論文 / 著書情報
Article / Book Information

題目(和文)	ディーゼルエンジンを用いたカーボンナノチューブ合成プロセスに関する研究
Title(English)	The study on the synthesis of carbon nanotubes using a diesel engine
著者(和文)	鈴木俊介
Author(English)	Shunsuke Suzuki
出典(和文)	学位:博士(工学), 学位授与機関:東京工業大学, 報告番号:甲第10954号, 授与年月日:2018年9月20日, 学位の種別:課程博士, 審査員:森 伸介,関口 秀俊,多湖 輝興,松本 秀行,小酒 英範
Citation(English)	Degree:Doctor (Engineering), Conferring organization: Tokyo Institute of Technology, Report number:甲第10954号, Conferred date:2018/9/20, Degree Type:Course doctor, Examiner:,,,,
学位種別(和文)	博士論文
Type(English)	Doctoral Thesis

Doctoral thesis 博士論文

The study on the synthesis of carbon nanotubes using a diesel engine

（ディーゼルエンジンを用いたカーボンナノチューブ合成プロセスに関する研究）

Shunsuke SUZUKI (鈴木俊介)

Supervisor: Shinsuke MORI(森伸介), Associate Professor

Department of Chemical Engineering 化学工学専攻

Graduate school of Science and Engineering 理工学研究科

Tokyo Institute of Technology, Japan 東京工業大学

2018

Abstract

A diesel engine has been utilized for a power source and/or electrical generator for more than one hundred years. On the other hand, the application of a diesel engine to other field has been considered in recent years. For instance, the utilization as a chemical reactor for the generation of syngas has been reported. In this study, a diesel engine was regarded as a combustion reactor to synthesize carbon nanomaterials such as carbon nanotube (CNT). CNT is quite promising nanomaterial because it possesses a number of outstanding physical/chemical properties. However, the applications using CNTs are limited even today due to its very high production cost. Flame process using a burner has been paid attention since not only CNTs but also the allotrope of CNT like carbon black and fullerene has been produced commercially in flame technique owing to its inherent characteristics such as easy scale-up and low investment cost. Similar features are provided for CNT formation process using a diesel engine. A diesel engine is an attractive system since simultaneous power generation and material synthesis can be achieved in one system, being expected that the CNT production cost is reduced in comparison with various conventional processes. Combustion reactions of injected fuel which provided adequate heat and carbon precursors were utilized for growing CNTs. Catalyst sources that were necessary for the synthesis of CNTs were also introduced into a reactor.

As a first step (Chapter 1), experimental conditions required for CNT formation in a diesel engine were examined when using a gas oil as base fuel. No CNT formation was observed when gas oil alone was employed even in the presence of catalyst sources. It was found that at least three conditions had to be satisfied for successful synthesis of CNTs, namely, (1) the introduction of catalyst precursor, (2) the usage of gas oil/ethanol mixing fuel, and (3) the addition of sulfur as an enhancer.

As a next step (Chapter 3), normal dodecane/ethanol mixing fuel was employed as base fuel in place of gas oil/ethanol because gas oil has very complicated compositions which makes some analyses difficult. Due to fixed compositions of fuel, the evaluation of the key factors such as combustion temperatures and gaseous species which contributed to CNT synthesis became possible. It was suggested that carbon monoxide affected CNT formation more strongly than a combustion temperature. Also, the analysis on catalytic nanoparticles revealed that sulfur seemed concentrated on iron catalyst.

Then, in Chapter 4, the impact of the molecular structure of fuel on CNT formation was investigated in the employment of fatty acid methyl ester (methyl laurate) and alcohol with long alkyl group (1-decanol) besides normal dodecane. This activity was motivated because combustion characteristics and emission properties were affected by the chemical structure of fuel according to a number of preceding papers. The difference of results was observed when a volumetric percent of ethanol in initial fuel was low, while it became tiny along with an increase of an ethanol fraction. It was implied that this difference was probably interpreted by the amounts of carbon monoxide in an exhaust. Also, elemental analysis showed that the state of catalyst nanoparticles should not be oxidized one but the metallic one for the growth of CNTs.

In-depth discussion on a promising CNT precursor and CNT growth mechanism/pathway was carried out through experimental, computational and modeling approaches (Chapter 5). Experimental approach employed an exhaust gas analysis, and combustion reactions were simulated in computational approach. The modeling of CNT growth reactions using CO, C_2H_4 and C_2H_2 as a carbon source were exploited based on several elemental reactions. All of them indicated that carbon monoxide might behave as a central role in CNT formation rather than other hydrocarbons like acetylene and ethylene. Also, it was suggested that fuel rich region was of advantage in forming gaseous carbon precursor and appropriate growth of catalyst nanoparticles. Given the combustion characteristics of a diesel engine, CNT synthesis might take place in fuel rich regions like the vicinity of fuel injection nozzle and/or the center of sprayed fuel.

In order to improve CNT productivity, the impacts of additional gaseous fuel were investigated (Chapter 6). H_2, CH_4 and C_2H_2 were selected as additional intake gas. A slight increase of CNT growth was found in the use of H_2 and CH_4, while CNT production was degraded in C_2H_2. This might be attributed to very high concentration of acetylene which deactivated catalysts at early reaction stage when C_2H_2 was employed as additive gaseous species.

Finally, in Chapter 7, the role of sulfur as a promoter in CNT growth was examined by means of chemical vapor deposition (CVD) process because the addition of sulfur was one of key factors for the successful CNT synthesis in a diesel system. In order to make analysis easier, CVD technique was employed. The introduction of sulfur significantly reduced the activation energy required for CNT growth which was revealed by Arrhenius plot. The shift of the rate-determining step in carbon diffusion process during CNT growth might take place in the presence of sulfur. According to some analyses on catalytic nanoparticles, it was suggested that the reduction of melting temperature of catalysts might occur, resulting in the enhancement of CNT synthesis.

In Chapter 8, overall summary obtained in this study and future works are described.

Contents

Chapter 1. Introduction

1-1 About a diesel engine

1-1-1 History of a diesel engine [1]

A diesel engine has been one of the most popular equipment that obtains driving force for various vehicles and/or generates power. Historically, the prototype of a diesel engine was developed by Dr. Diesel in Germany at the end of 19th century for the original use of heavy oil and vegetable oil. However, due to immature technology at the beginning, the utilization of a diesel engine was limited to ships and stationary equipment. From the early 1920's, a diesel engine was advanced by means of technological innovations such as the practical use of a direct fuel injection system, commercial production of fuel injection pump and nozzle, and so on. As a result, the application of a diesel engine to auto trucks, automobiles and railroad vehicles was initiated. In the 1950's and 1960's, through the achievement of high pressurization of a fuel injection system and improvements of a combustion chamber, fuel efficient diesel engine with lower noise emerged. When supercharger which supplies compressed air to a combustion chamber was started to be installed in the 1980's, the advantages like an increase of engine power output and a reduction of NOx emissions were provided. Since a diesel engine is currently available around the world as a power source, it possesses quite significant impact on world's environments. Since we moved into the 21st century, strict regulations for environments have been implemented in especially developed countries. Accordingly, a lot of studies and researches on a diesel engine are continued, such as replacement of a conventional fossil fuel with alternative fuel, the attainment of a hybrid system with the combination of a diesel system and electrical power, and others.

1-1-2 Basic of a diesel engine [1,2]

Both a diesel engine and gasoline engine generate power through the conversion from heat energy to mechanical energy via combustion of fuel inside a cylinder. The differences between a diesel engine and a gasoline engine are fuel used and an ignition system. As fuel, gasoline which is a mixture of a variety of hydrocarbons ranging from C4 to C10 is used for a gasoline engine, while gas oil and heavy oil whose carbon number is higher than C10 are used for a diesel engine. In general, gas oil is applied for automobiles and small-sized power generator, and heavy oil is for boilers and ships. Since the pre-mixture of gaseous fuel and air is ignited via spark plug in a gasoline engine, it is called a spark ignition engine. On the other hand, liquid fuel is spayed into compressed air and ignited automatically in a diesel engine system, hence it is called a compression ignition engine. Due to differences of fuel compositions and an ignition system, combustion cycle is different with each other. Gasoline engine basically obeys Otto cycle which is constant volume cycle, but diesel engine does Diesel cycle which is constant pressure cycle. Figure 1-1 shows the comparison of Otto cycle and Diesel cycle. Of course, since these schematics are an ideal cycle, both constant volume cycle and constant pressure volume

cycle possibly coexist in actual combustion of a diesel engine. Regarding the net thermal efficiency in automobiles which is defined as the ratio of shaft power divided by the energy of fuel introduced into an engine system, a gasoline engine ranges 25~35 %, while a diesel engine has 35~45 %. There are mainly three reasons why higher efficiency is gained in case of a diesel engine. First reason is larger compression ratio which is defined as the ratio of the chamber volume before compression (bottom dead point) by the chamber volume after compression (top dead point). Basically, the higher compression ratio becomes, the higher thermal efficiency can be obtained. A gasoline engine has the limited compression ratio up to about 10 due to knocking, while the compression ratio of a diesel engine being free from knocking is possible up to 20. Second reason is that a diesel engine is operated under fuel lean condition (oxygen rich condition), leading to the reduction of cooling loss during combustion as a result of the suppression of temperature increase. Third reason is that a diesel engine is free from throttling valve which controls intake volume. By contrast, it is installed in a gasoline engine, resulting in the degradation of efficiency because of pumping loss. Accordingly, a diesel engine is regarded as an economically kind system in comparison with a gasoline engine. However, the bottleneck of a diesel engine is the trade-off correlation between the generation of particulate matters and that of NOx. This is described in a later section.

Here, the burning process in a diesel engine is mentioned. In case of a diesel engine with 4 stroke system, the combustion process consists of 4 steps, intake of fresh air, compression of introduced air, expansion as a result of fuel combustion, and exhaust of burned gas to an outside. The operation of each step is schematically displayed in Figure 1-2. In general, the operation which starts from intake and finishes by exhaust is defined as one engine cycle. In a diesel engine, liquid fuel is injected after intake air is compressed, then, auto ignition of fuel occurs. Burning processes of a typical diesel engine per one cycle are exhibited in Figure 1-3. Pressure inside chamber, heat release rate and needle valve lift are employed to describe the combustion characteristics. Combustion processes in a diesel engine are divided into four stages, ignition delay, premixed combustion, diffusion combustion, and afterburning, shown in Figure 1-3. Since the combustion in a diesel engine is inhomogeneous (cf. homogeneous in case of a gasoline engine), sprayed liquid fuel firstly has to be vaporized to form the mixture of air and fuel. Then, air-fuel mixture starts ignition by triggering partial oxidation reactions. Ignition delay is defined as the required time from an initiation of fuel spray to an ignition after which enormous heat is released. Pressure inside chamber is sharply increased owing to significant heat release after ignition starts. During this period, combustion properties are similar with premixed ones because a part of liquid fuel is vaporized and mixed with air until ignition begins. After that, diffusion combustion becomes dominant because ignited combustion occurs simultaneously with fuel injection and combustion properties are controlled by the diffusion rate of air and fuel. Even after fuel injection ceases, some of unburned fuel continue to react with oxygen. This period is called afterburning period. It should be noted that combustion properties in a diesel engine are susceptible to various factors, like

fuel compositions, impurities in fuel, the design of an intake and exhaust system, a fuel injection system, and others. Accordingly, these factors may affect emission properties from a diesel engine which are one of the largest concerns in a current engine study.

1-1-3 Emissions from an internal combustion engine

An internal combustion engine (not to limited to a diesel engine) releases an effluent gas into atmosphere after combustion, and the exhaust gas potentially includes air pollutants such as NOx, unburned hydrocarbons, carbon monoxide, and particulate matter. Every country sets up regulations against emissions from an internal combustion engine in order not to make atmosphere poisoned. Thus, it is of importance to understand properties and the formation mechanism of combustion emissions. Here, descriptions about potential contaminants from a diesel engine are provided in the following sentence.

① NOx [3,4]

NOx is the abbreviation of nitrogen oxide mainly composed of NO, NO_2 and N_2O, and it is largely generated via reactions between N_2 and O_2 during combustion inside a cylinder. The formation mechanism of NOx can be divided into three categories according to its origin, thermal NOx, prompt NOx and fuel NOx. Thermal NOx is generated as a result of oxidation of air at high temperature usually larger than 1,800 K. Formation reactions of thermal NOx can be described by extended Zeldovich mechanism where N_2 and O_2 react with high activation energy. Prompt NOx is generated from N_2 in air even at mild temperature like 1,000 K, but its pathways are different from those of thermal NOx. Prompt NOx is rapidly formed inside flame zone via HCN, N, and NH radicals through reactions between N_2, CH, CH_2, C radicals, etc. with relatively low activation energy. Fuel NOx can be generated when nitrogen atom is contained in fuel. In general, the content percentage of nitrogen in coal and heavy oil is approximately 0.2~3.4% and 0.1~0.4%, respectively. The conversion from nitrogen atom included in fuel to NO is quick independently on temperature. Countermeasures for reducing NOx have been taken to date, such as controlling combustion processes and removal of NOx in an exhaust by additives and/or catalysts.

② Unburned hydrocarbons [3]

Fuel which is composed of a variety of hydrocarbons is decomposed during oxidation reactions to form various low molecular weight hydrocarbons as intermediate products. When oxygen is locally too short to oxidize intermediate hydrocarbons or oxidation reactions cease due to quenching caused by rapid heat release and/or mixing air at low temperature, hydrocarbons remain unburned and are emitted outside. As countermeasures to suppress emissions of unburned hydrocarbons, the improvement of mixing air and fuel and/or a gradual decrease of temperature

for avoiding quench have been proposed. Moreover, an aftertreatment system of emission gas using catalysts is also carried out in automobiles.

③ Carbon monoxide [3]

Basically, causes and the formation mechanism of CO are almost same with those of unburned hydrocarbons. In general, because a diesel engine is operated under oxygen rich condition, emission of CO tends to be smaller than that from a gasoline engine.

④ Particulate matter (PM) [2,4]

PM is defined as materials emitted from an internal combustion engine, including soluble organic fraction (SOF) which consists of unburned large molecular weight hydrocarbons and insoluble organic fraction (IOF) which is mainly made up of soot and sulfate (ash). Here, soot is the most interesting content for us because it is largely composed of elemental carbon. Soot cannot be ideally generated via complete combustion, however, it is potentially released by a shortage of air and/or quick cooling of flame. Primary particles of soot with a diameter of several tens of nanometers have the spherical structure that multiple graphite layers are irregularly piled up in the microscopic sense. The distance of graphite layer of soot is generally larger than that of ideal graphite (0.335 nm) due to the inclusion of other elements like hydrogen and oxygen present between layers. Primary particles coalesce each other to form aggregate which consists of several tens to several hundreds of primary particles. Although a lot of efforts have been devoted to reveal the mechanism of soot generation and growth, it remains a controversial item even today. Prevalent theory expresses that polycyclic aromatic hydrocarbon (PAH) such as naphthalene, pyrene and larger molecules is produced in gas phase through thermal cracking of fuel, and then an initial nucleation occurs as a result of condensation of PAH. Because the surface of soot particles is very reactive owing to the presence of a number of unpaired electrons, growth reactions between soot and active chemical species which is present around soot like acetylene and PAH make progress quickly (called surface growth). At the same time, soot nucleus collides with each other, resulting in particle enlargement (called coagulation). After soot growth, oxidation reactions by O and OH radicals takes place, leading to the reduction of soot amount. Soot amount emitted outside can be determined by not only growth reactions but also oxidation reactions. As the dependency of soot formation on temperature, soot is formed at temperature ranging from 1,000 K to 2,000 K, being maximum value at 1600 K according to the fundamental study using a burner system instead of an internal combustion system. This is because reactions via radicals cannot continue at low temperature while oxidation becomes in favor at high temperature. For the suppression of soot emission, it is important to mix air and fuel adequately in order to avoid locally fuel rich circumstance.

The typical dependence of NOx and soot on temperature and equivalence ratio (the ratio of fuel/air ratio in actual mixture divided by stoichiometric fuel/air ratio) is shown in Figure 1-4.

This relationship becomes quite important when considering an actual engine operation, in particular a diesel engine. Since in a diesel engine various equivalence ratios typically ranging from 0.4 to over 2.0 coexist even at one engine cycle, and corresponding adiabatic combustion temperature is higher than 1,500 K, this led us the trade-off correlation between soot formation and NOx generation. As a required condition for soot formation but no NOx generation according to this figure, fuel rich circumstance (generally higher than 2 as an equivalence ratio) and temperature larger than about 1,500 K should be satisfied. We believe that this perspective is qualitatively valid for the formation of carbon nanotubes in a diesel engine because main element in soot and carbon nanotube is carbon atom.

1-1-4 Recent improvements of a diesel engine

Here, we present three examples of recent improvement achieved in a diesel engine especially for automobiles, namely exhaust gas recirculation (EGR), aftertreatment equipment and a common rail system. These provisions have been considered in order to control emissions and/or abide by various regulations. EGR is an emerging system where a part of an exhaust gas is recirculated to an engine intake line and combustion takes place after mixing it with fresh air. EGR is a technique that enables the reduction of NOx emission because of lowering the combustion temperature inside an engine. Aftertreatment equipment is dedicated to the removal of PM and NOx which are present in an exhaust gas from a diesel engine. Apparatus termed diesel particulate filter (DPF) which is composed of porous metal or ceramics is used for the elimination of PM. PM up to 90 % at most is collected by DPF. Regeneration operation where PM is burned by heating filter is regularly required in order to prevent clogging by PM. Aftertreatment equipment for reducing NOx is in practical use, e.g. selective catalytic reduction (SCR) and NOx storage catalyst. In SCR, ammonia which is produced from the reaction of injected urea pyrolysis selectively reduces NOx, and NOx conversion efficiency at approximately 90 % is attained. NOx storage catalyst consists of two steps, lean-burn condition and rich-burn condition. In the former step, an engine is run under a normal operation and NOx is trapped on catalyst. Then, in the latter step, an engine is operated at fuel rich condition and NOx is purified by generated H_2 and CO. A common rail system is an emerging technique used in a fuel injection system since middle of 1990's. Typical configuration diagram of a common rail system is depicted in Figure 1-5 [5]. In a common rail system, a fuel injection is adjusted by electrical control, being different from the conventional system where the fuel injection is controlled mechanically. A common rail system contains some main component parts, supply pump, common rail, injectors and engine control unit (ECU) as shown in Figure 1-5. Pressurized fuel by supply pump up to about 200 MPa at maximum is stored in common rail, then fuel is sprayed into a cylinder via injectors depending on the operational situation. Not only injection timing and duration but also each injection number and amount are

tailored through electronic control in ECU. Table 1-1 displays the comparison of controllable factors in a conventional fuel injection system and a common rail system. Drastic improvements of emission properties from an engine have been achieved by introducing a common rail system owing to enhanced flexibility of a fuel injection via electrical control. Our group sees this fact from another standpoint. It is suggested that a common rail system has large potential to accomplish an appropriate fuel injection system for the synthesis of nanomaterials like CNTs in a diesel engine. Therefore, we believe that a diesel engine is a promising reactor to produce CNTs. In this study, a conventional diesel engine controlled by a mechanical system without EGR, DPF, SCR and a common rail was employed because the viability of a diesel engine for material synthesis had to be examined and fundamental insights on CNT synthesis in the use of a basic diesel engine was mandatory as a first step.

1-1-5 Applications of a diesel engine other than power sources

New applications of an internal combustion engine other than power sources have recently been proposed by taking advantages of its inherently dynamic high temperature/pressure system. Most intensively studied application is for the production of syngas by means of partial oxidation of methane in a gas engine without any catalysts. In these studies, the engine was treated as a chemical reactor, namely the engine reformer. Historically, attempts to use the engine reformer can be firstly found in U. S. patents by some companies such as Texas Co., Maschinenfabrik Augsburg, and Sun Oil Co. about half a century ago. These patents are expired at present. In 1960's, Hiratsuka performed partial oxidation of natural gas using a spark ignition engine [6], and McMillian and Lawson also utilized a spark ignition engine [7]. From 1990's, Karim et al. carried out partial oxidation of methane in a diesel engine where diesel fuel was used to trigger combustion [8,9,10]. Furthermore, numerical and modeling study on the production of syngas using a homogeneous closed compression ignition engine fueled with natural gas was performed for the optimization of experimental conditions [11,12]. The study by He et al. attained the production of CO/H_2 mixture gas through a spark ignited engine using either natural gas or ethanol, but their study aimed to improve an engine operation with EGR, not to synthesize CO/H_2 gas intentionally [13,14]. The group of Massachusetts Institute of Technology recently demonstrated partial oxidation of natural gas in a diesel engine with spark ignition and examined whether an engine reformer could be integrated into small-scale Gas-to-Liquids (GTL) plants as one system [15]. According to their description, not only syngas production but also other techniques like usage of hot effluent gas from an engine to heat the reactants, electric generation, operation of compressor etc. could be achieved in one system, providing economic advantages to small-scale GTL plants which did not employ an engine. In spite of some reports on syngas production by an engine, it is commonly operated at a high equivalence ratio up to 2.5 (fuel rich condition). Anderson et al. studied steam methane reforming in a variable volume reactor where H_2 separation

membrane, adsorptive agent for CO_2 and catalyst for reforming reaction were installed in a single reactor [16,17]. Although this system was far from an internal combustion engine in a strict sense due to no appearance of combustion reactions and quite slow piston speed, similar concept with studies regarding an engine as a chemical reactor was applied. Thanks to nice concept, they were able to acquire high purity hydrogen beyond equilibrium even at low temperature.

In this work, we regard a diesel engine as a reactor to synthesize carbon nanomaterials intentionally like carbon nanotube (CNT) together with generating power, and try to investigate the potential of it. To our knowledge, this is the first attempt to exploit a new process of material synthesis using a diesel engine. Our study is originally motivated by several researches where accidental synthesis of CNTs in an internal combustion engine was found for the purpose of warning about environmental and human health issues. Lagally et al. reported that CNTs and fullerene were contained in an exhaust gas in addition to PM when a spark-ignited engine was used in the absence of catalyst sources [18]. Jung et al. [19] and Swanson et al. [20] found that CNTs were emitted from a diesel engine fueled with diesel fuel when ferrocene which served as an iron catalyst source was added into fuel. According to the work by Jung et al, CNTs could only be observed in an exhaust gas in the presence of catalyst source in fuel, whereas emitted CNT amount was almost zero without catalyst sources. In their study, ferrocene concentration was 600 ppm by weight at a maximum, being too large for the inclusion of iron component in a normal engine operation accidentally. Hence, they claimed that CNT might be unable to be synthesized unless accidental incorporation such as mechanical wear or lube oil leakage occurred. The study by Swanson et al. provided additional information that the presence of both sulfur and ferrocene which acted as a promoter and catalyst source, respectively, significantly facilitated growth of CNT-like materials in comparison with the case in the presence of sulfur or ferrocene alone.

We believe that there are several advantages of a diesel engine as a chemical reactor. One of advantages is that reactions are completed instantly (usually within several miliseconds) under high temperature and pressure condition along with compression and combustion. As well as the utilization of high temperature and pressure environment, if rapid temperature and pressure decrease during expansion can be made use of for the cessation of reactions in a proper manner, it can become advantageous from the point of view of controllability.

1-1-6 Possibility of carbon nanotube (CNT) formation in a diesel engine

Here, let us discuss the possibility of CNT formation in a diesel engine. Initially, we would like to turn the spotlight on soot formation in a diesel engine because the main component of both CNT and soot is carbon. Soot formation mechanism in a diesel engine is already described in section 1-1-3. Morphology observations of particle matters emitted from a diesel engine without catalyst sources have been conducted by others, and may provide fruitful information [21,22,23,24,25]. Diesel

particulates observed by transmission electron microscopy (TEM) showed a chain-like agglomerates structure, which was composed of many spherical or near-spherical primary particles. In terms of engine operating conditions such as engine load, fuel type, and others, dominant contents of particulate matter could be varied, like soluble organic-fraction-rich particles and soot-rich particles. Particle matter morphology could be changed accordingly and it was revealed by TEM observations that the former showed nebulous morphology with unclear boundaries between primary particles but the latter showed more distinct and ordered structure. Actually, some characterization methods indicated that the latter possessed more graphitized structure compared with the former. Since CNT has a highly ordered structure with six-membered ring, one can expect that experimental conditions proper for the formation of soot-rich particles may be preferable for CNT growth. The possibility of CNT formation in a diesel engine is considered next. At least, three conditions have to be satisfied for CNT growth, namely the presence of heat, metallic catalysts and carbon precursor [26]. Heat can be provided via combustion of fuel. Catalyst precursors are able to be introduced into a cylinder through dissolution of ferrocene in fuel as done by Swanson et al. [20]. Taking account of intentional CNT synthesis in flame processes using a burner, carbon precursors such as ethylene, acetylene and carbon monoxide were usually employed [27,28]. Diesel fuel or its surrogate is pyrolyzed at high temperature to low-molecular weight hydrocarbons like ethylene, acetylene, and so on [29,30,31]. Furthermore, since combustion properties in a diesel engine are inherently inhomogeneous, fuel lean regions and fuel rich regions are generated at the same combustion cycle. As stated in section 1-1-3, low-molecular weight hydrocarbons and carbon monoxide are likely to be formed at fuel rich regions during combustion owing to the shortage of oxygen. Therefore, if a part of these low-molecular weight hydrocarbons produced during combustion become a precursor for not only PAH but also CNTs, it is very probable that CNTs are synthesized during combustion in a diesel engine.

1-2 About carbon nanotube (CNT)

1-2-1 Structures and types of CNTs

Carbon nanomaterials are one of the most intensively studied materials since its discovery such as fullerene [32] and carbon nanotube (CNT) [33,34], and a variety of applications using them have been proposed to date. Carbon materials show diverse structures according to its bonding type. For instance, in case of sp^3 bonding, solid diamond with 3D structure is formed, while in case of sp^2 bonding, graphite with laminated 2D structure is made up. When laminated graphite layers are peeled off to one layer, graphene is fabricated. Fullerene is the material that graphene layer is engineered to soccer ball like shape. When graphene is rolled up with concentric shape, it becomes CNT. CNT structure can be described by two fundamental vectors on graphene layer with 2 dimensions, termed chiral vector and translation vector. What is important is that some CNT physical properties like electrical conductivity

depend on chirality which is determined by the combination of chiral vector and translation vector. Furthermore, CNT can be categorized into three depending on the number of graphite layers, namely single walled CNT (SWNT), double walled CNT (DWNT), and multi walled CNT (MWNT). SWNT consists of only single graphene layer, DWNT comprises two graphene layers in its structure, and MWNT possesses multiple graphene layers larger than two. Figure 1-6 shows the structure of SWNT and MWNT. The growth of MWNTs does not necessarily require catalyst, while the presence of catalysts is generally crucial for synthesizing SWNTs. Sometimes, since SWNT shows quite distinct physical properties with MWNT, it is of significance to distinguish SWNT from MWNT according to some applications. As other CNT types which are not mentioned above, bamboo-like CNT and cap-stacked CNT have been reported. These special CNTs normally have multiple graphene layers. Due to its unique structure, CNTs have significant superiority in characteristics such as mechanical property (tensile strength, elasticity, flexibility), electrical property (electron mobility), chemical property (inertness, corrosive resistivity), thermal property (heat transfer).

1-2-2 Applications using CNTs

Because of its outstanding physical/chemical properties, a lot of applications using CNTs have been proposed to date. Among them, promising applications are introduced shortly as follows [35].

① Composite material

Composite materials including CNTs have two types, one is a complex of ceramics and CNTs and another is that of resin and CNTs. The former can be classified into two configurations further, surface modifications of CNTs via ceramics and the introduction of CNTs into ceramics matrix. The former aims to improve performance of some devices such as photocatalyst, gas sensor and so on. The latter intends to increase mechanical strength and give electrical specifications by means of CNTs as a filler. A complex of resin and CNTs is expected to serve as an excellent material in mechanical reinforcement, heat release for the use of electrical equipment, construction materials and others.

② Field emitter

When strong electrical field is applied to solid surface, electron is released from the surface due to tunnel effect. Though very large electric field higher than 10^9 V/m is usually necessary for achieving field emission, the reduction of applied electrical field becomes possible if a protruding object is used as an emitter. By taking advantage of superior physical properties of CNTs such as large aspect ratio, good electrical conductivity, chemical stability and inertness etc., some devices using CNTs as a field emitter have been proposed until now, e.g. light source, displays for TV and electron source as small X-ray source.

③ Material for battery electrode

The application of CNTs to lithium ion secondary battery, fuel cell and electric double layer capacitor (EDLC) is expected. As for lithium ion secondary battery, some usages have been proposed, for example, an electrode material instead of conventional activated carbon and additive for assisting electrical conductivity when activated carbon or alternative materials for it is used as an electrode material. With respect to fuel cell, CNT is a promising material as a catalyst support of Pt or Pt-Ru because it has capability of not only promoting charge/mass transport but also suppressing agglomeration of catalyst nanoparticles, contributing to the reduction of catalyst quantity used. Intriguingly, CNT with high defects shows high performance. Concerning EDLC, studies to employ CNT as a replacement of conventional carbon material by means of large specific surface area of CNT are continued.

④ Electronics and photonics

CNTs are expected to be applied for a number of devices in electronics technology. For instance, field effect transistor and thin-film transistor through the use of competent electron transport properties of CNT, a material as a trace in LSI circuit alternative to copper, transparent electrode as a substitution of currently prevalent indium tin oxide, and bio-sensor and gas sensor with high sensitivity. Also, a number of researches on applications to optical fiber laser and optical fiber communications with the assistance of optical features of CNT are put forward.

⑤ Microelectromechanical system (MEMS)/Nanoelectromechanical system (NEMS)

CNT is a promising candidate as a material for mechatronics devices in micrometer and/or nanometer size due to its special mechanical and electronic properties. CNT probe for scanning probe microscope and CNT oscillator for mass measurement have already been in practical use. Developments of other devices such as CNT motor and CNT radio are in progress.

⑥ Gas storage

Because CNT possesses large specific area and nano-sized pore, it has been paid attention as a material to store some kinds of gas like hydrogen and methane. Besides, it was demonstrated that CNT was able to be used for selective D_2 separation against H_2 due to the difference of adsorption properties.

⑦ Medical application

In recent years, studies for the purpose of in vivo use of CNTs are performed, in particular as a carrier in a drug delivery system (DDS) through a proper modification. DDS studies aimed at cancer treatment are current mainstream, but applications to other diseases are in expansion. Moreover, the composite material using CNT as a biomaterial is in consideration for the field of orthopedics because CNT has a strong compatibility with bone tissue. Also, studies to use CNT composite materials as a scaffolding in tissue engineering are actively carried out.

According to applications stated above, required CNT specifications and configuration structures differ from each other. Both SWNT and MWNT have been tried to be applied. As for the arrangement

of grown CNTs, vertically aligned CNTs on substrate are preferable for one application, but dispersed form is preferred in another application. In any case, it is of importance in commercial scale to produce CNTs with uniform length and diameter as much as possible in order to accelerate the implementation of applications using CNTs.

1-2-3 Synthesis processes of CNTs and current drawbacks

Until now, four CNT growth processes have been mainly proposed, namely, arc discharge, laser ablation, chemical vapor deposition (CVD), and flame process. In the following sentence, let us review general characteristics of each synthesis process.

① Arc discharge [36,37,38]

In this process, arc discharge is generated between two carbon electrodes usually under He or Ar atmosphere. Carbon of anode is vaporized during discharge, resulting in the deposition on cathode and chamber wall. This deposition includes not only soot but also CNTs. It is possible to grow MWNT, DWNT and SWNT selectively by adjusting experimental conditions properly. Carbon electrode including catalyst metal is used for the synthesis of SWNT and DWNT, however, growth of MWNT generally requires no catalyst. Arc discharge has advantages such as relatively large CNT production, while it is difficult to control synthesis conditions and the purity of CNT in products is low.

② Laser ablation [39,40]

Carbon rod including metal which behaves as a catalyst is employed in this process. Carbon and metal atoms are evaporated by irradiation of laser at high temperature under blowing inert gas. The nucleation and growth of CNTs takes place in backward region where temperature ranges from 850 to 1,250 ^{o}C. High CNT yield is acquired via laser ablation process with small formation of other carbonaceous materials. However, mass production of CNT is quite challenging due to its productivity.

③ Chemical vapor deposition (CVD) [41,42,43,44,45,46]

CVD is most intensively studied among four processes. A variety of hydrocarbons such as methane, acetylene, ethylene, ethanol and carbon monoxide are employed as a carbon source and metal catalysts like iron, cobalt and nickel are frequently utilized for growing CNTs. Thermal CVD process is often carried out where temperature ranges from 600 to 1200 ^{o}C, while plasma enhanced CVD is also studied for the purpose of reducing growth temperature by microwave plasma and RF plasma. CVD technique is advantageous to mass production because apparatus is simple and scale-up is relatively easy. Furthermore, tuning conditions like a catalyst source, carbon source and reaction temperature enables us to grow SWNT, DWNT and MWNT selectively. Practically, mass production of CNTs has been achieved by some CVD methods

[47,48,49]. In particular, the production scheme for vapor growth carbon fibers proposed by Endo has provided the basis for current CNT commercial production processes [50]. Moreover, CVD processes can be usually divided into two categories according to growth region of CNTs. One is substrate growth process where CNTs are grown directly on solid substrate. In this process, catalysts are normally prepared on substrate before carbon sources are fed. The other is floating catalyst process where both carbon sources and catalyst sources are supplied at the same time, leading to CNT growth in gas phase. Here, let us mention the details of each method.

A) Substrate growth process

A variety of materials such as silicon, quartz, alumina etc. are employed as a substrate, and metal catalysts like Fe, Co and Ni are immobilized on it. Metal layer is often prepared by dip-coating or sputtering. Patterning of catalyst deposition is accomplished by using masks, resulting in area-selective growth of CNTs. The structure of CNTs, namely SWNT and MWNT, can be controlled by adjusting conditions like loading amounts of catalysts, CVD methodology (thermal decomposition or plasma enhanced), CVD temperature, CVD time, partial pressure of carbon source and so on. Furthermore, some groups try to synthesize CNTs by using porous materials like zeolite as a support for preventing catalytic particles from coagulating. CoMoCat process where cobalt and molybdenum are employed as catalyst sources and carbon monoxide is used as a carbon source has been commercialized as a representative of substrate growth process [49].

B) Floating catalyst process

Because both carbon and catalyst sources are fed in gas phase, continuous production of CNT can be achieved in principle. As a catalyst precursor, metalocene such as ferrocene or pentacarbonyl like iron pentacarbonyl are frequently utilized due to its easy sublimation. This process also enables us to achieve selective synthesis of SWNT or MWNT through the optimization of synthesis conditions. The group of Smalley developed commercial production termed HiPco, in which carbon monoxide with high pressure (1~10 atm) and iron pentacarbonyl are employed [48].

④ Flame process [51,52,53,54,55,56,57]

In this method, a burner to generate flame is commonly employed. However, burner configurations and used catalysts are dependent on systems. The flame system mainly consists of two configurations dependent on how to supply fuel and oxygen, pre-mixed flame and diffusion flame. The former is the process where fuel and oxygen are pre-mixed before being fed to combustion field. The latter is the one that fuel and oxygen are supplied to a reactor separately. Both systems are employed for both SWNT and MWNT synthesis. Methane, ethylene, acetylene and ethanol were popular fuel, being supplied with inert gas like nitrogen as usual and hydrogen as a carrier gas in some cases. Also, there are two procedures to supply catalyst sources, one is

that catalyst sources like metalocene or metalpentacarbonyl are mixed with feed gas and then fed to a chamber, and the other is that metal substrate such as stainless steel is used as a catalyst. In general, flame process using a burner possesses several advantages like easy scale-up and low investment costs. Actually, there is a company, Nano-C, Inc., to produce CNTs commercially using the combustion process [58]. Moreover, carbon black and fullerene which are known as an allotrope of CNT have already been produced commercially using a burner flame process, and as a result the production cost has been significantly suppressed compared with conventional methods like arc discharge [59,60]. We believe this information stated above provides a motivation to study flame process further. The large difference between the flame method for carbon black/fullerene production and that for CNT production is whether catalysts for growing such a carbon material are included in feedstock or not. Flame process for carbon black and fullerene does not require catalysts while that for CNT does. Although the reduction of CNT production cost using flame processes has been expected, a great challenge is anticipated; the availability of carbon and catalyst sources still remains low. Figure 1-7 shows the typical schematic of an apparatus using a burner.

Summary of each CNT production technique to describe both its general advantages and disadvantages is shown in Table 1-2. It should be noted that mass production has been achieved by CVD process at present. However, there are some problems in spite of high potentials of CVD process. The biggest problem is CNT production cost, in particular SWNT. The purchase price of SWNT remains over several hundreds of US dollars per one SWNT gram. Hence, the reduction of CNT production cost is still required even today.

In this study, we regard a diesel engine as a combustion reactor to produce carbon nanomaterials in addition to power generation. As a result, a diesel engine is a potential candidate to produce CNTs with a low cost because a part of generated power is able to be used for CNT separation and purification processes. The concept of our idea is presented in Figure 1-8.

1-2-4 Separation process of CNTs from impurities

After synthesis of CNTs, it is important to separate synthesized CNTs from impurities like carbonaceous materilas (soot) and catalytic nanoparticles [35]. Until now, three separation processes have been proposed, thermal treatment, oxidative treatment and centrifugal separation. Thermal treatment is used for the separation of carbonaceous materials. In this process, the relative difference of reactivity in CNTs and carbonaceous materials is utilized. CNTs are oxidized in air at higher than 500 ^{o}C, while carbonaceous impurities are oxidized at around 200~350 ^{o}C. There is disadvantage that a part of CNTs are damaged in thermal treatment. Oxidative treatment is a process where acid solution such as sulfuric acid and/or nitric acid is employed for the removal of both soot and catalysts. In this

process, the relative difference of reactivity in CNTs and carbonaceous materials is utilized. Catalyst particles can be removed through the dissolution into acid solution. As a disadvantage of acid treatment, functional groups like –OH are formed on the CNT surface. Centrifugal separation where relative difference of density is used is applied for the removal of both carbonaceous impurities and catalysts. Firstly, samples are dispersed ultrasonically in the solution including surfactant agent, and then centrifugation is performed. After evaporation of both solution and surfactant agent, followed by low-temperature heat treatment, the purification of CNTs is enabled. Centrifugal separation requires a number of steps for the purification of CNTs. These three separation processes are able to be applied for the separation of CNTs synthesized via a diesel engine. Since CNTs generated in a diesel engine has disorder graphite structure (shown in later chapter), it can be considered that the separation of soot from CNTs may become more difficult than CVD because the relative difference of oxidative reactivity between soot and CNTs is reduced. Also, since CNTs and soot/catalytic particles form an aggregate in a diesel engine (shown in later chapter), the removal of impurities may become hard even when centrifugal approach is employed.

1-3 The objective in this study

The purpose in this study is to synthesize CNTs intentionally as much as possible using a conventional diesel engine with mechanically controlled fuel injection system as a basic reactor. As was stated earlier, this is the first attempt to utilize a diesel engine for the intentional material synthesis process. Studies where an engine was employed as a reforming reactor strongly support our study because of good economic performance. The reduction of CNT production cost can be expected through taking advantage of generated power and effluent gas with high temperature. Firstly, it was demonstrated whether the formation of CNTs was possible in our diesel system. Then, we investigated the experimental condition suitable for CNT synthesis as a function of an engine load, compositions of starting fuel, the amount of catalyst source, introduction of additives, etc. Also, we attempted to elucidate key factors which contributed to CNT formation in a diesel engine because of the pioneering work that intentional synthesis of CNT is carried out by an internal combustion system. Moreover, identification of a promising CNT precursor was performed, and CNT growth path/synthesis mechanism was explored through a number of experimental/calculated approaches in order to increase CNT production. We evaluated and proposed the effect and role of a promoter like sulfur on CNT growth in the employment of CVD because the addition of a promoter was one of keys to succeed in synthesizing CNTs in a diesel engine which is described in final chapter and corroborates our results obtained in a diesel system.

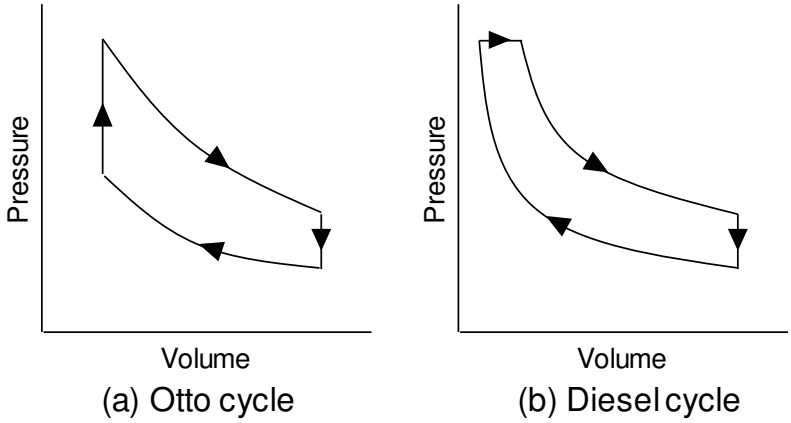

Figure 1- 1 Comparison of a combustion cycle between (a) a gasoline engine and (b) a diesel engine.

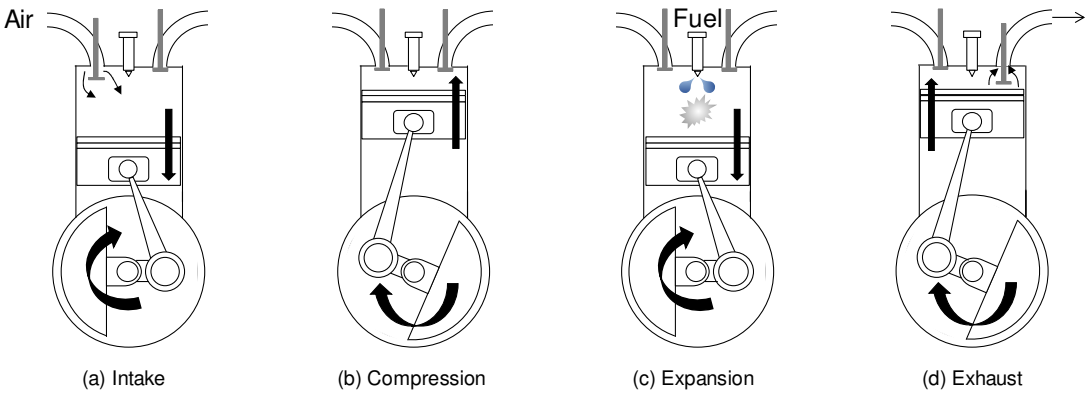

Figure 1- 2 Schematic of the operation of 4 stroke diesel engine.

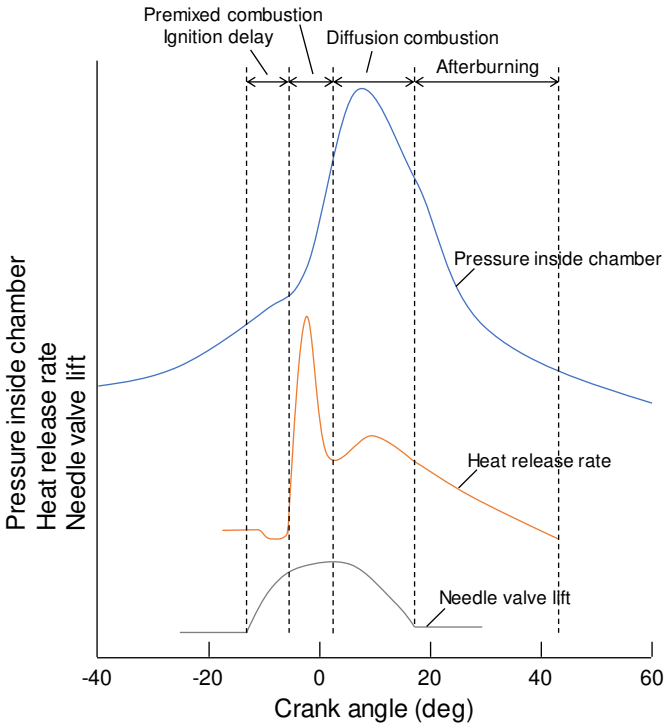

Figure 1- 3 Combustion process per one cycle of a typical diesel engine.

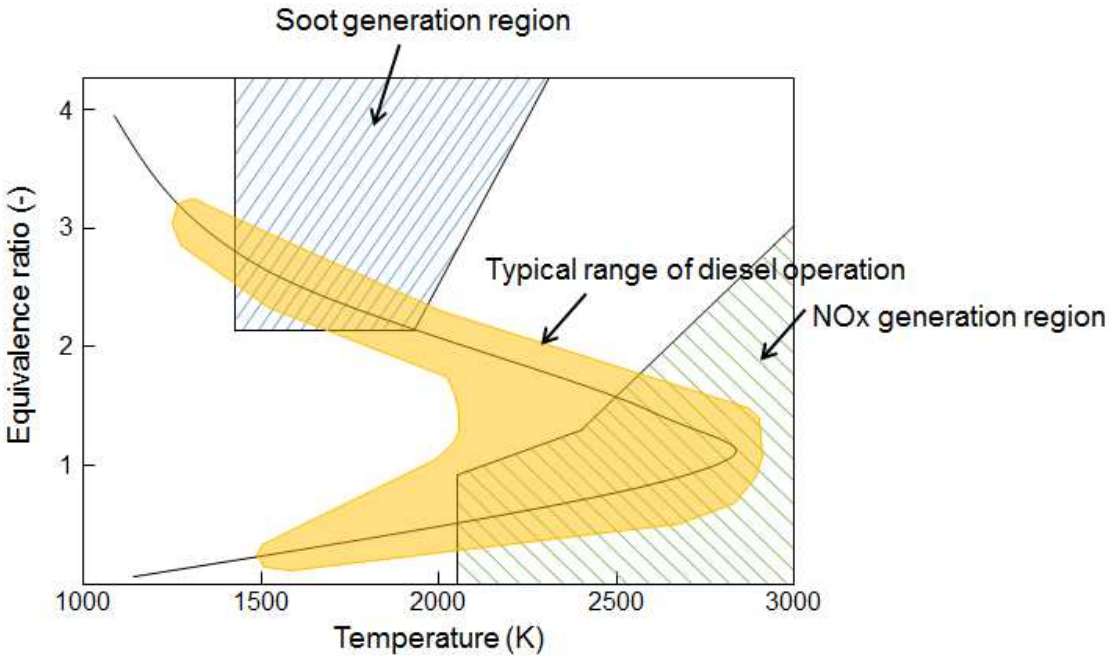

Figure 1- 4 The dependence of soot and NOx generation on equivalence ratio and temperature.

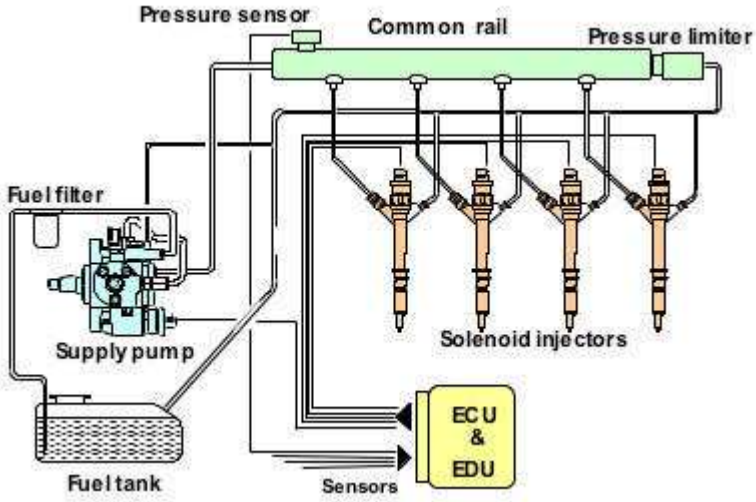

Figure 1- 5 Schematic representation showing overall view of a common rail system.

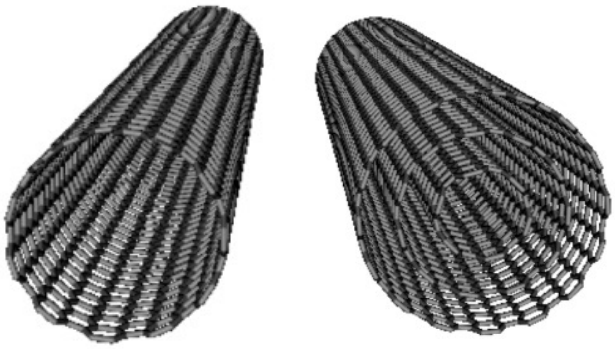

Figure 1- 6 Structure of SWNT (left) and MWNT (right).

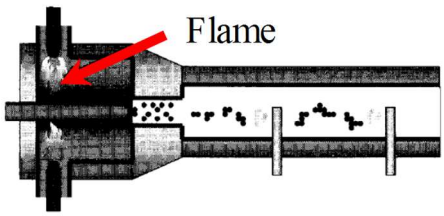

Figure 1- 7 Typical schematic of flame process to produce carbon materials.

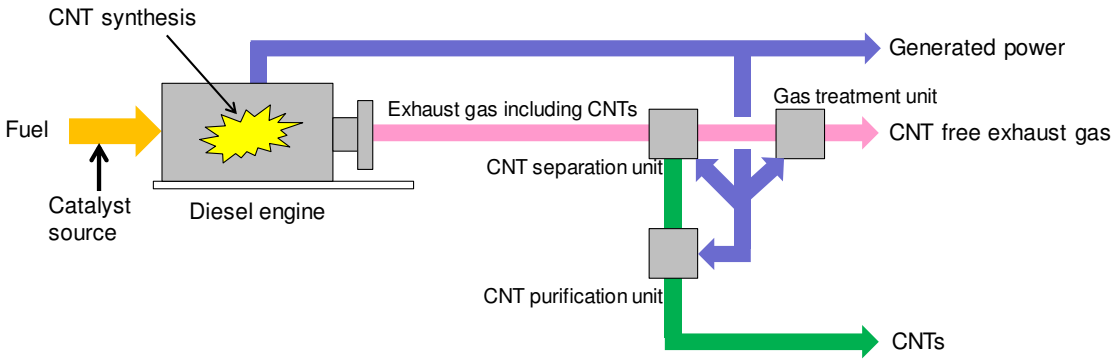

Figure 1- 8 Schematic of our concept to produce CNTs using a diesel engine.

Table 1- 1 Comparison of fuel injection manner between conventional system and common rail system.

System	Conventional system	Common rail system
Control	Mechanical control	Electrical control
Sketch of fuel injection manner		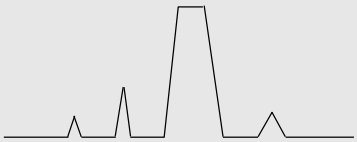
Controllable factors	• Injection timing • Injection duration	• Injection timing • Injection duration • Injection number • Injection amount

Table 1- 2 Summary of CNT production methods and its characteristics.

Method	Advantage	Disadvantage
Arc discharge	・Production○ ・Variety○	・Purity× ・Controllability△
Laser ablation	・Yield○ ・Purity◎	・Production× ・Price×
CVD	・Production◎ ・Scale-up◎	・Price△ ・Controllability△
Flame	・Scale-up◎ ・Production◎	・Know-how△ ・Controllability△

Chapter 2. CNT Synthesis Using Gas Oil as Fuel

2-1 Background of this chapter

Firstly, we employed gas oil (i.e. diesel fuel) as main fuel for operating an engine. Gas oil is one of the petroleum products produced through atmospheric distillation of crude oil and has a boiling point ranging from 180 to 350 ^{o}C, and consists of hydrocarbons whose carbon number ranges from 10 to 26. In Japan, Gas oil is manly utilized as fuel for an operation of a diesel engine in automobiles and generators. Besides gas oil, alcohol fuel such as ethanol and butanol was mixed with it since CNTs were unable to be synthesized by using gas oil alone. Alcohol fuel has received much attention recently because it can be produced from biomass processes and are expected to be used as a clean alternative fuel source for conventional fossil fuel. Practically, ethanol is mainly used as additives to gasoline for increasing octane number in many countries such as USA, Brazil, India, and others. Although ethanol has ever been utilized for spark-ignition engines for academic and practical purpose, attempts to apply it to a diesel engine have been launched recently because a low percentage mixing of ethanol with diesel fuel does not require any modification in a conventional diesel system. Actually, according to other works, an ethanol fraction in mixing fuel up to several tens of volume percentage could be allowed and an operation stability was not affected even in the use of gas oil/alcohol mixing fuel [61,62]. Furthermore, ethanol has been used as a feedstock for CNT growth in CVD methods and high-purity SWNTs were successfully synthesized [63,64,65,66]. Even in the flame process using a burner, CNTs were synthesized as well by supplying ethanol as feed gas [67]. These facts offer that ethanol becomes a strong candidate as a carbon source in our system. Moreover, ferrocene was added into mixing fuel as a catalyst source because catalyst sources were necessary for the formation of CNTs in a diesel engine [68,69]. Ferrocene is decomposed during combustion to release Fe atom, and then generated iron atoms collide with each other to form Fe nanoparticles which are expected to serve as a catalyst for the growth of CNTs. In this work, sulfur and molybdenum were also added as a promoter. According to some reports, sulfur is quite effective for the synthesis of carbon nanomaterials like carbon fibers [70,71] and CNTs [72,73] in a CVD process. Likewise, Mo promoted CNT production in floating catalyst CVD [74]. The purpose of this chapter is to investigate experimental conditions that can produce CNT in a diesel engine employing gas oil/ethanol as starting fuel.

2-2 Experimental methods

The diesel engine used in this study was a direct injection, 4-stroke cycle engine (KIPOR KDE.2.0E). We employed a diesel engine with mechanical control in a fuel injection system instead of that with electrical control. Main specifications of this engine are shown in Table 2-1. In this study, gas oil/ethanol mixing fuel was used instead of gas oil only because formation of CNT was observed only when mixing fuel was used. An ethanol fraction in fuel was changed from 0 to 40 volume% of total mixing fuel. Gas oil/ethanol mixing fuel was prepared by mixing gas oil (Idemitsu Kosan Co., Ltd.,

JIS No.1) and ethanol (99.5+%, Wako Pure Chemical Industries, Ltd.) without any purification treatment before mixing. In order to prevent a phase separation, 4 volume % of 1-octanol (98.0+%, Wako Pure Chemical Industries, Ltd.) was added. This mixing fuel was used as a carbon source for CNT formation and a heat source. As a catalyst source, 10,000 ppm by mass of ferrocene (98.0+%, Wako Pure Chemical Industries, Ltd.) was dissolved in gas oil/ethanol mixing fuel. This amount was equivalent to ca. 3,000 ppm iron by mass. Molybdenum acetate dimer (98%, Sigma-Aldrich) was dissolved in mixing fuel so that an atomic ratio of Mo/Fe to be 0.01. Sulfur powder (97.0+%, Wako Pure Chemical Industries, Ltd.) was dissolved into fuel so that an atomic ratio of S/Fe to be 0-3.85. Since dissolution of sulfur in fuel was limited, S/Fe of 3.85 was nearly the upper limit in this research when ferrocene amount was 10,000 ppm by weight, and sulfur content in this condition was corresponding to about 7,000 ppm by weight. When sulfur was added more than this amount, undissolved sulfur could be confirmed. A fuel flow rate to an engine was controlled by an electronic governor actuator in order to keep a constant engine rotation number of approximately 3,000 rpm. An engine load was adjusted by varying the power of an external heater which was connected to an alternator coupled to the engine. The power of an external heater ranged from 0 kW to 1.05 kW in this chapter. For sampling, a part of an exhaust was introduced into a sampling gas line using a vacuum pump and a mass flow controller to collect particles and CNT from an exhaust on a membrane filter with mean pore size of 200 nm and filter diameter of 25 mm (ADVANTEC, K020A052A) or TEM grid (Okenshoji Co.). Sampling was started after an engine operation became stable. The flow rate to a sampling holder was fixed to be about 350 sccm by a mass flow controller and sampling duration time was 20 seconds through all measurements. Exhaust gas temperatures were measured by a thermocouple (Type K, sheath diameter of 1.0mm), which was located right behind the muffler. A schematic diagram of an experimental setup and a sampling system is shown in Figure 2-1. Produced CNTs were evaluated by means of field emission scanning electron microscopy (FE-SEM, JEOL JSM-7500F) and transmission electron microscopy (TEM, HITACHI H-7650 Zero. A). For SEM analysis, samples were coated with a layer of Pt-Pd by ion sputtering (HITACHI E-1030, estimated thickness: 2-3 nm). Energy dispersive X-ray (EDX) analysis was conducted by high-resolution transmission electron microscopy (JEOL JEM-2010F) in order to elucidate chemical compositions of emitted particles.

2-3 Results and discussions

In this work, CNT formation could not be observed in any cases in the absence of ferrocene in fuel. This trend is consistent with the study by Jung et al. [68] although iron loading is different with each other. Therefore, in the following paragraph, we pick up results under the condition of ferrocene presence only.

2-3-1 Effect of an ethanol fraction in fuel

Figure 2-2 shows SEM and TEM images of carbon products collected on a sampling holder when the ethanol fraction in mixing fuel was varied from 20 volume% to 40 volume%. It should be noted that almost no CNT was synthesized at an ethanol fraction lower than 20 volume% and a diesel engine could not be operated at an ethanol fraction higher than 40 volume%. For these measurements, an atomic ratio S/Fe of 2.75 was employed. Formed CNTs are indicated by arrows in SEM micrograph. Exhaust gas temperature in an ethanol fraction of 20 volume%, 30 volume%, and 40 volume% was 232, 301, and 336 ºC, respectively. It is clear from SEM images in Figures 2-2 (a)–(c) that CNT production was increased sharply when an ethanol fraction in fuel reaches to 30 and 40 volume%. According to preceding investigations, suppression of soot emissions could be confirmed by using gas oil/alcohol blended fuel in experiments [61] and in computational simulations [62] in comparison with the use of gas oil only. A tendency to inhibit soot may be desirable for CNT formation because catalysts deactivation by carbonaceous materials which hinder CNT growth is avoided. Figure 2-3 is a TEM image under the same experimental condition with Figure 2-2 (c) but shows the agglomerate. This agglomerate consists of soot and iron particles which show a darker color than soot and are incorporated in soot. It is known in the CNT growth study that catalyst particles lose their catalytic activity when they are encapsulated by carbonaceous materials like soot, so a similar situation may occur in our experiments. Some iron particles that can avoid catalyst deactivation may contribute to CNT growth. What is important in Figure 2-2 is that a high ethanol fraction in fuel may bring about the environment proper for CNT formation. EDX analysis was carried out for the points that are indicated in Figure 2-3 (a), and the results are shown in Figures 2-3 (b) and (c). Because Figure 2-3 (b) is for a carbonaceous-rich point, the dominant element was carbon but small amounts of O, Fe, Si, and S could be detected. On the other hand, an increased Fe peak intensity could be exhibited in Figure 2-3 (c), since the iron particle coated by carbonaceous material was examined. Besides Fe, peaks attributed to C, O, Si, and S were detected. Detection of C, O, S, and Fe is reasonable because these elements are included in feedstock and/or feed gas to a diesel engine, while Si is not contained in such a feed material. It may be probable that Si may be derived from lubricant oil. Other peaks that are not labeled in Figures 2-3 (b) and (c) stem from Cu, which is used as the framework of TEM grid. CNTs observed in this work have a diameter of about 10–25 nm (average diameter: 18.9 nm, maximum diameter: 25.0 nm, minimum diameter: 11.5 nm) and a length of more than several hundreds of nanometers, sometimes more than 1 μm. Based on the estimation using several SEM images, the average, maximum, and minimum lengths were 630, 1170, and 240 nm, respectively. The total analyzed number of CNT for an evaluation of average diameter and length was 25. Histogram of CNT outer diameter and CNT length is presented in Figure 2-4. Due to its large diameter, it can be deduced that synthesized CNTs were MWNT. Synthesized CNT diameters in this work are very similar to those

synthesized in other diesel engine systems [68,69]. On the other hand, CNT length is relatively longer than that in preceding researches. Here, let us consider the suitability of CNT length synthesized by a diesel engine for some applications. Required CNT length strongly depends on applications, and it ranges from several hundreds of nanometers to several hundreds of micrometers. Based on the average CNT length in a diesel engine (about 600 nm) and the assumption that CNT growth rate is independent on an engine rotation speed, average CNT length can reach from 360 nm to 3.6 μm if an engine rotation speed can arbitrarily be altered from 500 rpm to 5,000 rpm (currently 3,000 rpm). This means that CNTs synthesized via a diesel engine are limited to a part of applications such as secondary lithium battery, catalyst support, and others. Based on a rough estimation using SEM photographs, the CNT productivity and yield in this work were 9.3×10^{-3} g/hr and 9 ppm by injected fuel weight, respectively, on the assumption that CNT-like material mass density was 1.35 g/cm^3. Furthermore, we investigated the number fraction of CNT based on TEM images, and it was calculated to be approximately 3% at most. We suppose in this estimation that agglomerates were regarded as one particle. Thus, actual number fraction of CNT in an exhaust gas might be smaller than this estimated value. For this analysis, total 390 particles were analyzed.

2-3-2 Effect of sulfur amount

The impact of sulfur on CNT formation was investigated by varying an atomic ratio S/Fe from 0 to 3.85. For these measurements, a mixture of 80 volume% of gas oil and 20 volume% of ethanol was employed. TEM images are shown in Figure 2-5 (a) as a function of an atomic ratio S/Fe in mixing fuel. Exhaust gas temperature when the S/Fe ratio was 0, 0.11, 0.55, 2.75, and 3.85 was 373, 384, 304, 232, and 219 ℃, respectively. Figure 2-5 (a) indicates that no CNT is observed and agglomerate instead of CNT is collected on a sampling holder when the S/Fe ratio is 0 and 0.11. However, CNT formation in addition to agglomerate is observed when the S/Fe ratio is equal to or higher than 0.55. It should be noted that TEM image at S/Fe of 0.55 shows that CNT-like material is put on the collodion film, which is a part of the TEM grid. Figure 2-5 (b) is an SEM photograph when the S/Fe ratio is 0 and shows agglomerates composed of a number of particles without CNT. Analogously to Figure 2-3, these agglomerates may be constructed by carbonaceous material like soot and iron particles. Moreover, SEM micrograph at S/Fe = 0.55 in mixing fuel is also displayed in Figure 2-5 (c) for reference, where CNT formation was observed as indicated by an arrow. This experimental result suggests that the presence of sulfur may be one of key factors for success in CNT synthesis, and this tendency is coincident with the study by Swanson et al [69]. Effects of sulfur addition on promoted CNT formation were seen in CNT or carbon fibers synthesis through CVD processes, like lowered adhesion energy between Fe and C [73], the prevention of catalyst deactivation by carbonaceous materials [70], and/or the reduction of catalyst melting temperature [71]. The real role of sulfur on CNT growth is controversial even today, but we tried to elucidate effects of sulfur on CNT synthesis

in later chapter.

The summary table which shows our experimental trials and its outcomes is presented in Table 2-2, where experimental conditions leading to CNT formation and/or no CNT formation are summarized. It is apparent that mixing of ethanol and the addition of sulfur which both exceeded a certain value were essential in growing CNTs successfully. The trend in Table 2-2 may be versatile even in the employment of other engine load, such as 1.65 kW.

Here, let us shortly discuss CNT growth mechanism in a diesel engine. Promising CNT precursors such as acetylene, ethylene and carbon monoxide may be produced during combustion as a result of pyrolysis of fuel, especially in fuel rich regions. At the same time, iron particles used for CNT growth catalysts can be formed through decomposition of ferrocene. Hence, the potential mechanism for CNT formation in a diesel engine is that CNT precursors and iron particles produced during combustion meet with each other, and then CNTs grow like CVD processes. Of course, some iron particles are oxidized, while the other maintain a metallic state, leading to catalytically growing CNTs. In-depth discussions on CNT growth mechanism are carried out in Chapter 5.

2-4 Summary of this chapter

In this chapter, we investigated preferable conditions for CNT growth during internal combustion in a diesel engine by employing gas oil/ethanol mixing fuel with ferrocene as catalyst precursors and sulfur/molybdenum as a promoter. Remarkable points were acquired as follows.

- Following three conditions have to be satisfied at the same time for the successful synthesis of CNTs: high ethanol fraction in mixing fuel, high sulfur loading, and the presence of catalyst sources in fuel. If at least one of these three conditions was not satisfied, almost no CNT could be observed in an exhaust gas.

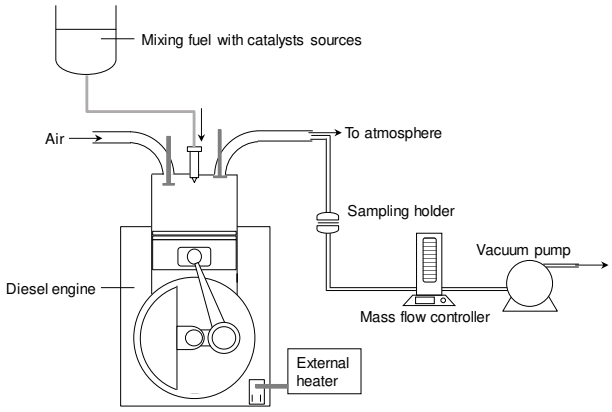

Figure 2- 1 Schematic diagram of an experimental setup and a sampling system

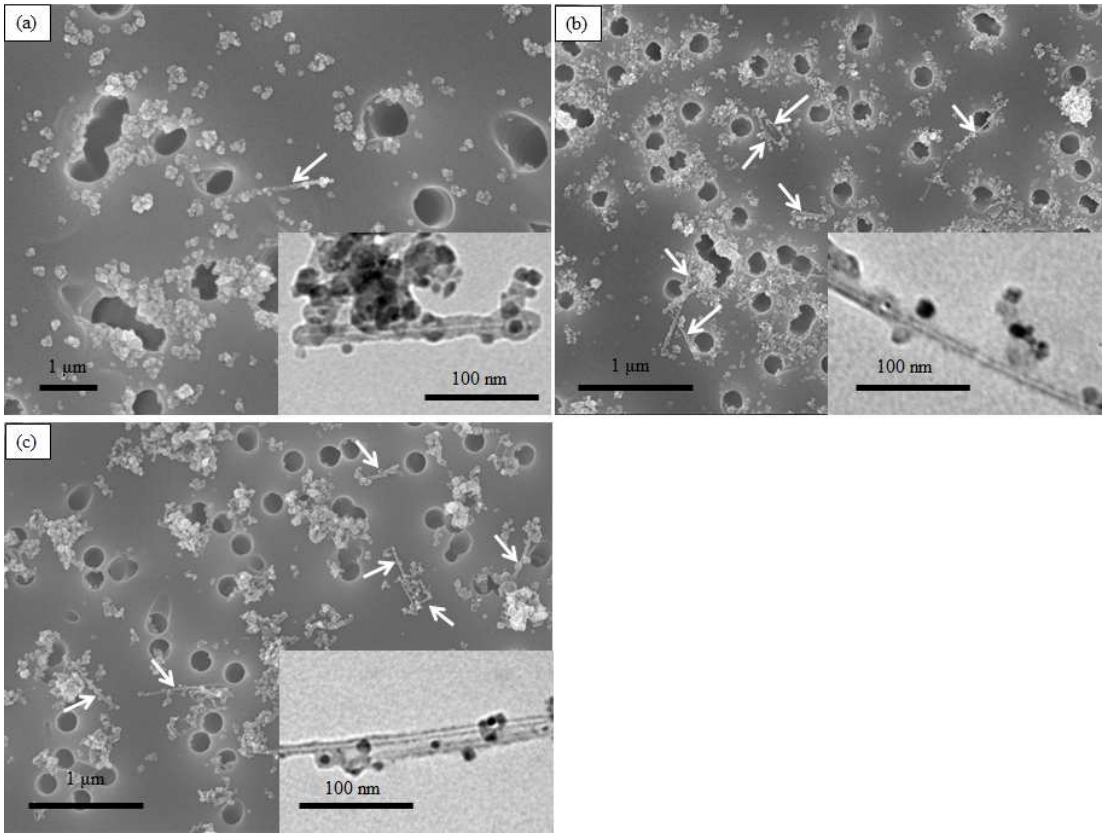

Figure 2- 2 SEM and TEM images (inserted) of carbon materials collected on a sampling holder. (a) Mixture of 80 volume% gas oil and 20 volume% ethanol. (b) Mixture of 70 volume% gas oil and 30 volume% ethanol. (c) Mixture of 60 volume% gas oil and 40 volume% ethanol. Synthesized CNTs are indicated by arrows in SEM images in (a), (b), and (c). An atomic ratio of S/Fe in mixing fuel was 2.75.

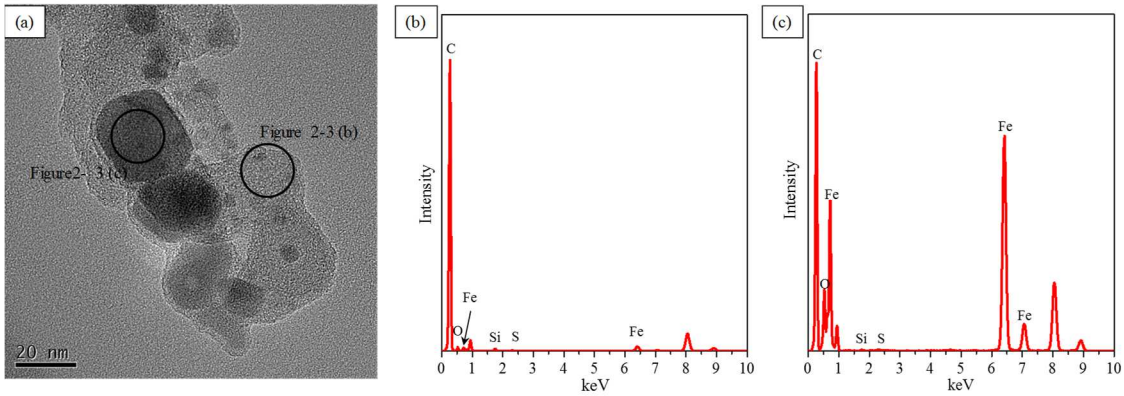

Figure 2- 3 (a) High-resolution TEM image showing the aggregation consisting of soot and iron particles in the absence of CNT in the case of a mixture of 60 volume% gas oil and 40 volume% ethanol. (b, c) EDX analysis results pointed out in (a).

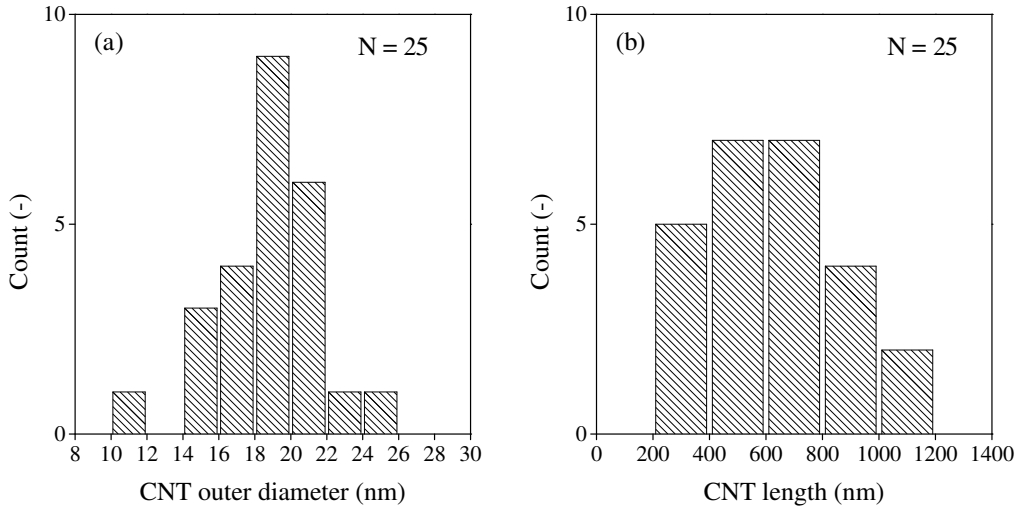

Figure 2- 4 Histogram of (a) CNT outer diameter and (b) CNT length when gas oil/ethanol mixing fuel was used.

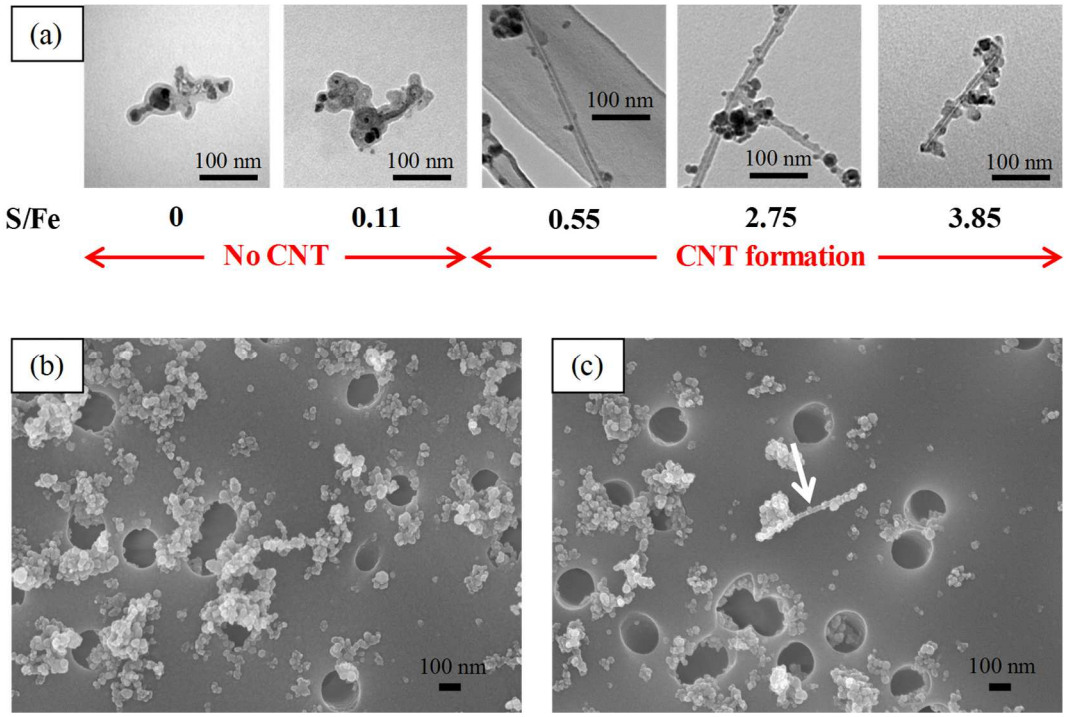

Figure 2- 5 (a) TEM images of synthesized carbon materials when the S/Fe ratio was varied from 0 to 3.85. SEM images (b) without sulfur (S/Fe = 0) and (c) with sulfur (S/Fe = 0.55) as a reference. Fuel condition was gas oil (80 volume%)/ethanol (20 volume%).

Table 2- 1 Specifications of the diesel engine used in this work.

Model	KIPOR KDE.2.0E
Number of cylinder	1
Fuel injection	Direct injection
Number of stroke	4
Diameter (mm) × stroke (mm)	70 × 55
Cylinder volume (cm^3)	211
Compression ratio	20
Rated power	2.5 kW at 3,000rpm

Table 2- 2 Summary of experimental results performed in this chapter.

S/Fe in mixing fuel (-)	Ethanol volume percent (%)				
	0	5	20	30	40
0	×	-	×	-	-
0.11	-	-	×	-	-
0.55	×	×	○	○	○
2.75	-	-	○	○	○
3.85	-	-	○	-	-

×: No CNT formation
○: CNT formation
- : No measurement

Chapter 3. CNT Synthesis Using n-Dodecane as Fuel

3-1 Background of this chapter

In Chapter 2, it was revealed that MWNTs could be synthesized when both of a sulfur addition and a high ethanol fraction in fuel were satisfied. However, detailed analysis has not been done in gas oil system. An evaluation such as combustion temperature was quite difficult in gas oil because it has complicated compositions due to inclusion of a lot of substances like normal alkanes, branched alkanes, cycloalkanes, alkenes, and aromatics. This complicated composition makes it difficult to estimate a combustion temperature in a chamber from enthalpy balance and to discuss the reaction mechanism. Since fixed fuel composition is favorable for estimating a combustion temperature, normal dodecane (n-dodecane) is employed as main fuel in this chapter instead of gas oil.

N-dodecane has been used as a model fuel of commercial transport fuel such as jet fuel and diesel in order to mimic physical and chemical properties of real fuel. The oxidation reaction pathway of n-dodecane has been explored widely and elucidated that n-dodecane is a potential candidate to represent the paraffin class in transportation fuel [75,76,77,78]. Also, ethanol is utilized as fuel in this study besides n-dodecane because preferable outcomes were brought about in Chapter 2. Thus, n-dodecane/ethanol mixing fuel is employed as heat and carbon sources for CNT growth in this chapter.

One of main purposes in this chapter is to determine the mean adiabatic combustion temperature in a chamber of a diesel engine when an ethanol fraction in fuel and an engine load are varied as experimental parameters. For the evaluation of a mean adiabatic combustion temperature, the mass balance of oxygen between the inlet and outlet of an engine is carried out by analyzing the composition in an exhaust gas through gas chromatography. Then, a mean adiabatic combustion temperature is calculated using the enthalpy difference between the inlet gas and outlet gas, and details are expressed in an experimental section. After an estimation of a mean adiabatic combustion temperature, the correlation between experimental conditions showing CNT formation and combustion properties such as a mean adiabatic combustion temperature and exhaust gas composition is described.

3-2 Experimental methods

The diesel engine used in this chapter is the same with the one in Chapter 2. N-dodecane/ethanol mixing fuel was prepared by mixing n-dodecane (99.0+%, Wako Pure Chemical Industries, Ltd.) and super dehydrated ethanol (99.5+%, Wako Pure Chemical Industries, Ltd.). An ethanol fraction in mixing fuel was altered from 0 volume% to 50 volume%. In order to prevent a phase separation, 4 volume% of 1-octanol (98.0+%, Wako Pure Chemical Industries, Ltd.) was added into mixing fuel. As a catalyst source, 200 ppm, 1,000 ppm and 5,000 ppm by mass of ferrocene (98.0+%, Wako Pure Chemical Industries, Ltd.) were dissolved in n-dodecane/ethanol mixing fuel. It should be noted that the upper limit of ferrocene solubility in mixing fuel restricted us to dissolve ferrocene higher than 5,000 ppm by weight in this study. Additionally, molybdenum acetate dimer (98%, Sigma-Aldrich)

and sulfur powder (97.0+%, Wako Pure Chemical Industries, Ltd.) which played a promoter for CNT synthesis were dissolved into fuel so that an atomic ratio of Mo/Fe and S/Fe to be 0.01 and 2.2, respectively. When ferrocene concentration was reduced to 200 ppm or 1,000 ppm, the contents of molybdenum and sulfur in mixing fuel were identical with Mo/Fe = 0.01, S/Fe = 2.2, respectively, on the basis of 5,000 ppm as ferrocene concentration. An engine load was provided by an external heater and its load was varied from 0 to 1.65 kW. A summary of experimental conditions in this research appears in Table 3-1. Sampling duration and sampling method of carbon materials are identical with those in Chapter 2. Gas chromatograph (Shimadzu Ltd., GC-8A) with a gas sampling system was used to detect the composition of an exhaust gas. SHINCARBON ST (Shimadzu Ltd.) was installed in gas chromatograph as a packed column to separate O_2, CO and CO_2. These species eluting from a column were sensed by a thermal conductivity detector (TCD) using He as a carrier gas. Overall diagram of experimental setup is shown in Figure 3-1. Absolute mole amount of O_2, CO and CO_2 in an exhaust gas was estimated by carrying out the mass balance of oxygen between the inlet and outlet of an engine. For implementing mass balance calculation, it was assumed that inlet air was atmospheric ideal gas at a temperature of 15 ^oC and an intake air volume per one engine cycle was equal to a cylinder volume. Moreover, a hypothesis was also provided that oxidized products from mixing fuel were only CO, CO_2 and H_2O, and the formation of aldehyde like acetaldehyde or formaldehyde or other low molecular weight hydrocarbons was ignored. The mixing fuel amounts which were oxidized through combustion could be calculated using the mole amount of CO and CO_2 at an outlet. An intake fuel amounts per one engine cycle were estimated by measuring fuel consumption rate and revolutions per minute in each experiment. Then, the conversion of mixing fuel and the yield of CO and CO_2 from intake mixing fuel were calculated. Conversions for three different fuel components, normal dodecane, ethanol and 1-octanol, were considered to be equal. After gas compositions of an inlet and outlet of an engine were determined, the enthalpy difference between an inlet and outlet could be obtained. A mean adiabatic combustion temperature inside a cylinder could be estimated by satisfying the above enthalpy difference. For calculating a mean adiabatic combustion temperature, some additional assumptions were provided as follows. Firstly, a gas composition inside an engine chamber was uniform. As a second one, other reactions such as nitrogen oxidation or thermal dissociation of steam did not take place during combustion. Actual combustion temperature would be lower than the above estimated temperature due to heat release from a combustion chamber wall to an atmosphere. However, it is quite helpful to utilize the above estimated adiabatic temperature for evaluating CNT growth inside a diesel engine. Several cautions should be taken care of when mean adiabatic combustion temperatures estimated through above procedure are used for discussions. Mean adiabatic combustion temperature in our method may be unable to eliminate inaccuracy because combustion region and non-combustion region are not separated. Since combustion temperature inside sprayed fuel generally gets up to about 2,000 K, large differences of combustion temperature between in our approach and in sprayed fuel

may be generated. Hence, there is the possibility that we underestimate the importance of the contribution by combustion temperature to CNT growth. When the pressure behavior inside a cylinder is measured during an engine operation, it is possible to evaluate the local flame temperature through the method using the two-region model which consists of burned gas region and unburned air region [79]. These advanced quantitative approach shall be carried out in future by tracking the pressure behavior inside a cylinder. Produced CNTs and other carbon materials were evaluated by means of field emission scanning electron microscopy (FE-SEM, JEOL JSM-7500F) and transmission electron microscopy (TEM, HITACHI H-7650 Zero. A). Energy dispersive X-ray (EDX) analysis was carried out to study catalyst particles in detail through scanning transmission electron microscopy (HITACHI SU9000) equipped with EDX detector. For EDX analysis, the same TEM grid sample used in TEM observations was employed. Raman spectra (JASCO NRS-4100, 532 nm diode laser) of a sample was obtained without any purification treatment of a sample. In order to avoid the detection of information originated from a sampling filter itself, Pt-Pd sputtering was performed on a sampling filter before collecting carbon materials. We confirmed that sputtering suppressed our concern and did not disrupt signals stemmed from carbon structures emitted from an engine.

3-3 Results and discussions

3-3-1 Observation results

The impact of ferrocene content on CNT formation was examined by varying it from 200 ppm to 5,000 ppm by weight. Besides SEM and TEM micrographs, the histogram of CNT outer diameters was prepared as well in Figure 3-2. For these measurements, mixing fuel of n-dodecane (55 volume%)/ethanol (45 volume%) including Mo and S at 1.65 kW as an engine load was employed. When ferrocene concentration becomes low (200 ppm), no CNT formation was observed. In place of CNT, particulate matters which primarily consisted of soot and iron-based particles were found. With the increase of ferrocene content in mixing fuel (1,000 ppm and 5,000 ppm), CNTs were started to be formed as indicated by arrows in SEM images, and larger CNT production was obtained at 5,000 ppm. However, histogram at 1,000 ppm showed that thinner CNT diameter, namely the improved distribution of CNT outer diameter, was gained in comparison with 5,000 ppm. Since we put weight on CNT production rather than the uniformity of CNT diameter, ferrocene amounts of 5,000 ppm were employed in later experiments.

Figure 3-3 shows typical SEM and TEM images when an ethanol fraction was varied. An ethanol fraction in mixing fuel in Figure 3-3 (a), (b) and (c) was 20, 40 and 50 volume%, respectively. For these measurements, an engine load was fixed to be 1.05 kW. Growth CNTs are indicated by arrows in SEM pictures. At an ethanol fraction of 20 volume%, a lot of aggregation which consists of small catalyst particles or soot could be observed instead of CNT observation. When an ethanol fraction in

fuel reached 40 volume%, the formation of CNT started to be observed but produced CNT number was still small. When an ethanol fraction in fuel was further enlarged up to 50 volume%, produced CNT number was further incremented. The dependence of CNT synthesis on an ethanol fraction in fuel is similar with that found in gas oil system. Produced CNT had a diameter ranging from several nanometers to less than twenty nanometers. Wall thickness can be calculated from the difference between an outer diameter and an inner diameter of tubes by means of TEM images, and the result shows it has more than one nanometer which is larger than ideal graphene interlayer distance (0.335 nm). This supports the idea that synthesized CNT in this study is MWNT.

Figure 3-4 shows typical SEM and TEM images when an engine load was varied while an ethanol fraction was kept at 45 volume%. An engine load in Figure 3-4 (a), (b) and (c) was 0 kW, 1.05 kW and 1.65 kW, respectively. CNTs could be observed on a sample filter in all conditions. A diameter of synthesized CNTs reached several nanometers, thus CNT type was considered as MWNT. Produced MWNT number was increased with growing an engine load. Based on the SEM image of Figure 3-4 (c), the CNT productivity and yield in this study were estimated to be 2.2×10^{-3} g/h and 3 ppm by injected carbon weight, respectively, on the assumption that CNT mass density was 1.35 g/cm^3. The mass-basis yield of CNT using n-dodecane is smaller than that in gas oil because thicker CNTs were synthesized in a gas oil system although the number of grown CNTs is identical with each other. The CNT selectivity for impurities like soot or catalyst particles was also estimated to be 6% on the basis of occupied domain.

Raman spectrum with n-dodecane (55 volume%)/ethanol (45 volume%) at 1.05 kW is displayed in Figure 3-5 (a). This condition showed CNT synthesis. As a reference, Raman spectrum under the condition which showed no CNT growth is also presented, Figure 3-5 (b). Figure 3-5 (a) indicates sharp G peak and relatively weak D peak which are stemmed from an ordered graphite structure with six membered ring and a disordered/defective graphite structure, respectively. The intensity ratio of G peak and D peak which is frequently utilized as a criterion for evaluating the crystallinity of graphite structure is approximately 5. On the other hand, the shape of Raman spectrum in Figure 3-5 (b) resembles that stemmed from typical soot emitted from a diesel engine in preceding articles [80,81]. Hence, it is probable that sharp and strong G peak against D peak in Figure 3-5 (a) is attributed to the presence of CNTs.

In order to gain information on iron particles, EDX analysis was carried out as shown in Figure 3-6. Analyzed sample was the one that an ethanol fraction was 45 volume% and an engine load was 1.65 kW. Iron catalyst particle which seems to contribute to CNT synthesis is marked by an arrow. According to this elemental mapping, CNT is grown from a metallic iron nanoparticle not from oxidized ones in spite of oxidized atmosphere during combustion because catalyst particle encapsulated by carbon layers did not include oxygen. Figure 3-6 also shows that sulfur seemed to be concentrated on the iron particle which grew CNT rather than the ones which did not grow CNT. Also,

as an interesting tendency, the region which reflects strong O intensity does not overlap that of sulfur intensity. This fact implies that sulfur played a crucial role in CNT synthesis in our system as indicated in Chapter 2.

3-3-2 Gas compositions in an exhaust and mean adiabatic combustion temperature

Figure 3-7 (a) and (b) show variations of the mole amount of CO and CO_2 per one engine cycle which were detected at the engine outlet, respectively, when an ethanol fraction in fuel and an engine load were altered. It can be seen from Figure 3-7 (a) that no or almost no CO was detected at an ethanol fraction below 20 volume%, but it gradually increased with growing an ethanol fraction. This tendency that larger amounts of CO are emitted at a high ethanol concentration in fuel can be acceptable taking into consideration several reports by other researches. As Curran et al. pointed out, C-O bond in the oxygenated compounds is very strong and prone to remain connected during combustion [82]. According to the low temperature (800 K) oxidation of ethanol proposed by Mittal et al., a path to form CO via the formation of acetaldehyde or formaldehyde is one of the major reaction routes [83]. Meanwhile, when CO amounts at the same ethanol fraction in fuel is compared, larger CO was obtained at a higher engine load as significantly indicated in an ethanol fraction of 45 volume%. It is well known that formation of CO is facilitated in the fuel rich regions due to incomplete combustion. Since injected quantity of fuel is increased along with increasing an engine load shown in Figure 3-7 (c), it is probable that a fuel rich region is extended, especially in the vicinity of the fuel injection nozzle. As a consequence, larger CO amounts might be produced when an engine load was increased. Since the rotation number per one minute is around 3,000 rpm almost irrespective of experimental conditions in our diesel engine, Figure 3-7 (c) provides the indirect information about fuel consumption rate per unit time. For instance, fuel injection rate of 1.37×10^{-2} (mL/1-cycle) is equal to 1.23 (L/h) when an ethanol fraction is 45 volume% and an engine load is 1.05 kW. The behavior of CO and CO_2 emission in an exhaust resembles each other, namely, they are enlarged with the increase of both an ethanol fraction in fuel and an engine load.

Mean adiabatic combustion temperatures in each experimental condition which were estimated by means of CO and CO_2 mole amounts in an exhaust gas are shown in Figure 3-7 (d). The behavior of a mean adiabatic combustion temperature resembles especially that of CO_2 in Figure 3-7 (b) through all the conducted experiments. The contribution of CO to a combustion temperature is minor in comparison with that of CO_2 because amounts of CO in an exhaust gas is one order smaller than those of CO_2 and reaction enthalpy to form CO from feedstock fuel is about 280 kJ/mol lower than that to form CO_2 under the standard condition. A combustion temperature is one of the most critical parameters for CNT growth. Actually, Figure 3-3 and Figure 3-4 tend to present a large fraction of CNT under an experimental condition with a high adiabatic combustion temperature.

As well as adiabatic combustion temperatures, other experimental results to determine an engine

performance were exhibited in Figure 3-8. These items were calculated based on gas compositions in an exhaust as a function of an engine load and an ethanol concentration in mixing fuel. Figure 3-8 (a) is the variation of thermal efficiency, where it is defined as the ratio of an engine load provided by an external heater to actually introduced heat calculated by lower heating value of mixing fuel. Thermal efficiency was reduced with the increase of an ethanol fraction, but it became improved when a higher engine load was provided. Figure 3-8 (b) shows the dependence of an average equivalence ratio on an ethanol content in fuel and an engine load. An equivalence ratio was estimated on the basis of measured fuel injection rate and intake air volume. The behavior of an equivalence ratio resembles that of CO_2 amount in an exhaust and adiabatic combustion temperature shown in Figure 3-7. Although all conditions were operated under fuel lean circumstance (smaller than 1.0) as a whole, an equivalence ratio increased when an engine load and an ethanol contents became large, meaning that local fuel rich regions were extended. Figure 3-8 (c) displays the variation of fuel conversion to CO and CO_2 which is calculated on the assumption that components included in mixing fuel possess the equal conversion. Fuel conversion is primarily enlarged at a high load, but it is less dependent on an ethanol fraction at the same engine load. It should be noted that actual fuel conversion has to be slightly higher than the ones presented in Figure 3-8 (c) because the conversion from fuel to soot or hydrocarbons other than CO and CO_2 was not taken into account.

3-3-3 Discussions

SEM and TEM analysis was carried out for all samples in order to evaluate the presence of CNTs on filter. According to its observations, each experimental condition was divided into two categories as follows. One is that no CNT could be observed and another is that CNT could be observed. The distinguishing line which separates the regions for CNT formation and no CNT formation is indicated in Figure 3-7. It is confirmed that the growth of CNT was found when an ethanol fraction in fuel was equal to or higher than 30 volume%. It is implied from these results that ethanol strongly affects CNT growth in a diesel engine directly or indirectly.

One of notable effects when an ethanol fraction became high was that mixing fuel injection rate into a chamber was increased (Figure 3-7 (c)), resulting in an increase of CO_2 emission in Figure 3-7 (b) and a higher adiabatic combustion temperature in Figure 3-7 (d). In particular, the latter is important. From the standpoint of the effect of a combustion temperature on CNT synthesis, there was a tendency to be rise in formed CNT number at a higher combustion temperature as seen in Figure 3-3 and Figure 3-4. According to preceding reports, a temperature corresponding to the region of massive CNT synthesis was 1,500–1,800 K [84] and 1,400–1,600 K [85] in flame process, and about 1,200 ^{o}C [86,87] in CVD process, which were close to the combustion temperature (1,150 ^{o}C) at an ethanol fraction of 50 volume% and an engine load of 1.05 kW in our study where a number of CNTs was grown. Another effect observed when an ethanol fraction became high was that CO emission in an

exhaust was increased as indicated in Figure 3-7 (a). According to some preceding papers, CO has been utilized as a feedstock [88,89,90] or one of the main precursors [85,91] for CNT formation. Hence, it may be reasonable to consider that a higher combustion temperature and/or larger CO amounts would be the essential reason for increasing CNT number when an ethanol fraction became large. In order to compare the significance of these two factors, Figure 3-9 was prepared, where the relationship between them is shown. The region of CNT formation and no CNT formation can be clearly distinguished by the vertical line which intersects the horizontal axis into two CO amount zones. On the other hand, such a distinguishing is impossible by the horizontal line which intersects vertical axis into two temperature zones. It seems to be obvious in this figure that CNT synthesis in a diesel engine is allowed when CO emission in an exhaust surpasses a certain value. These results suggest that whether CNT growth can be achieved in a diesel engine or not is strongly governed by CO amounts produced during combustion in an engine, and a mean adiabatic combustion temperature has less impact on CNT growth. Although CO is inferred to be a promising CNT precursor in our system, we recognize that other chemical species such as acetylene [92,93,94] and/or ethylene [95,96,97] may be able to synthesize CNTs according to some reports. Actually, we cannot rule out this possibility because oxidation reactions of n-dodecane [76,78] and ethanol [98,99] produce acetylene and ethylene during combustion. However, detailed discussions to compare the importance in CNT growth are carried out in a later chapter.

3-4 Summary of this chapter

In this chapter, we attempted to synthesize CNTs in a diesel engine by replacing gas oil with n-dodecane as main fuel in order to perform detailed analysis including the estimation of a mean adiabatic combustion temperature in a cylinder on the basis of oxygen mass balance and heat balance at an inlet/outlet of an engine. Remarkable points in this chapter were acquired as follows.

- Through SEM/TEM observations in each experimental condition, it was found that CNTs were prone to be synthesized when an ethanol content in mixing fuel and an engine load were enlarged. This may be because higher combustion temperatures and larger emissions of carbon monoxide were achieved.
- It was suggested via EDX analysis that the catalytic particle contributing to CNT growth was metallic state rather than oxidized one.
- It was implied that the formation of CNTs in a diesel engine was strongly correlated with CO emission rather than a combustion temperature because the distinguishing line separating CNT growth condition and no CNT growth condition could be drawn against CO amounts.

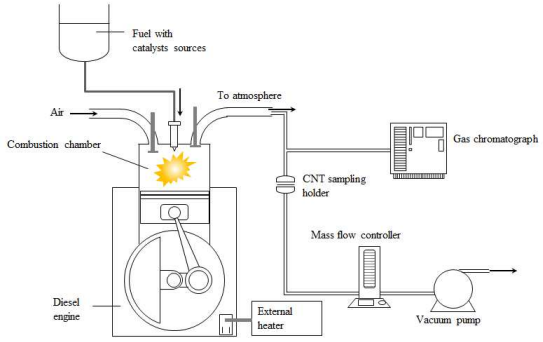

Figure 3- 1 Schematic diagram of an experimental setup. The same engine with that in Chapter 2 was employed. The sketch of gas chromatograph is added.

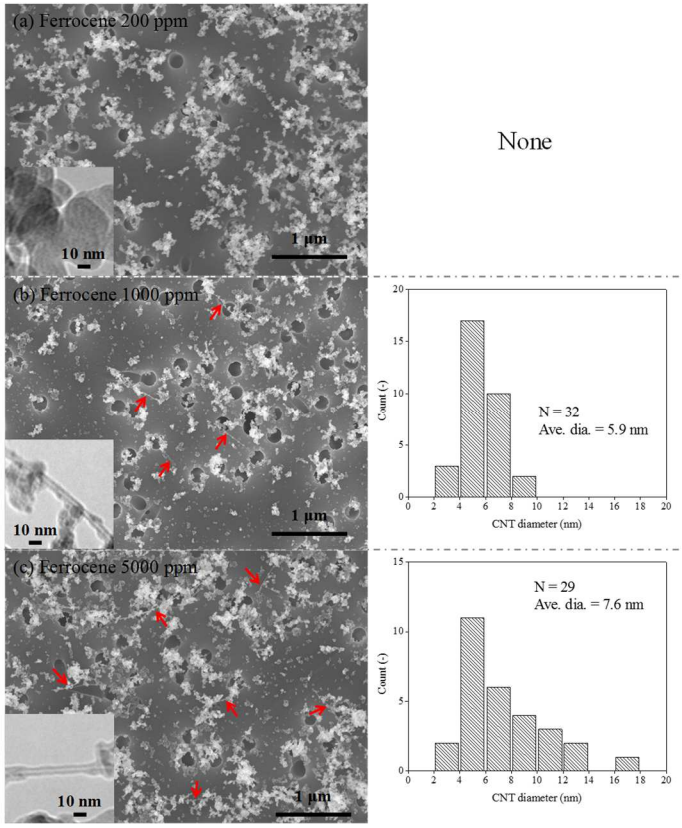

Figure 3- 2 SEM photograph and corresponding histogram of CNT outer diameter as a function of ferrocene concentration in mixing fuel. Ferrocene concentration is (a) 200 ppm, (b) 1,000 ppm and (c) 5,000 ppm by weight. TEM images are inserted in each SEM image for a reference. Mixing fuel of n-dodecane (55 volume%)/ethanol (45 volume%) including Mo and S at 1.65 kW as an engine load was employed.

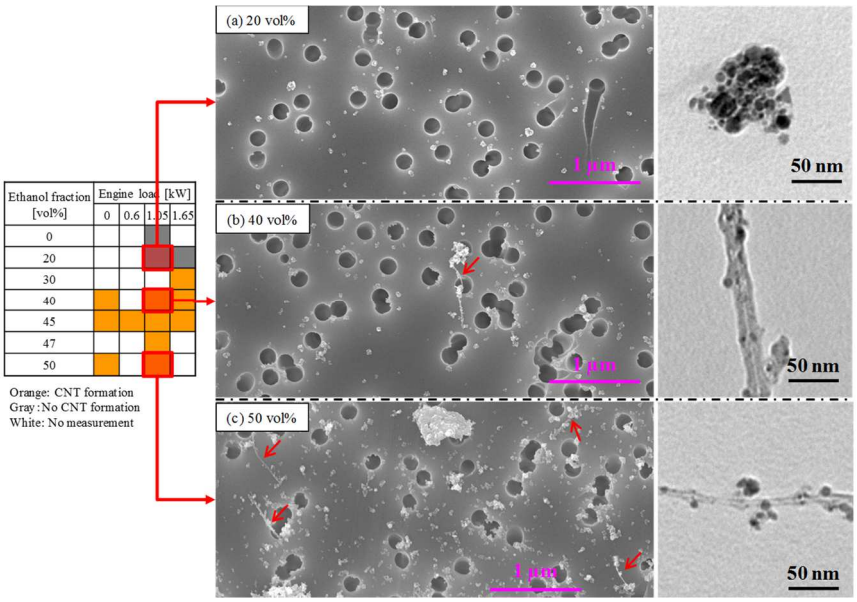

Figure 3- 3 Typical SEM and TEM images when an ethanol fraction in fuel was varied, (a) 20 volume%, (b) 40 volume% and (c) 50 volume%. An engine load was 1.05 kW for all samples. As a reference, mean adiabatic combustion temperature in (a), (b) and (c) was 520, 670 and 1,150 ^{o}C, respectively.

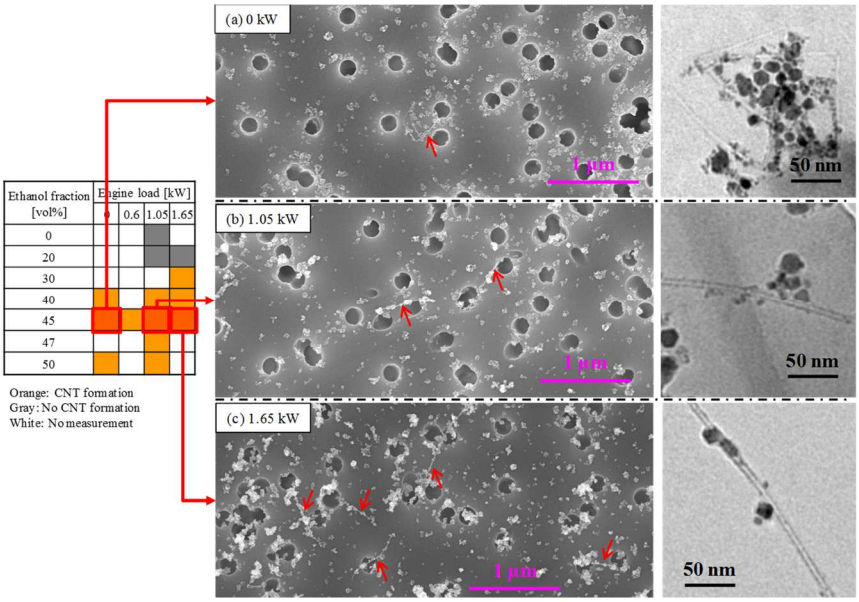

Figure 3- 4 Typical SEM and TEM images when an engine load was varied, (a) 0 kW, (b) 1.05 kW and (c) 1.65 kW. An ethanol fraction was 45 volume% for all samples. As a reference, mean adiabatic combustion temperature in (a), (b) and (c) was 460, 780 and 1,060 ^{o}C, respectively.

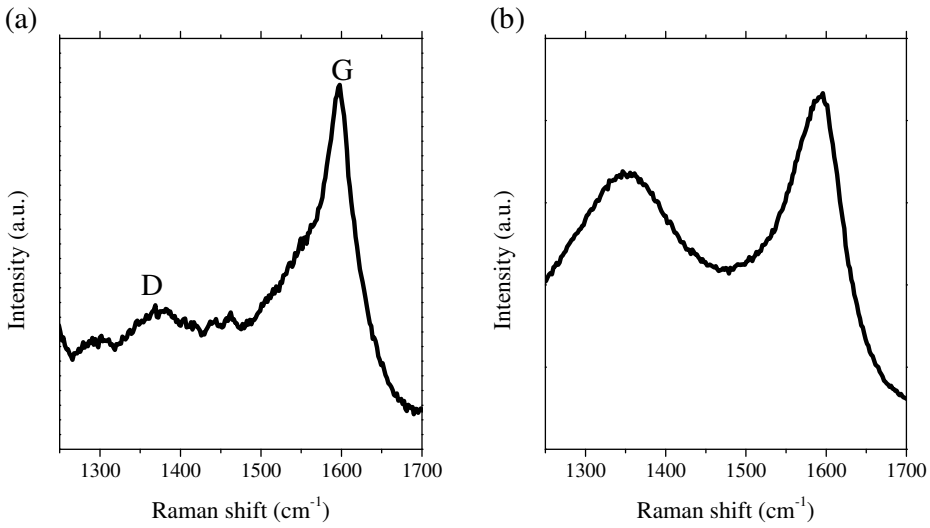

Figure 3- 5 Raman spectra under the condition which shows (a) CNT growth and (b) no CNT growth. (a) n-dodecane (55 volume%)/ethanol (45 volume%) at 1.05 kW using ferrocene 5,000 wt ppm and Mo/S (Mo/Fe = 0.01, S/Fe = 2.2). (b) gas oil 100 volume% at 1.05 kW without any additives.

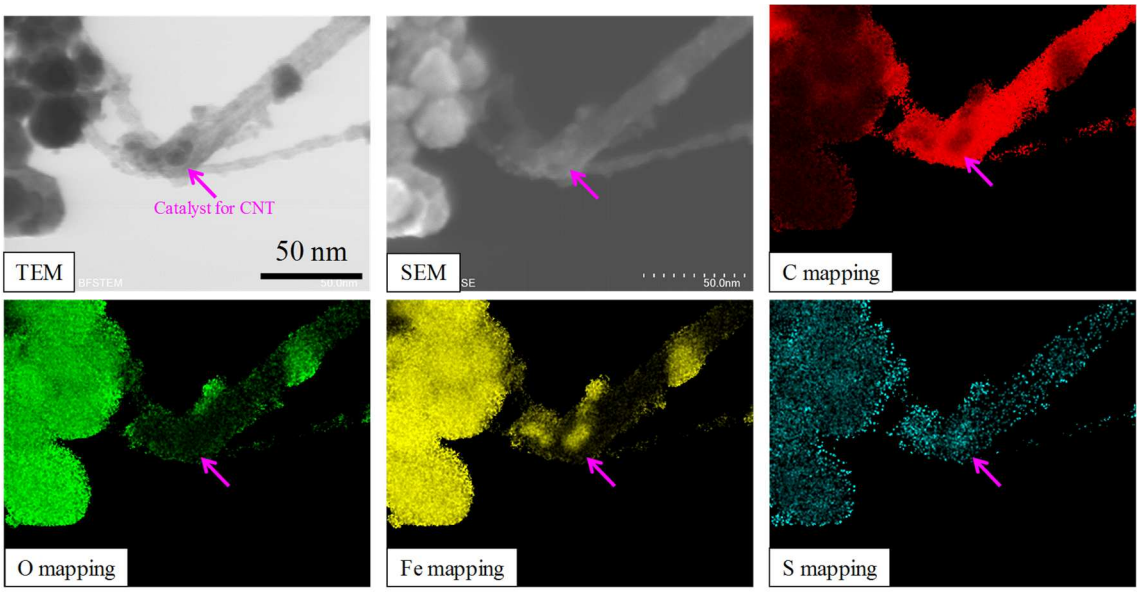

Figure 3- 6 EDX analysis for investigating the chemical state of catalyst particles under 45 volume% as an ethanol fraction and 1.65 kW as an engine load.

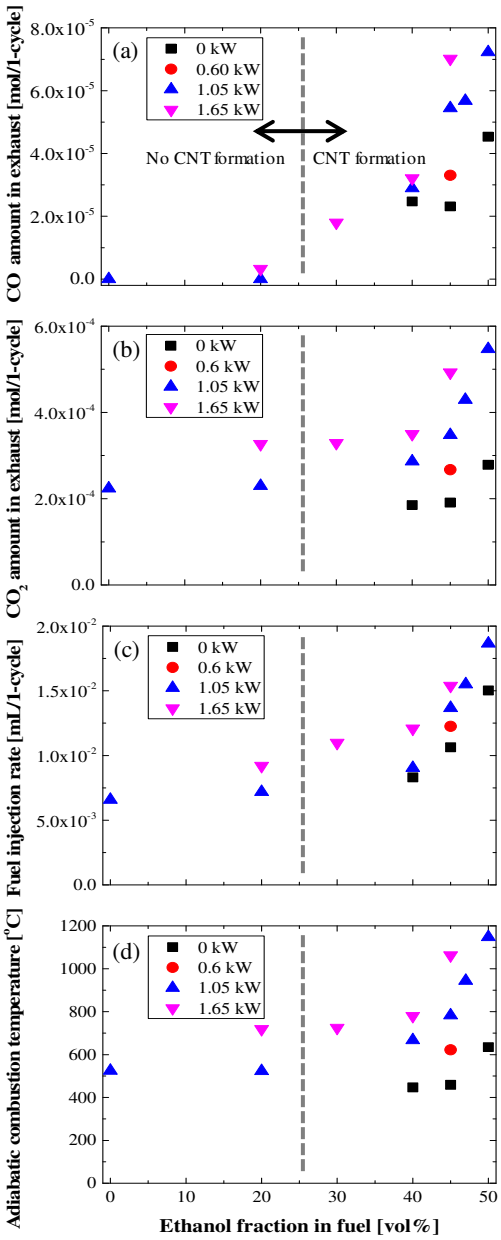

Figure 3- 7 Experimental results using gas chromatograph when an ethanol fraction in fuel and an engine load were varied. (a) CO mole amount in an exhaust gas, (b) CO_2 mole amount in an exhaust gas, (c) mixing fuel injection rate and (d) mean adiabatic combustion temperature in an engine chamber.

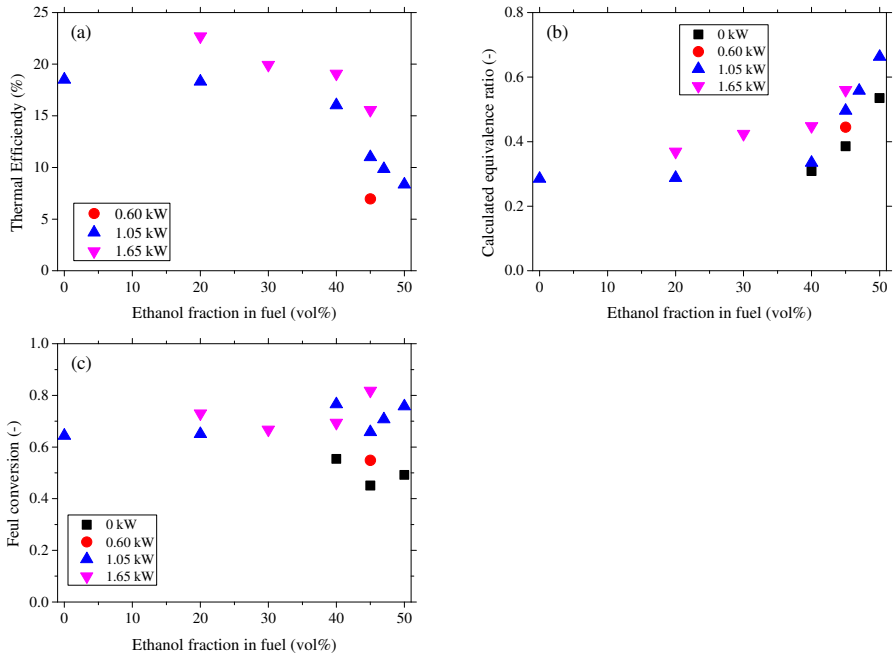

Figure 3- 8 Variation of evaluations items calculated by gas compositions in an exhaust as a function of an ethanol content in mixing fuel and an engine load. (a) thermal efficiency, (b) equivalence ratio and (c) fuel conversion.

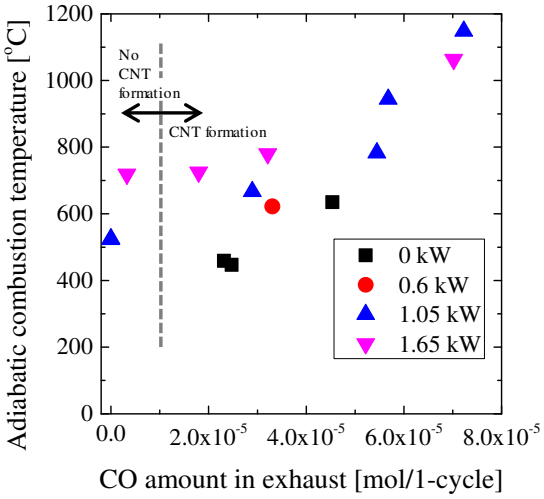

Figure 3- 9 Relationship between CO amount in an exhaust and adiabatic combustion temperature.

Table 3- 1 Summary of experimental conditions in this chapter.

Fuel	Normal dodecane (balance) + Ethanol (0–50 volume %)
Catalyst	Ferrocene: 5,000 ppm by weight
	Molybdenum acetate dimer: Mo/Fe = 0.01
	Sulfur powder: S/Fe = 2.2
Engine load	0, 0.60, 1.05, 1.65 kW

Chapter 4. Effects of Fuel Type on CNT Synthesis

4-1 Background of this chapter

The applications of alternative fuels such as fatty-acid methyl ester (FAME) instead of conventional diesel fuel for a diesel engine operation have been studied in recent years because of its renewable ability or the necessity for preventing global warming [100,101,102,103]. It is well known that FAME is vegetable-origin fuel and regarded as biodiesel. Merits of employing vegetable-origin fuel are, for examples, cleaner emissions from its combustion, the reduction of CO_2 by carbon-neutral through combining water and CO_2 by photosynthesis and consuming by combustion, similar properties with diesel fuel such as cetane number, and so on [104]. Since raw vegetable oils cannot be utilized for a present diesel engine, they have to be converted to FAME. FAME can be produced from not only a wide variety of vegetable oils, but also diverse animal fats and waste grease by means of a transesterification reaction usually with methanol. Depending on the area and oil feedstock, typical compositions of biodiesel are different with respect to one another [104,105,106]. For instance, methyl linoleate ($C_{19}H_{34}O_2$) is a dominant compound from soybean oils in USA, methyl oleate ($C_{19}H_{36}O_2$) is most included in case of rapeseed oils in Europe, methyl palmitate ($C_{17}H_{34}O_2$) and methyl oleate are primary constituents from palm oils in Southeast Asia, and methyl laurate ($C_{13}H_{26}O_2$) consists mainly of biodiesel when coconut oils are used as a feedstock in Philippines. Of course, the mixture of several FAMEs with different carbon number is applied to an actual engine operation. In any case, due to its simple production process and an intensive expectation as an alternative fuel, emission properties or oxidation pathways when FAME was employed as fuel have been explored by a lot of research groups with the application for an actual engine in mind [106,107,108]. Not only FAME but also other candidates such as normal alkane and alcohol have been attempted for a diesel engine operation in laboratory scale until today [109,110]. In Chapter 3, we utilized n-dodecane as one of fuel, but normal alkanes larger than heptane (C_8H_{18}) are able to be viable in a diesel engine operation. In practice, combustion properties and/or emission properties of normal alkanes have been intensively studied [111,112]. Although investigations of alcohol with large carbon chain for the use of a diesel operation is very few when compared with normal alkane and FAME, Julis and Leiter reported recently that 1-octanol ($C_8H_{18}O$) could be synthesized effectively via an outstanding catalyst from acetone and furfuran which is known as a biomass-derived material [113]. Along with that, the study to use 1-octanol or 1-decanol ($C_{10}H_{22}O$) as diesel fuel has been begun [109,114], and thus it can be expected that articles dealing with long chain alcohol are going to be increased more in future. Here, let us review comparative studies where effects of fuel types with different chemical structures on combustion/emission properties were investigated. Jakob et al. reported emissions from a diesel engine when n-decane or 1-decanol was utilized and their experiments showed that emissions of carbon monoxide and unburned hydrocarbons were larger in 1-decanol than those in n-decane [114]. Kerschgens et al. investigated the impact of the fuel chemical structure on combustion in a diesel engine and exhibited that shorter ignition time was obtained in n-octane than that in 1-octanol, and

higher amounts of carbon monoxide and unburned hydrocarbons at an engine outlet were measured in 1-octanol than those in n-octane [109]. The study by Cai et al. evaluated the ignition delay time in a high-pressure shock tube, in which similar ignition delay times were observed between n-octane and 1-octanol at high temperature (> 1,000 K) but it became shortened in case of n-octane at temperature below 1,000 K [115]. Shen and coworkers measured the ignition delay time of normal alkane ranging from heptane to tetradecane ($C_{14}H_{30}$), indicating that an ignition time was independent on fuel carbon number [111]. Witkowski et al. evaluated sooting properties of methane, n-heptane and n-tetradecane using a laminar diffusion flame burner and the sooting tendency was increased along with increasing carbon number included in its molecular structure [112]. Pinzi et al. reported that when methyl ester was employed for a diesel engine operation instead of ordinary diesel fuel, PM emissions from an engine were decreased [100]. Moreover, they used several methyl esters whose carbon numbers ranged from 12 to 18 and found that emissions of carbon monoxide, unburned hydrocarbon and PM were monotonously incremented with the increase of carbon number included in its molecular structure [100]. The study by Feng et al. presented interesting comparative information that soot volume produced from methyl ester was lower compared to the corresponding normal alkane in atmospheric pressure non-premixed flame [108]. Saggese and coworkers provided kinetic modeling for biodiesel combustion where similar ignition delay time under a stoichiometric condition was observed irrespective of constituent carbon numbers if methyl ester was saturated [105]. Herbinet et al. suggested that the production rate of CO and CO_2 from methyl ester at low temperature (ca. 800 ^oC) was larger than that from normal alkane [107]. Since combustion and emission properties are strongly dependent on the fuel chemical structure as seen above, it is plausible to consider that such differences may influence CNT growth in a diesel engine. As an observed tendency, when oxygen-containing fuel like methyl ester and alcohol is used, larger emissions of CO and unburned hydrocarbons are generated but there is less difference in combustion properties.

The synthesis of carbon nanomaterials like CNT and graphene from natural or wasted hydrocarbons as a carbon source is one of the hot topics in recent years. In place of conventional carbon feedstock such as methane, ethylene, toluene, etc. which are produced from fossil fuel, many processes utilizing alternative materials like natural hydrocarbon or industrial carbonaceous waste has been proposed to date [116]. As examples of CNT synthesis, camphor [117,118,119], turpentine oil [120], eucalyptus oil [121], palm oil [122], jatropha derived biodiesel [123], castor oil [124], sesame oil [125] and others were studied in laboratory stage. In these reports, the technique to carry out CVD process with CNT growth on substrates has been employed. On the other hand, one of characteristics in our method is to use a diesel engine for the synthesis of CNTs where renewable hydrocarbons such as FAME and ethanol are employed as heat and carbon source.

In this chapter, we employed three types of fuel for a diesel engine operation: mixture of methyl laurate as FAME and ethanol, mixture of 1-decanol as long chain alcohol and ethanol, and mixture of

n-dodecane as normal alkane and ethanol. Then, we tried to examine how the chemical structure of fuel affected the CNT growth in a diesel engine.

4-2 Experimental methods

The diesel engine and sampling system for products are identical with that described in Chapter 3. As main fuel, n-dodecane (99.0+%, Wako Pure Chemical Industries, Ltd.), methyl laurate (98.0+%, Wako Pure Chemical Industries, Ltd.) and 1-decanol (>98.0%, Tokyo Chemical Industry Co., Ltd.) were employed. The chemical structure of each fuel is shown in Figure 4-1. Super dehydrated ethanol (99.5+%, Wako Pure Chemical Industries, Ltd.) was mixed with main fuel and an ethanol fraction was changed from 0 volume% to 40 volume% for methyl laurate and 1-decanol and from 0 volume% to 50 volume% for n-dodecane. In order to prevent a phase separation, 4 volume% of 1-octanol (98.0+%, Wako Pure Chemical Industries, Ltd.) against mixing fuel was added in case of n-dodecane. No phase separation was observed in the use of methyl laurate and 1-decanol even when ethanol was mixed. As a catalyst source, 5,000 ppm by mass of ferrocene (98.0+%, Wako Pure Chemical Industries, Ltd.) was dissolved in mixing fuel. Additionally, molybdenum acetate dimer (98%, Sigma-Aldrich) and sulfur powder (97.0+%, Wako Pure Chemical Industries, Ltd.) which played a promoter for CNT synthesis were dissolved into fuel so that an atomic ratio of Mo/Fe and S/Fe to be 0.01 and 2.2, respectively. An engine was operated under a load ranging from 0 kW to 1.65 kW. A summary of experimental conditions in this chapter is presented in Table 4-1. The impacts of differences in the fuel chemical structure were evaluated by means of field emission scanning electron microscopy (FE-SEM, JEOL JSM-7500F) and transmission electron microscopy (TEM, HITACHI H-7650 Zero. A). For analyzing CNT structure in detail, high-resolution transmission electron microscopy (HR-TEM, JEOL JEM2010F) was used. An elemental analysis of our samples was performed using energy dispersive X-ray analysis (EDX) equipped with JEM-2010F. Two types of gas chromatograph (Shimadzu Ltd. GC-8A) were adopted to detect compositions of an exhaust gas. One is thermal conductivity detector (TCD) equipped with SHINCARBON ST (Shimadzu Ltd.) as a packed column for detecting O_2, CO, CO_2 in an exhaust gas. The other is flame ionization detector (FID) equipped with Unipak S (GL Sciences Inc.) as a packed column for detecting C1–C3 hydrocarbons, namely CH_4, C_2H_2, C_2H_4, C_2H_6, C_3H_4, C_3H_6 and C_3H_8. Mean adiabatic combustion temperature inside a cylinder was estimated in the similar manner as described in Chapter 3. Through these approaches, we evaluated effects of fuel type on CNT synthesis in a diesel engine.

4-3 Results and discussions

4-3-1 Gas compositions of an exhaust gas

The emissions of CO_2 and CO in an exhaust gas evaluated via a TCD system are shown in Figure 4-2 (a) and (b), respectively, when an ethanol fraction and an engine load are varied. Variations of a mean adiabatic combustion temperature inside a chamber calculated by means of CO and CO_2 amounts are displayed in Figure 4-2 (c). It is obvious from these figures that larger CO and CO_2 amounts in an exhaust tend to be acquired in case of methyl laurate and 1-decanol based fuel at an ethanol concentration lower than 40 volume% when compared at the same engine load. For instance, at an ethanol fraction of 40 volume% and an engine load of 1.65 kW, mixing fuel based on methyl laurate and 1-decanol produces larger amounts of CO and CO_2 than n-dodecane blended fuel. The emissions in n-dodecane system catch up with those in methyl laurate and 1-decanol when an ethanol fraction in fuel increases larger than 40 volume%. The distinguishing line which separates CNT growth conditions and no CNT growth conditions based on SEM and TEM observations conducted for all samples is inserted in Figure 4-2. Such a line can be very clearly inserted against CO amounts in an exhaust, suggesting that CO may be more important for CNT growth in a diesel engine than CO_2 amounts and/or adiabatic combustion temperatures, which is consistent with the implication in Chapter 3.

Figures 4-3 (a), (b) and (c) exhibit total C1–C3 hydrocarbon amounts in an exhaust per one engine cycle, ethylene amounts in an exhaust and acetylene amounts in an exhaust, respectively, when an ethanol content in fuel is varied. Since the importance of ethylene and acetylene in CNT synthesis as a promising precursor is well recognized, their behavior is picked up specially. Figures 4-3 (a)–(c) show a similar tendency with each other, that is to say, emissions in an exhaust gas are boosted suddenly when an ethanol fraction surpasses a certain value. In case of mixing fuel based on 1-decanol, a sharp jump is achieved at an ethanol fraction larger than 15 volume%. On the other hand, such a sharp jump can be observed at a higher ethanol fraction over 40 volume% when n-dodecane/ethanol mixing fuel is used. Methyl laurate based fuel shows an intermediate propensity between 1-decanol and n-dodecane. The increase of emitted amounts of low molecular hydrocarbons found in Figure 4-3 resembles the trend of CO and CO_2 shown in Figure 4-2. However, the distinguishing line which separates CNT growth conditions and no CNT growth conditions cannot be drawn against any low molecular hydrocarbon, whose tendency is different from that in CO amounts in Figure 4-2 (b).

Figure 4-4 shows the dependence of fuel injection rate, thermal efficiency, mean equivalence ratio and fuel conversion on experimental parameters (fuel type, an ethanol concentration in mixing fuel and an engine load). In Figure 4-4 (a), the variation of fuel injection rate which is measured via experiments is displayed. Injection rate is increased with the increase of an ethanol content and an engine load irrespective of fuel type. The order of injection rate becomes 1-decanol ≈ methyl laurate > n-dodecane when compared at the equal ethanol fraction. Figure 4-4 (b) shows the variation of thermal efficiency which is defined in a similar manner in Chapter 3. Thermal efficiency is deteriorated when an ethanol fraction becomes large, however, it is improved at a high engine load. These

tendencies are common in all fuel. In general, the order of thermal efficiency offers n-dodecane > methyl laurate ≈ 1-decanol when compared at the same ethanol fraction and engine load. The dependence of an average equivalence ratio at an engine inlet basis is shown in Figure 4-4 (c). The way to calculate equivalence ratio is the same with that described in the previous chapter. We can confirm the propensity that mean equivalence ratio inside a cylinder is made large in the order corresponding to 1-decanol, methyl laurate and n-dodecane when compared at the equal ethanol fraction/engine load. Figure 4-4 (d) is the variation of mixing fuel conversion which is calculated similarly in Chapter 3. Higher fuel conversion is presented in case of methyl laurate, but this suggestion is not explicit.

4-3-2 SEM/TEM images of synthesized CNTs

SEM and TEM micrographs of carbon materials produced from three different main fuel at an ethanol fraction of 20 volume% and an engine load of 1.65 kW are displayed in Figure 4-5. TEM images are inserted in SEM images, and observed CNTs are indicated by arrows in SEM photographs. Soot and iron-based nanoparticles covered by carbonaceous materials were found instead of CNT formation in n-dodecane, while methyl laurate and 1-decanol based fuel showed slight CNT formation although a large amount of soot and iron particles were observed as well. Even when CNT was observed, soot and/or iron nanoparticles which did not contribute to CNT growth were attached on CNT. As indicated in Figure 4-2, an experimental condition with a low ethanol content in fuel like 20 volume% is located on the boundary to separate CNT growth region and no CNT growth region. It should be noted that both methyl laurate and 1-decanol based fuel produce larger CO amounts than n-dodecane according to Figure 4-2, while methyl laurate and n-dodecane based fuel show little difference but 1-decanol based fuel generates higher emissions of low molecular hydrocarbons at corresponding conditions as shown in Figure 4-3. Taking into account SEM/TEM micrographs and measured gas data, it is suggested that CO contributed more strongly to CNT formation in a diesel engine. In-depth discussions on an influential CNT precursor in our system are carried out in Chapter 5.

The number of formed CNT was increased regardless of fuel type when an ethanol fraction in fuel became high as shown in Figure 4-6. In case of n-dodecane, the mixture of n-dodecane 55 volume% plus ethanol 45 volume% was selected, while 65 volume% main fuel blended with ethanol of 35 volume% was adopted in methyl laurate and 1-decanol system. These three conditions possess almost similar CO amounts in an exhaust gas of ca. 7×10^{-5} mol/1-engine cycle, but an adiabatic combustion temperature at 1-decanol condition has 990 °C which is 150 °C lower than that of n-dodecane and methyl laurate case. The quantity of formed CNTs in Figure 4-6 was increased in all three conditions in comparison with the one at a low ethanol fraction in Figure 4-5. Further increase of an ethanol content in fuel did not cause any acceleration of CNT synthesis, and to make matters worse an additional increasing led to an unstable engine operation. Figure 4-6 includes histogram of synthesized

CNT outer diameters under corresponding conditions with SEM and TEM images. Three conditions show relatively similar propensity that maximum peak of an outer diameter appears from 4 nm to 8 nm and not negligible amounts of large diameter over 10 nm are produced. An average diameter was estimated to be 7.5 nm, 6.5 nm and 6.5 nm for n-dodecane, methyl laurate and 1-decanol based fuel, respectively. Although an average diameter formed from n-dodecane based fuel indeed possesses slightly larger value compared with the other two cases, its difference is tiny. The reasons why similar experimental results were given at a high ethanol fraction in fuel may be because CO amounts contained in an exhaust were almost equal with each other. With the increase of an ethanol concentration in fuel, CO emissions from n-dodecane/ethanol mixing fuel catch up with those from mixing fuel of methyl laurate or 1-decanol with ethanol. This is because ethanol is likely to generate CO due to strong C-O bond [126]. Also, the kinetic model of ethanol oxidation shows that ethanol tends to mainly produce CO via the formation of aldehyde during combustion, and less C_2H_4 and C_2H_2 are formed compared with CO [127,128]. Then, CNT production becomes less affected by fuel type at a high ethanol fraction. On the other hand, at a low ethanol content in fuel, methyl laurate and 1-decanol are likely to produce more CO than n-dodecane due to the presence of oxygen atom in their molecular structure [107,109]. Consequently, whether CNT is formed or not in a diesel engine at a low ethanol fraction depends on fuel chemical structures because CO which is primarily produced from methyl laurate and 1-decanol is expected to play a significant role in CNT growth. Further considerations on the CNT growth mechanism in our system are provided in Chapter 5.

4-3-3 HR-TEM images and elemental analysis of catalysts

In order to acquire more detailed information on as synthesized CNTs, HR-TEM analysis was carried out for samples using n-dodecane, methyl laurate and 1-decanol. The experimental conditions for HR-TEM were consistent with those in Figure 4-6. Figure 4-7 exhibits HR-TEM pictures. Single-walled carbon nanotube (SWNT) could be observed among synthesized CNTs, but it was quite rare, Figure 4-7 (a). On the contrary, multi-walled carbon nanotubes (MWNTs) occupied a major portion of synthesized CNTs irrespective of a fuel type as shown in Figure (b)–(d). MWNTs prepared in these conditions undoubtedly possessed multiple layers, but it was difficult to count with accuracy because they showed the unclear and irregular structure. Such a defective structure might be induced by oxygen which was present in a cylinder and might attack carbon network during or after carbon layer formation. These TEM micrographs also show iron-based particles attached or included in CNT side wall which are observed frequently during HR-TEM evaluation.

In order to obtain elemental information about iron-based particles, EDX analysis was performed. The experimental conditions considered for EDX analysis were the same with the ones in Figure 4-7, but for comparison purpose, data obtained from n-dodecane (80 volume%)/ethanol (20 volumes%) mixing fuel with 1.65 kW where no CNT growth was observed was added. Figure 4-8 (a) is an

exemplary TEM photograph showing EDX point and its EDX spectra for estimating elemental ratio. Average O/Fe atomic ratio through randomly picked-up several iron-based particles is displayed in Figure 4-8 (b). It is clear from Figure 4-8 (b) that CNT growth conditions showed lower O/Fe ratio after combustion reactions than that without CNT growth, i.e. n-dodecane (80 volume%)/ethanol (20 volume%) mixing fuel, and among CNT growth conditions there were not large differences in O/Fe ratio. According to preceding studies, both metallic iron and oxidized iron are capable of catalytically growing CNTs. Nasibulin et al. [129], Teblum et al. [130] and Wen et al. [131] argued that metallic iron particles had higher activity for CNT growth than iron oxide particles in CVD technique and flame process. In contrast, Sato et al. [132] and de los Arcos et al. [133] indicated that iron oxide catalysts promoted CNT growth in CVD system, and Unrau et al. [134] considered that FeO particles played a dominant role in growing SWNT in flame process. Moreover, even when iron oxide, for example Fe_2O_3, was used as a catalyst feedstock, it was reduced during CNT growth to metallic iron or Fe_3C [132,135,136]. Some researchers consider that such reduced metallic iron particles exhibited catalytic function for carbon material growth [132,137]. Hence, following scenario is plausible to take place. Once metallic iron is formed from raw iron oxide, it may catalytically grow CNTs, keeping metallic state till the end of reaction time. Similar phenomena could be observed in aerosol studies to evaluate effects of iron additives into fuel on characteristics of particulate emission from flames, where metallic iron particles were observed at the exit in addition to iron oxide particles in spite of the presence of oxygen [138,139]. The reduction of iron oxide to metallic iron may proceed in a similar way to the well-known blast furnace reactions, namely iron oxide reacts with solid carbon or carbon monoxide to form iron [140]. According to reactions in blast furnace, some particles in aerosol are reduced from oxidized state to metallic state and then emitted maintaining metallic state. Our experiments might undergo similar reactions because an operation temperature in blast furnace ranging from several hundreds to over one thousand Celsius resembles adiabatic combustion temperatures in our study. Therefore, metallic iron particles produced through reduction reactions might exhibit catalytic ability for CNT growth when considering above preceding studies and experimental results presented in Figure 4-8. During CNT formation, metallic state was maintained to some degree because carbon layers surrounding such particles might prevent oxidizer from accessing to catalyst particles. On the other hand, oxidized iron particles without experiencing reduction processes and/or other particles which underwent reoxidation reactions immediately after reduction might not contribute to CNT growth.

4-4 Summary of this chapter

In this chapter, we attempted to investigate and evaluate impacts of the chemical structure of fuel on CNT growth in a diesel engine. Three different types of fuel, i.e. normal dodecane (n-dodecane),

FAME (methyl laurate) and alcohol (1-decanol), were employed as main fuel. Remarkable points are listed as follows.

- At a low ethanol content (e.g. 20 volume%), CNT could be grown in case of mixing fuel using methyl laurate and 1-decanol, while n-dodecane system did not show any CNT growth. At a high ethanol fraction, CNT production was facilitated and there was almost no difference in CNT production between fuel type.
- The behavior of CNT growth in different fuel type may be able to be interpreted by the contribution of CO amounts in an exhaust. Higher CO emissions could be obtained from methyl laurate and 1-decanol than from n-dodecane at a low ethanol content. On the other hand, at a large ethanol fraction, CO amounts became similar because it could be produced mainly from ethanol, resulting in very less difference in CNT production.
- According to HR-TEM evaluation, SWNT was rarely formed while majority of synthesized CNTs was MWNT irrespective of fuel conditions. Carbon layers consisting of CNTs were damaged probably due to oxygen.
- EDX analysis of iron nanoparticles showed that lower O/Fe atomic ratio was obtained in case of CNT growth condition. Based on various preceding papers, it is implied that metallic iron particles contributed to CNT growth in our study.

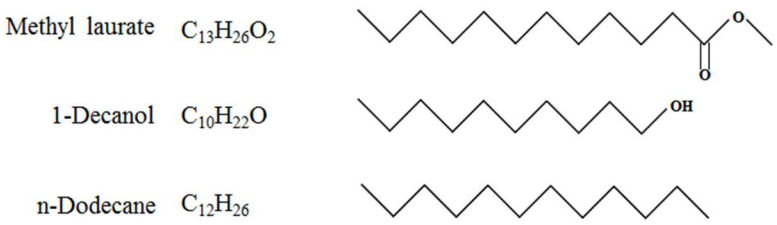

Figure 4- 1 Chemical structure of main fuel used in this chapter for a comparison study.

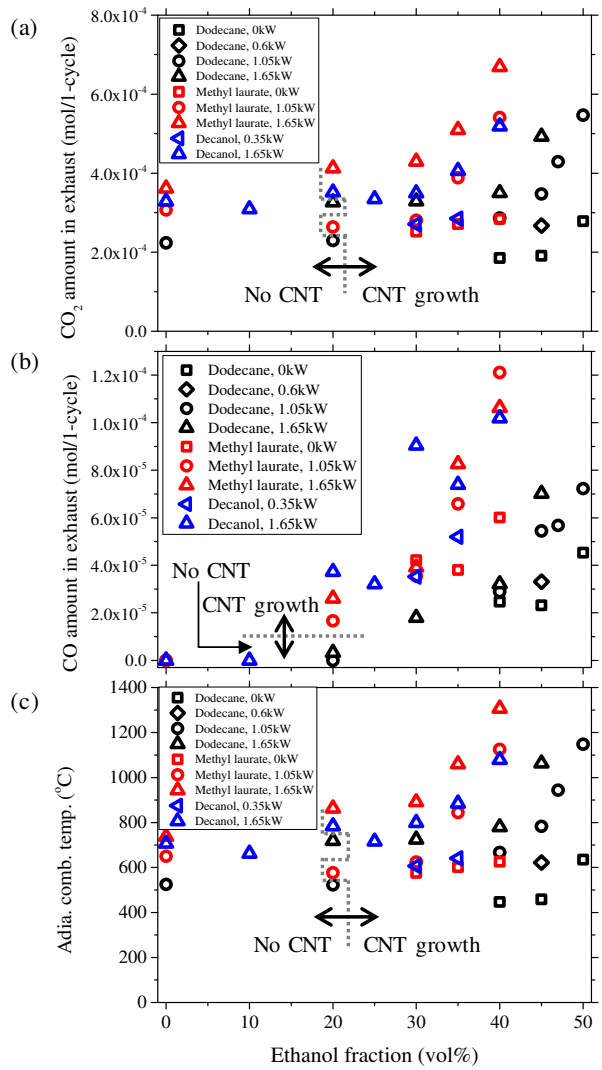

Figure 4- 2 Variations of (a) CO amount in an exhaust gas, (b) CO_2 amount in an exhaust gas and (c) mean adiabatic combustion temperature when main fuel, an ethanol fraction and an engine load were changed. The uniform color was used for the same main fuel and the uniform shape was used for the same engine load.

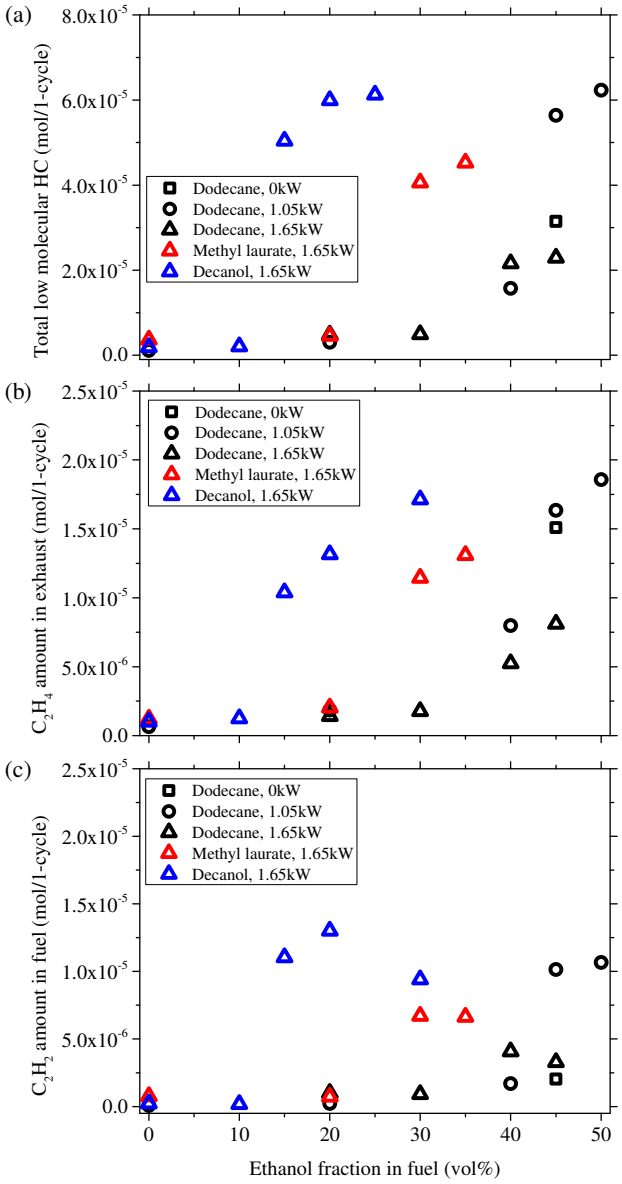

Figure 4- 3 Variations of (a) total C1–C3 hydrocarbon amount in an exhaust gas, (b) ethylene amount in an exhaust gas and (c) acetylene amount in an exhaust gas when main fuel and an ethanol fraction in fuel were changed.

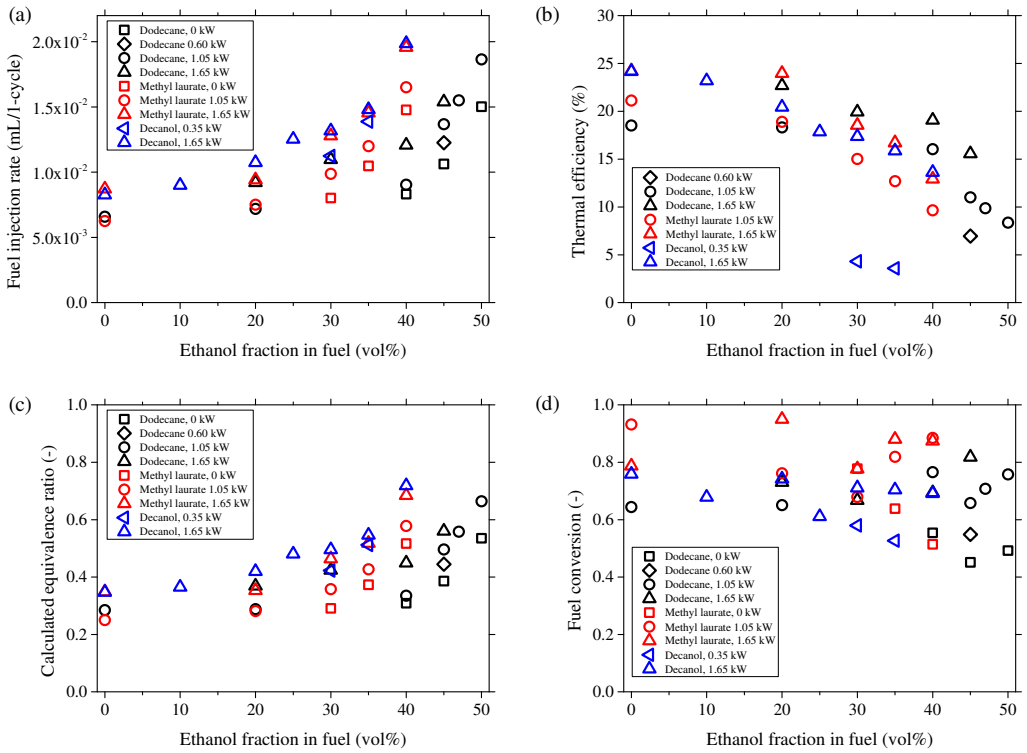

Figure 4- 4 Variation of evaluations items calculated by gas compositions in an exhaust when experimental conditions (fuel type, ethanol content, engine load) were changed. (a) fuel injection rate. (b) thermal efficiency. (c) equivalence ratio. (d) fuel conversion. The definition and estimation procedure of thermal efficiency, equivalence ratio and fuel conversion were identical with those in Chapter 3.

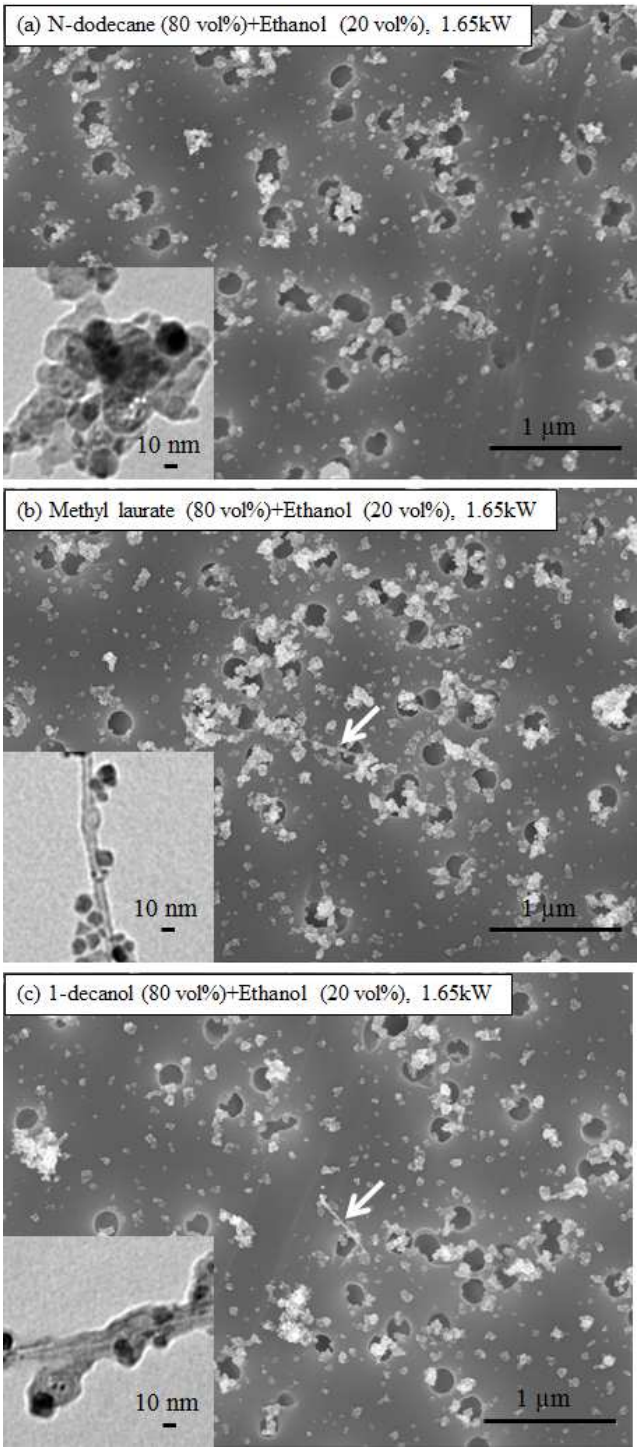

Figure 4- 5 Typical SEM images with inserted TEM images of synthesized CNTs when main fuel was varied while an ethanol fraction (20 volume%) and an engine load (1.65 kW) were identical. (a) n-dodecane (80 volume%)/ethanol (20 volume%) mixture, (b) methyl laurate (80 volume%)/ethanol (20 volume%) mixture and (c) 1-decanol (80 volume%)/ethanol (20 volume%) mixture. Synthesized CNTs are indicated by arrows in SEM images.

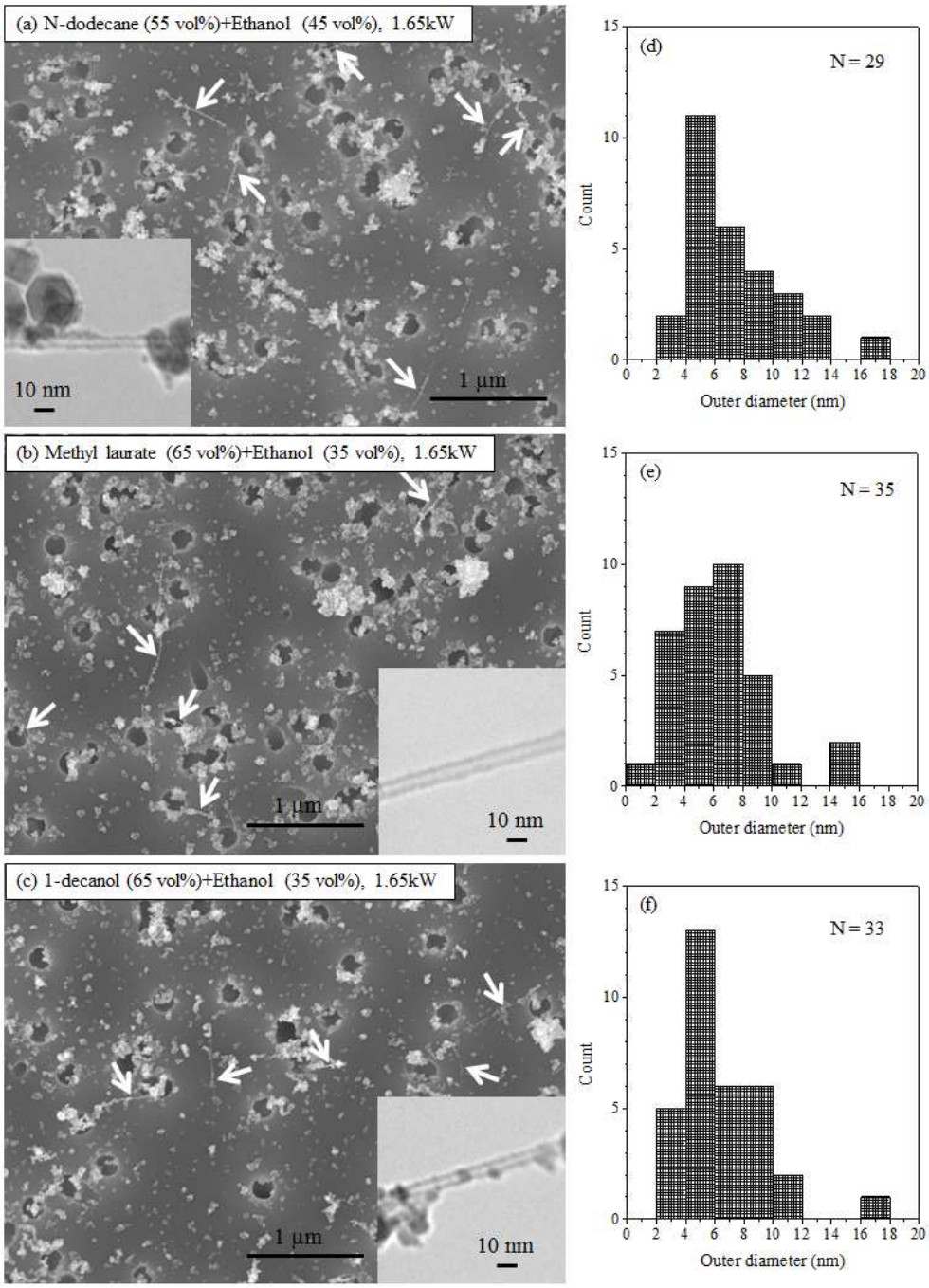

Figure 4- 6 SEM images with inserted typical TEM images of synthesized CNTs at higher ethanol fraction in fuel and histogram of CNT outer diameter synthesized at the comparable condition. (a) n-dodecane (55 volume%)/ethanol (45 volume%) mixing fuel with 1.65 kW as an engine load, (b) methyl laurate (65 volume%)/ethanol (35 volume%) mixing fuel with 1.65 kW as an engine load and (c) 1-decanol (65 volume%)/ethanol (35 volume%) mixing fuel with 1.65 kW as an engine load. Synthesized CNTs are indicated by arrows in SEM images.

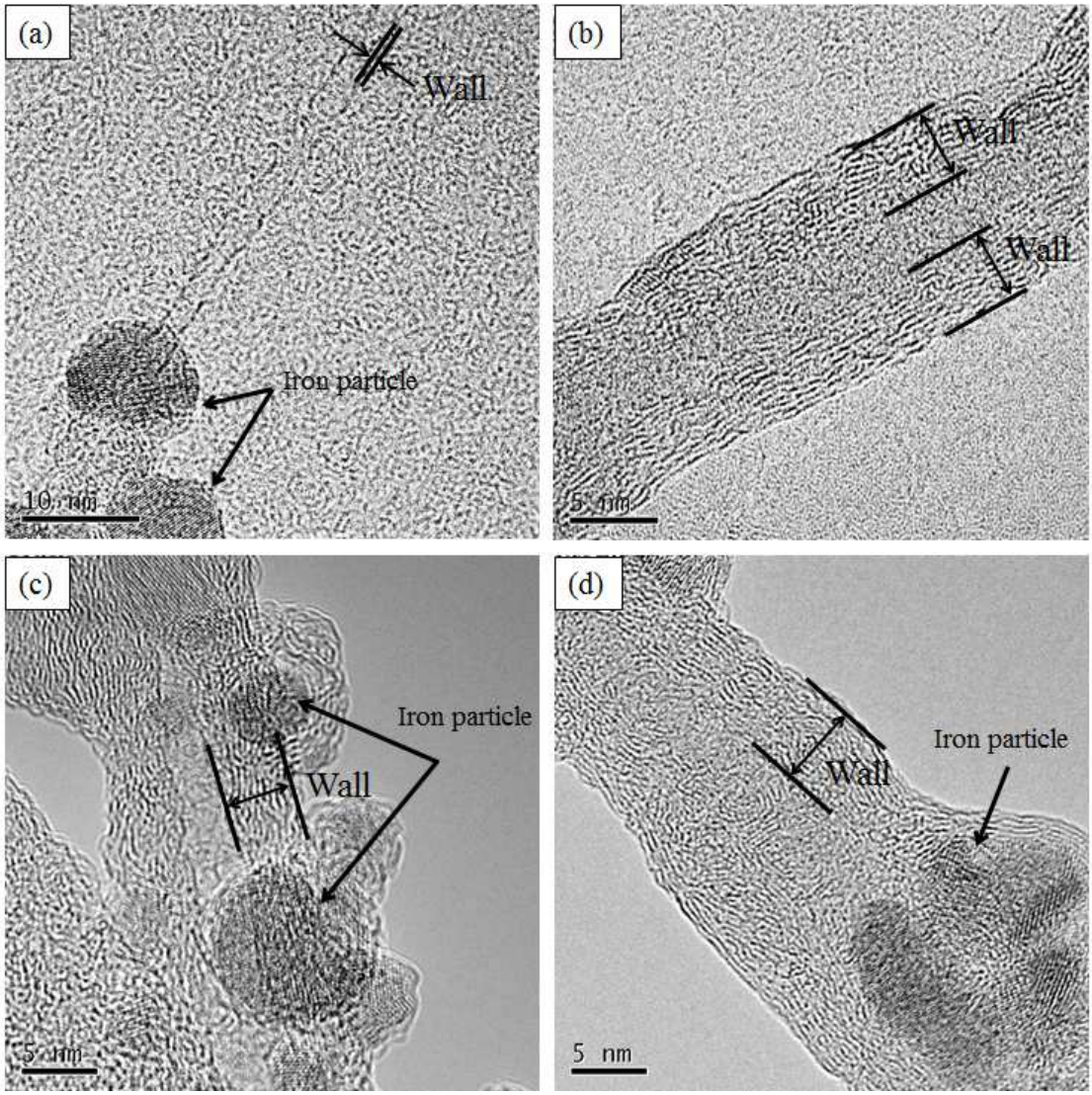

Figure 4- 7 HR-TEM images of synthesized CNT. (a) and (b) n-dodecane (55 volume%)/ethanol (45 volume%) mixing fuel with 1.65 kW as an engine load, (c) methyl laurate (65 volume%)/ethanol (35 volume%) mixing fuel with 1.65 kW as an engine load and (d) 1-decanol (65 volume%)/ethanol (35 volume%) mixing fuel with 1.65 kW as an engine load. SWNT was rarely observed and the majority of CNTs were MWNTs in each condition. Iron-based nanoparticles attached or encapsulated in CNT are indicated by arrows.

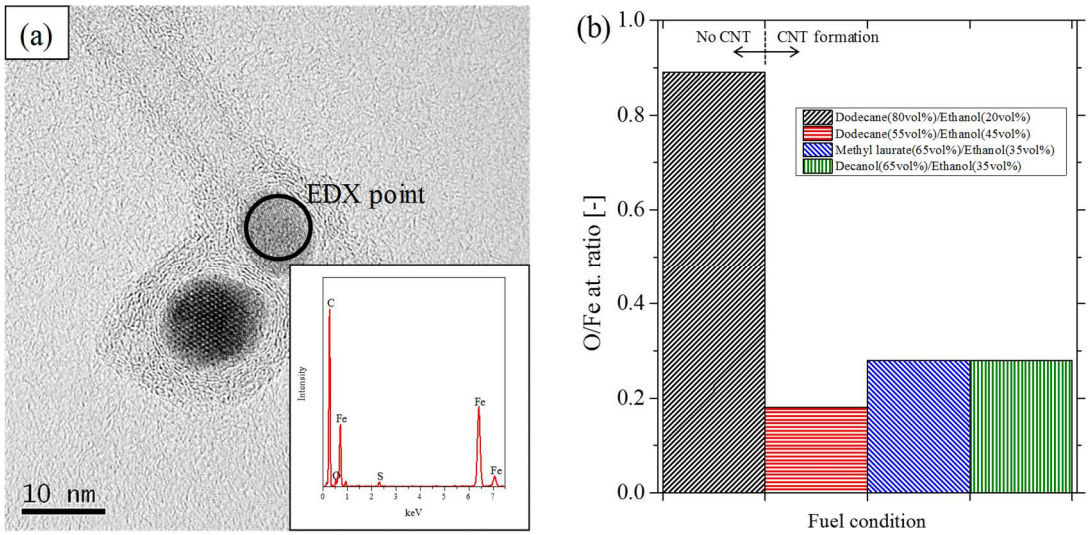

Figure 4- 8 EDX analysis of iron particles for estimating atomic ratio when different fuel was used. (a) HR-TEM image and EDX spectrum where pointed out in HR-TEM image when n-dodecane (55 volume%)/ethanol (45 volume%) mixing fuel was used and an engine load was 1.65 kW. (b) average O/Fe atomic ratio of several iron-based particles when different fuel was used. The same engine load of 1.65 kW was employed.

Table 4- 1 Summary of experimental conditions conducted in this chapter.

Fuel	N-dodecane (balance) + Ethanol (0–50 volume%)
	Methyl laurate (balance) + Ethanol (0–40 volume%)
	1-decanol (balance) + Ethanol (0–40 volume%)
Catalyst	Ferrocene: 5,000 ppm by weight
	Molybdenum acetate dimer: Mo/Fe = 0.01
	Sulfur powder: S/Fe = 2.2
Engine load	0, 0.60, 1.05, 1.65 kW

Chapter 5. Considerations on CNT Growth Mechanism in a Diesel Engine

5-1 Background of this chapter

In previous chapters, the importance of carbon monoxide is suggested for the synthesis of CNTs using a diesel engine. However, it is insufficient to interpret the key CNT precursor and/or the CNT growth route in a cylinder although several experimental data like gas compositions in an exhaust gas and mean adiabatic combustion temperature were acquired. Hence, major purpose in this chapter is to identify the key factor which contributes to CNT formation in our system, and to provide clues leading to understanding the CNT growth mechanism and/or CNT synthesis path in a diesel engine. In order to corroborate our purpose, we employed three approaches, namely, experiments, simulations and modeling.

5-2 Methods

5-2-1 Experiments/analysis

Experimental setup and sampling system which is the same with that in Chapter 3 and 4 was employed in this chapter. Also, tailored mixing fuel identical with Chapter 4 was used for measurements. Carbon materials in an exhaust gas were collected on a membrane filter and the surface of filter was observed by FE-SEM. CNT growth rate in each experimental condition was estimated based on the sum of CNT length per SEM images on the assumption that synthesis duration was 5 milliseconds and CNT diameter was independent on experimental conditions. 5 milliseconds originated in an average engine rotation speed. Because it was approximately 3,000 rpm, maximum allowable time for CNT growth was consistent with 5 milliseconds in case of the current engine. In order to strengthen the reliability of our estimation approach, the average value of several SEM images was employed. This calculated CNT growth rate was compared with numerical one in a modeling work.

5-2-2 Simulations and modeling

Gas-phase chemical kinetic simulations using CHEMKIN-PRO (version 17.2) software were carried out to obtain helpful information to support experimental results from the qualitative point of view. Three different starting materials, n-dodecane 100%, ethanol 100% and their mixture (n-dodecane 55 volume%/ethanol 45 volume%) with a low equivalence ratio (fuel lean condition, 0.5) and a high equivalence ratio (fuel rich condition, 1.5) were employed. The n-dodecane combustion model proposed by Luo et al. [141] which included 106 chemical species and 420 elemental reactions was applied. Although some ethanol combustion models were available [142,143], the model published by Marinov [143] with 57 chemical species and 372 elemental reactions was adopted because this model was used in other CNT study [144]. Moreover, kinetics of the sulfur oxidation proposed by Bongartz and Ghoniem [145] was taken into account as well. Since they studied impacts of a sulfur addition on

methane combustion, only sulfur involved parts with 33 chemical species and 245 elemental reactions were extracted for our study. Both the ethanol combustion model and the sulfur combustion model were integrated into the n-dodecane combustion model. Following item was kept in mind when integrating; thermodynamic properties and elemental reactions in the model proposed by Luo et al. had a higher priority when we found duplicated chemical species and elemental reactions between n-dodecane and ethanol combustion models. The integrated kinetic model possessed 140 chemical species and 910 elemental reactions totally. It should be noted that heterogeneous reactions such as CNT growth on catalytic surface are not taken into consideration in this kinetic model. As a reactor type in a simulation, although actual combustion phenomena in a diesel engine are inhomogeneous, a closed homogeneous reactor was employed where oxidation reaction proceeded at constant pressure and temperature. Also, homogeneous closed compression ignition was employed as a reactor model for the comparative purpose. The dynamics of this model is close to that of an actual engine because computation underwent compression-ignition process similar to an actual diesel engine under given compression ratio (20) and engine speed (3,000 rpm). Nonetheless, we believe that calculation results based on homogeneous combustion enable us to provide qualitative information for understanding the key CNT precursor and CNT growth pathway.

Moreover, formation processes of metallic iron particles which might behave as a catalyst for CNT synthesis during combustion were also simulated using CHEMKIN-PRO. Growth processes of iron particles consist of several steps, such as ferrocene decomposition to form atomic Fe, formation of Fe clusters, agglomeration process of Fe clusters to form larger particles, and oxidation of some atomic iron by oxygen. We collected several documents and integrated them into overall reactions describing from ferrocene decomposition to formation of metallic iron particles. For instance, kinetics of ferrocene decomposition to form atomic Fe in gas phase and thermodynamic properties of chemical species were proposed by Hirasawa et al. [146] and Kuwana et al. [147], the model of iron particle formation from atomic Fe via Fe clusters was referred to the work by Wen et al. [148], and oxidation reactions of atomic Fe in gas phase with oxidizer to form FeO were formulated by Rumminger et al. [149,150]. Growth processes of iron particles which consist of 75 chemical species and 498 elemental reactions were integrated into the kinetic model of n-dodecane/ethanol for performing simulations. In this study, only metallic iron particles were paid attention because not oxidized state but metallic state generally displays catalytic capability of growing CNTs. A closed homogeneous reactor and homogeneous closed compression ignition were selected for the simulation of iron particle formation. From these two cases, we expect that qualitative discussions on CNT synthesis pathways are possible. For simulations, mixture fuel of n-dodecane 55 volume%/ethanol 45 volume% was adopted.

Furthermore, modeling of CNT growth rate was performed using carbon monoxide or ethylene or acetylene as a carbon source. The detailed procedure how we developed the kinetic model of CNT growth rate is described in latter section.

5-3 Results and discussions

5-3-1 Experimental results

SEM and TEM micrographs of as synthesized CNTs can be referred to Chapter 3 and 4. Those SEM images shown in previous chapter were used for evaluating CNT growth rates in a modeling work. The remarkable point given in former chapters is that emitted hydrocarbons and an adiabatic combustion temperature tended to rise under the condition that CNT formation could be observed. It was implied from these results that CO emissions were most important for CNT synthesis than other factors. In order to confirm that implication, a comparison work of experimental data obtained was performed. Figure 5-1 shows the relationship between adiabatic combustion temperatures and CO, C_2H_4 and C_2H_2 amounts in an exhaust. Ethylene and acetylene were selected as a representative of low molecular weight hydrocarbons because many reports in CVD process indicated they were one of the most effective CNT precursors. As shown in Figure 5-1 (a), the distinguishing line which separates CNT growth conditions and no CNT growth conditions can be inserted horizontally against CO amounts irrespective of fuel types. On the other hand, such a line was unable to be drawn clearly for adiabatic combustion temperatures. In Figure 5-1 (b) and (c), the distinguishing line which separates CNT growth region and no CNT growth region cannot be created against both adiabatic combustion temperatures and ethylene/acetylene amounts in an exhaust gas. This strongly suggests that CO more strongly affects CNT formation in a diesel engine in comparison with adiabatic combustion temperatures and low molecular weight hydrocarbons. In order to make this propensity more comprehensible, Figure 5-2 was prepared, where the correlation between CO amounts in an exhaust and ethylene/acetylene amounts in an exhaust was shown. In Figure 5-2, the same data in Figure 5-1 were taken over, and the horizontal axis was altered from mean adiabatic combustion temperature to CO amounts in an exhaust while the vertical axis was maintained in ethylene and acetylene amounts in an exhaust. The distinguishing line which separates CNT growth conditions and no CNT growth conditions can be inserted against CO amounts, corroborating the suggestion found in Figure 5-1. Since the importance of carbon monoxide was indicated, the dependence of CNT growth rate estimated from SEM images on CO amounts in an exhaust gas was illustrated in Figure 5-3. Two SEM micrographs were selected as representative examples. In this figure, experimental results related to only n-dodecane were picked up. The relationship between estimated CNT growth rate and CO amounts infers that CNT growth rate seems to be linear with respect to CO amounts when CO amounts surpass a certain threshold value. The threshold value can be calculated from x-intercept to be 9.4×10^{-6} mol/1-cycle. This proportionality is roughly in line with CNT generation in inserted SEM images in Figure 5-3.

Quantities of hydrocarbons at an engine outlet were explored in the presence and absence of catalyst

sources in fuel. Measured data are shown in Figure 5-4 where both absolute amounts and relative amounts based on the case without catalyst sources are provided. It is clear that lower CO amounts but larger amounts of low molecular weight hydrocarbons were acquired under the condition with catalyst sources. It seems reasonable to consider that Fischer-Tropsch reactions might take place on iron particle surface. In Fischer-Tropsch reactions, CO reacts with hydrogen which may be produced during combustion as an intermediate product in our study, forming hydrocarbons ranging from C1 hydrocarbons to long chain hydrocarbons larger than C5 on transition metals such as iron, cobalt and nickel. Typical Fischer-Tropsch reactions are expressed in following equations; $nCO + (2n+1)H_2 \Leftrightarrow C_nH_{2n+2} + nH_2O$, $nCO + 2nH_2 \Leftrightarrow C_nH_{2n} + nH_2O$, etc. Fischer-Tropsch process and CNT growth mechanism share certain similarities in that CO molecule adsorbs on catalyst surface as a first step and then CO dissociation reaction occurs [151,152]. The schematic to compare pathways of CNT growth reactions and Fischer-Tropsch reactions is shown in Figure 5-5. After dissociation, two processes take a different path and form a different product as a result. In case of Fischer-Tropsch reactions, atomic carbon adsorbed on catalyst reacts with atomic hydrogen to form hydrocarbons like paraffin and olefin [151]. On the other hand, carbon atom adsorbed on catalyst dissolves into catalyst, diffuses and precipitates on the surface which is expected to become a feedstock for carbon network in CNT. In our study, it is plausible to consider that Fischer-Tropsch reactions and CNT growth reactions take place simultaneously in the similar region. Therefore, taking into account our experimental results shown in Figure 5-4 and reaction similarities in between Fischer-Tropsch process and CNT growth process, it seems appropriate to claim that CO preferentially reacts with catalysts quickly in comparison with other hydrocarbons.

5-3-2 Simulations

Calculated results of combustion reactions using CHEMKIN-PRO are exhibited in Figure 5-6, where profiles of major intermediate products are shown as a function of reaction time. Calculations were carried out at 1,500 K and 75 atm by changing staring materials and an equivalence ratio. Mole fractions were normalized by an initial carbon molar fraction. Although we integrated sulfur related reactions into current simulations, negligible impacts on our outputs were provided. Under a fuel lean condition (equivalence ratio = 0.5), carbon monoxide is rapidly oxidized to form CO_2 soon after it is produced owing to abundant oxygen in a reaction region. Ethylene, acetylene and hydrogen disappear very faster than CO. It should be noted that the maximum mole fraction of ethylene and acetylene is reduced with increasing an ethanol fraction in fuel. On the other hand, a portion of carbon monoxide remain unchanged irrespective of starting materials under a fuel rich condition (equivalence ratio = 1.5), and hydrogen does not disappear similarly at all time. It is worth noting that ethylene and acetylene mole fraction both at maximum and at the end of reaction is decreased when an ethanol fraction in initial fuel becomes large. This tendency is consistent with that under fuel lean condition.

These results corroborate relative importance of carbon monoxide during combustion for CNT synthesis. Actual experiments showed that an equivalence ratio tended to increase with increasing an ethanol fraction in feedstock (Figure 4-4), meaning that it was easy for carbon monoxide to remain in a reaction field because combustion properties conceptually shifted from Figure 5-6 (a) to (d). Hence, Figure 5-6 presents a qualitative insight that CO may play a crucial role in growing CNT during combustion compared with C_2H_4 and C_2H_2.

As a comparative study, oxidation reactions in the use of homogeneous closed compression ignition model were computed in Figure 5-7. In these simulations, n-dodecane (55 volume%)/ethanol (45 volume%) mixing fuel with different equivalence ratio (0.5 and 1.5) was employed. As well as the profile of intermediate chemical species, the variation of temperature and pressure in a cylinder is shown. Both temperature and pressure were increased with progression of compression, and combustion was initiated just before 0.005 seconds shown by sharp increase of temperature/pressure and rapid disappearance of n-dodecane/ethanol. Regarding the behavior of intermediate products, observed tendency was similar with that in Figure 5-6, namely, CO, ethylene and acetylene were consumed very quickly at fuel lean condition (equivalence ratio = 0.5), while CO and hydrogen remained unoxidized even after reaction at fuel rich condition (equivalence ratio = 1.5). Intriguingly, ethylene and acetylene reacted quite rapidly even at fuel rich condition, supporting the relative significance of CO.

Moreover, combustion reactions in case of methyl laurate/ethanol mixing fuel were simulated using a closed homogeneous reactor model in Figure 5-8. Kinetic model provided by Herbinet et al. was referred as the oxidation of methyl laurate [153]. This reaction model was integrated with the kinetic model of ethanol [143] and sulfur oxidation [145]. Figure 5-8 depicts the profile of chemical species computed at 1,500 K and 75 atm using methyl laurate (65 volume%)/ethanol (35 volume%) mixing fuel. The behavior of each species is well consistent with that in n-dodecane (55 volume%)/ethanol (45 volume%) system in both fuel rich/lean condition. In Chapter 4, these two conditions showed similar CNT production when an engine load was 1.65 kW, maybe due to similar combustion properties with each other.

Variation of average metallic iron nanoparticle size via the process initiating from ferrocene decomposition was simulated using n-dodecane (55 volume%)/ethanol (45 volume%) mixing fuel as a feedstock with different equivalence ratio in Figure 5-7. Different reactor type was selected, a closed homogeneous reactor for Figure 5-9 (a) and homogeneous closed compression ignition for Figure 5-9 (b). The simulated condition was 1,500 K and 50 atm in Figure 5-9 (a). Both figures indicate the similar qualitative point of view that the higher equivalence ratio becomes (namely fuel rich condition), the larger particle diameter formed becomes, although absolute value of size is different with each other. According to TEM analysis showing that particle size formed (not limited to metallic one) ranged from several nanometers to dozen nanometers, it is suggested from Figure 5-9 that proper iron

catalyst for CNT synthesis may be formed in locally fuel rich regions.

5-3-3 Modeling

Since experimental and simulated results strongly indicated that CO was the key CNT precursor in our system, modeling of CNT growth rate using CO, C_2H_2 and C_2H_4 as a feedstock was carried out for further investigation. Firstly, a modeling work using CO was attempted, and then fitting performance of modeled CNT growth rate employing CO, C_2H_2 and C_2H_4 as a carbon source is compared later. CNT growth model using CO was developed based on CO disproportionation (Boudouard) reactions to deposit carbon on catalyst surface. It was assumed that other reactions like CO hydrogenation were ignored and CO disproportionation proceeded through Langmuir-Hinshelwood mechanism. The kinetic study of carbon deposition on transition metals via CO disproportionation reactions was performed by using preceding articles as a reference [154,155,156,157]. Elemental reactions on catalytic surface can be described in the following steps [154,157].

CO adsorption: $CO + * \Leftrightarrow CO*$ (1)

CO dissociation: $CO* + * \Leftrightarrow C* + O*$ (2)

CO_2 desorption: $CO* + O* \Leftrightarrow CO_2 + * + *$ (3)

where * signifies an adsorption site on catalyst surface and CO*, C* and O* are chemisorbed species. In addition to above steps, a step of carbon diffusing through catalyst to form CNT should be taken into account as follows.

Carbon diffusion: $C* \Rightarrow C_{CNT} + *$ (4)

where C_{CNT} is carbon atom constituting of CNT. An overall reaction considered in this study can be given as below.

Overall reaction: $CO + CO \Rightarrow C_{CNT} + CO_2$ (5)

In this work, two types of models were considered in case of carbon monoxide. First model termed as Model 1 was based on the assumption that the rate-limiting step was step (2), CO dissociation reaction, and CNT growth rate was equal to the production rate of C* in step (2). This is because some articles studying CO disproportionation reactions found that CO dissociation reaction was a rate-limiting step [155,156]. These assumptions provide the following expression for the rate of CNT formation, R_{CNT}

$$\boldsymbol{R_{CNT}} = \frac{\boldsymbol{k_2 K_1 P_{CO}}}{\left[\boldsymbol{1+K_1 P_{CO}+K_B(P_{CO_2}/P_{CO})}\right]^2} \quad (6)$$

The definition of each character is expressed in nomenclature list at the end of this chapter (before Figures). In the second model termed as Model 2, it was assumed that step (4), carbon diffusion, was rate-determining and other steps were in quasi-equilibrium for estimating CNT growth rates. This is because it was reported that carbon diffusion was a rate-limiting step according to some studies on

CNT growth [158,159]. Based on that, the following equation can be given as a CNT growth rate, R_{CNT}

$$\boldsymbol{R_{CNT}} = \frac{k_4 K_A P_{CO}^2}{P_{CO_2}\left[1+K_1 P_{CO}+K_B\left(\frac{P_{CO_2}}{P_{CO}}\right)+K_A(P_{CO}^2/P_{CO_2})\right]} \quad (7)$$

In CNT synthesis, the possibility that other steps than the ones stated above such as building-up reaction of CNTs and transportation of carbon feed gas to catalyst surface become a rate-determining is very limited according to the investigation on CNT growth dynamics [160]. In Fischer-Tropsch reaction, CO dissociation reaction or chain growth step can control the reaction rate [152]. Also, as stated early, CO dissociation reaction on catalyst surface becomes a rate-limiting step in CO disproportionation reaction. Hence, from a comprehensive point of view, we took notice of above two steps in this study, CO dissociation step and carbon diffusion step. In these reaction models, it was supposed that rate constants and equilibrium constants complied with Arrhenius equation and van't Hoff equation, respectively. Also, additional assumption was presented that gas compositions inside a chamber were the same with those at an engine outlet for estimating P_{CO} and P_{CO_2}. Then, we compared CNT growth rates in Model 1 and 2 by tuning fitting parameters with actual CNT growth rates which were estimated by SEM images. Only experimental findings of n-dodecane were adopted for the modeling study.

Fitting parameters in Model 1 and Model 2 (ΔE_2, ΔE_4, ΔH_1, ΔH_A, ΔH_B, k_{20}, k_{40}, K_{10}, K_{A0} and K_{B0}) were all adjusted for making CNT growth rates using both models fitted well with experimentally estimated growth rates, shown in Figure 5-10 where modeled and measured CNT growth rates were plotted in the horizontal axis and vertical axis, respectively. For optimization, fitting parameters other than k_{20} and k_{40} were tuned so that R^2 which shows the degree of linear relationship between modeled CNT growth rate and actual one in Figure 5-10 can approach unity as much as possible, in which a least-square technique was employed. Whereas, k_{20} and k_{40} were tuned so that values in modeled CNT growth rate can be the same order with those in measured one. Fitting parameters in both models are summarized in Table 5-1 where not only estimated values but also corresponding literature data are provided if they are available. Both models show good agreement with values in measurements, especially Model 2 as presented in Figure 5-10. In CNT synthesis study, if the rate of carbon supply is higher than that of carbon diffusion, abundant amorphous carbon is formed on catalyst surface, resulting in the deactivation of catalysts. In our experiments, since substantial deactivated catalyst nanoparticles by amorphous carbon were observed in TEM analysis, it is indicated that the probable rate-determining step in our system is carbon diffusion step, termed Model 2. Considerations whether fitting parameters are within an acceptable range compared with those values in similar researches are carried out in discussion section. In sum, all fitting parameters are generally in line with literature data.

As well as the procedure in carbon monoxide, modeling of CNT growth rate using ethylene and acetylene as a carbon source was carried out. We assumed that CNT synthesis occurs via ethylene or

acetylene decomposition on catalyst surface through Langmuir-Hinshelwood mechanism. Firstly, elemental reactions on catalytic surface using C_2H_4 are displayed as follows.

C_2H_4 adsorption: $C_2H_4 + * \Leftrightarrow C_2H_4*$ (8)

C_2H_4 dissociation: $C_2H_4* + * + * + * + * + * \Leftrightarrow 2C* + 4H*$ (9)

H_2 desorption: $2H* \Leftrightarrow H_2 + * + *$ (10)

Carbon diffusion: $C* \Rightarrow C_{CNT} + *$ (11)

Then, elemental reactions in case of acetylene are exhibited in following steps.

C_2H_2 adsorption: $C_2H_2 + * \Leftrightarrow C_2H_2*$ (12)

C_2H_2 dissociation: $C_2H_2* + * + * + * \Leftrightarrow 2C* + 2H*$ (13)

H_2 desorption: $2H* \Leftrightarrow H_2 + * + *$ (14)

Carbon diffusion: $C* \Rightarrow C_{CNT} + *$ (15)

C_2H_4*, C_2H_2* and H* represent chemisorbed species on catalyst surface, and the definition of other symbols is identical with that in the model using CO. Although surface reactions should take place in a sequential manner and non-sequential reaction (9) and (13) is not realistic from a practical viewpoint, we attempted to simplify the reaction model as described above reactions and actually confirmed that fitting performance is not much affected regardless whether reactions proceeded in sequential or non-sequential manner (see supporting information). Hence, non-sequential mode was adopted here. Because there was little difference of fitting performance regardless of a rate-limiting step in case of CO, carbon diffusion step was assumed to be a rate-limiting one in ethylene and acetylene as well. Consequently, CNT growth rate, R'_{CNT} for ethylene and R''_{CNT} for acetylene, can be kinetically described as below.

$$\boldsymbol{R'_{CNT}} = \frac{\boldsymbol{k_{11}(K_C P_{C_2H_4})^{0.5}}}{\boldsymbol{P_{H_2} + K_8 P_{C_2H_4} P_{H_2} + \frac{P_{H_2}^{1.5}}{K_{10}^{0.5}} + (K_C P_{C_2H_4})^{0.5}}} \quad (16)$$

$$\boldsymbol{R''_{CNT}} = \frac{\boldsymbol{k_{15}(K_D P_{C_2H_2})^{0.5}}}{\boldsymbol{P_{H_2}^{0.5} + K_{12} P_{C_2H_2} P_{H_2}^{0.5} + \frac{P_{H_2}}{K_{14}^{0.5}} + (K_D P_{C_2H_2})^{0.5}}} \quad (17)$$

The definition of each character is summarized in nomenclature list. Although $P_{C_2H_4}$ and $P_{C_2H_2}$ were calculated based on the analysis of gas chromatograph, P_{H_2} was estimated according to mass balance between fuel fed into an engine inlet and low molecular weight hydrocarbons at an outlet. If chemical formula, CH_xO_y and $C_\alpha H_\beta$, signifies mixing fuel (n-dodecane/ethanol/octanol) fed into a cylinder and sum of low molecular weight hydrocarbons (methane, acetylene, ethylene, ethane, propyne, propylene and propane) in an exhaust gas, respectively, we assumed that the following equation is satisfied and other reactions did not take place.

$CH_xO_y \Rightarrow C_\alpha H_\beta + \gamma H_2 + (y/2)O_2$ (18)

Since total amounts of low molecular weight hydrocarbons in an exhaust gas were measured by gas chromatograph, H_2 amount in an exhaust gas can be estimated via mass balance using equation (18), resulting in getting partial pressure of hydrogen. Modeled CNT growth rate based on ethylene and

acetylene and measured one were plotted in Figure 5-11 after tuning fitting parameters in a similar manner in CO. For comparison, the result using CO is also shown. Fitting parameters in ethylene and acetylene modeling are summarized in Table 5-2 and Table 5-3, respectively. It is apparent from Figure 5-11 that CO based model shows better linearity with measured CNT growth rate, indicating stronger connection between CO amount and CNT growth rather than ethylene amount and acetylene amount. Discussions on the rationality of fitting parameters in ethylene/acetylene models against literature data are performed in discussion section. Basically, values of fitting parameters in models using ethylene and acetylene are within an acceptable range predicted by preceding studies. Therefore, these modeling works that modeled CNT growth rates using CO fitted with measured CNT rates better than those using ethylene and acetylene strongly gives favor to our idea that CO dominantly acts as a CNT precursor in a diesel system.

5-3-4 Discussions

5-3-4-1 Fitting parameters in modeling work

Firstly, let us discuss the validity of fitting parameters in CNT growth models based on CO disproportionation reaction. Regarding ΔE_2 which represents the activation energy in CO dissociation reaction, our model indicates 105 kJ/mol as an optimum value, being in agreement with previously reported values, 20±5 kcal/mol = 84±21 kJ/mol [161] in experiments and 1.11–1.18 eV = 107 – 114 kJ/mol [162] in density functional theory (DFT) calculations. Our models provides -100 kJ/mol as a value of ΔH_1 which is the CO adsorption energy, matching the energy of -92.5 kJ/mol estimated by Snoeck et al. [163] and -48.1 – -26.0 kcal/mol = -201 – -109 kJ/mol by Sorescu et al. [164]. Furthermore, considering the energy required for CO adsorption (ΔH_1 = -92.5 kJ/mol) and CO_2 desorption (ΔH_3 = 89.8 kJ/mol) by Snoeck et al. [163], and the reaction energy of CO dissociation (ΔH_2) ranging from -0.5 to 0.5 eV (-48 to 48 kJ/mol) which was dependent on crystal face and/or structure of catalysts calculated by Melander et al. [152], $\Delta H_A = 2\Delta H_1 + \Delta H_2 + \Delta H_3$ = -50 kJ/mol and $\Delta H_B = -(\Delta H_1 + \Delta H_3)$ = 5 kJ/mol in our model are enough acceptable. The activation energy in carbon diffusion, ΔE_4 = 25 kJ/mol, shows relatively similar value if it is assumed that carbon diffusion proceeds in liquid phase (37 kJ/mol, [165]) or surface diffusion (34 kJ/mol, [166]). Furthermore, estimated value of K_{10} (= 0.5 atm^{-1}) which is an equilibrium constant in step (1) at 873 K lies within literature data ranging from 0.3 to 7.5 bar^{-1} estimated at the same temperature [163,167,168]. On the other hand, although K_{B0} (= 0.09 at 873 K) shows good agreement with 0.021 at 798 K [163] and 0.056±0.015 at 613 K [154] as a reference when calibrated by using van't Hoff equation with ΔH_B = 5 kJ/mol, there is little literature with respect to other integrated equilibrium constant, K_{A0} (= 350 atm^{-1} at 873 K). However, since our fitting parameters generally match well with values in preceding papers, our modeling work using CO can be regarded as reliable one.

Next, we checked the rationality of each fitting parameter in ethylene and acetylene modeling as long

as there are available literature data. As for ΔE_{11} and ΔE_{15}, the same value in CO modeling was adopted because carbon diffusion step is not interfered by the difference of a carbon source. k_{110} and k_{150} were adjusted so that the gradient becomes unity in Figure 5-11 (b) and (c), but they show the same digit with that in CO. Regarding ΔH_8, we estimated -60 kJ/mol, being well consistent with other studies, -49 kJ/mol [169] and -80 kJ/mol [170] on Fe and -62 kJ/mol on Ni [171]. ΔH_{12} in our study indicates -250 kJ/mol which is located between calculated values via DFT studies, -206 kJ/mol [169], -273 kJ/mol [170] and -285 kJ/mol [172]. According to original research by Sellers et al. [171] and Huang et al. [173], K_{80} on Ni catalyst became 1.96×10^{-5} at 350 K and 1.8 cm^3/mol at 298 K, respectively. These are able to be converted to 1.4×10^{-12} atm^{-1} and 8.7×10^{-12} atm^{-1} at 873 K, respectively, on the assumption that van't Hoff equation and perfect gas are satisfied. In a similar way, K_{120} at 873 K can be estimated as 1.1×10^{-29} atm^{-1} [171] and 5.6×10^{-27} atm^{-1} [173]. K_{80} and K_{120} in this work shows 5.0×10^{-12} atm^{-1} and 1.0×10^{-27} atm^{-1}, respectively, being in relatively good agreement with literature data. Because hydrogen desorption step is independent on ethylene and acetylene, following relation, $K_{100} = K_{140}$ and $\Delta H_{10} = \Delta H_{14}$, were applied in our study. Due to literature data by Sellers and Gislason [171], K_{100} (= K_{140}) can be estimated as 1.4×10^{-10} atm at 873 K. Zou et al. calculated the reaction enthalpy of dissociative hydrogen adsorption on Fe surface and the results exhibited that it was 38 – 71 kJ/mol depending on surface sites [174]. Similarly, Ozbek and Niemantsverdriet studied adsorption energy of hydrogen on iron carbide via DFT simulation where it ranged from 6 to 92 kJ/mol according to coverage [175]. These references match estimated values in this study. Although we could not find direct supporting data in regard to K_{C0}, K_{D0}, ΔH_C, and ΔH_D to our knowledge, the validness of ΔH_C and ΔH_D can be discussed because literature data of ΔH_9 and ΔH_{13} is available. Calculations done by Mueller et al. showed that ΔH_9 and ΔH_{13} were 2.5 – 77 kJ/mol and 86 – 124 kJ/mol, respectively [176]. Since ΔH_C is equal to $\Delta H_8 + \Delta H_9 + 2\Delta H_{10}$ according to its definition, ΔH_C of 100 kJ/mol in this study seems plausible when ΔH_8 = -60 kJ/mol and ΔH_{10} = 60 kJ/mol is used. In the same manner, ΔH_D (= $\Delta H_{12} + \Delta H_{13} + \Delta H_{14}$) of -80 kJ/mol in this work is within an acceptable value range if ΔH_{12} of -250 kJ/mol and ΔH_{14} of 60 kJ/mol are taken into account. Therefore, fitting parameters in ethylene/acetylene modeling are generally consistent with values in preceding studies.

5-3-4-2 CNT precursor in our system

Investigation works to study effective chemical species for CNT growth have been quite popular, in particular in CVD technique [144,177,178,179,180,181,182,183,184,185,186,187,188]. For example, Franklin et al. [177] and Tian et al. [179] proposed C_6H_6 while Teblum et al. [186] identified one benzene ring connected to different substituents like xylene as favored compounds for CNT growth. However, a number of studies reported that C2 hydrocarbons should be the key species. Eres et al. [180], Zhong et al. [182] and Sugime et al. [144] indicated that C_2H_2 was the main precursor while C_2H_4 was an efficient species capable of facilitating CNT growth as proposed by Shukla et al. [183] and Inoue et al. [184]. Zhang et al. argued that both C_2H_2 and C_2H_4 played an important role in CNT

nucleation stage and CNT development stage, respectively [185]. It should be noted that CH_4 was considered by some researchers as less effective species even when it was employed as a feed gas [182,183]. Meanwhile, Shandakov et al. [187] investigated aerosol CVD process in the use of ethanol as a carbon precursor, and stated that the utilization of ethanol was equivalent to the use of the mixture of methane and carbon monoxide as precursors to produce SWNTs. According to the comparative study done by Futaba et al. [188], highly efficient SWNT growth was achieved by C_2H_2 and C_2H_4 than CO, showing the superiority of acetylene and ethylene over carbon monoxide. As addressed by Anoshkin et al. [189] who employed dual carbon sources ($CO+C_2H_4$) and obtained the enhanced CNT synthesis compared with the case using solely CO evidenced especially at higher temperature than 900 ^oC, the possibility might take place that SWNT was formed by CO at early stage and then it was elongated by primarily C_2H_4 at high temperature. In spite of a lot of efforts dedicated to studying a promising CNT precursor, it is still an open issue because of the strong dependency on experimental conditions and systems. However, the trend in CVD system was found that C2 hydrocarbons such as acetylene and ethylene seemed to be a more efficient source rather than other hydrocarbons.

Although publications in flame technique are limited in comparison with those in CVD process, some studies can give us fruitful information. Flame processes provide a different situation with CVD system because not only carbon sources but also O_2 takes part in reactions and affects intermediate chemical species in gas phase. In spite of complicated circumstances, some articles reported a promising chemical species for CNT synthesis in flame technique with a burner system [190,191,192,193,194,195]. Though C2 hydrocarbons such as C_2H_2 and C_2H_4 were indeed proposed as an important compound for CNT growth [190,195], a number of researches elucidated that CO was a strong candidate leading to CNT growth regardless of fuel type [190,191,192,193,194,195]. In particular, Wen et al. [194] conducted the modeling work to predict CNT growth where CO played a monopolistic role in CNT growth via disproportionation and hydrogenation, and their result was in line with measured data. Also, there is possibility that both CO and C_2H_2 affect CNT growth but its role is different with each other, the former contributes to CNT nucleation and the latter does to CNT elongation after nucleation as suggested by Hall et al. [191]. In spite of limited publications in flame process, we can find the propensity that carbon monoxide becomes a predominant species in CNT growth.

It can be claimed from experimental approaches shown in Figure 5-1 and Figure 5-2 that carbon monoxide is the most important factor in our study because the distinguishing line which separates CNT growth region and no CNT growth region can be explicitly inserted against CO amounts in an exhaust, while such a line cannot be drawn against adiabatic combustion temperatures or amounts of low molecular weight hydrocarbons at an outlet. Analysis on amounts of hydrocarbon in an exhaust gas shown in Figure 5-4 indicates that carbon monoxide preferentially reacts with catalyst particles compared with other hydrocarbons. Calculated results in Figure 5-6 also shows relative importance of

carbon monoxide than low molecular weight hydrocarbons like ethylene and acetylene, especially at a high equivalence ratio. Moreover, modeling works of CNT growth rates based on CO as a carbon source are in better agreement with experimentally estimated CNT growth rates in comparison with those based on ethylene or acetylene as a carbon source, shown in Figure 5-11. Our experimental results, simulations and modeling all show carbon monoxide is an effective chemical species in CNT synthesis. The propensity is basically in line with other findings in flame processes to produce CNTs as stated above, where burners and gas phase feedstock were employed instead of an internal combustion system. Vander Wal et al. [192] and Naha et al. [193] pointed out carbon monoxide was a main source of CNTs, and Wen et al. [194] performed CNT modeling works using CO as a sole carbon supplier, fitting well with experimental observations. Other research groups such as Unrau et al. [190] and Hall et al. [191] argued that besides CH_4 and/or C_2H_2, carbon monoxide was of value in synthesizing CNTs. Although there are some differences in combustion properties between a diesel engine and a burner system in some degree, above-mentioned studies are useful for corroborating our idea that carbon monoxide is the most promising precursor for CNT formation in a diesel engine.

5-3-4-3 CNT growth path inside a diesel engine

From results obtained until now, let us speculate CNT growth passes in our study. All our results indicate the significance of CO as a CNT precursor. CO tends to be produced during an incomplete combustion where there is shortage of oxygen to oxidize CO to CO_2, and as a result it becomes one of main components under fuel rich conditions. This behavior can be suggested in Figure 5-6 (b), (d) and (f) where as a result of creation of fuel rich condition CO stayed unoxidized even after 0.003 sec. At fuel rich circumstances, abundant hydrogen was produced as well, being unreacted with oxidizer, as shown in Figure 5-6 (b), (d) and (f). This might be helpful for growing CNT because hydrogen induces the reduction of iron catalyst surface which exhibits good catalytic capability. Based on calculated results in Figure 5-6, both carbon monoxide and hydrogen which is preferable for CNT growth are most likely to be formed in fuel rich regions. Moreover, according to simulated results showing the dependence of metallic iron size on equivalence ratio (Figure 5-9), suitable particles diameter for CNT growth is prone to be formed at a high equivalence ratio. Since actual combustion in a diesel engine is inhomogeneous, an equivalence ratio generally ranging from 0.2 to 2.0 coexists in a cylinder per one engine cycle. Large equivalence ratio regions, in other words fuel rich conditions, are created in the vicinity of fuel injection nozzle and the center of sprayed fuel. Here, let us propose CNT formation mechanism in a diesel engine which reflects findings in this study. Firstly, iron nanoparticles are produced as a result of ferrocene decomposition soon after combustion reactions are initiated. At the same time, through pyrolysis and/or partial oxidation of fuel fed into a cylinder, low molecular weight hydrocarbons such as carbon monoxide, ethylene, acetylene, etc. which is a prospective candidate as a CNT precursor are also generated. Then, generated carbon monoxide reacts with metallic iron particles preferentially than ethylene and acetylene. Some of carbon monoxide induce Fischer-Tropsch

reaction, while the other contributes to the formation of graphite layers on catalyst surface. Although most of iron particles may lose their catalytic ability due to graphite layers, some of them grow CNTs probably via CO disproportionation reaction. It can be considered that these processes may take place mainly in fuel rich region. We believe this is the major route of CNT synthesis in a diesel engine. Finally, Here, let us compare our results with those by Nikolaev et al. who commercialized SWNT production through floating catalyst CVD technique using CO as a carbon source termed HiPco process [196]. The production rate of SWNTs approached 450 mg/h in their study [196], which is significantly higher than our production rate (2 mg/h). Hence, the production rate in our system has to be improved further for achieving commercial production by a diesel engine. Our study using a conventional diesel engine until now revealed some important points. Thus, as specific approaches to improve CNT yield in future, the change in a fuel injection system from currently used mechanical control to the electrical control for the enhancement in fuel/air mixture can be considered as future works.

The depiction that summarizes all findings obtained in this study and shows CNT synthesis pathway is presented in Figure 5-12.

5-4 Summary of this chapter

In this chapter, we attempted to identify the key factor which contributes to CNT formation in a diesel system, and to investigate CNT synthesis path in a diesel engine through several approaches such as experiments, simulations and modeling. Remarkable points are listed as follows.

- By comparing gas amounts examined via gas chromatograph, the importance of carbon monoxide was disclosed because the distinguishing line separating CNT growth region and no CNT growth region could be clearly inserted.
- Measurements of hydrocarbons in an exhaust with and without catalyst sources indicated that reactions between CO and catalysts preferentially occur compared with those between other hydrocarbons and catalysts.
- According to profiles of chemical species calculated by CHEMKIN-PRO software, relative importance of carbon monoxide in comparison with other hydrocarbons such as ethylene and acetylene was emphasized.
- Fitting performance of modeled CNT growth rate using carbon monoxide or ethylene or acetylene as a carbon source against experimentally measured CNT growth rate was compared, and then the model based on CO showed better agreement with measured data.
- All approaches in this chapter suggested the significance of carbon monoxide as a promising candidate of CNT precursor, being in line with previous studies in flame processes to synthesize CNTs using burners.

- CNT synthesis pathway expected in our system; CO is generally generated via imperfect combustion where there is shortage of oxygen, namely fuel rich conditions (larger equivalence ratio than unity). Taking into account the fact that the equivalence ratio inside a general diesel engine ranges from 0.2 to 2.0 during one combustion stroke and high equivalence ratio regions are concentrated in the vicinity of fuel injection nozzle and the center of sprayed fuel, the most probable route of CNT growth is that iron particles and carbon monoxide produced at fuel rich regions react each other, resulting in CNT growth.

Nomenclature list

ΔE_i: activation energy of reaction rate constant k_i

ΔH_i: reaction enthalpy of reaction step (i)

K_A (= $K_1^2 K_2 K_3$): integrated equilibrium constant in CO disproportionation reaction

K_B (= $1/K_1 K_3$): integrated equilibrium constant in CO disproportionation reaction

K_C (= $K_8 K_9 K_{10}^2$): integrated equilibrium constant in ethylene decomposition reaction

K_D (= $K_{12} K_{13} K_{14}$): integrated equilibrium constant in acetylene decomposition reaction

k_i (= $k_{i0}\exp(-\Delta E_i/RT)$): reaction rate constant of forward reaction of reaction step (i)

Ki (= $K_{i0}\exp[-\Delta H_i(1/T - 1/T_0)]$): equilibrium constant of reaction step (i)

$P_{C_2H_2}$: partial pressure of acetylene

$P_{C_2H_4}$: partial pressure of ethylene

P_{CO}: partial pressure of carbon monoxide

P_{CO_2}: partial pressure of carbon dioxide

P_{H_2}: partial pressure of hydrogen

R: gas constant

R_{CNT}: modeled CNT growth rate

T: temperature

superscript

': ethylene related reaction/coefficient

": acetylene related reaction/coefficient

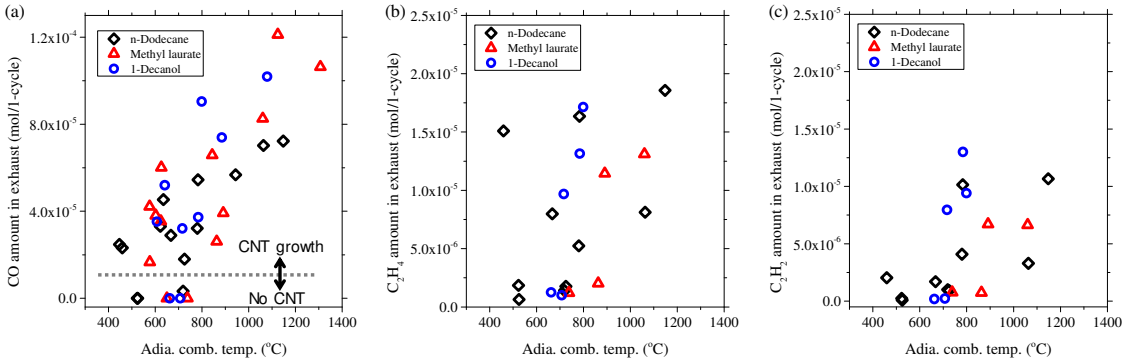

Figure 5- 1 Comparisons of data measured in our experiments. Relation between (a) adiabatic combustion temperatures and CO amounts in an exhaust, (b) adiabatic combustion temperatures and C_2H_4 amounts in an exhaust, and (c) adiabatic combustion temperatures and C_2H_2 amounts in an exhaust. The distinguishing line which separates CNT growth conditions and no CNT growth conditions is inserted in (a), but it cannot be inserted in (b) and (c).

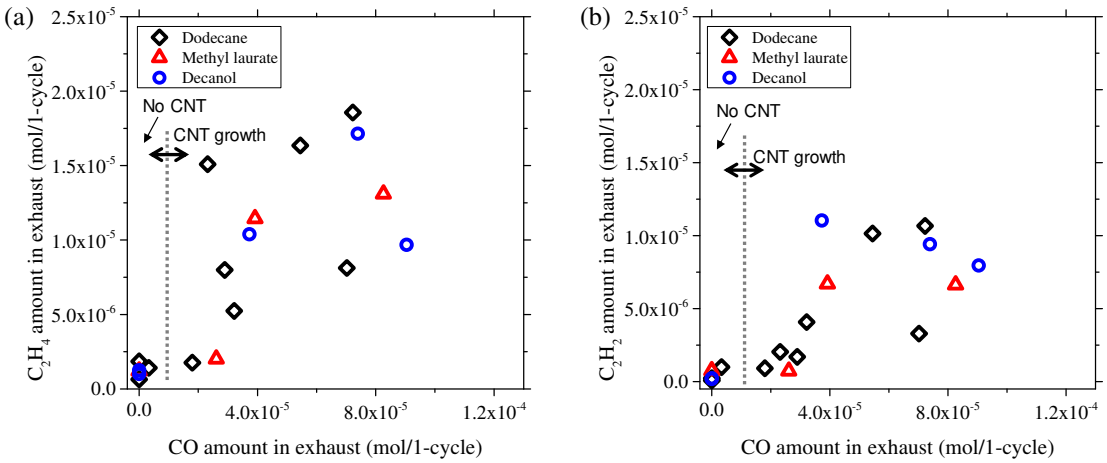

Figure 5- 2 Comparisons of data measured in our experiments. Correlation between (a) CO amounts in an exhaust and C_2H_4 amounts in an exhaust, (b) CO amounts in an exhaust and C_2H_2 amounts in an exhaust. The distinguishing line which separates CNT growth conditions and no CNT growth conditions can be inserted for CO.

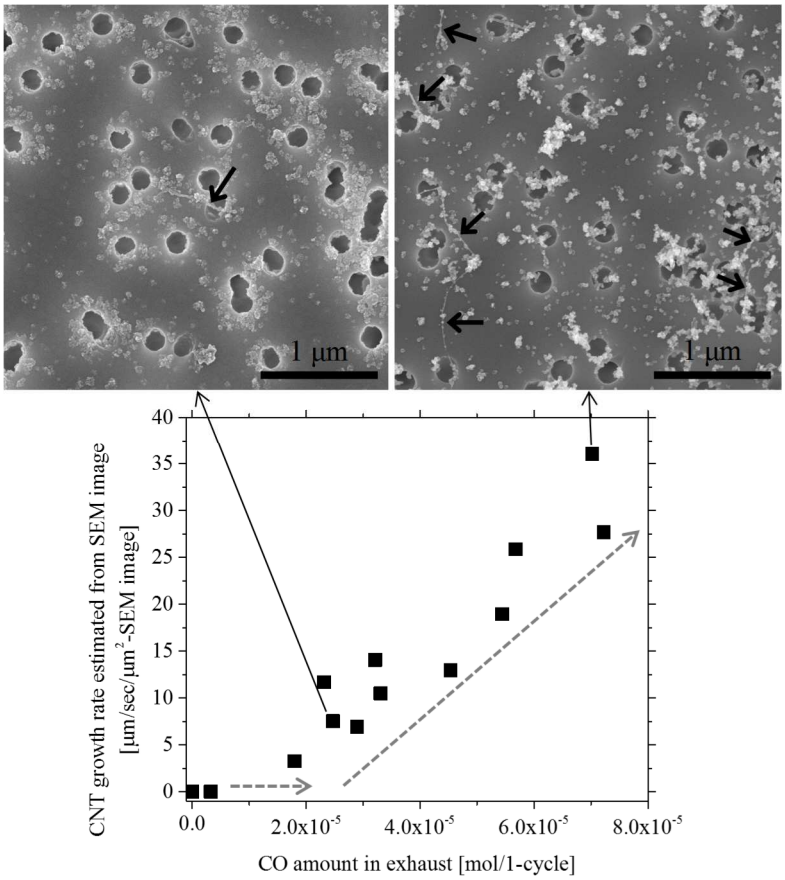

Figure 5- 3 Variation of CNT growth rates estimated from SEM images as a function of CO amount in an exhaust gas. Some SEM photos which show an increase of CNT growth in line with CO amount are shown as well. Synthesized CNTs are pointed by arrows.

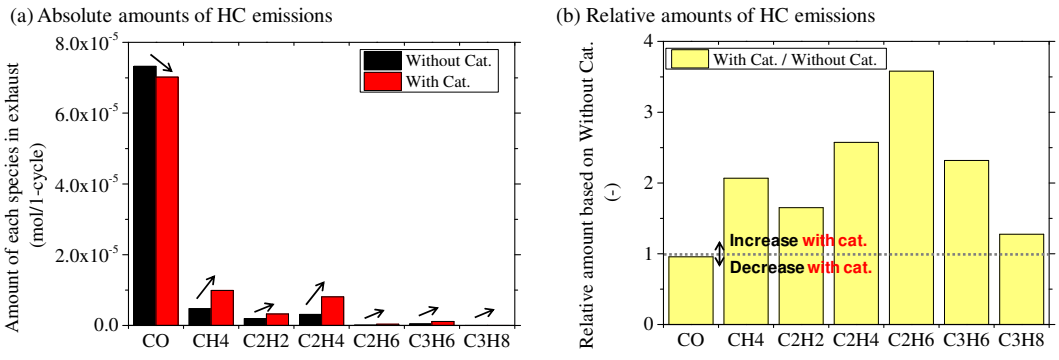

Figure 5- 4 Amounts of hydrocarbons in an exhaust with and without catalyst sources in fuel. (a) absolute amounts of hydrocarbons and (b) relative amounts of hydrocarbons based on those without catalyst sources.

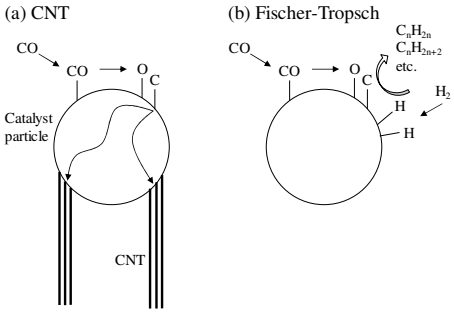

Figure 5- 5 Schematic of reaction pathway of (a) CNT growth and (b) Fischer-Tropsch reaction.

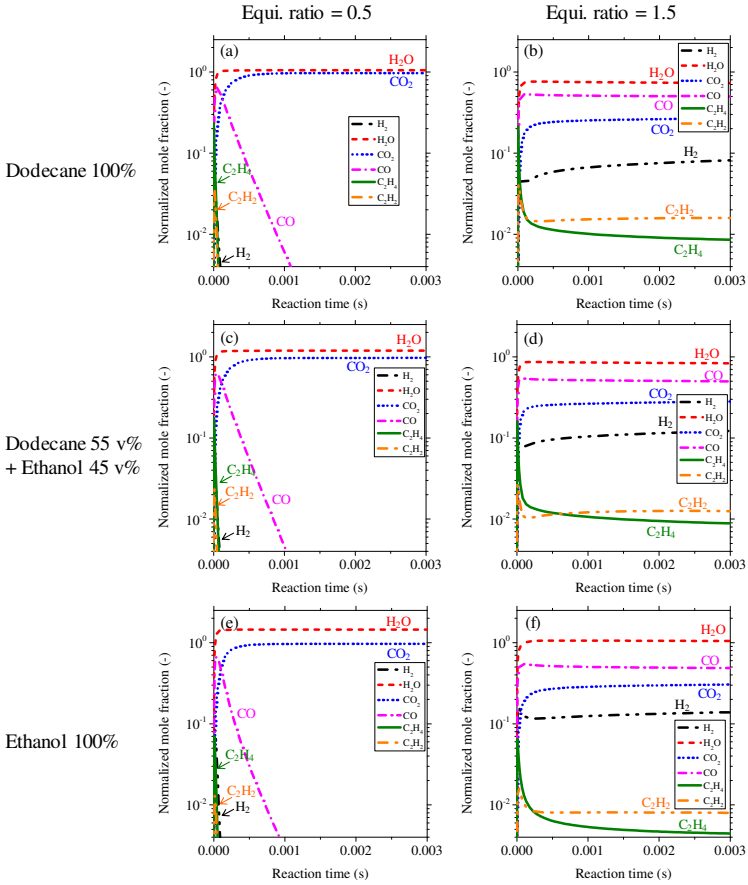

Figure 5- 6 Normalized mole fractions of intermediate species during combustion calculated at 1,500 K and 75 atm using a closed homogeneous reactor type in CHEMKIN-PRO. (a) n-dodecane as starting fuel at an equivalence ratio of 0.5, (b) n-dodecane as starting fuel at an equivalence ratio of 1.5, (c) n-dodecane(55 vol%)/ethanol(45 vol%) mixture as starting fuel at an equivalence ratio of 0.5, (d) n-dodecane(55 vol%)/ethanol(45 vol%) mixture as starting fuel at an equivalence ratio of 1.5, (e) ethanol as starting fuel at an equivalence ratio of 0.5, and (f) ethanol as starting fuel at an equivalence ratio of 1.5.

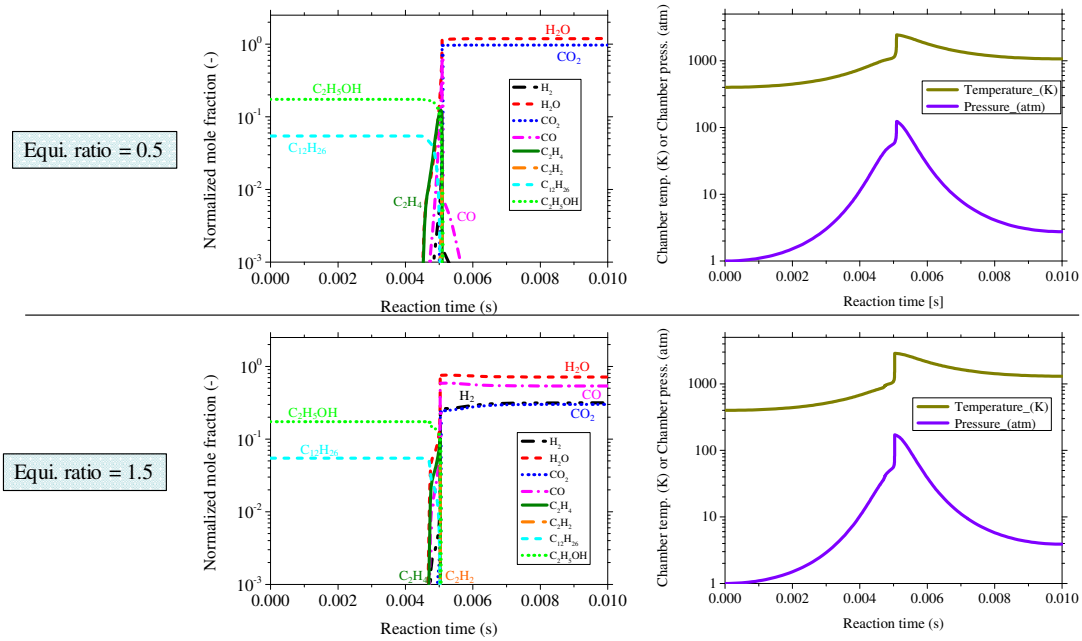

Figure 5- 7 The variation of normalized mole fraction of important chemical species, combustion temperature and pressure during reaction simulated by CHEMKIN-PRO using a homogeneous closed compression ignition engine as a model reactor. Fuel condition was the mixture of n-dodecane (55 vol%) and ethanol (45 vol%), and both fuel rich and lean conditions were employed.

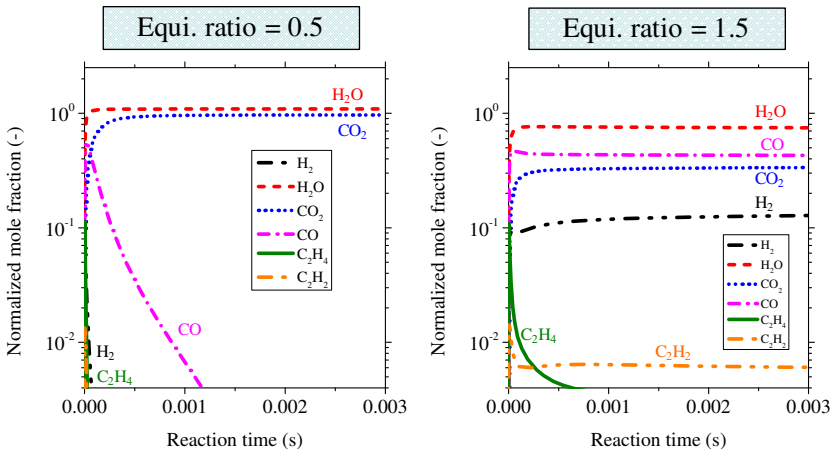

Figure 5- 8 Normalized mole fractions of intermediate species during combustion calculated at 1,500 K and 75 atm using methyl laurate (65 vol%)/ethanol (35 vol%) as fuel in a closed homogeneous reactor type in CHEMKIN-PRO.

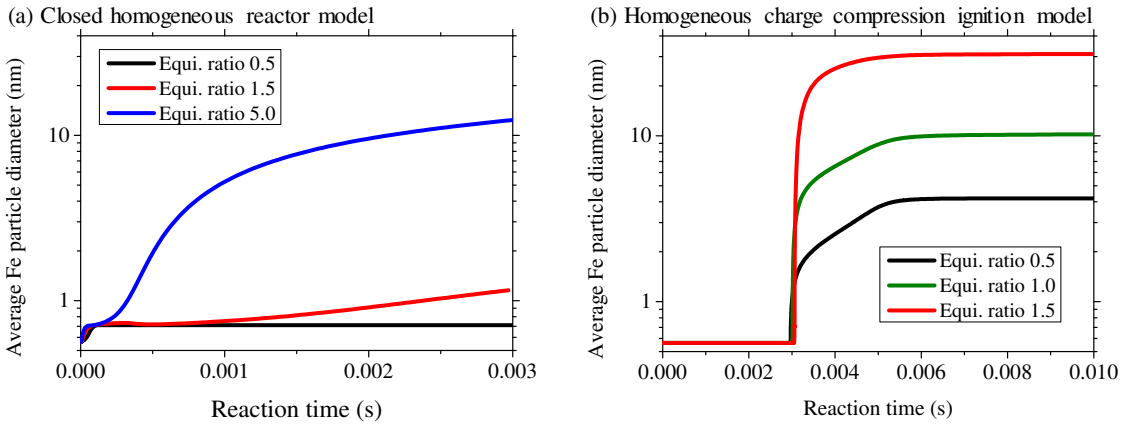

Figure 5- 9 Variation of average Fe catalytic nanoparticle size using a different reactor type in CHEMKIN-PRO. (a) closed homogeneous reactor type at 1500 K and 50 atm and (b) homogeneous closed compression ignition engine type. It should be noted that initial setting temperature was 1000 K in homogeneous closed compression ignition engine for convergent calculation.

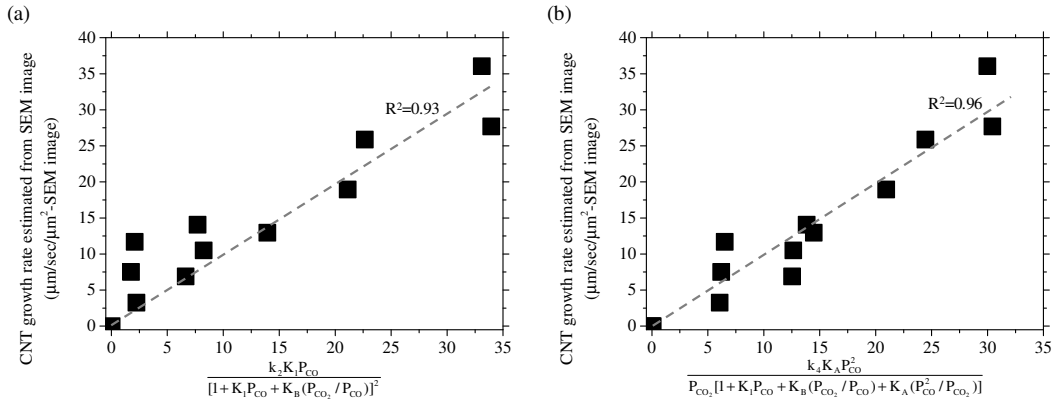

Figure 5- 10 Comparison of modeled CNT growth rates and measured ones. (a) Model 1 in which CO dissociation step is assumed to be rate-limiting, and (b) Model 2 where carbon diffusion step is assumed to be rate-limiting. In both models, carbon monoxide was supposed to be a sole CNT precursor.

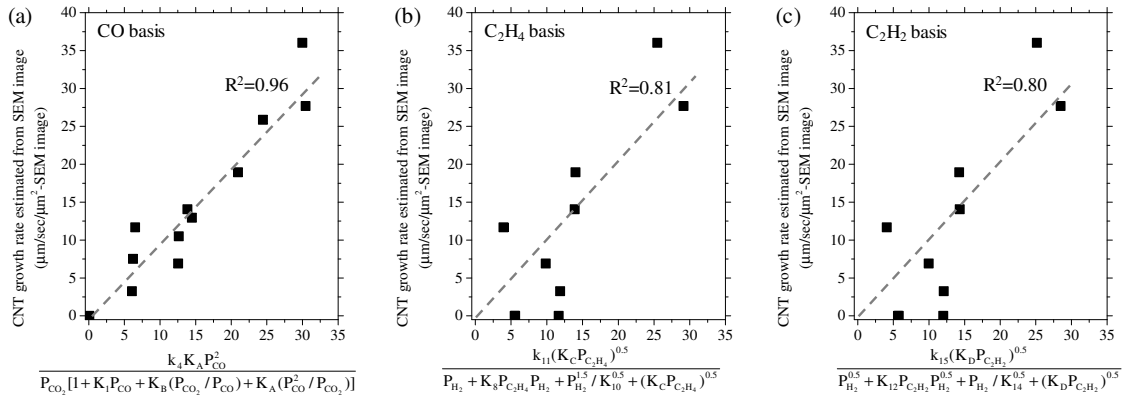

Figure 5- 11 Comparison of modeling performance employing different hydrocarbons. (a) carbon monoxide basis. (b) ethylene basis. (c) acetylene basis.

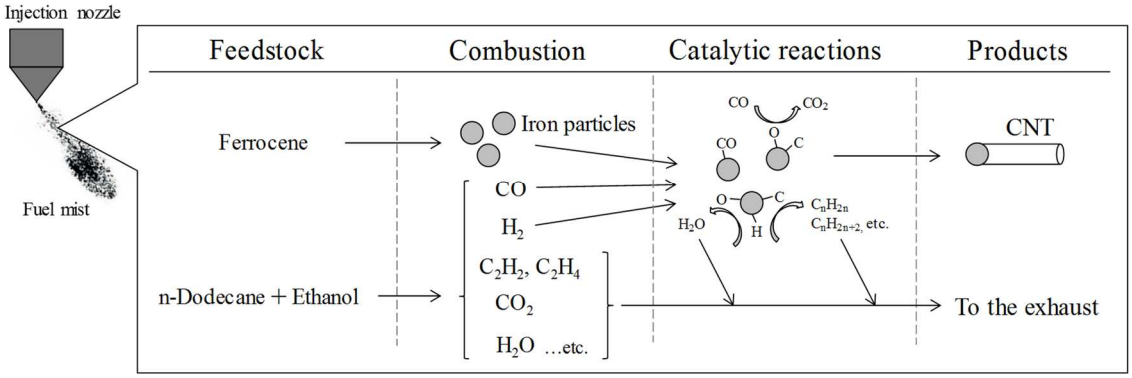

Figure 5- 12 Schematic representation showing various processes present in a diesel engine and CNT growth pathway based on findings obtained in this study.

Table 5- 1 Summary of fitting parameters in models (termed Model 1 and Model 2) using carbon monoxide and corresponding literature data if it is available.

Fitting parameters	Estimated value	Literature data
k_{20}	4.7×10^8 s^{-1}	-
ΔE_2	105 $kJmol^{-1}$	84±21 kJ/mol [161] , 107 – 114 kJ/mol [162]
k_{40}	4.5×10^2 s^{-1}	-
ΔE_4	25 $kJmol^{-1}$	37 kJ/mol [165], 34 kJ/mol [166]
K_{10}	0.5 atm^{-1} at 873 K	0.3 bar^{-1} [163], 0.9 bar^{-1} [167], 7.5 bar^{-1} [168] at 873 K
ΔH_1	-100 $kJmol^{-1}$	-92.5 kJ/mol [163], -201 – -109 kJ/mol [164]
K_{A0}	350 atm^{-1} at 873 K	-
ΔH_A	-50 $kJmol^{-1}$	-143 kJ/mol – -47 kJ/mol*
K_{B0}	0.09 at 873 K	0.021 at 798 K [163], 0.056±0.015 at 613 K [154]
ΔH_B	5 $kJmol^{-1}$	3 kJ/mol*

* Calculated from literature data presented in reference [152] and [163].

Table 5- 2 Summary of fitting parameters in a model based on ethylene and corresponding literature data if it is available.

Fitting parameters	Estimated value	Literature data
k_{110}	2.4×10^2 s^{-1}	-
ΔE_{11}	25 $kJmol^{-1}$	37 kJ/mol [165], 34 kJ/mol [166]
K_{80}	5.0×10^{-12} atm^{-1} at 873 K	1.4×10^{-12} atm^{-1} at 873 K [171], 8.7×10^{-12} atm^{-1} at 873 K [173]
ΔH_8	-60 $kJmol^{-1}$	-49 kJ/mol [169], -62 kJ/mol [171], -80 kJ/mol [170]
K_{100}	1.0×10^{10} atm at 873 K	1.4×10^{10} atm at 873 K [171]
ΔH_{10}	60 $kJmol^{-1}$	38 – 71 kJ/mol [174], 6 – 92 kJ/mol [175]
K_{C0}	1.0×10^4 atm at 873 K	-
ΔH_C	100 $kJmol^{-1}$	63 – 137 kJ/mol**

** Calculated from literature data presented in reference [176] and estimated ΔH_8 and ΔH_{10}.

Table 5- 3 Summary of fitting parameters in a model using acetylene and corresponding literature data if it is available.

Fitting parameters	Estimated value	Literature data
k_{150}	2.5×10^{2} s^{-1}	-
ΔE_{15}	25 $kJmol^{-1}$	37 kJ/mol [165], 34 kJ/mol [166]
K_{120}	1.0×10^{-27} atm^{-1} at 873 K	1.1×10^{-29} atm^{-1} at 873 K [171], 5.6×10^{-27} atm^{-1} at 873 K [173]
ΔH_{12}	-250 $kJmol^{-1}$	-206 kJ/mol [169], -273 kJ/mol [170], -285 kJ/mol [172]
K_{140}	1.0×10^{10} atm at 873 K	1.4×10^{10} atm at 873 K [171]
ΔH_{14}	60 $kJmol^{-1}$	38 – 71 kJ/mol [174], 6 – 92 kJ/mol [175]
K_{D0}	1.0×10^{4} at 873 K	-
ΔH_D	-80 $kJmol^{-1}$	-104 – -66 kJ/mol***

*** Calculated from literature data presented in reference [176] and estimated ΔH_{12} and ΔH_{14}.

Chapter 6. CNT Synthesis via Adding Hydrocarbons in Intake Line

6-1 Background of this chapter

In the previous chapter, it was strongly suggested that the most promising precursor for CNT formation in a diesel was carbon monoxide rather than other low-molecular weight hydrocarbons like acetylene and ethylene. In order to verify this implication and improve CNT productivity, we demonstrated CNT synthesis where a part of intake air was replaced with hydrocarbons.

A number of studies to investigate effects of hydrocarbon addition in intake air line on combustion characteristics, emission properties and engine performance have been carried out, e.g. hydrogen [197,198,199,200,201], CO [200], C_2H_2 [202,203], C_2H_4 [204], CH_4 [200], mixture of CH_4 and H_2 [201,205,206] and mixture of CH_4 and CO_2 [201,207,208]. Among these results, we looked into the impact on emission properties. When H_2 was added in the intake port, the quantity of unburned hydrocarbons and soot was prone to decrease because of no inclusion of atomic carbon in hydrogen molecule. In the use of CO as additive gas, emitted CO from an engine was increased while soot in an exhaust was reduced. It was reported that soot amount was increased in case of C_2H_4. Intriguingly, whether the quantity of unburned CO and soot was increased or decreased depended on the system and experimental conditions in C_2H_2. When the replacement gas based on CH_4 was employed, the general propensity that unburned CO increased but soot emission decreased was found. It is worth noting that the qualitative effect of CH_4 and CO is similar with each other in emission properties. Since additive hydrocarbons in the intake air line to a diesel engine possess some influences, it is plausible to consider that CNT formation process inside a diesel engine may be affected accordingly. According to the knowledge found in the previous chapter, carbon monoxide is most influential on CNT synthesis rather than other hydrocarbons such as acetylene and ethylene. Therefore, it can be expected that CNT production is improved by adding CO into the intake port while acetylene addition brings about undesirable or no effects on CNT synthesis. Hence, we attempted to perform the growth of CNTs through partial exchange of intake air with hydrocarbons system.

6-2 Experimental methods

Figure 6-1 displays the depiction of the experimental apparatus in this chapter. A diesel engine itself is the same one used in the previous chapter, but the intake line to an engine was modified so that additional hydrocarbons can be introduced. The mixture of n-dodecane (99.0+%, Wako Pure Chemical Industries, Ltd.) and super dehydrated ethanol (99.5+%, Wako Pure Chemical Industries, Ltd.) was used as fuel. 4 volume% of 1-octanol (98.0+%, Wako Pure Chemical Industries, Ltd.) was added for the prevention of phase separation. 5,000 ppm by mass of ferrocene (98.0+%, Wako Pure Chemical Industries, Ltd.) and sulfur powder (97.0+%, Wako Pure Chemical Industries, Ltd., S/Fe = 2.2) were dissolved into mixing fuel. An engine load was 1.65 kW in all conditions. As an additive hydrocarbon, methane, hydrogen and acetylene were employed. Although we would like to utilize CO, we gave up

using it due to its high toxicity. However, as stated in introduction, similar impacts in methane with those in CO for emission properties can be expected from the qualitative point of view. Hence, methane was employed as an alternative to carbon monoxide in this study. Besides methane, hydrogen and acetylene were used as well. It should be noted that the former does not include carbon atom in its structure but are regarded as popular gaseous fuel. The latter has been considered as one of promising CNT precursor primarily in CVD technique but its impact on CNT synthesis in a diesel engine was inferior to CO. The table to summarize experimental conditions is presented in Table 6-1. The maximum amounts of gaseous hydrocarbons introduced into the intake line were determined by the capability of current mass flow controller which was proofed by CF_4 gas in shipping. For a comparative study in reaction simulations, the concept that the replacement fraction by gaseous fuel reached approximately ten percent in injected heating value basis was adopted. For instance, the replacement fraction was about 11.7%, 11.9% and 11.4% by hydrogen 5.0 L/min, methane 1.8 L/min and acetylene 1.1 L/min, respectively. Totally, 9 samples were prepared, and CNT production was evaluated by means of microscope.

Computed calculations of combustion reactions when different gaseous fuel was added were carried out via CHEMKIN-PRO (ver. 19.0) software in order to support experimental results. The same kinetic model with that described in Chapter 5 which comprised oxidation reactions of n-dodecane, ethanol and sulfur was used in this chapter. Thermodynamic data was also identical with the one employed in the previous chapter. Closed homogeneous reactor was selected as a reactor type for the simulation. Initial gaseous fuel was the mixture of n-dodecane, ethanol and additive fuel (hydrogen or methane or acetylene) in computation. Two equivalence ratios as a representative of fuel lean (0.5) and rich (1.5) condition were employed.

6-3 Results and discussions

Figure 6-2 shows typical SEM and TEM images when H_2 gas was employed as additive gaseous fuel. CNTs were formed in all conditions and indicated by arrows in SEM image. A slight increase of CNTs was found according to SEM micrograph, but a drastic improvement was not found.

Figure 6-3 displays typical SEM and TEM micrographs as a function of methane amounts added into an intake port. It seems that there is an increase of CNT production particularly at CH_4 0.8 L/min and 1.8 L/min, however, the promoted effect of methane addition on CNT synthesis is not so large because further increase of methane up to 3.6 L/min does not provide the facilitation of CNT growth any more in comparison with CH_4 0.8 L/min and 1.8 L/min.

Figure 6-4 exhibits SEM and TEM images in the use of acetylene as an intake gas, showing different trend with hydrogen and methane. The addition of small amount of acetylene such as 0.5 L/min and 1.1 L/min brought about very slight increase of CNT formation or little change of CNT growth from

the case without any additive gas. On the other hand, when acetylene was additionally increased (3.5 L/min), CNT growth was deteriorated and actually no CNT formation was observed in this condition. In place of CNTs, aggregates consisting of soot particles and iron-based particles were found as shown in TEM micrograph. This tendency observed in acetylene is different from that in hydrogen and methane because the addition of hydrogen or methane did not present a degradation of CNT growth even when the additive amount was increased. Anyhow, according to our experimental results, the impacts of additive gaseous fuel on CNT production in a diesel engine become the following order, $CH_4 \approx H_2 > C_2H_2$.

In order to interpret the difference in behavior among hydrogen, methane and acetylene from the qualitative standpoint, combustion reactions were simulated via CHEMKIN-PRO. Figure 6-5 shows simulated results which depict the variation of mole fraction of main chemical species as reaction time proceeded up to 0.003 seconds when different gaseous fuel was added. For the comparison purpose, the cases employing H_2 5.0 L/min, CH_4 1.8 L/min and C_2H_2 1.1 L/min were simulated. The temperature and pressure for the calculation were 1,150 K and 60 atm, respectively, since the combustion temperature using n-dodecane (70 volume%) and ethanol (30 volume%) without any additive gaseous species was relatively mild as shown in the previous chapter. The molar fraction which was put on the vertical axis was not normalized because the similar behavior was given even in normalization. Let us compare the profile at fuel lean condition (equivalence ratio = 0.5) even because the similar conclusion is able to be obtained at fuel rich condition (equivalence ratio = 1.5). The similar mole fraction of interested chemical species is provided after 0.002 seconds irrespective of additive gaseous fuel. The difference among conditions become clear from reaction initiation to 0.001 seconds, while the period between 0.001 and 0.002 seconds is the transition one. What we should take care is the period from reaction initiation (0 seconds) to 0.001 seconds. When comparing H_2 addition case and CH_4 addition case, very similar profile other than H_2 and CH_4 was obtained. Hydrogen cannot be a CNT growth precursor due to no inclusion of carbon atom in its structure. As discussed in the previous chapter, CH_4 is regarded as less effective species for CNT growth. Hence, since the difference in mole fraction of H_2 and CH_4 is not influential on CNT synthesis so much, similar experimental tendency might be observed. On the other hand, the calculation in case of acetylene is important. Since C_2H_2 is present as fuel before the initiation of reaction, the maximum mole fraction of C_2H_2 in Figure 6-5 (c) is about one order of magnitude larger than that in Figure 6-5 (a) and (b). Acetylene is considered as highly reactive chemical, so the difference in C_2H_2 concentration might bring about the difference in the behavior of CNT growth shown in Figure 6-2, 6-3 and 6-4. The addition of acetylene in the intake line exhibited the negative effect on CNT growth (Figure 6-4). It might occur that abundant acetylene present in the reaction region deactivated catalytic nanoparticles owing to very rapid encapsulation by graphitic structure. On the other hand, when hydrogen and methane was used as additive gas, such a deactivation might take place less frequently, and it is probable that carbon

monoxide produced during oxidation reactions might contribute to CNT growth. This idea is consistent with the promising suggestion in the previous chapter that carbon monoxide plays a key role in CNT growth in a diesel engine rather than other hydrocarbons such as acetylene and ethylene.

6-4 Summary of this chapter

In this chapter, we attempted to investigate the effects of additive gaseous fuel in an intake line to a diesel engine on the CNT synthesis. Remarkable points are listed as follows.

- When either hydrogen or methane was utilized as additive fuel, a slight increase of CNT production was achieved. On the other hand, the degradation of CNT growth was found in the use of acetylene fed to an engine.
- The difference in the performance of CNT formation depending on additive gaseous species might be interpreted via the calculation through CHEMKIN. The large concentration of acetylene at an early stage of combustion reactions when acetylene was added might involve catalyst deactivation, resulting in the deterioration in CNT production. In the use of H_2 and CH_4, such a dire situation might be avoided.

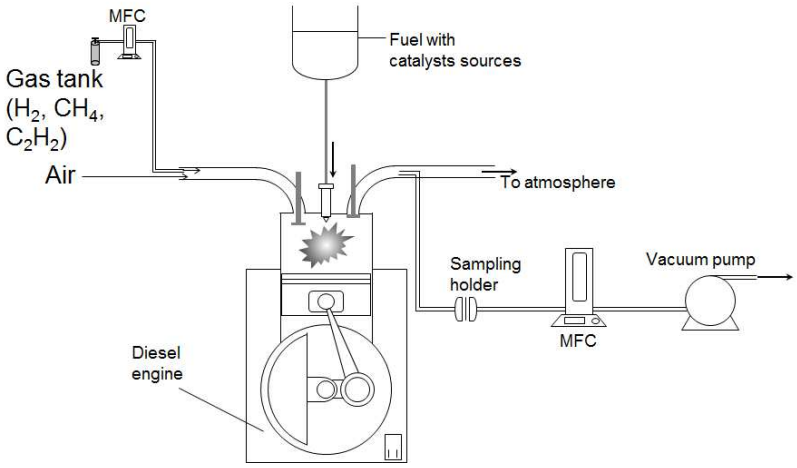

Figure 6- 1 Schematic of experimental setup for the investigation on the effect of gas replacement in intake air line.

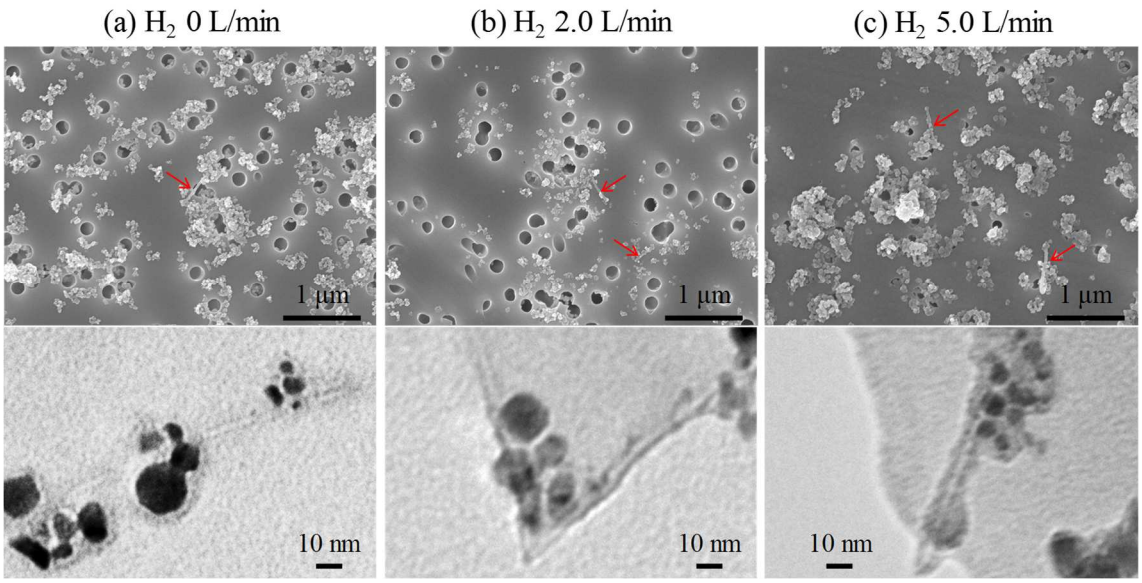

Figure 6- 2 Typical SEM and TEM micrographs of formed CNTs when hydrogen was used as an additive gas into the intake line. (a) without H_2 addition, (b) the amount of added H_2 was 2.0 L/min, and (c) the amount of added H_2 was 5.0 L/min.

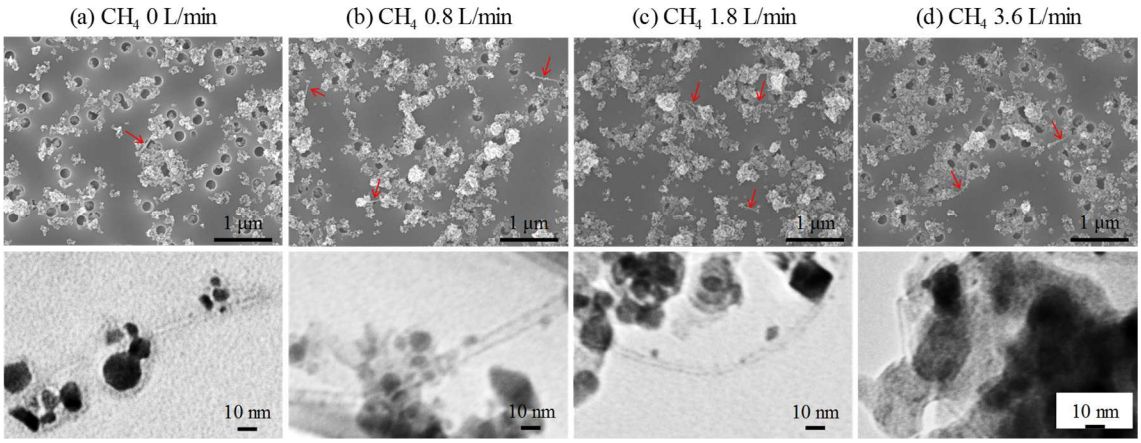

Figure 6- 3 Typical SEM and TEM micrographs of formed CNTs when methane was used as an additive gas into the intake line. (a) without CH_4 addition, (b) the amount of added CH_4 was 0.8 L/min, (c) the amount of added CH_4 was 1.8 L/min, and (d) the amount of added CH_4 was 3.6 L/min.

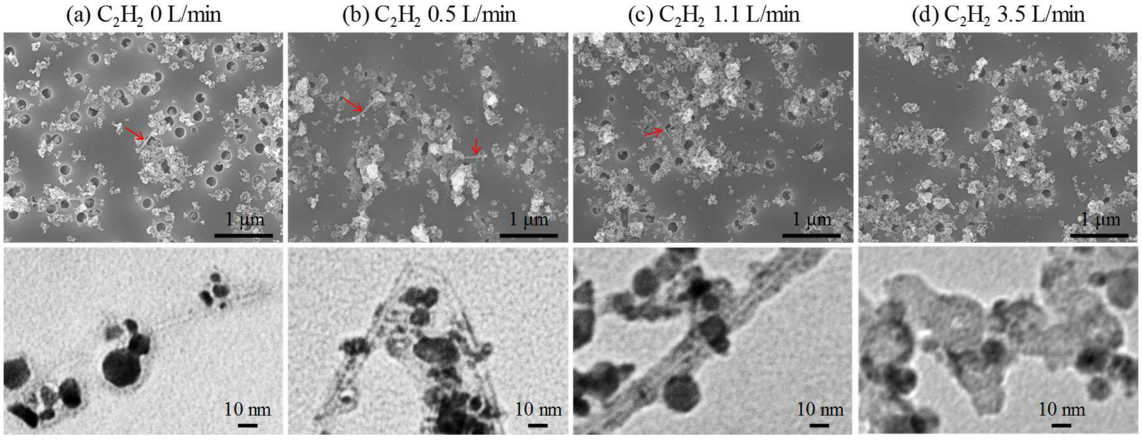

Figure 6- 4 Typical SEM and TEM micrographs of formed CNTs when acetylene was used as an additive gas into the intake line. (a) without C_2H_2 addition, (b) the amount of added C_2H_2 was 0.5 L/min, (c) the amount of added C_2H_2 was 1.1 L/min, and (d) the amount of added C_2H_2 was 3.5 L/min. In case of 3.5 L/min, no CNT formation was observed.

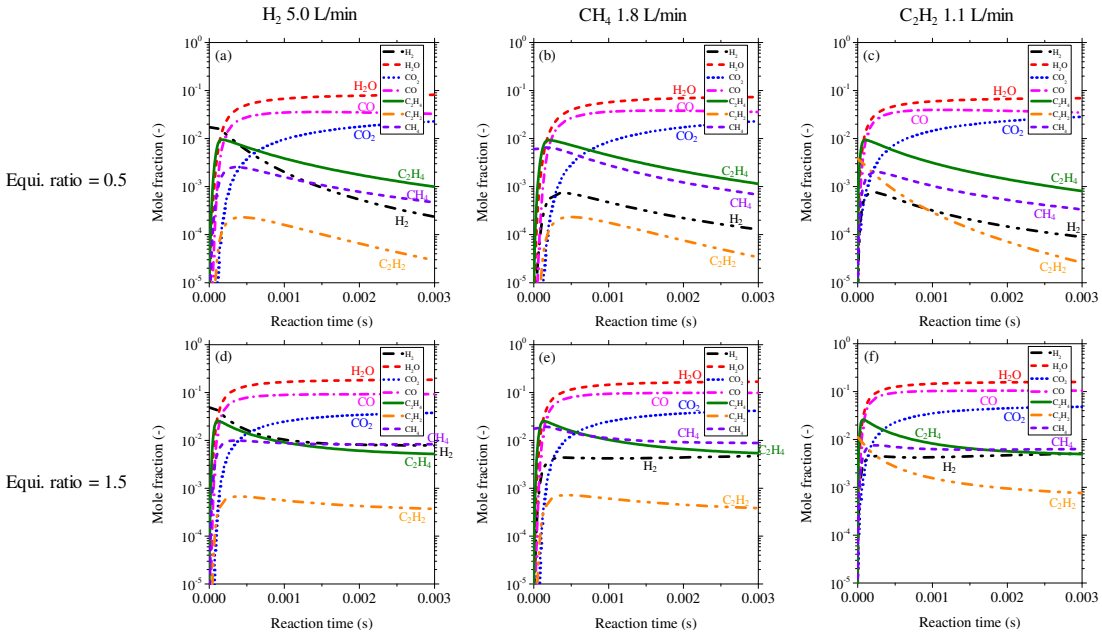

Figure 6- 5 Mole fractions of intermediate species during combustion calculated at 1,150 K and 50 atm using a closed homogeneous reactor type in CHEMKIN-PRO. The composition of liquid fuel was the mixture of n-dodecane (70 volume%) and ethanol (30 volume%) and additive gaseous fuel was changed as a parameter. Both fuel lean (equivalence ratio = 0.5) and fuel rich (equivalence ratio = 1.5) were conducted. (a) H_2 addition at an equivalence ratio of 0.5, (b) CH_4 addition at an equivalence ratio of 0.5, (c) C_2H_2 addition at an equivalence ratio of 0.5, (d) H_2 addition at an equivalence ratio of 1.5, (e) CH_4 addition at an equivalence ratio of 1.5, and (f) C_2H_2 addition an equivalence ratio of 1.5.

Table 6- 1 The summary table of experimental condition

Fuel	N-dodecane (70 volume%) + Ethanol (30 volume%)
Catalyst	Ferrocene: 5,000 ppm by weight
	Sulfur powder: S/Fe = 2.2
Engine load	1.65 kW
Additive gas	H_2: 0, 2.0, 5.0 L/min
	CH_4: 0, 0.8, 1.8, 3.6 L/min
	C_2H_2: 0, 0.5, 1.1, 3.5 L/min

Chapter 7. Impacts of Sulfur on CNT Growth in Chemical Vapor Deposition

7-1 Background of this chapter

In our study to use a diesel engine for the synthesis of CNTs, one of key factors was the introduction of sulfur as a CNT growth promoter. However, the real role of sulfur in CNT synthesis is still an open question in spite of a lot of efforts by a number of research groups. Hence, we tried to elucidate the role of sulfur in CNT growth in the employment of chemical vapor deposition (CVD) process instead of flame process because flame process is a rather complicated system. Firstly, after we mention several approaches using several additives for the purpose of CNT synthesis promotion, various influences of sulfur addition on the growth of CNTs reported until now are given in this section. The influences which are picked up in this section are mainly correlated with CVD method, but not limited to it. Then, from next sections, detailed experimental methods and obtained results will be expressed. We believe that findings obtained in this chapter strongly supports our results in an internal combustion system in terms of the role of sulfur.

Some techniques such as introducing additives in gas phase or into a catalyst layer have been employed till now for increasing the CNT production. For instance, chlorine was employed as a CNT growth enhancer in arc discharge [209] and CVD process [210]. Phosphorous also exhibited promotion effects of carbon fiber growth [211] and CNT synthesis [212] probably due to interaction with catalyst. Further interestingly, Huang et al. [213] and Mas et al. [214] employed selenium as an enhancer in arc discharge and floating-catalyst CVD, respectively. However, the most well-known and frequently used promoter is sulfur or sulfur-included compounds like hydrogen sulfide and thiophene for the growth of carbon fiber [215,216] and CNTs [217,218,219,220,221,222,223,224,225,226]. The addition of sulfur-containing compounds is a versatile approach because it hardly limits the catalyst choice according to preceding articles, namely the performance of Fe [216,217,219,220,221,222,223,224,226], Fe/Cu/quartz [225], Co [215,227] and Co/Mo [218] was improved via a sulfur addition. Thus, we can regard influences caused by sulfur on CNT synthesis as generalized phenomena. In our study to use a diesel engine as a reactor for the successful synthesis of CNTs, one of key factors is the introduction of sulfur. Not only our research but also other group reported recently that the presence of both Fe catalyst and sulfur increased CNT production in a diesel engine system [228]. The approach to form CNTs via an internal combustion system is very similar with floating catalyst CVD in terms of mechanism in catalyst particle formation and CNT growth. Most of works to study the effect of sulfur have been primarily dedicated to the floating catalyst CVD system. Several ideas to explain the role of sulfur as a promoter have been put forth so far, e.g. the prevention of catalyst deactivation by sulfur adsorption due to mild carbon supply [215], enhanced carbon diffusion in catalyst because of the reduction of catalyst melting point as a result of alloy formation between metal and sulfur [216], lowered catalyst surface energy in a metal-sulfur system leading to easy lift-off of carbon cap [229,230] and others. Although many studies have been devoted to investigate effects of sulfur on CNT formation, its role during CNT growth is still controversial

even today and further work to reveal it is required. In spite of the fact that sulfur has been recognized as a poisoning agent to degrade catalyst performance, a small amount of sulfur surprisingly functions as an improver of catalyst activity and/or selectivity such as in Fischer-Tropsch reaction and steam reforming [231]. According to this review, the catalyst performance is basically dependent on sulfur content added into the system [231]: when sulfur amount is low, catalyst activation becomes improved. When it is increased, catalyst selectivity is modified, and a further increase of sulfur leads to the loss of catalyst performance. These transitions of catalyst performance may be attributed to the electron dispersion change on catalyst surface and/or the alteration of adsorption properties owing to a coverage by sulfur, but explicit reasons to interpret the role of sulfur as a catalyst modifier are not enough presented in this field too. Interestingly, the addition of sulfur brings a lot of impacts on CNT, e.g. not only its growth promotion but also CNT morphology, CNT diameter, chirality and so on. Some research groups have reported that sulfur contributed to grow Y-shaped CNTs with many branches [232,233,234,235,236,237]. Wang et al. found that CNT morphology was changed from bamboo-like structure to compartment-free CNTs [238]. With regards to CNT diameter and the number of graphite layer, some studies observed that CNT diameter size and wall number increased via sulfur addition [222,226,229,239,240,241], but only a few results showed a different propensity that a small amount of sulfur reduced the CNT size at first while it was increased at an elevated sulfur concentration [242]. According to some publications, sulfur is also useful for selectively synthesizing single-walled carbon nanotube (SWNT) with specific chirality [243,244,245,246]. Sulfur affects catalyst particle as well: the enlargement of particle size could be suppressed due to the prevention of coalescence in the presence of sulfur [246,247,248], while Lee et al. found that whether catalyst particle size became increased or decreased depended on the combination of sulfur/carbon source used [249]. We are convinced that detailed analysis on catalyst nanoparticles performed here may provide helpful information to understand the behavior of sulfur in CNT formation, not only in CNT growth enhancement but also in the change of CNT morphology, the size shift of CNT/catalyst nanoparticles and others. In this chapter, we attempted to present insights on the role of sulfur mainly through kinetic approach and various characterization methods.

This chapter consists of mainly three sections. Firstly, we carried out a comparison study using a two types of catalyst conditions, basic catalyst (Co and Mo) free from sulfur and basic catalyst + sulfur (sulfur powder), in order to confirm the effectiveness of sulfur in CNT formation. Then, some characterization methods were performed for the interpretation of the difference between above two catalytic conditions and for the proposal on the role of sulfur during CNT growth. Finally, the impacts of sulfur source on CNT synthesis were investigated in the employment of sulfur powder and thiourea as a sulfur source.

7-2 Experimental methods

7-2-1 CNT growth

In this study, cobalt-molybdenum co-catalyst was employed as a base catalyst because this catalyst has been authorized and practically enabled commercial production of CNTs [250,251]. Though we wanted to use Fe-base catalyst in this chapter because Fe catalyst was employed from Chapter 2 to Chapter 6, CNT growth was hardly found in the employement of Fe alone or Fe/Mo co-catalyst on a substrate even in similar conditions/procedures with those in Co/Mo. In order to grow CNTs in the use of Fe/Mo catalyst, reduction operation should be initiated at the same time as temperature rising and CO/H_2 mixing gas should be supplied during CVD. As well as condition/procedure change, longer CVD time was required in Fe/Mo catalyst compared with Co/Mo even when condition and procedure were improved. We suppose that the similar effect of sulfur on CNT synthesis in both Fe and Co catalyst may take place because CNT growth promotion was found not only in Fe but also in Co according to preceding papers. Quartz with 0.3 millimeter thickness (Tokyo Glass Kikai Corp.) and carbon monoxide were used as a substrate and carbon precursor, respectively. Two kinds of sulfur sources were employed in this study, sulfur powder and thiourea. We prepared three types of samples for a comparison study, namely, Co/Mo alone, Co/Mo/S derived from thiourea, and Co/Mo/S derived from sulfur powder. A synthetic process of CNTs from several catalyst layers is schematically described in Figure 7-1 (a). Quartz substrate was calcined at 900 ^oC in air for more than one hour before utilization in order to eliminate carbonaceous impurities on it. A dip-coating method was utilized for forming a catalyst layer on a substrate. Cobalt acetate (95%, Wako Pure Chemical Industries, Ltd.) and molybdenum acetate dimer (98%, Sigma-Aldrich) used as a Co and Mo precursor respectively were dissolved in super dehydrated ethanol (99.5+%, Wako Pure Chemical Industries, Ltd.) through ultra-sonication. Their concentration was 0.05 wt% against ethanol. When Co/Mo/S derived from thiourea was prepared, thiourea (98.0+%, Wako Pure Chemical Industries, Ltd.) was put into an ethanol solvent in addition to cobalt acetate and molybdenum acetate dimer. After immersing a substrate in a tailored solution for 10 minutes, it was drawn from the solution at a constant speed of 0.96 cm/min. Then, the substrate was calcined in air at 400 ^oC for 5 minutes to decompose precursors to form catalyst particles, and then cooled down to room temperature. In case of Co/Mo and Co/Mo/S stemmed from thiourea, the substrate was moved to a furnace to carry out a next operation (reduction operation). On the other hand, for preparing Co/Mo/S derived from sulfur powder, an additional dip-coating was required to load sulfur on a substrate. Quartz substrate was again dip-coated into the tailored solution that sulfur powder (98.0+%, Wako Pure Chemical Industries, Ltd.) was dissolved in a toluene solvent (99.5+%, Wako Pure Chemical Industries, Ltd.). An immersion time in toluene and a drawing speed of a substrate from it were identical with that for forming a Co/Mo layer. Then, all substrates were inserted into a furnace and temperature was elevated up to 800 ^oC under Ar atmosphere. A reduction operation was carried out at 800 ^oC for 30 minutes to form active catalyst particles under

the condition that flow rates of Ar (>99.999%) and H_2 (>99.99%) were 60 sccm and 40 sccm, respectively. Temperature inside a furnace was adjusted to given temperatures for CVD under Ar atmosphere after a reduction operation was completed. CVD process to deposit carbon on a substrate was performed at given temperatures under the condition that flow rates of carbon monoxide (>99.95%) and Ar were 45 sccm and 155 sccm, respectively. When impacts of oxygen on CNT synthesis were investigated, O_2 was also fed into a reactor besides CO and Ar. Both a reduction and CVD were carried out at atmospheric pressure. Schematic of an experimental set-up for a reduction and CVD operation is displayed in Figure 7-1 (b). When CVD was completed, a flow of carbon monoxide was stopped and a furnace was quenched to room temperature with Ar flowing. The substrate was then taken out from a furnace.

7-2-2 Characterizations

Field emission scanning electron microscopy (FE-SEM, JEOL JSM-7500F) was employed to know CNT production on the substrate after CVD. Samples were coated with a layer of Pt-Pd by ion sputtering (HITACHI E-1030) with a current of 15 mA for 60 seconds before observations. In order to obtain information about CNT morphology, high-resolution transmission electron microscopy at 200 kV (HR-TEM, JEOL JEM2010F) was performed. For CNT observations, CNTs grown on a substrate were directly scratched to a TEM grid. For observation of catalyst nanoparticles in HR-TEM, silicon substrate with SiO_2 layer (approximately one hundred nanometers) on surface was employed instead of quartz. We confirmed that there is no difference in CNT production between SiO_2/Si and quartz substrate. Raman spectroscopy (JASCO NRS-4100, 532 nm diode laser) was implemented to evaluate a CNT quality and speculate the presence of SWNT and its diameters. Laser was irradiated from a top direction on samples and a spot diameter was 100 μm. A substrate surface was explored by means of atomic force microscopy (AFM, SHIMADZU SPM-9600) to get surface information. Samples with and without sulfur, and before and after CVD were prepared for AFM analysis. Samples before CVD mean that a substrate undergoes up to a reduction operation, and those after CVD are that CVD is done at 800 ^oC for 10 minutes after catalyst deposition. Survey area was 250 nm × 250 nm in each measurement. Time-of-flight secondary ion mass spectroscopy (TOF-SIMS, HITACHI TOF-SIMS 5-100-AD) was available for examining elemental profile data of catalyst layer in depth direction. We used Cs ion gun at current 20 nA to detect negative ions of substrate with the area of 100 μm × 100 μm. Inductive coupled plasma (ICP, AGILENT 5100 VDV ICP-OES) was used to estimate bulk compositions of catalyst layer. Because catalyst amounts loaded on a substrate was tiny, large coated area of approximately 9 cm^2 was prepared for the detection. Two types of samples were made, the substrate coated with Co/Mo/S derived from sulfur powder and one coated with only sulfur power. Both samples underwent up to a reduction (no CVD). The chemical states of catalyst particles were determined by X-ray photoluminescence spectroscopy (XPS, ULVAC-PHI Perkin Elmer X-ray

Photoelectron Spectrometer 5500MT). Spectra were acquired using a monochromatic Al Kα source operated at 14.0 kV under charge neutralization. For detection of Co and Mo, a substrate was dip-coated one time. On the other hand, in case of S detection, Co/Mo layer was dip-coated many times because sulfur could not be detected through only one Co/Mo dip-coating due to the overlapping of strong Si peak and weak S peak. It should be noted that dip-coating of sulfur powder was done only one time in this case. For deconvolution of obtained peaks, a Shirley background was used. For the estimation of CNT growth rate, three approaches were employed. First one was to use top-viewed SEM micrographs and to treat them by image processing free software, ImageJ, and then to assess CNT growth rate per substrate (k, $\mu m^2/cm^2$-substrate/min) on the basis of the occupied area by CNTs in SEM images. Several images were employed for the purpose of ensuring reliability. Second one was to use the transmission of substrate in nearly visible light (350–800 nm as wavelength) and to estimate CNT quantity on substrate by means of Lambert-Beer relation, then CNT growth rate was calculated. Transmittance of sample was measured by double beam spectrophotometer (HITACHI, U-2910). Relative CNT production on a substrate via the change in several experimental parameters was evaluated by this technique in the past [252]. Third approach was to use sheet resistance of grown CNT on a substrate. Since the thickness of CNT layer on substrate, namely CNT quantity, has inverse relationship with sheet resistance, CNT growth rate is able to be estimated by means of sheet resistance [253]. 4-points probes resistivity processor (NPS, Inc.) was used for measuring resistance of CNT. All three methods possess advantages and disadvantages. For instance, there is the possibility that the evaluation via image treatment may underestimate CNT growth owing to overlapping of CNTs with each other, but this technique is quite facile and simple. On the other hand, the evaluation through transmission has a potential to reflect information stemmed from not only CNTs but also amorphous carbon formed during CVD in the final result. It can be considered that electrical characteristics of grown CNTs may be affected by the change of CVD temperature, which may influence not only the graphitization of CNTs but also the chirality of them. Moreover, if there is no connecting path between CNTs, sheet resistance cannot be measured even when CNTs were formed on the substrate. However, by performing three approaches, there is increase in the possibility that we are able to gain highly reliable results and conclusion.

7-3 Results and discussions

7-3-1 Promoted growth of CNTs using sulfur

As a first step, since we tried to confirm whether promoted growth of CNTs occurred through the addition of sulfur, two samples, Co/Mo free from sulfur and Co/Mo/Sulfur powder, were compared.

In order to identify the optimum sulfur loading, CNT growth on a substrate was carried out as a function of sulfur amounts as shown in Figure 7-2. These figures show top-view SEM images of the

substrate using sulfur powder as a sulfur source after CVD was carried out at 800 °C for 30 minutes, and Raman results of each condition were inserted in corresponding SEM photographs. In Figure 7-2 (a) and (b), dissolved amounts of sulfur powder in toluene were changed while a drawing speed of a substrate from a solution was 0.96 cm/min. On the other hand, in Figures 7-2 (b) and (c), a drawing speed was increased from 0.96 cm/min to 9.96 cm/min keeping a dissolved amounts of sulfur powder 2.0 wt%. Because the concentration of sulfur powder in a toluene solution, 2.0 wt%, was close to the upper limit in this study, we had to alter a drawing speed of dip-coating from 0.96 cm/min to 9.96 cm/min to load sulfur powder on a substrate more. This condition was comparable with sulfur powder of approximately 9.5 wt% in toluene at a drawing speed of 0.96 cm/min. The maximum point of CNT production was observed in Figure 7-2 (b). Two characteristic peaks were detected at around 1590 cm^{-1} (G peak) and 1340 cm^{-1} (D peak) which was stemmed from six-membered ring structure and its defects, respectively. In general terms, when CNT production is increased, G peak intensity becomes strong. The ratio of peak intensity of G band and D band (I_G/I_D) has been widely used as a criterion which indicates the degree of graphitization in a graphite structure. As a reference, I_G/I_D in the employment of sulfur powder 2.0 wt% and 0.96 cm/min was calculated to be 27, revealing the formation of highly graphitized CNTs. The presence of a maximum point of CNT production was also presented in other works using phosphorous [211] and sulfur [236,245] as a promoter. The phenomenon seen in sulfur powder may be explained by the idea that poisoning effects by sulfur counteract promotion effects when sulfur amounts in a catalyst layer are too increased. Sulfur powder of 2.0 wt% in solvent was employed in the following measurements.

Next, in order to confirm the effectiveness of sulfur in CNT formation, SEM images of samples with and without a sulfur powder after CVD were compared. Figure 7-3 shows top-view SEM images of the substrate after a CVD process for 30 minutes when the catalyst condition and CVD temperature are changed. Raman spectra corresponding to SEM micrograph are also inserted. At 800 °C, small quantity of CNTs were grown on the substrate with Co/Mo alone in Figure 7-3 (a). On the other hand, when a sulfur source was added into a catalyst layer, the formation of CNTs which were grown in a carpet-like structure was found in Figure 7-3 (d). When CVD temperature was reduced to 750 °C, CNT growth was indeed enhanced in the presence of sulfur but the difference in CNT production between the cases with and without sulfur seemed to be diminished as shown in Figures 7-3 (b) and (e). When temperature was further decreased to 700 °C, the promoting effect by sulfur could be still found although absolute CNT production was reduced in two conditions as shown in Figures 7-3 (c) and (f). The behavior of G peak intensity in Raman spectra was roughly consistent with CNT formation amount. Importantly, it could be confirmed that CNT growth was facilitated by adding sulfur in our system, which is in line with other CVD processes like floating catalyst CVD.

Figure 7-4 shows the dependence of CNT growth on O_2 flow rate in feedstock. One of our motivations in this study is originated from the flame process synthesizing CNTs by a diesel engine,

where it was difficult to synthesize CNTs owing to the presence of O_2, but the addition of sulfur was one of key factors for the successful synthesis of CNTs even in the presence of oxygen. Hence, it is of importance to investigate impacts of O_2 present in feed gas on CNT growth. CVD was carried out at 750 ^oC for 60 minutes in all conditions. When O_2 was introduced into feedstock to check the effect of oxygen on CNT growth, O_2 flow rate was varied from 0 sccm to 0.3 sccm and the flow rate of carbon monoxide and Ar was 45 sccm and balanced, respectively, so that the total flow rate became 200 sccm. According to SEM pictures in Figure 7-4, the catalytic ability was very sensitive to O_2 flow rate. Lots of CNTs were grown in the absence of oxygen (O_2 = 0 sccm) irrespective of sulfur addition in this condition. By contrast, CNTs hardly grew in all catalyst conditions at O_2 flow rate larger than 0.2 sccm. Distinct differences between catalyst conditions can be recognized at O_2 = 0.1 sccm, showing that the growth of CNTs was rarely found without sulfur powder, but CNTs were surely produced in the presence of sulfur. Although absolute CNT production is reduced with increasing O_2 flow rate from 0 to 0.1 sccm, it is reasonable to consider that promoting effects of sulfur on CNT formation compensate the negative effect caused by oxygen. From Figure 7-4, it was confirmed that sulfur was effective as a CNT growth enhancer even when oxygen was present in feedstock, being consistent with our previous findings in a diesel engine system.

Based on SEM micrographs like Figure 7-3, CNT growth rate, k, was estimated in each experimental condition. Then, the relationship between natural logarithm of CNT growth rate, $\ln(k)$, and the inverse of a CVD temperature between 600 and 800 ^oC, $1/T$, was drawn in Figure 7-5. The evaluation technique to utilize image treatment was employed here. It should be noted that CVD duration was extended at low CVD temperatures for an appropriate estimation. Both catalyst conditions clearly showed Arrhenius relation under 750 ^oC, $\ln(k) = \ln(A) - E_a/RT$, where A is a frequency factor, E_a is activation energy required for CNT growth and R is a gas constant. When CVD temperature was higher than 750 ^oC, the relationship deviated from the Arrhenius law in both conditions. This deviation is explained by thermodynamic point of view because CO disproportionation reaction became disadvantageous in such high temperature and carbon deposition became deteriorated. Estimated activation energy in Co/Mo/Sulfur powder 2.0 wt% and Co/Mo was 15 and 95 kJ/mol, respectively. It is obvious that the addition of sulfur greatly reduced activation energy. Information on the activation energy for CNT growth is quite important because it gives us fruitful clues about a rate-limiting step. According to the criteria provided by Jourdain and Bichara [254], it can be implied that the rate-limiting step in case of Co/Mo/Sulfur powder 2.0 wt% (15 kJ/mol) is surface diffusion of carbon atom on catalyst or bulk diffusion of carbon atom in liquid phase catalyst, while that in Co/Mo (95 kJ/mol) is bulk diffusion of carbon atom in solid phase catalyst. Detailed discussion will be carried out in a later section.

7-3-2 Characterizations on catalytic particles

As shown in the previous section, CNT growth is enhanced in the presence of sulfur, and this may mean that the properties of catalytic nanoparticles were significantly affected. Therefore, several characterizations on catalytic particles were performed in order to provide the insight on the role of sulfur in CNT synthesis and to clarify the difference in CNT growth using sulfur powder or no sulfur.

Surface morphologies of substrates before and after CVD surveyed by AFM are shown in Figure 7-6. The pictures before CVD (Figures 7-6 (a) and (b)) were taken for samples after reduction in H_2/Ar at 800 ^oC for 30 minutes, and those after CVD (Figure (c) and (d)) were taken after CVD with CO/Ar at 800 ^oC for 10 minutes. This short CVD time hardly grow CNTs even when sulfur was employed. Regardless of before and after CVD, AFM observations provided the similar tendency that the surface of Co/Mo with sulfur powder seemed smooth while that of Co/Mo without sulfur was rough, implying the presence of smaller particles formed in the case using sulfur powder. However, since information of z-direction (height direction) is emphasized in AFM, actual difference in particle size may not be so large. It should be noted that some valleys in AFM images (for instance, Figure 7-6 (d)) could be observed in all catalyst conditions, probably due to cracks inherent in substrate and/or formed during annealing.

Figure 7-7 shows typical HR-TEM images of catalyst nanoparticles formed on a substrate in the absence and presence of sulfur after CVD at 750 ^oC for 180 minutes. HR-TEM micrograph of Co/Mo shows clear lattice fringe of catalyst particles whose distance was approximately 0.2 nm in Figure 7-7 (a). This spacing of lattice fringe obtained is well consistent with metallic cobalt according to preceding articles [255,256,257]. Thus, we can consider that cobalt behaved as a catalyst for growing CNTs instead of molybdenum, being supported by Sugime et al. [252]. On the other hand, in Figure 7-7 (b) where Co/Mo/Sulfur powder 2.0 wt% was used as a catalyst condition, ambiguous lattice fringe was observed, suggesting a less crystal structure compared with a Co/Mo system. We speculate that the catalyst particle which contributes to CNT growth in Co/Mo/Sulfur powder 2.0 wt% may be cobalt sulfides instead of metallic cobalt because other researches using sulfur as a promoter in CNT growth indicated that the chemical state of catalytic particles was cobalt sulfides [234,258]. Also, if cobalt sulfide is formed, it can be expected that the melting temperature is reduced according to Co-S phase diagram owing to the presence of eutectic point [259,260], corroborating ambiguous lattice fringe in Co/Mo/Sulfur powder 2.0 wt%. Histogram of catalyst particle diameters was prepared on the basis of a number of HR-TEM images shown in Figure 7-7. It shows narrower particle size distribution in Co/Mo/Sulfur powder 2.0 wt% although average diameters are almost identical with each other. The presence of large particle size in a Co/Mo free from sulfur may interpret the results in Figure 7-6, namely, this kind of large particles may make the surface in Co/Mo rougher.

In order to confirm whether sulfur formed some kinds of chemical bond with catalytic metals, further characterizations were performed. Firstly, elemental depth profile was examined via TOF-SIMS as shown in Figure 7-8. Figure 7-8 (a) is a depth profile of Co/Mo/Sulfur powder 2.0 wt% and Figure 7-

8 (b) is that of a sample when sulfur powder alone was coated on a quartz substrate without Co and Mo deposition. Both samples underwent up to the reduction operation and no CVD was conducted. It should be noted that because minus ion of Mo was too weak, the intensity of MoS^- was shown instead. If sulfur coexisted with Co and Mo, the detection of sulfur was possible, Figure 7-8 (a). However, the signal of sulfur in Figure 7-8 (b) was almost constant, indicating the absence of sulfur in this case since relative intensity is meaningful rather than absolute intensity in TOF-SIMS. Sulfur deposited on a substrate might be removed during heating-up and/or reduction operation probably because sulfur had no capability of forming chemical bonds with quartz. On the other hand, Figure 7-8 (a) suggests that sulfur could bind with cobalt and/or molybdenum when they were present on a substrate. Similar propensity was acquired in ICP analysis as well. All three elements, Co, Mo and S, could be detected in the analysis of Co/Mo/Sulfur powder 2.0 wt%, while the intensity of S in a sample coated with only sulfur was lower than the detection limit which was approximately several tens of parts per billion. This fact also supports the idea proposed in Figure 7-7 that the chemical bond between sulfur and transition metal is likely formed. Another remarkable point in Figure 7-8 (a) is that sulfur peak appears earlier than cobalt peak, implying that sulfur mainly exists near on the surface of catalyst and does not penetrate into catalyst deeply. Sulfur was preferentially present in the vicinity of surface rather than inside the bulk probably because sulfur acted as an agent to reduce the surface energy, and actually very thin layer including sulfur was formed on the surface of metals as reported by some publications, e.g. floating catalyst CVD technique [224,261] for CNT synthesis and the study on Fe-C-S melts in metallurgy [262]. The elemental depth profile of Co/Mo/Sulfur powder 2.0 wt% after CVD was carried out at 800 ^oC for 10 minutes showed similar behavior with Figure 7-8 (a).

To obtain information on chemical states of catalyst, XPS analysis was performed for the sample of Co/Mo/Sulfur powder 2.0 wt% as shown in Figure 7-9. Spectra of cobalt $2p_{3/2}$ were separated into three peaks, 778.1 eV, 781.0 eV and 786.0 eV at its center, Figure 7-9 (a). These peak locations provide us clues to understand the chemical state of cobalt. According to previous publications, the binding energy attributed to metallic cobalt (Co^0) and cobalt sulfide ranged 777.8–778.5 eV [263,264,265] and 778.1–778.6 eV [266,267,268,269], respectively. Co $2p_{3/2}$ levels corresponding to Co^{+2} in CoO and $CoMoO_x$ were reported to be 780.0–781.9 eV [263,264,266,269] and 780.5–781.2 eV [263], respectively. There are two scenarios that Co $2p_{3/2}$ binding energy at 778.1 eV in our work are assigned to metallic Co and/or cobalt sulfide due to their peak overlapping in references. By contrast, 781.0 eV in our work is obviously assigned to Co^{+2}, probably being stemmed from cobalt oxide. The binding energy at 786.0 eV in our XPS results can be regarded as a satellite. Spectra of molybdenum were analyzed as well in Figure 7-9 (b), and the chemical state of Mo was Mo^{+4} (228.5 eV in Mo $3d_{5/2}$) and Mo^{+6} (232.0 eV in Mo $3d_{5/2}$), being consistent with preceding papers [263,264,265,267,268]. Although spectra of Co $2p_{3/2}$ and Mo 3d presented some information, it was inadequate for us to elucidate exact chemical bonding, e.g. metallic state and/or sulfide state. On the other hand, the spectrum of sulfur 2p

seems helpful for rationalizing chemical bonding formed in a catalyst layer since two peaks, S $2p_{3/2}$ (160.7 eV) and S $2p_{1/2}$ (161.7 eV), were found as a result of deconvolution. These values are well consistent with those attributed to metal sulfide such as Co-S [265,268,270]. This information strongly indicates that cobalt sulfides and/or molybdenum sulfides are formed on the substrate surface. The presence of reduced state of sulfur is consistent with results in TOF-SIMS (not shown here) that no detection of positive ions of sulfur was observed.

In order to confirm the implication in TOF-SIMS and XPS, thermodynamic approach was employed. By means of calculations using Outokumpu HSC Chemistry for Windows (ver. 2.0), the differences of reaction Gibbs energies from metal oxides with sulfur to metal sulfides and sulfur dioxide become negative over the whole temperature range interested in this work, as shown in Figure 7-10. In addition, the formation of cobalt sulfide from cobalt oxide and sulfur is facilitated in the presence of hydrogen. According to this calculation, it is suggested that in our system, chemical bonds between sulfur and catalytic metals might be formed during not only heating-up from room temperature to given temperature for reduction but also reduction itself.

7-3-3 Impacts of sulfur source on CNT growth

Finally, we examined impact of different sulfur sources on CNT growth by using not only sulfur powder but also thiourea as a sulfur source. To our knowledge, there is hardly reported on the influences of different sulfur compounds on CNT synthesis in substrate catalyst CVD process. Hence, it is of importance to grasp advantage/disadvantage brought by various sulfur species in order to improve the understanding of CNT synthesis technique employing sulfur more sophisticatedly.

As well as the optimization of sulfur loading in case of sulfur powder (Figure 7-2), CNT production as a function of thiourea content in solvent was explored in Figure 7-11. The concentration of thiourea was altered from 0.14 wt% to 3.5 wt%. It should be noted that thiourea of 3.5 wt% was close to the upper limit of thiourea dissolution in ethanol. As shown in this figure, CNT production was increased along with the increase in thiourea concentration. Thus, we employed 3.5 wt% as a thiourea content in the following experiments.

Figure 7-12 shows top-viewed SEM micrographs of the substrate when catalyst conditions and CVD temperature are altered. As an example of the effect of temperature on CNT growth, 750 ^{o}C and 650 ^{o}C were selected. CVD duration was 30 minutes except for Figure 7-12 (d), in which it was 60 minutes. Abundant CNTs were synthesized at 750 ^{o}C irrespective of catalyst condition in Figure 7-12 (a)–(c). On the other hand, large difference was found among catalytic conditions at 650 ^{o}C in Figure 7-12 (d)–(f). The sample using thiourea and sulfur powder showed CNT production while CNTs were hardly grown in Co/Mo free from sulfur source even when CVD time was extended twice. Although absolute CNT production was larger in Co/Mo/Sulfur powder than Co/Mo/Thiourea, sulfur certainly possessed the effect to promote CNT synthesis.

High resolution TEM images of as-grown CNTs with and without sulfur source are shown in Figure 7-13. CVD was performed at 750 ºC for 180 minutes for making it easy to transfer synthesized CNTs to a TEM grid. Synthesized CNTs were predominantly SWNTs, including very little multi-walled carbon nanotube (MWNT) with a few layers such as double walled carbon nanotube irrespective of catalytic conditions. The presence of SWNTs in both samples could be supported by the appearance of radial breathing mode (RBM) in Raman spectra. Although SWNTs were primarily synthesized irrespective of sulfur addition, the distribution of CNT outer diameters was a little different as indicated by histogram in Figure 7-13. Histogram which was prepared based on TEM photographs shows that the average CNT diameter using Co/Mo catalyst including sulfur tends to be slightly smaller than that using Co/Mo catalyst free from sulfur. RBM behaviors show that strong peaks at a larger Raman shift appear in Co/Mo catalyst including sulfur, suggesting that CNTs with a smaller diameter are formed in the presence of sulfur because Raman shifts in the RBM region have an inverse relationship with CNT diameters [271,272]. When compared between thiourea and sulfur powder, the former provided a little smaller CNT diameter than the latter.

Figure 7-14 displays the dependence of CNT growth rate on CVD temperature evaluated via three approaches, (a) is the evaluation by image treatment through SEM images, (b) is the evaluation by transmission in visible light and (c) is assessed via sheet resistance of grown CNTs on a substrate. Natural logarithm of CNT growth rate, ln(k), is put on the vertical axis, and the inverse of CVD temperature, 1/T, is put on horizontal axis. It should be noted that there is shortage of data points in assessment technique using sheet resistance owing to unmeasurably high resistivity for the sample with thin CNT layers. Since all three approaches indicate the good linearity within the studied temperature range, activation energy required for CNT growth, E_a, was calculated by Arrhenius equation. Activation energy in each experimental condition is summarized in Table 7-1, which shows similar propensity that the lowest activation energy is given in Co/Mo/Sulfur powder, the largest one is obtained in Co/Mo alone, and its intermediate is found in Co/Mo/Thiourea. When compared among three evaluation methods, the conclusion cannot be affected because there exist relatively small differences in the value of activation energy given by these three technique. The considerations on the difference in the activation barrier between thiourea and sulfur powder are conducted in later section.

The relation between transmittance and sheet resistance of samples prepared with different catalyst conditions are depicted in Figure 7-15. This relationship becomes important in transparent conductive film. Since CNTs are directly grown on a substrate in our work, several data in similar works where carbon materials were directly synthesized on a substrate are also provided in this figure, e.g. SWNT film [273,274] and multi-walled CNT/graphene composite film [275]. According to the previous paper, the trade-off relation between transmittance and sheet resistance can be expressed by the following equation [253].

$$T = \exp\left(-\frac{\alpha\rho}{R}\right) = \exp(-\frac{A}{R}) \qquad (1)$$

where T and R are the transmittance and sheet resistance, respectively, of a sample, α and ρ are the resistivity and absorption coefficient, respectively, of the CNT film material, and A is the integrated constant defined as $A = \alpha\rho$. By adjusting A (= 330 Ω) in equation (1), the fitting curve to our experimental data was prepared as shown in the solid line in Figure 7-15. Among our measurements, they all were located in the vicinity of the fitting line. Moreover, data in other similar work are consistent with the fitting line in our study, being slightly higher performance as a transparent conductive film than our work. This figure indicates that the synthesis process using sulfur provides the promoted growth of CNTs without losing the competitiveness as a transparent conductive film.

7-3-4 Discussions

7-3-4-1 Interpretation of activation energy (without sulfur vs with sulfur powder)

Here, let us focus on the results without additives and with sulfur powder. Since the distinct difference in the activation energy required for CNT growth was found, we would like to speculate the rate-limiting step in CNT synthesis. CNT growth process can be mainly divided into three sequential steps, e.g. (1) decomposition reactions of supplied carbon sources, (2) diffusion of formed carbon atom in or on catalyst, and (3) CNT formation reactions on catalyst surface. Since a number of references representing activation energies in each step have been published until now, let us look over them one by one in the following sentence.

(1) Decomposition reactions of supplied carbon sources

Hydrocarbons are decomposed on catalyst surface to form atomic carbon, and activation energies in this step depend on carbon sources used, e.g. 230–270 kJ/mol for ethanol [276], 120–180 kJ/mol for acetylene [277,278,279], larger than 190 kJ/mol for ethylene [276], and 70–160 kJ/mol for carbon monoxide [280,281,282,283]. It should be noted that these values are based on not only Co catalysts but also other transition metals like Fe and Ni. It is particularly required to look after publications where carbon monoxide and sulfur are stated. Curulla-Ferré et al. performed density functional theory (DFT) calculations and they showed that the activation energy for CO dissociation on pure Fe was 110 kJ/mol while that on sulfur-precovered Fe surface was 120–125 kJ/mol [284]. According to the study by Habermehl-Ćwirzeń that the effect of sulfur treatment on CO desorption properties on cobalt surface, the activation barrier for CO desorption via sulfur treatment was reduced compared with that on pure cobalt surface [285]. This means that CO adsorption is disturbed on sulfur-covered cobalt surface. These researches indicate that sulfur degrades CO adsorption and dissociation properties on metal surface.

(2) Diffusion of formed carbon atom in or on catalyst

After the formation of carbon atoms as a result of decomposition of hydrocarbon feedstock, this step takes place in parallel via mainly three routes, e.g. bulk diffusion in solid-phase catalyst, bulk

diffusion in liquid-phase catalyst, and surface diffusion on catalyst surface. The activation energies in case of bulk diffusion in solid-phase catalyst for CNT synthesis ranged 90–160 kJ/mol in iron based catalysts [286,287,288,289], 120–140 kJ/mol in nickel based catalysts [278,290,291,292] and 110–140 kJ/mol in cobalt based catalysts [290,292,293,294]. These values are quite similar with each other. Many researchers attribute these activation energies to carbon diffusion in solid catalyst due to the analogy with those of carbon diffusion in solid metal reported in metallurgy, e.g. 80–140 kJ/mol for solid iron [295,296] and 140–150 kJ/mol for solid cobalt [297,298]. On the other hand, activation energies in case of bulk diffusion in liquid-phase catalyst indicated significantly reduced values, for instance, 30–40 kJ/mol in CNT growth works [292,299], being similar values with those of carbon diffusion in metallurgy, 10–40 kJ/mol in molten iron and cobalt [299,300,301]. According to the phase diagram of metal-sulfur system, melting temperature of alloy is significantly decreased in comparison with that of pure metal as in Fe-S [216] and Co-S [259,260]. This fact infers that the state of catalytic nanoparticles may be shifted from solid state to melted one in the presence of sulfur at high temperature used for CNT synthesis. The activation energies in surface diffusion on catalyst surface resemble very well those in bulk diffusion in liquid phase. Hofmann et al. showed the activation energies in surface diffusion of approximately 20–30 kJ/mol depending on employed catalysts [278], and Mojica and Levenson estimated the activation energy of carbon on nickel to be 30 kJ/mol [302]. Li et al. showed activation energy of 10–40 kJ/mol for carbon atoms to diffuse on metallic Co [303].

(3) CNT formation reactions on catalyst surface

After carbon atoms reach CNT growth site through diffusion, surface reactions for constructing carbon lattice take place on catalyst surface, e.g. integration of carbon atoms into carbon networks and graphite cap lift-off from catalyst surface. Lin et al. estimated the activation energy of 260 kJ/mol required for the integration of carbon atoms into hemispherical graphene sheet during nucleation [304]. According to DFT calculation by Yuan et al. [305], the energy barrier related to the integration of carbon atoms into hexagon carbon networks was 180 kJ/mol on Ni (111) and 220 kJ/mol on Fe (111)/Co (0001) catalysts. The activation energies for the formation of heptagon structure built by carbon atoms were estimated through experiments to be 250 kJ/mol [306]. Anyhow, the energy barriers required for carbon atoms being integrated into carbon networks are in general significantly large. Some literatures indicated the enhancement of graphitization by sulfur. They dealt in petroleum cokes including 1.7% sulfur but no metal catalyst, and graphitization was accelerated usually at larger temperature than 1,500 ^{o}C [307,308,309]. The energy barrier for graphitization was estimated, e.g. 250–380 kJ/mol at 1,400–2,200 ^{o}C [307] and 190 kJ/mol at higher than 1,500 ^{o}C [309]. Furthermore, graphene formation using hydrocarbons and sulfur (S_8) as a feedstock under the mild temperature (300–600 ^{o}C) was reported probably due to cross-linking by sulfur [310,311]. No metal catalyst was employed in these studies. However,

similar effects observed in graphene formation by sulfur might be inapplicable to our system because no growth of CNTs was found in the use of a substrate with sulfur alone free from metal catalysts in our measurements (not shown here). We should also pay attention to the adhesion energy between catalyst surface and graphite sheet as one of surface reactions because it plays an important role in graphite cap lift-off during CNT growth [312,313]. The adhesion energies between graphite and Ni/Co catalyst were around 10–15 kJ/mol [312]. It is necessary for graphite cap extrusion that kinetic energy ($E \approx k_B T$) has to surpass the adhesion energies, where k_B is Boltzmann constant and T is temperature. Generally, if temperature (T) is higher than 700 K, lift-off of graphite cap from catalyst surface takes place easily because adequate energy is provided by heat [313]. It is well known that sulfur functions as an agent to reduce the metal surface energy [314], leading to actual decreasing of adhesion energy between graphite and Fe melts [315]. Although the presence of sulfur on catalyst surface is favorable for graphite cap lift-off, we speculate that sulfur is influential in a very limited way because carbon cap lift-off occurs with no difficulty under our CVD temperatures even in the absence of sulfur as stated above. Summary table which depicts activation energies in literatures addressed until here and those in our experiments is presented in Table 7-2 for a comparison purpose.

(4) Suggested role of sulfur in CNT synthesis

Considering the agreement in the value of energy barriers between our study and preceding studies, let us identify the rate-limiting step in our system and elucidate the effect of sulfur on CNT growth. Although we introduced a number of articles, Jourdain and Bichara showed versatile and helpful criteria to determine a rate-limiting step from activation energies, in which activation barrier of 20–60 kJ/mol for CNT growth was basically stemmed from bulk diffusion in liquid-phase or surface diffusion, activation energy of approximately 70–150 kJ/mol in CNT synthesis was mainly due to bulk diffusion in solid-phase, and activation barrier larger than 150 kJ/mol was primarily attributed to decomposition of supplied hydrocarbons or CNT formation reaction on surface [254]. These criteria largely match the range of activation energies in Table 7-2. In our system, we can remove the possibility that CNT formation reactions on catalyst surface become a rate-limiting step due to its extreme mismatch in activation energy. In Co/Mo catalyst, we acquired the activation energy of 94 kJ/mol, being coincident with that in bulk diffusion of carbon in solid-phase catalyst or CO dissociation reaction. Though this value is within the range of activation barrier of CO dissociation reaction, we can rule out the possibility that it becomes a rate-determining step because CNT growth should be deteriorated in the presence of sulfur owing to the hindrance of CO adsorptive dissociation according to literatures [284,285]. Hence, it is plausible to consider that the rate-limiting step in Co/Mo free from sulfur is bulk diffusion in solid-phase catalyst. Here, one may consider that the step with largeer activation energy like CNT formation reactions on catalytic surface does not become a rate-determining step. The rate of

reaction/diffusion can be expressed as $\boldsymbol{A}\exp(-\boldsymbol{E_a}/\boldsymbol{RT}) \times [\textbf{Concentration term}]$ where A is pre-exponential constant (frequency factor), E_a is activation energy, R is gas constant and T is temperature. When A and/or concentration term are large enough, the process with high activation energy (E_a) cannot become a rate-limiting step. Thus, we can identify a rate-limiting step based on the agreement of the value of activation energy. On the other hand, strikingly reduced activation energy of 25 kJ/mol was found in Co/Mo/Sulfur powder 2.0 wt%, being stemmed from surface diffusion of carbon atoms on catalyst or bulk diffusion in liquid-phase catalyst. Through some characterization methods, the formation of Co-S chemical bond was indicated, meaning that the melting temperature of Co-S binary system was reduced in comparison with that of bulk Co. Moreover, its reduction is accelerated due to nano-sized effect. Actually, HR-TEM images in Figure 7-7 showed that the ambiguous lattice fringe in the presence of sulfur powder was observed. Therefore, above hypothesis is valid in our system from the qualitative point of view. Of course, it should be noted that the degree of reduction of melting point depends on the composition of Co-S system and also that there are some differences in physical properties between bulk system and nano-sized system. As a consequence of the decrease in melting temperature of catalytic particles during CVD operation, the diffusion barrier for atomic carbon inside the bulk was quite lowered, resulting in the significant reduction of the activation energy. Based on the finding in Figure 7-8, since sulfur was concentrated near the catalytic surface, the potential diffusion path for atomic carbon might be the region in the vicinity of surface. To sum up, the expected role of sulfur during CNT synthesis in this study is that it improved the diffusivity of carbon in catalyst nanoparticles particularly near the surface and shifted the rate-determining step in CNT formation. Figure 7-16 depicts the difference between conditions with and without sulfur powder. The largest difference appears in the diffusion of atomic carbon inside catalytic particles which finally affects CNT production.

7-3-4-2 Interpretation of activation energy (sulfur powder vs thiourea)

The activation energy required for CNT growth was explicitly reduced by introducing sulfur, however, its degree depended on sulfur source. Sulfur powder showed the significant performance in CNT growth enhancement, while thiourea could not reach the level attained by sulfur powder. Activation barrier in sulfur powder was 25 kJ/mol. On the other hand, that in thiourea was 55 kJ/mol, which was the intermediate value between Co/Mo/Sulfur powder 2.0 wt% and Co/Mo (94 kJ/mol). This value is too large to assign bulk diffusion of carbon atom in liquid-phase catalyst like Co/Mo/Sulfur powder 2.0 wt%, while it is too small to assign bulk diffusion of carbon in solid-phase catalyst like Co/Mo alone. Although sulfur atom in thiourea clearly functioned for promoting CNT growth due to the reduced activation energy compared with that free from sulfur, it can be considered that there may exist some factors to diminish the promoting effect by sulfur in case of thiourea due to the increased activation energy in comparison with that in sulfur powder.

Sulfur powder is composed of only sulfur atom while thiourea includes not only sulfur but also nitrogen in its chemical structure. When temperature is elevated at ~220 ^{o}C, thiourea is thermally decomposed into ammonia (NH_3), hydrogen sulfide (H_2S), isothiocyanic acid (HNCS), carbon disulfide (CS_2) and carbodiimide (HNCNH) [316,317]. Formed chemical species may act as sources of nitrogen and sulfur, probably interacting with catalyst consisting of cobalt and molybdenum. The effect and behavior of nitrogen during CNT formation has been proposed until now. In summary, CNT nucleation and growth was hindered in the presence of nitrogen from experimental [318] and computational [319,320] approaches, and this was probably because nitrogen atoms tended to be energetically located at the edge of carbon network, resulting in the inhibition of carbon atoms being incorporated into carbon lattice. However, we may be able to rule out this possibility because constructing reactions of CNT on catalytic surface cannot become a rate-determining step in our system as discussed early. Thus, we paid attention to the diffusivity of light elements (C, N, S) in transition metals in order to attempt to interpret the difference in activation energy between thiourea and sulfur powder because the diffusion step of atomic carbon in CNT formation was the key. When nitrogen and carbon coexisted in iron-based materials, mutual effects among diffusing elements occurred [321,322], leading to the implication that the lower diffusive atom, N, disturbed the transfer of C which had higher diffusivity [321,323]. On the other hand, a number of publications to study the diffusivity of individual element in transition metals such as Fe and Co have been carried out in metallurgy, e.g. carbon/metal [296, 324 , 325], nitrogen/metal [296, 326 , 327] and sulfur/metal [328,329,330]. If the state of host material was molten one, the diffusion coefficient was in the similar order of magnitude and showed the following order, carbon ≈ sulfur > nitrogen. Meanwhile, when host metals were in solid state, the diffusion coefficient between 600 ^{o}C and 750 ^{o}C used as a CVD temperature in this study was significantly reduced from that in molten state, and was in the following order, carbon > nitrogen >> sulfur. Here, we propose two scenarios to reveal the intermediate value of activation energy in thiourea. One is that the coexistence of sulfur and nitrogen affected carbon diffusion in catalyst nanoparticles being kept in solid state. Another is that the presence of sulfur and nitrogen affected carbon diffusion in molten catalyst. The former may be eliminated because it is likely that catalyst nanoparticles in the use of sulfur source in our system are melted during CNT growth probably due to the formation of Co-S alloy and nanosized effect. Thus, second scenario should be considered. According to some reports stated above which examined the diffusive ability of light elements in transition metals, it seems reasonable to suppose that the presence of nitrogen is disadvantageous to carbon diffusion in molten metal while sulfur is less influential on carbon transportation because the diffusivity of carbon and sulfur is the similar order but that of nitrogen is lower in the molten host material. Therefore, the difference in activation energy between the case using thiourea and sulfur powder may be stemmed from the existence of nitrogen and its relatively low diffusivity against other diffusing atoms, resulting in slightly larger activation energy in thiourea in

comparison with sulfur powder. This work suggests that the promoted effect of CNT growth caused by sulfur is sometimes deteriorated if hetero atoms other than sulfur such as nitrogen coexist in catalysts during CNT synthesis. However, since this does not leave the hypothesis stage, further studies to elucidate the role of hetero atoms during CNT synthesis are required in future.

7-4 Summary of this chapter

In this chapter, we explored the role of sulfur as a growth promoter during CNT synthesis via CVD process where Co/Mo binary system and carbon monoxide was employed as a basic catalyst and carbon source, respectively. Furthermore, impacts of sulfur type on CNT growth were investigated by means of sulfur powder and thiourea as a sulfur source. Remarkable findings are listed as follows.

- The introduction of sulfur into catalyst layer exhibited the enhancement in CNT production even when oxygen which was regarded as an unfavorable gas was fed into the reactor.
- The role of sulfur as a promoter in CNT growth was implied that it shifted the rate-limiting step from the bulk diffusion of atomic carbon in solid-phase catalyst to the bulk diffusion of atomic carbon in liquid-phase catalyst, especially shown in the use of sulfur powder.
- The activation energy required for CNT growth was significantly reduced from 94 kJ/mol in Co/Mo alone to 25 kJ/mol in Co/Mo/Sulfur powder 2.0 wt%. The intermediate value of 55 kJ/mol was gained in Co/Mo/Thiourea 3.5 wt%.
- Through some characterizations on catalytic nanoparticles, it was strongly suggested that the chemical bonding between Co and sulfur was formed and sulfur was prone to be concentrated in the vicinity of particle surface. Thermodynamic calculation corroborated this propensity.
- According to the phase diagram of Co-S binary system, the melting point was reduced in comparison with that of pure Co. This may explain the reason why sulfur was effective in CNT growth. Since sulfur decreased the melting temperature of catalyst particles, the diffusion of atomic carbon inside catalyst was facilitated, probably resulting in the promotion of CNT production.
- The difference in the value of activation energy between sulfur powder and thiourea may be attributed to the presence of hetero atom like nitrogen. Because the diffusivity of nitrogen was lower than that of carbon and sulfur in molten state, nitrogen might disturb the diffusion of carbon, probably resulting in the enlarged activation energy.

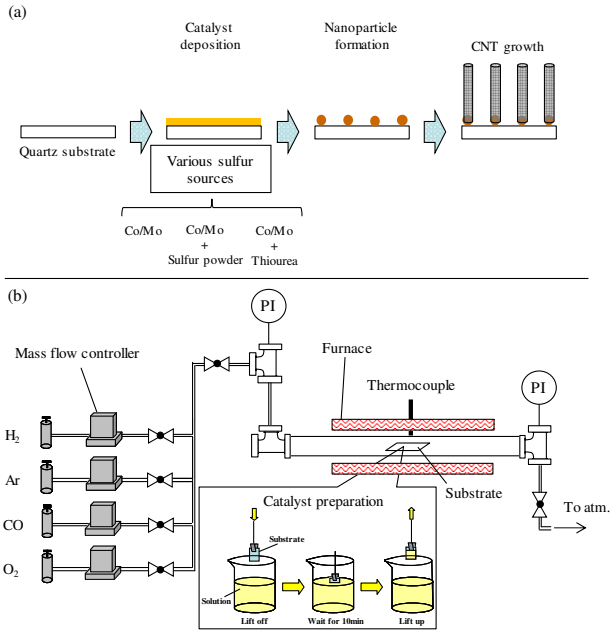

Figure 7- 1 Schematic representation which depicts (a) the synthetic process of CNT from various catalyst conditions and (b) the experimental apparatus for performing a reduction and CVD.

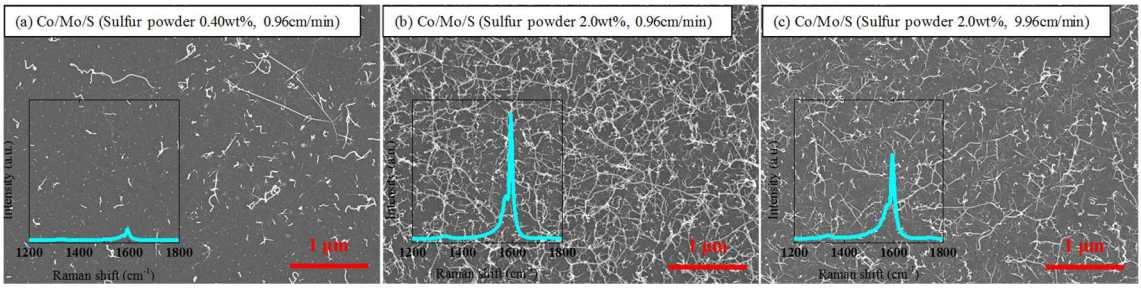

Figure 7- 2 SEM images after a CVD process at 800 °C for 30 minutes when sulfur amounts coated on a substrate were changed. Raman spectra were inserted in each SEM image. The images (a–c) were taken for a sample as a function of sulfur powder which dissolved in toluene. For the case (c), since the upper limit of sulfur powder which could dissolve in toluene was approximately 2.0 wt% in our work, a drawing speed from a toluene solution with 2.0 wt% of sulfur powder was increased from 0.96 cm/min to 9.96 cm/min, which was corresponding to sulfur amount of about 9.5 wt% in toluene on the basis of 0.96 cm/min as a drawing speed.

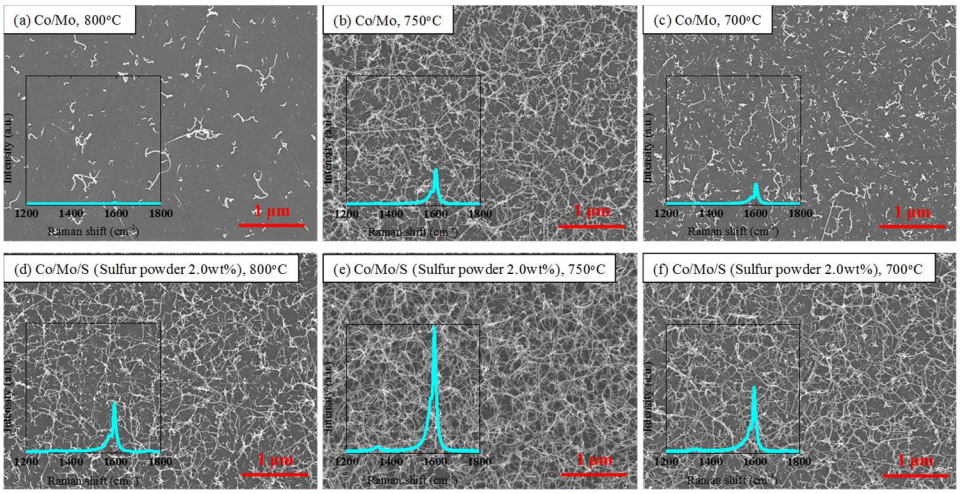

Figure 7- 3 SEM photographs after CVD process with different catalytic condition was carried out for 30 minutes as a function of CVD temperature. The catalyst condition and CVD temperature were (a) Co/Mo, 800 °C, (b) Co/Mo, 750 °C, (c) Co/Mo, 700 °C, (d) Co/Mo/S (Sulfur powder 2.0wt%), 800 °C, (e) Co/Mo/S (Sulfur powder 2.0wt%), 750 °C, and (f) Co/Mo/S (Sulfur powder 2.0wt%), 700 °C, respectively. Raman spectra corresponding to each SEM image were inserted.

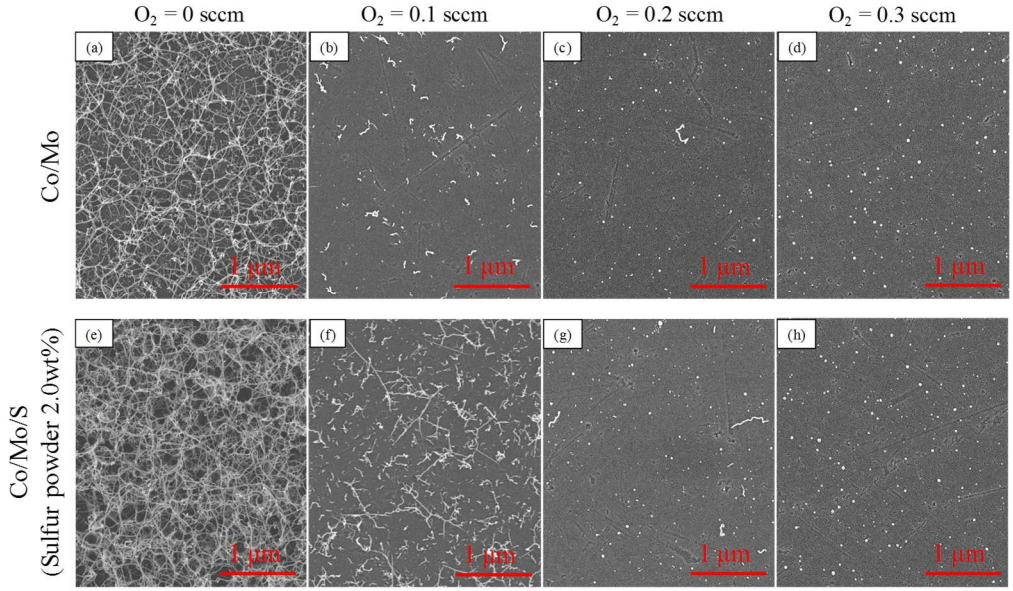

Figure 7- 4 Impacts of O_2 flow rate in feed gas on CNT growth. During CVD, CO flow rate was fixed to be 45 sccm and O_2 flow rate was varied from 0 to 0.3 sccm, while Ar flow rate was adjusted so that the total flow rate (CO+H_2+Ar) was 200 sccm. CVD was performed at 750 °C for 60 minutes. SEM images (a–d) were taken for a sample with Co/Mo free from sulfur after CVD. The images (e–h) were taken for a sample with Co/Mo/S using sulfur powder of 2.0 wt% after CVD.

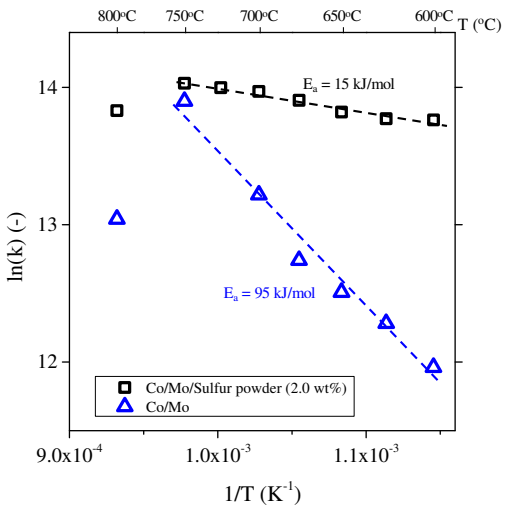

Figure 7- 5 Kinetic dependence of ln(k) on inverse CVD temperatures using a different catalyst layer. The activation energy required for CNT growth is shown as well.

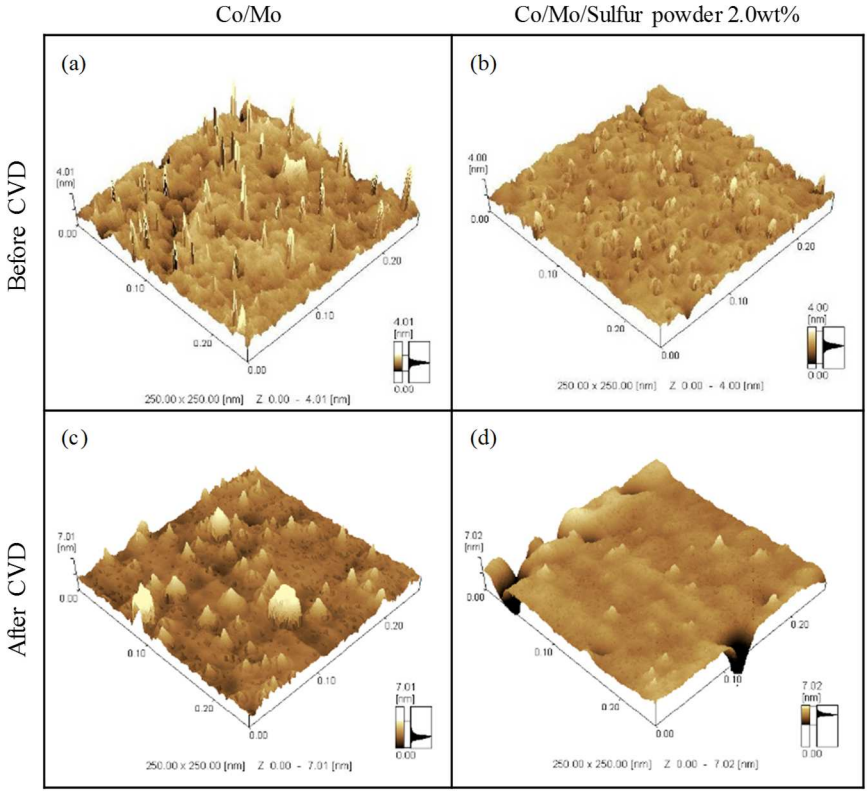

Figure 7- 6 AFM images of the substrate with and without sulfur sources and before and after CVD. The images before CVD (a) and (b) were taken for samples after the reduction in H_2/Ar at 800 °C for 30 minutes. The images after CVD (c) and (d) were taken after CVD with CO/Ar at 800 °C for 10 minutes.

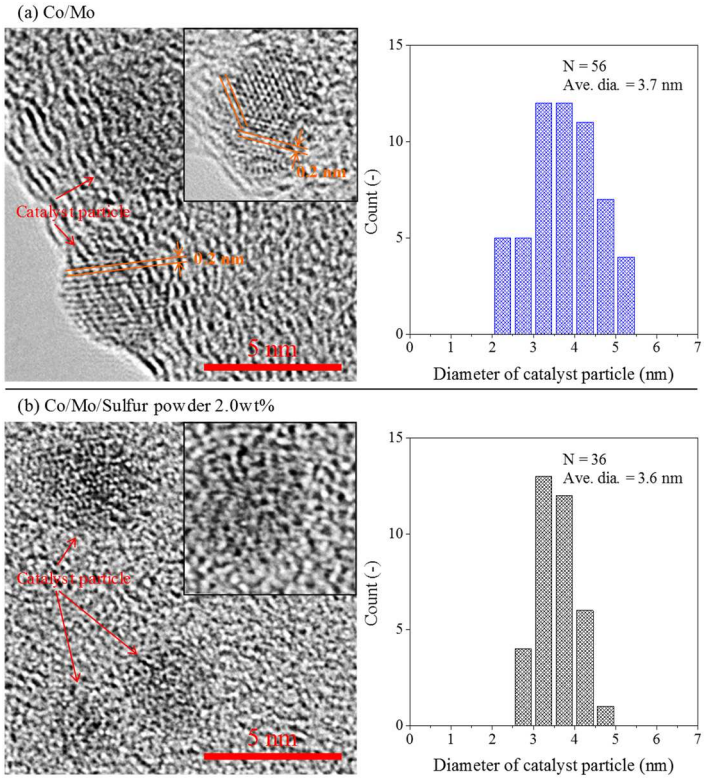

Figure 7- 7 HR-TEM images of catalyst particles when a condition of catalyst layer was changed. (a) catalyst condition was Co/Mo free from sulfur. (b) catalyst condition was Co/Mo/Sulfur powder 2.0 wt% in a toluene solution. Additional pictures of catalyst particles are inserted as another example. TEM micrographs were taken for the sample after CVD was performed at 750 ºC for 180 minutes. Histogram of catalyst nanoparticles size was prepared based on HR-TEM images.

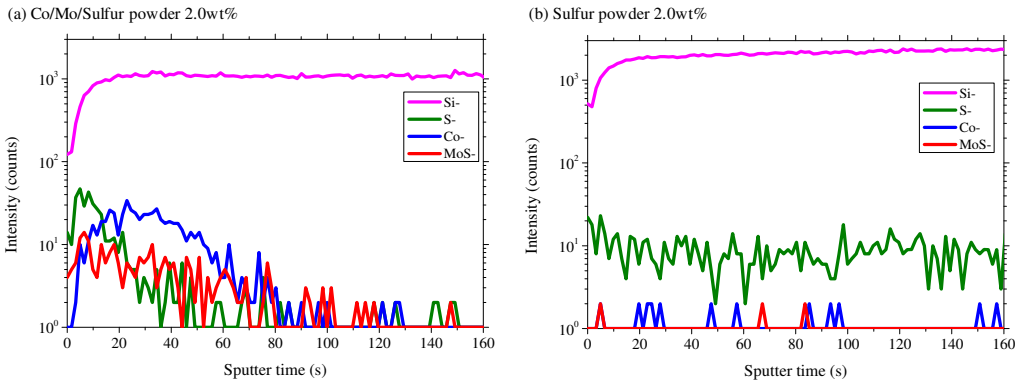

Figure 7- 8 Elemental depth profile using TOF-SIMS analysis of samples after a reduction (no CVD was done). (a) a sample coated by Co/Mo/Sulfur powder 2.0 wt% in toluene. (b) a sample coated by only sulfur powder of 2.0 wt% in toluene. Co and Mo was not deposited on this sample.

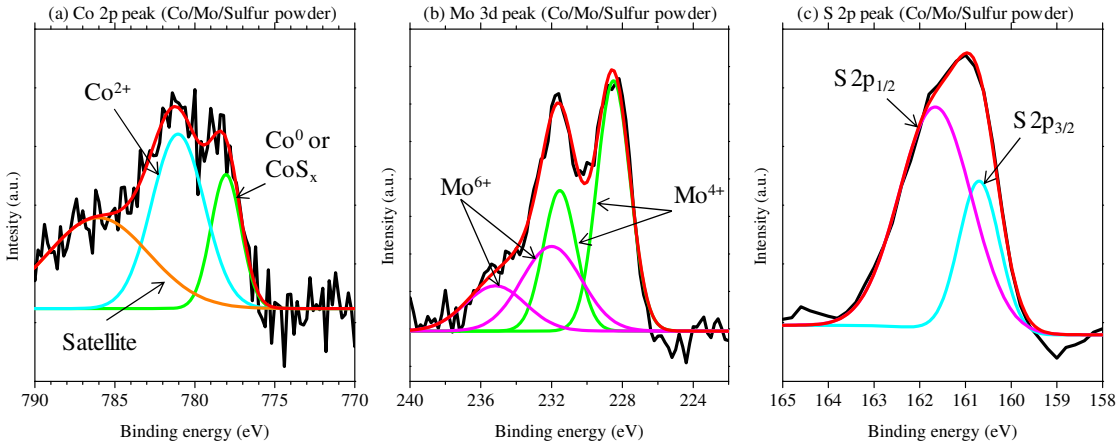

Figure 7- 9 XPS spectra of a sample deposited by Co/Mo/Sulfur powder 2.0 wt%. (a) Co 2p, (b) Mo 3d, and (c) S 2p regions. For detecting Co and Mo spectra, a substrate was dip-coated only one time. For detection of sulfur, Co/Mo layers were dip-coated a lot of times while sulfur was deposited only one time. CVD at 800 ºC was conducted for detecting (a) and (b) for 10 minutes and (c) for 5 minutes, respectively.

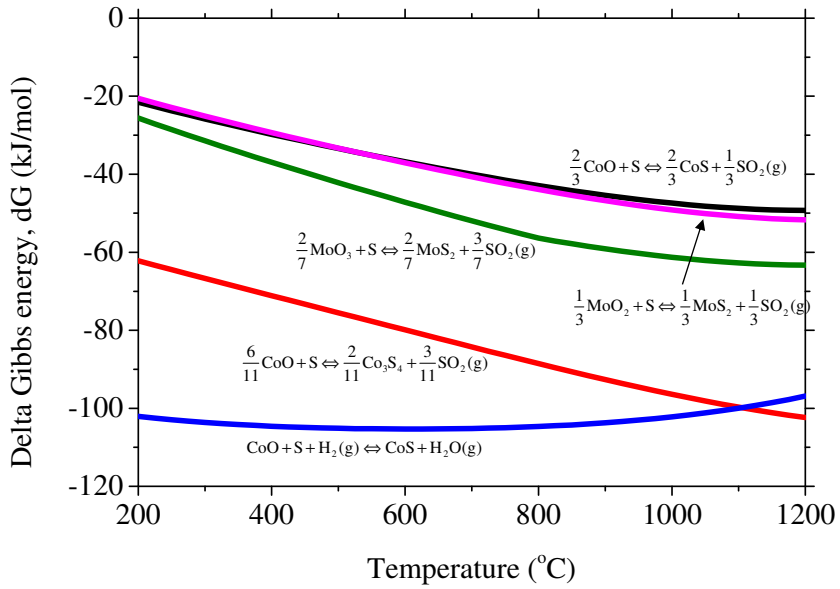

Figure 7- 10 Delta Gibbs energies of several reactions from metal oxides plus sulfur to form metal sulfides using a calculation software.

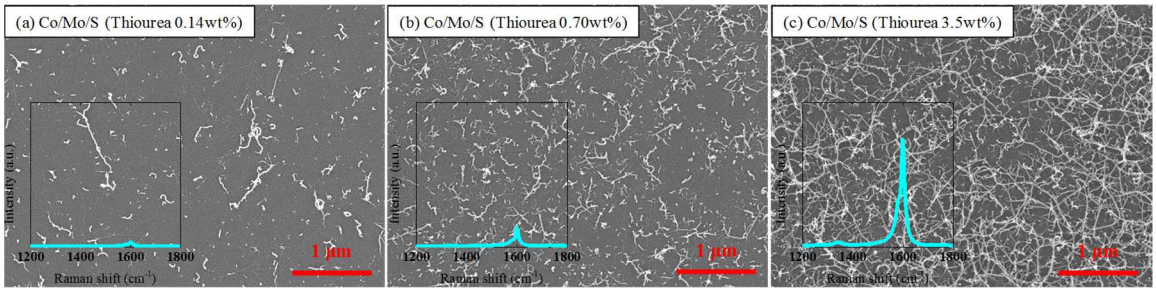

Figure 7- 11 SEM images after a CVD process at 800 ºC for 30 minutes when thiourea amounts in ethanol solution were changed. Raman spectra were inserted in each SEM image.

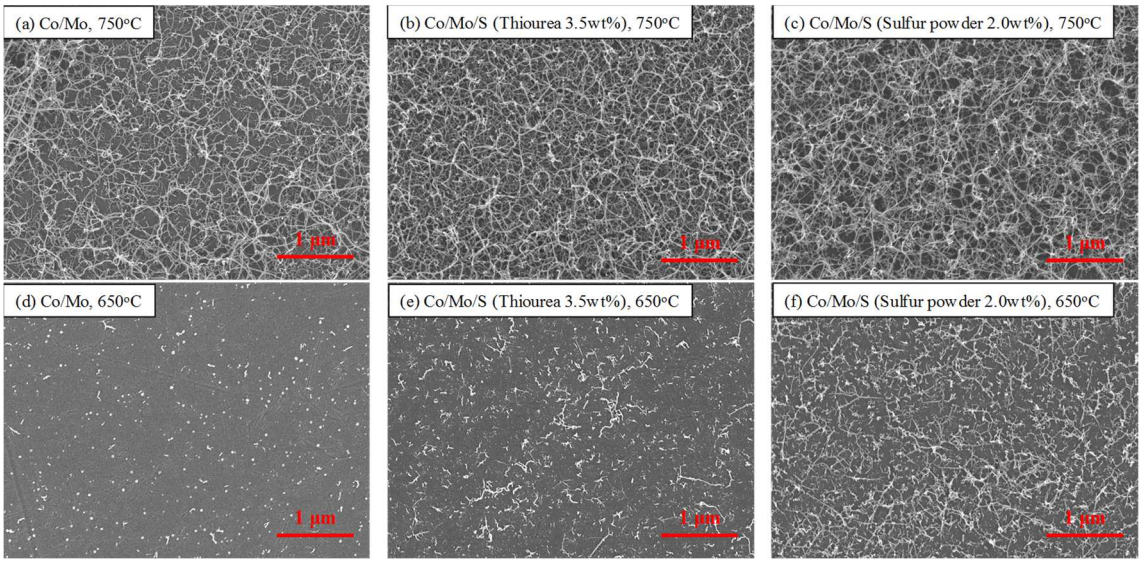

Figure 7- 12 Typical SEM micrographs when catalyst conditions and CVD temperature were varied. (a) Co/Mo alone under 750 ºC as a CVD temperature, (b) Co/Mo/Thiourea under 750 ºC, (c) Co/Mo/Sulfur powder under 750 ºC, (d) Co/Mo alone under 650 ºC, (e) Co/Mo/Thiourea under 650 ºC and (f) Co/Mo/Sulfur powder under 650 ºC. CVD was carried out for 30 minutes in samples other than (d), and it was extended to 60 minutes in (d). Even when CVD time was extended, CNT was rarely grown in (d).

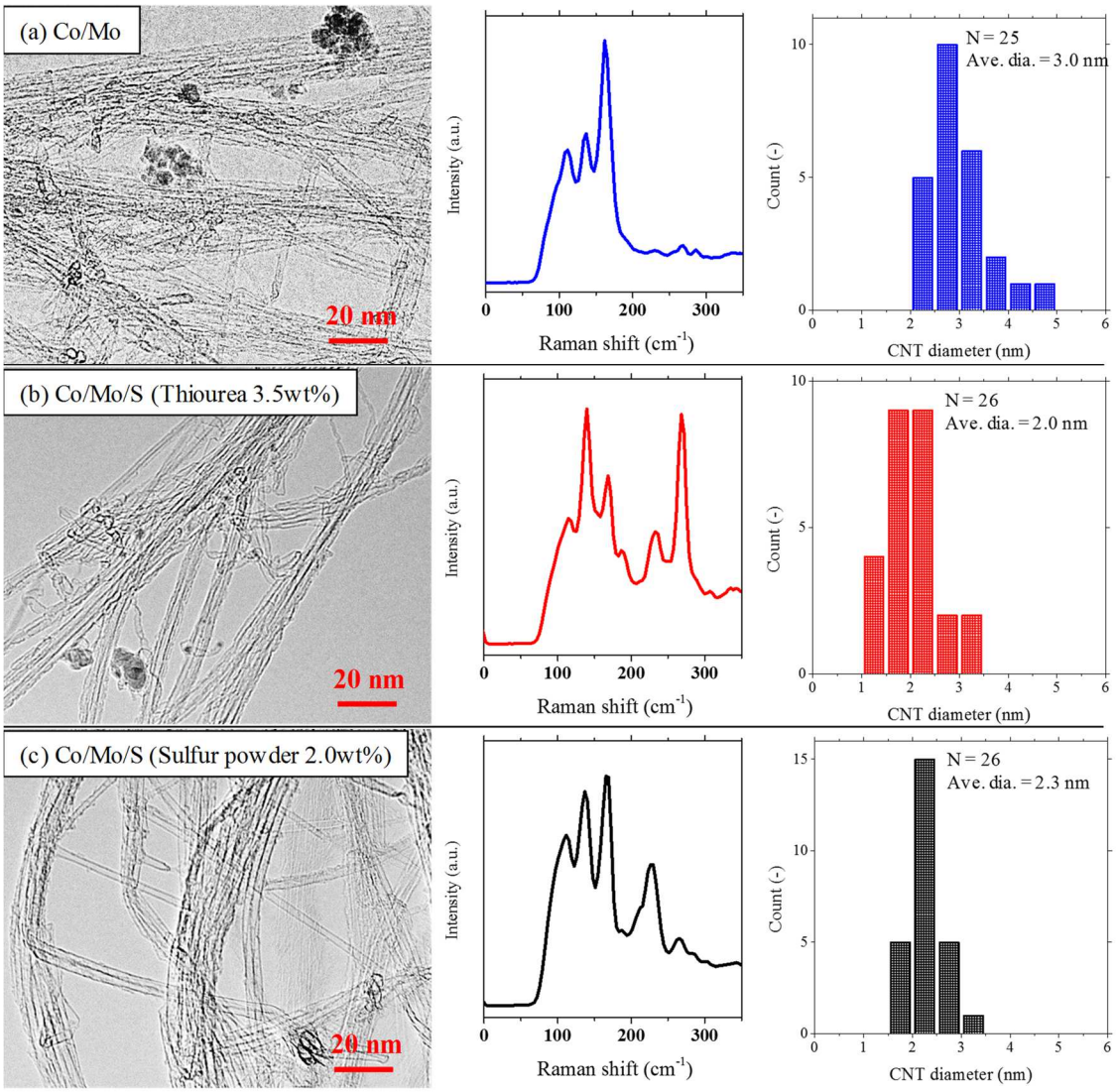

Figure 7- 13 High resolution TEM images of synthesized CNTs with and without sulfur sources, corresponding RBM of Raman spectra and histogram of CNT diameters. CVD duration was 180 minutes and CVD temperature was 750 °C. Histogram of synthesized CNT outer diameters was prepared based on corresponding TEM images. (a) sample whose catalyst condition was a Co/Mo layer alone (b) sample whose catalyst condition was Co/Mo/S derived from thiourea of 3.5 wt% in an ethanol solution as a sulfur source (c) sample whose catalyst condition was Co/Mo/S derived from sulfur powder of 2.0 wt% in a toluene solvent as a sulfur source.

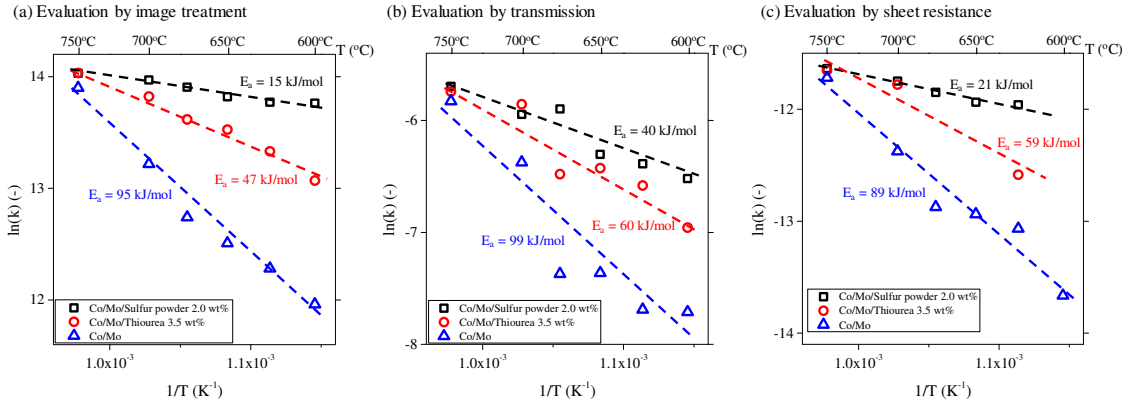

Figure 7- 14 Kinetic dependence of ln(k) on inverse CVD temperatures using a different catalyst layer. CNT growth rate was evaluated by means of (a) image treatment, (b) transmittance and (c) sheet resistance.

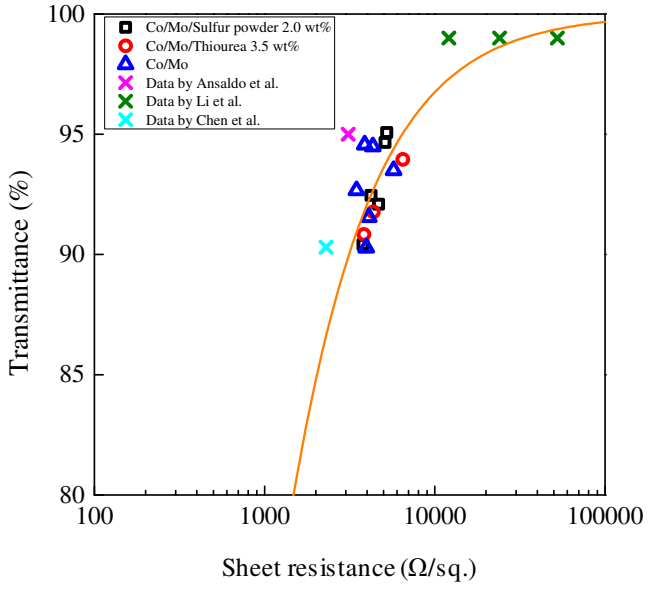

Figure 7- 15 Transmittance plotted as a function of sheet resistance of CNT film prepared from different catalytic conditions. Literature data where carbon materials were directly grown on a substrate are also presented. The solid curve represents the fitting line to our measured data expected from the relation between transmittance and sheet resistance.

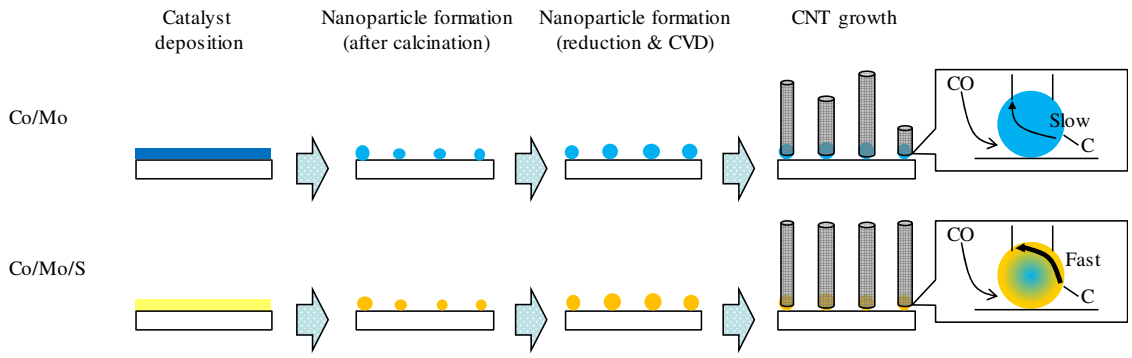

Figure 7- 16 The depiction that emphasizes the role of sulfur during CNT growth, which was implied from the experimental results using sulfur powder and no sulfur additive.

Table 7- 1 Summary table of activation energy estimated in this study using different evaluation technique.

Condition	Image treatment	Transmission	Sheet resistance	Average
Co/Mo/Sulfur powder 2.0 wt%	15 kJ/mol	40 kJ/mol	21 kJ/mol	25 kJ/mol
Co/Mo/Thiourea 3.5wt%	47 kJ/mol	60 kJ/mol	59 kJ/mol	55 kJ/mol
Co/Mo	95 kJ/mol	99 kJ/mol	89 kJ/mol	94 kJ/mol

Table 7- 2 Summary table of activation energies from both literatures and our experiments. Literature data shown here are mixed up based on Fe, Co and Ni as a catalyst.

		activation energy, E_a
literature data	decomposition reaction	70–160 kJ/mol[a]
	bulk diffusion in solid-phase	80–160 kJ/mol
	bulk diffusion in liquid-phase	10–40 kJ/mol
	surface diffusion on catalyst	10–40 kJ/mol
	CNT formation reaction	180–260 kJ/mol
our experiments	Co/Mo	94 kJ/mol[b]
	Co/Mo/Sulfur powder 2.0 wt%	25 kJ/mol[c]

[a]Only carbon monoxide. [b]The rate-limiting step is bulk diffusion in solid-phase. [c]The rate-limiting step is bulk diffusion in liquid-phase or surface diffusion on catalyst.

Chapter 8. Overall Conclusions and Future Scope

In this study, the development of a process using a diesel engine for the synthesis of CNTs was investigated. Not only required conditions for the CNT formation but also the identification of key factor contributing to CNT synthesis in a diesel engine and its growth mechanism were studied.

When gas oil/ethanol mixing fuel was used, it was revealed that three conditions had to be satisfied simultaneously for the successful synthesis of CNTs: high ethanol fraction in mixing fuel, high sulfur loading, and the presence of catalyst sources in fuel. If at least one of these three conditions was not satisfied, almost no CNT could be observed in an exhaust gas.

Instead of gas oil, n-alkane (n-dodecane) or fatty-acid methyl ester (methyl laurate) or alcohol (1-decanol) was employed in order to improve and simplify analysis. CNT production was prone to be increased when an ethanol content in mixing fuel and an engine load were enlarged. This may be because higher combustion temperatures and larger emissions of carbon monoxide were achieved. At a high ethanol fraction in mixing fuel, there was very less difference in CNT production among fuel used in this study, probably because almost equal CO amounts in an exhaust was obtained mainly from ethanol. On the other hand, at a low ethanol fraction, CNT could be grown in case of mixing fuel using methyl laurate and 1-decanol, while n-dodecane system did not show any CNT growth. The behavior of CNT growth in different fuel type may be able to be interpreted by the contribution of CO amounts in an exhaust. Higher CO emissions could be obtained from methyl laurate and 1-decanol than from n-dodecane at a low ethanol content because methyl laurate and 1-decanol have C-O bond in its chemical structure.

The attempt to identify promising CNT precursor in a diesel engine was carried out by means of three approaches, the analysis on an exhaust gas, the simulation of combustion reaction, and the modelling work of CNT growth rate using a CO or ethylene or acetylene as a carbon source. All approaches suggested the significance of carbon monoxide as a promising candidate of CNT precursor, being in line with previous studies in flame processes to synthesize CNTs using burners. The importance of fuel rich region for CNT formation was also indicated. Hence, CNT formation pathway was proposed; CO is generally generated via imperfect combustion where there is shortage of oxygen, namely fuel rich conditions (larger equivalence ratio than unity). Taking into account the fact that the equivalence ratio inside a general diesel engine ranges from 0.2 to 2.0 during one combustion stroke and high equivalence ratio regions are concentrated in the vicinity of fuel injection nozzle and the center of sprayed fuel, the most probable route of CNT growth is that iron particles and carbon monoxide produced at fuel rich regions react each other, resulting in CNT growth.

According to the observations via microscope and elemental analysis, SWNT was rarely formed while majority of synthesized CNTs was MWNT irrespective of fuel conditions. Carbon layers consisting of CNTs were damaged probably due to oxygen. EDX analysis on catalytic nanoparticles showed that lower O/Fe ratio (metallic state) was desirable for the growth of CNTs and sulfur seemed to be concentrated on nearly the surface of catalysts. And, we estimated the CNT productivity and

yield in this study (in case of gas oil system) to be 9.3×10^{-3} g/h and 9 ppm by injected fuel weight, respectively, which was lower than that by two-orders of magnitude in HiPco process which are known as one of commercial processes in CNT production. Therefore, the CNT productivity and yield in a diesel engine shall be improved.

Through the introduction of additional hydrocarbons into the intake air line, it was revealed that a slight improvement of CNT formation was attained in the employment of H_2 and CH_4 as additive gas, while C_2H_2 addition presented the opposite effect. This might be stemmed from the deactivation of catalyst particles caused by high acetylene concentration at an early reaction stage in the latter case.

The role of sulfur in CNT growth was investigated through CVD process to support experimental results attained by a diesel engine because the addition of sulfur was one keys for the successful synthesis of CNT in a diesel engine. The activation energy required for CNT growth was significantly reduced by the introduction of sulfur. This may result from the formation of metal-sulfur alloy in catalytic particles, leading to the decrease of melting temperature which facilitated the diffusion of atomic carbon. The effectiveness as a CNT growth enhancer depended on sulfur source, sulfur powder showed remarkable effect but thiourea did mild one. This may be interpreted by the presence of hetero atoms which made carbon diffusion slow.

As a summary, the overall CNT growth mechanism in a diesel engine reflecting findings in Chapter 5 and Chapter 7 is depicted in Figure 8-1. Ferrocene as a catalyst source was decomposed to form iron particles. Some of them underwent oxidation while the others reacted with sulfur powder to form Fe/FeSx nanoparticles. At the same time, fuel was pyrolyzed and/or oxidized, resulting in the formation of a number of intermediate species like CO, C2 hydrocarbons and stable products such as H_2O and CO_2. Among those species, carbon monoxide reacted with Fe/FeSx catalysts preferentially, and CNTs were grown due to the facilitated carbon diffusion in catalysts. Some of carbon monoxide reacted with hydrogen on the catalyst surface and formed various hydrocarbons via Fischer-Tropsch reaction, being emitted to an exhaust. CNT formation path might take place in the fuel rich regions during combustion.

Based on the overall results presented in this thesis, future works can be considered as follows.

- The modification of a current engine system to a sophisticated one shall be required for increasing CNT productivity and yield. The following plan can be regarded as a candidate; e.g. the adjustment of fuel injection timing/amount/number for accurately controlling catalytic particle size and nucleation timing of CNTs, the adjustment and control of an engine rotation speed in order to tailor the available CNT growth time. What is significant in synthesizing CNTs using a diesel engine is how precisely control contact timing not only between iron and sulfur but also iron catalyst and CNT precursor, and how suitably create fuel rich condition not leading to soot formation but contributing to CNT growth. Thus, a diesel engine equipped with a common rail

system is a promising because it enables us to tune injection amount, injection timing, injection number, and so on.

- In future, dual fuel utilization like Chapter 6 expressed in this thesis but under more highly control system of liquid/gaseous fuel shall be considered. In this sense, options such as the direct usage of CO as additive gaseous fuel or the direct introduction of gaseous species into a cylinder not into the intake air line should be taken into account. Moreover, the combination of a common rail system and duel fuel utilization may become an ambitious project for improving CNT production in a diesel engine.
- The application of the engine with homogeneous combustion like gas engine or spark-ignition engine to the synthesis of CNTs should be considered because it may easy to control combustion properties inside a cylinder.

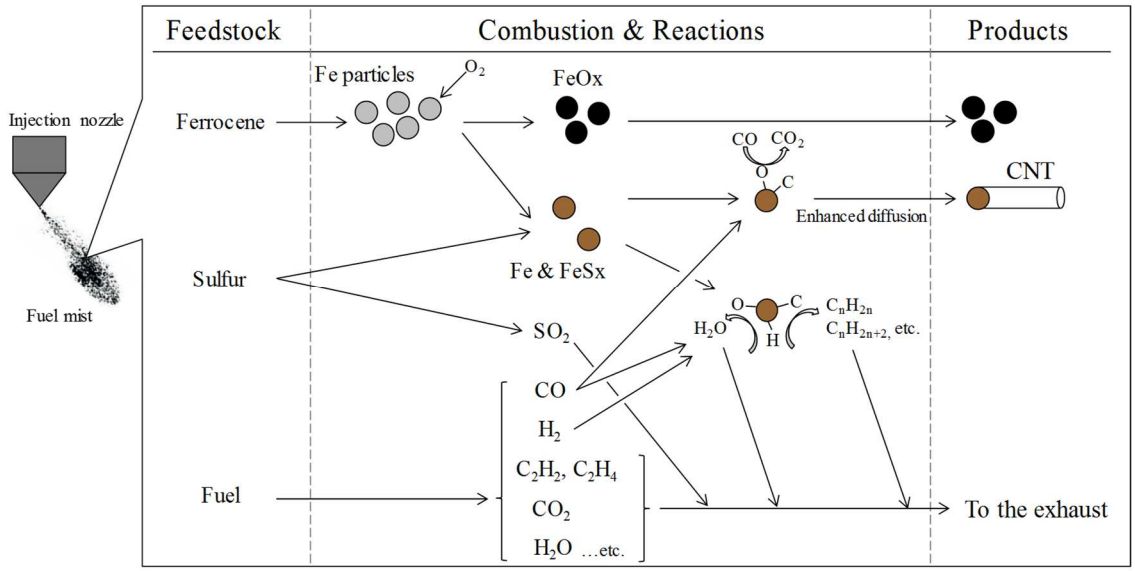

Figure 8- 1 Schematic showing overall CNT growth mechanism in a diesel engine where findings in Chapter 5 and Chapter 7 are reflected.

Acknowledgment

森准教授には本研究のような興味深く、またチャレンジングなテーマを与えていただき感謝しています。研究の方向性を自由に描き決定させてくれるなど、私の自主性を大いに尊重してくれました。また、ディスカッション時には私が見落としていた点を指摘してくださるなど、研究のレベルを引き上げてくれました。このように博士論文を書き上げることができたのも、先生の多大なる献身と熱意のお陰です。本当に感謝しています。

本論文の審査教官を務めていただいた、東京工業大学工学院システム制御系/機械系・小酒英範教授、東京工業大学物質理工学院応用化学系・関口秀俊教授、同・多湖輝興教授、同・松本秀行准教授からは貴重な助言を多数頂きました。新しい視点を得ることができ、本論文も洗練されたものとなりました。大変感謝しております。

東京工業大学技術部大岡山分析部門には本研究で使用したほとんどの分析機器を利用させていただきました(SEM、EDX、TEM、Raman、TOF-SIMS、ICP)。特にスタッフである堀さん、大塚さん、菊地さん、源関さん、幸喜さん、多田さんには私の度重なる分析依頼などにも親切に、かつ非常に辛抱強く対応していただきました。本論文の内容の大部分が貴部門の分析機器に支えられていることを考えると、感謝してもしきれません。本当にありがとうございました。

また東京工業大学物質理工学院材料系の矢野哲司教授には研究室の XPS 装置を使用させていただきました。深謝いたします。また金井さんには XPS 装置の使い方だけではなく、使用中のトラブルにも親切に対応いただきました。ありがとうございます。

最後になりましたが、本論文を書き上げるのにお世話になった全ての人に感謝いたします。

Appendix (Supplemental data)

General

Table S- 1 Summary table of physical properties of hydrocarbons used in this study

Fuel	Density [kg/m^3@20 ºC]	Boiling Point [ºC]	Lower Heating Value [MJ/kg]	Kinematic Viscosity [mm^2/s]	Cetane Number	Latent Heat of Vaporization [kJ/kg]
Gas oil	810	140~400 (a)	43.1 (b)	>2.7 (c)	>50 (c)	250 (b)
n-Heptane	684 (d)	98.6 (d)	44.6 (d)	0.51 @30ºC (d)	56 (e)	323 (f)
n-Dodecane	746 (d)	216.5 (d)	44.6 (d)	1.46 @40 ºC (d)	80 (e)	261 (f)
Methanol	792	64.7	20.1 (j)	0.75 @20 ºC (i)	2~5 (b)	1099 (h)
Ethanol	788 (b)	78 (b)	26.8 (b)	1.33 @20 ºC (f)	8 (b)	840 (b)
1-Butanol	813 (b)	117 (b)	33.1 (b)	3.62 @20 ºC (f)	18 (b)	585 (b)
1-Decanol	828~834	221 (g)	38.9 (g)	8.33 (g)	50 (g)	501 (g)
Methyl Laurate	869 (k)	260 (k)	35.3 (l)	4.48 @ 25 ºC (l)	54~70 (e)	820 (l)

(a) MSDS (Idemitsu Kosan Co., Ltd.)

(b) S. Yamamoto et al., Trans. JSME B 79 (2013) 380–389

(c) http://www.idemitsu.co.jp/factory/hokkaido/quality/

(d) Y. Miyamoto et al., 日本機械学会 2011 年度年次大会 DVD-ROM 論文集 (2011) G070055

(e) J. Yanowitz et al., Technical Report NREL/TP-5400-61693 (2014)

(f) Simulation by HYSYS V7.3 (Pressure: 1 atm, Property package: SRK)

(g) M. Jakob et al., Combust. Flame 159 (2012) 2516–2529

(h) Calculation using Advanced Chemistry Development (ACD/Labs) Software V11.02 (by Sci Finder)

(i) http://www.viscopedia.com/viscosity-tables/substances/methanol/

(j) Biomass Energy Data Book 2001 Appendix A, http://cta.ornl.gov/bedb/appendix_a/Lower_and_Higher_Heating_Values_of_Gas_Liquid_and_Solid_Fuels.pdf

(k) http://www.siyaku.com/uh/Shs.do?dspCode=W01W0113-0358

(l) Simulation by HYSYS V7.3 (Pressure: 1 atm, Property package: UNIPAC)

About the estimation of cetane number of mixing fuel

Cetane number of mixing fuel can be expressed in the following equation [331].

$$\textbf{Cetane number of mixing fuel} = \Sigma[(\textbf{volume fraction}, \textbf{vol}\%) \times (\textbf{cetane number of pure material})]$$

The evaluation of mixing fuel consisting of n-dodecane/ethanol, methyl laurate/ethanol and 1-decanol/ethanol is shown below. It should be noted that 1-octanol of 4 vol% against n-dodecane/ethanol system was added. In this estimation, cetane number of pure n-dodecane, methyl laurate, 1-decanol, ethanol and 1-octanol was 80, 62, 50, 8, and 36, respectively. The behavior of cetane number of mixing fuel when an ethanol fraction in mixing fuel is varied is shown in Figure S-1.

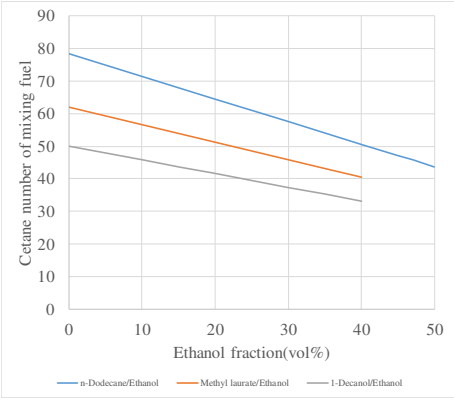

Figure S- 1 The dependence of cetane number of mixing fuel on an ethanol fraction in mixing fuel.

Here, we compared three examples, n-dodecane (55 vol%)/ethanol (45 vol%), methyl laurate (65 vol%)/ethanol (35 vol%) and 1-decanol (65 vol%)/ethanol (35 vol%), and cetane number of mixing fuel is 47.2, 43.1 and 35.3, respectively. The SEM/TEM images corresponding to above fuel condition are presented in Figure 4-6 in the manuscript (an engine load: 1.65 kW). CNT production and CNT structure are almost identical irrespective of fuel condition. In general, when cetane number is decreased, ignition delay time is increased, leading to higher proportion of premixed combustion and reduced proportion of diffusion combustion in a cylinder. The combustion properties of mixing fuel may be different accordingly. However, the result is not affected by the difference of fuel condition. Therefore, this fact suggests that combustion properties caused by the difference of fuel condition does not influence CNT synthesis in a diesel engine so much. Of course, further detailed analysis on combustion properties through the measurement of pressure behavior inside a cylinder should be required for correct evaluation.

Chapter 2

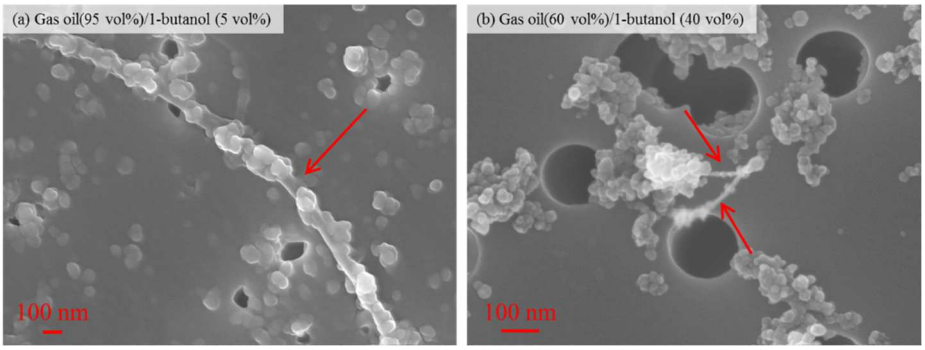

Figure S2- 1 SEM images when gas oil/1-butanol mixing fuel was used. A 1-butanol fraction in fuel was (a) 5 volume% and (b) 40 volume%. Ferrocene concentration was 10,000 ppm by weight, ratio of Mo/Fe was 0.01, and ratio of S/Fe was 0.55. An engine load was 1.05 kW. Observed CNTs are indicated by arrows. The formation of CNT was also confirmed when 1-butanol was used instead of ethanol.

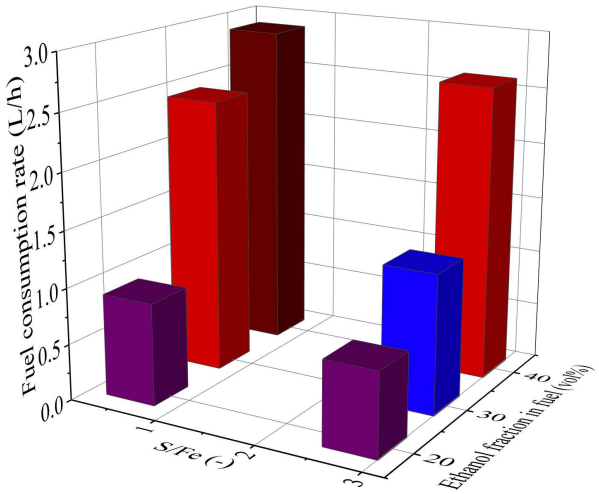

Figure S2- 2 Fuel consumption rate measured in the variation of S/Fe and an ethanol fraction in fuel when gas oil/ethanol mixing fuel was employed. Ferrocene concentration was 10,000 ppm by weight and Mo/Fe was 0.01. An engine load was 1.05 kW. Fuel consumption rate was increased with increasing an ethanol fraction in fuel, while it was decreased when sulfur amount introduced into fuel was increased.

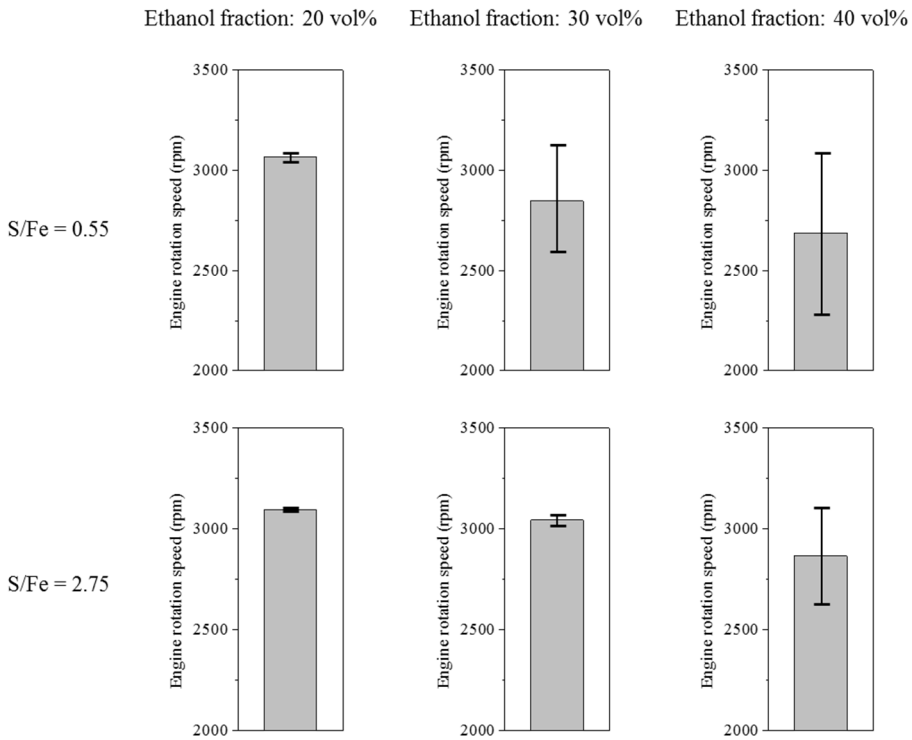

Figure S2- 3 Variation of an engine rotation speed as a function of S/Fe and an ethanol fraction in mixing fuel. When an ethanol fraction was increased, an engine rotation speed was dropped and an engine operation became unstable as indicated by progressively large error bar. When sulfur amount was increased (S/Fe = 2.75), similar tendency was observed, but stability of an engine operation was greatly improved as indicated by smaller error bar in comparison with low sulfur (S/Fe = 0.55). In particular, conditions in an ethanol fraction of 20 volume% and an ethanol fraction of 30 volume% with S/Fe = 2.75 were stable.

Chapter 3

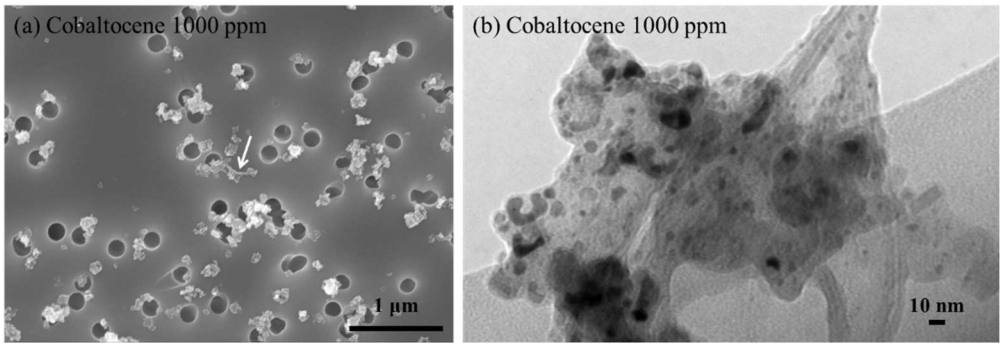

Figure S3- 1 (a) SEM and (b) TEM image when cobaltocene (1,000 ppm by weight) was used as a catalyst source instead of ferrocene. Mixing fuel of n-dodecane (55 volume%)/ethanol (45 volume%) including Mo (Mo/Co = 0.05) and S (S/Co = 11). An engine load was 1.65 kW. CNT synthesis was surely confirmed.

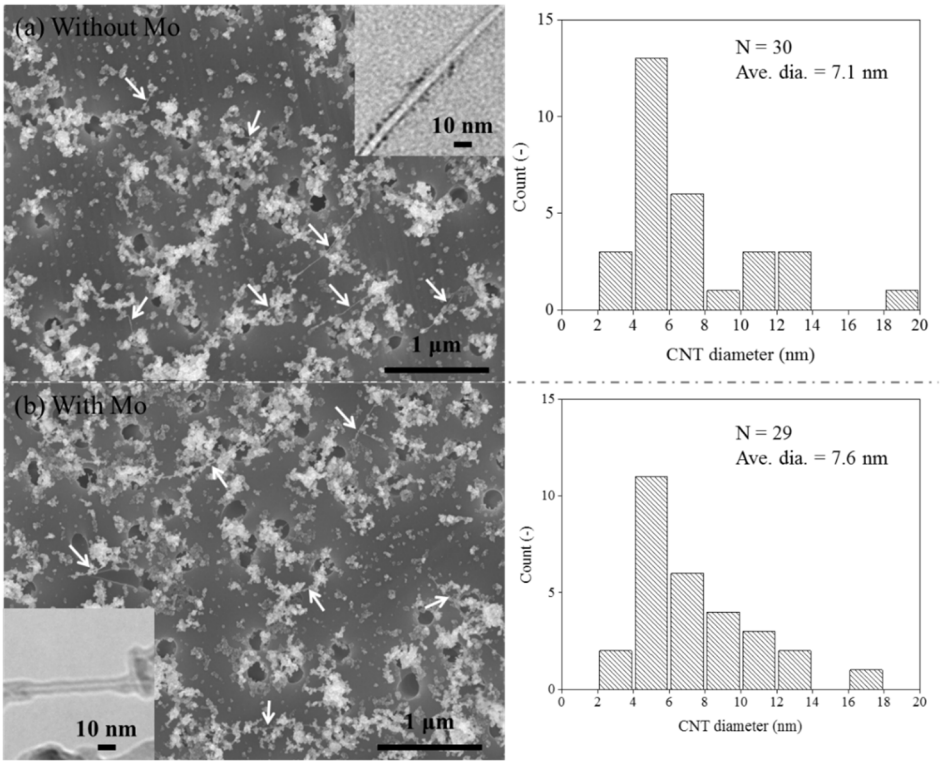

Figure S3- 2 SEM image and corresponding histogram of CNT outer diameter synthesized (a) without Mo and (b) with Mo. TEM photograph is inserted in SEM image. Mixing fuel of n-dodecane (55 volume%)/ethanol (45 volume%) including ferrocene 5,000 ppm by weight and sulfur (S/Fe = 2.2). An engine load was 1.65 kW. CNT production and distribution of CNT outer diameter are almost identical with each other.

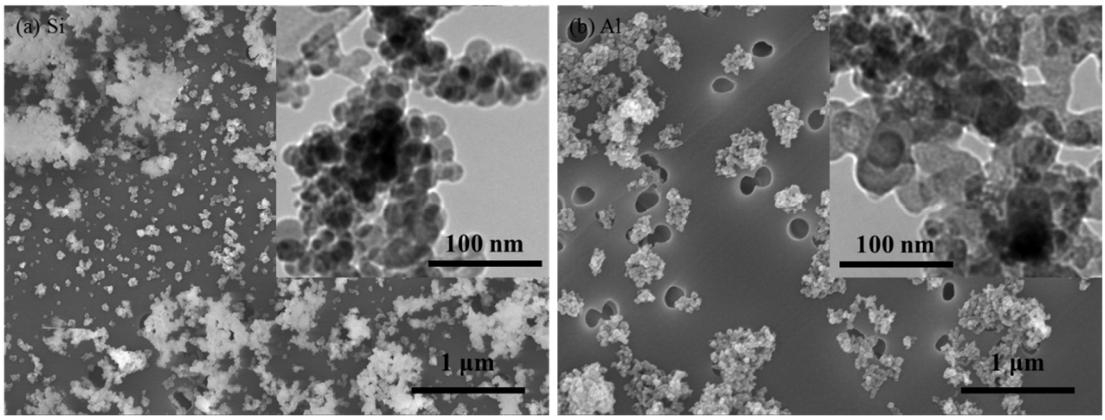

Figure S3- 3 SEM and inserted TEM images when (a) Si (Si/Fe = 2.2) and (b) Al (Al/Fe = 2.2) is used instead of sulfur. Mixing fuel of n-dodecane (55 volume%)/ethanol (45 volume%) including ferrocene 5,000 ppm by weight and Mo (Mo/Fe = 0.01) at 1.65 kW as an engine load. No CNT synthesis was found, but two-phase, separated structure which may be composed of Si and Fe could be observed particularly in case of Si.

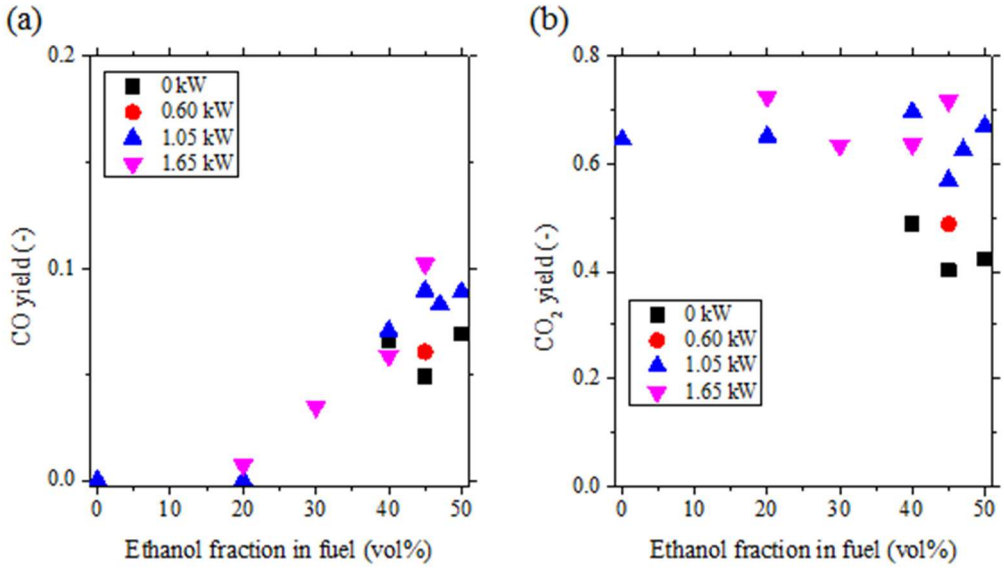

Figure S3- 4 The dependence of (a) CO yield and (b) CO_2 yield in an exhaust gas on an ethanol fraction in fuel and an engine load when n-dodecane/ethanol mixing fuel was employed. Both yields are calculated based on measurements through gas chromatograph in an exhaust gas. CO yield is quite lower than CO_2 yield through all experimental conditions, but its difference becomes relatively small at a high ethanol fraction.

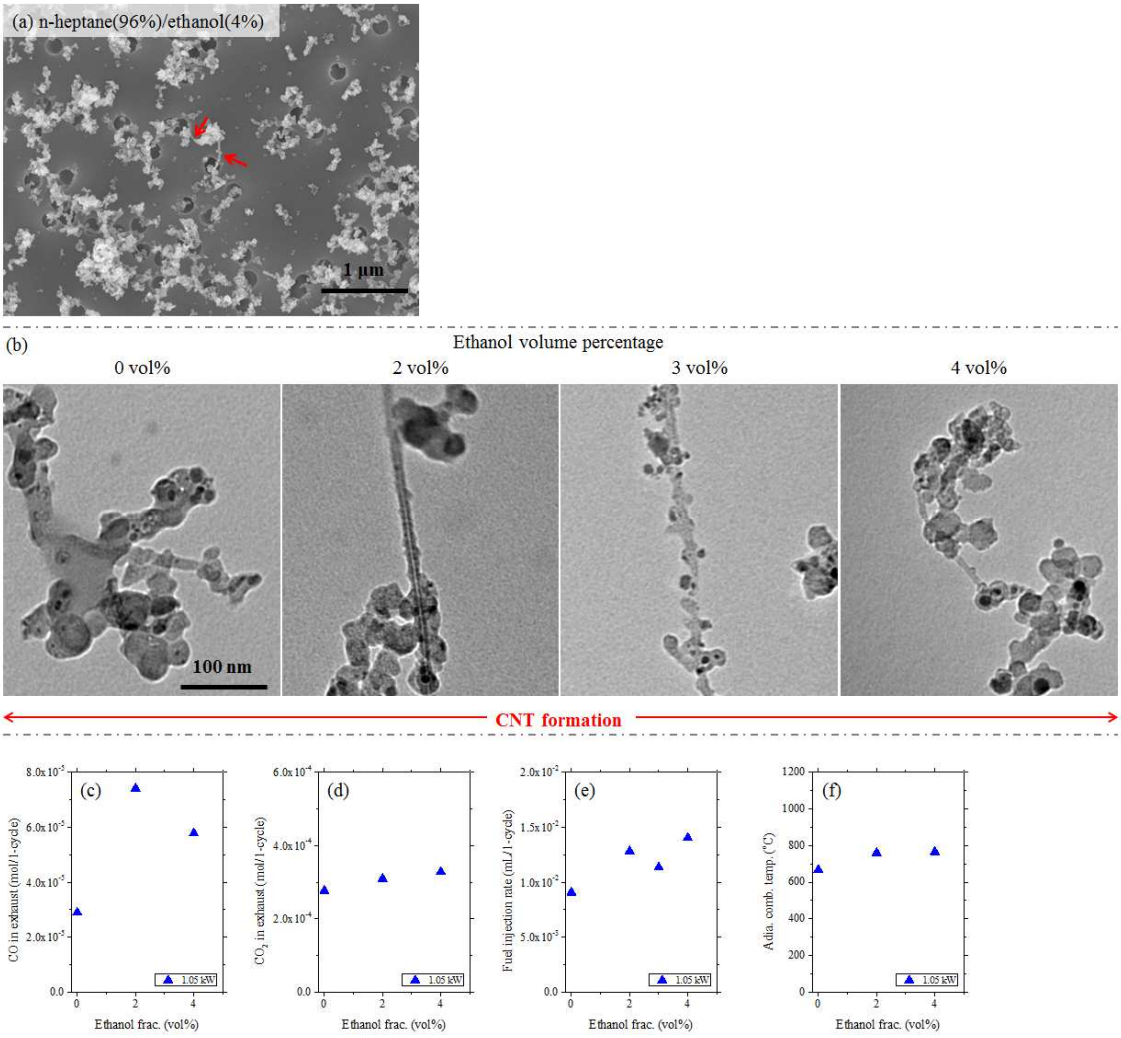

Figure S4- 1 Experimental results when n-heptane/ethanol mixing fuel was used. (a) SEM micrograph where synthesis condition was n-heptane (96 volume%)/ethanol (4 volume%) at 1.05 kW with ferrocene 5,000 ppm by weight and Mo/S (Mo/Fe = 0.01, S/Fe = 2.2). (b) TEM images as a function of an ethanol fraction in mixing. An engine load was 1.05 kW and ferrocene concentration was 5,000 ppm by weight with Mo (Mo/Fe = 0.01) and S (S/Fe = 2.2). CNT seemed to be synthesized at any ethanol fraction. An engine operation became unstable when it was larger than 5 volume%. (c) CO mole amounts in an exhaust gas, (d) CO_2 mole amounts in an exhaust gas, (e) fuel injection rate and (f) mean adiabatic combustion temperature inside a cylinder as a function of an ethanol content.

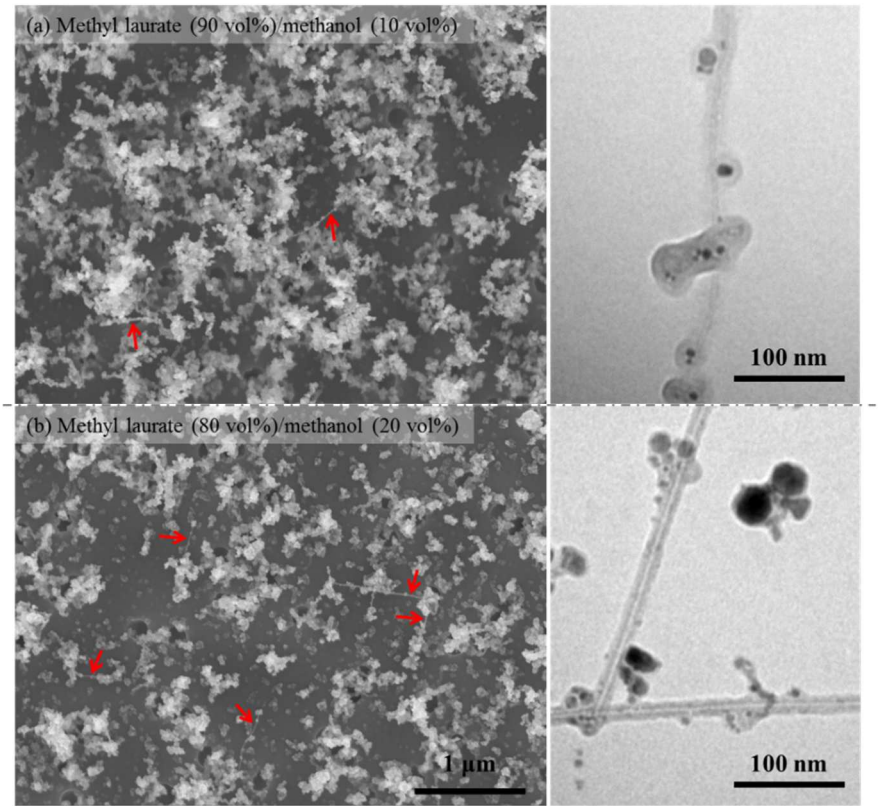

Figure S4- 2 SEM and corresponding TEM images when methanol is employed as an alternative of ethanol. Main fuel is methyl laurate and ferrocene concentration is 5,000 ppm by weight with Mo (Mo/Fe = 0.01) and sulfur (S/Fe = 2.2). An engine load is 1.65 kW. As a methanol content is increased, CNT production is also increased.

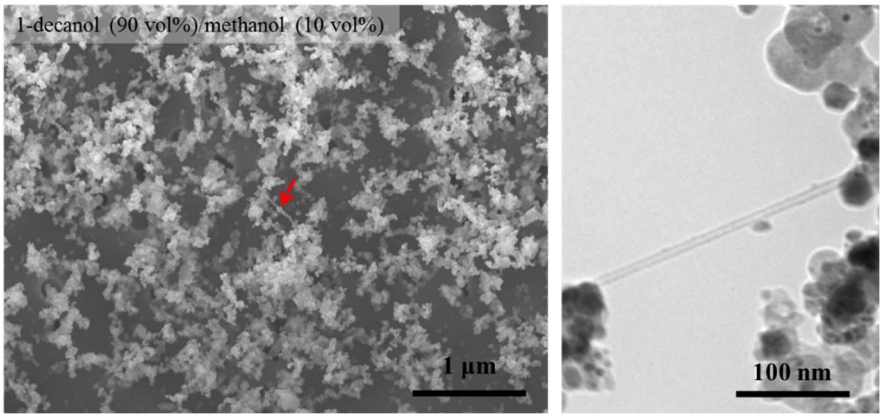

Figure S4- 3 SEM and corresponding TEM images when methanol is employed as an alternative of ethanol. Main fuel is 1-decanol and ferrocene concentration is 5,000 ppm by weight with Mo (Mo/Fe = 0.01) and sulfur (S/Fe = 2.2).

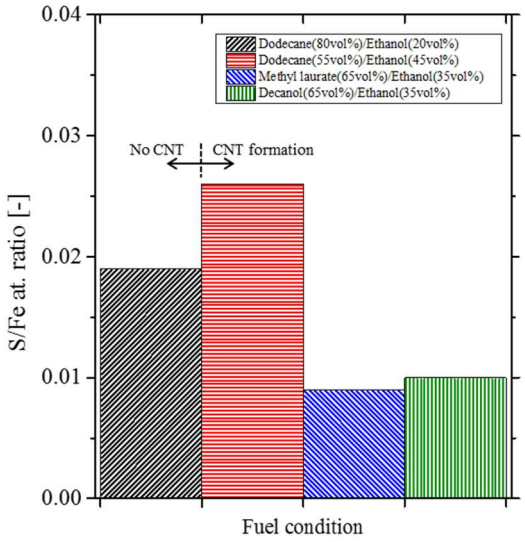

Figure S4- 4 S/Fe atomic ratio of iron particles based on EDX analysis when fuel type is varied. All conditions show the presence of sulfur in catalyst particles. However, whether CNTs are formed or not is independent on sulfur contents.

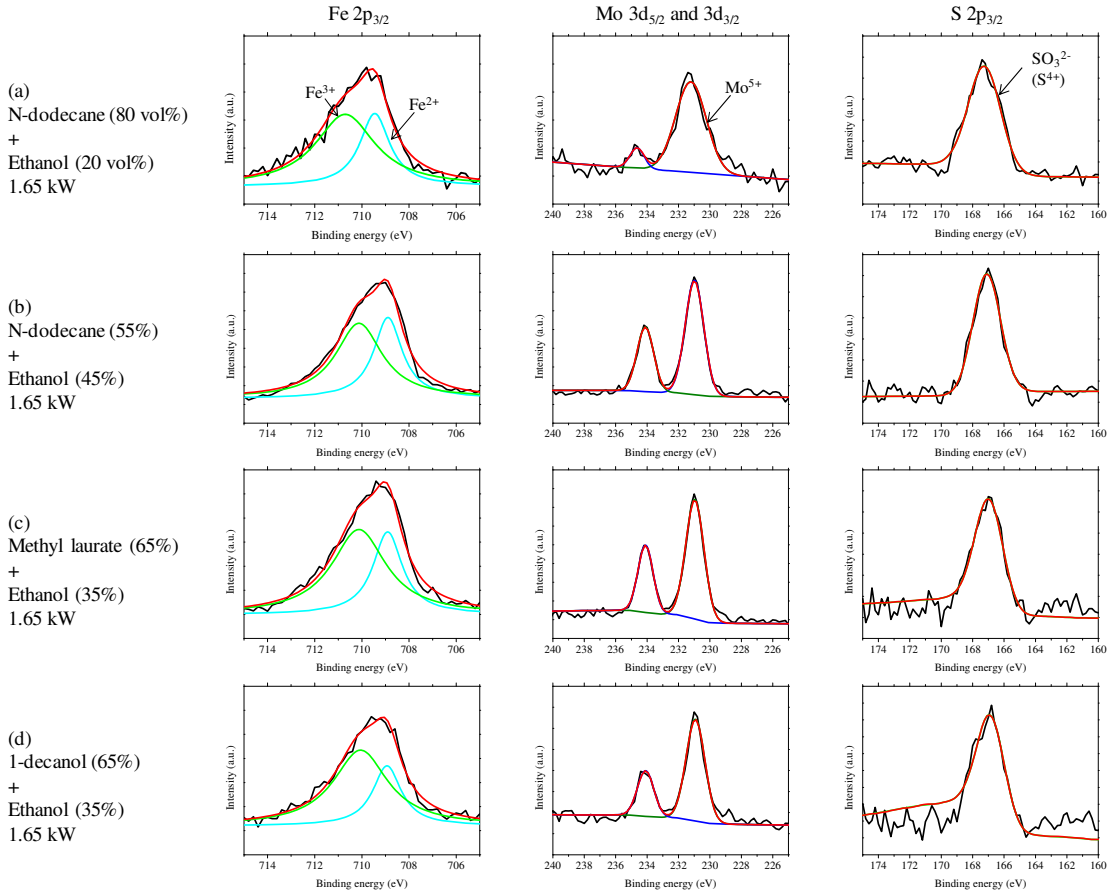

Figure S4- 5 XPS analysis on Fe $2p_{3/2}$, Mo $3d_{5/2}$ and $2d_{3/2}$, and S $2p_{3/2}$ orbital when fuel conditions are varied. X-ray is irradiated against a filter including carbonaceous materials and iron-based particles without any purification treatment. (a) n-dodecane (80 volume%)/ethanol (20 volume%) with 1.65 kW as an engine load. This condition does not show any CNT formation. (b) n-dodecane (55 volume%)/ethanol (45 volume%) with 1.65 kW as an engine load. (c) methyl laurate (65 volume%)/ethanol (35 volume%) with 1.65 kW as an engine load. (d) 1-decanol (65 volume%)/ethanol (35 volume%) with 1.65 kW as an engine load. In latter three conditions, CNT synthesis is found. Ferrocene concentration in mixing fuel is 5,000 ppm by weight, and Mo (Mo/Fe = 0.01) and sulfur (S/Fe = 2.2) is contained as well. There are very less differences in chemical state between experimental conditions.

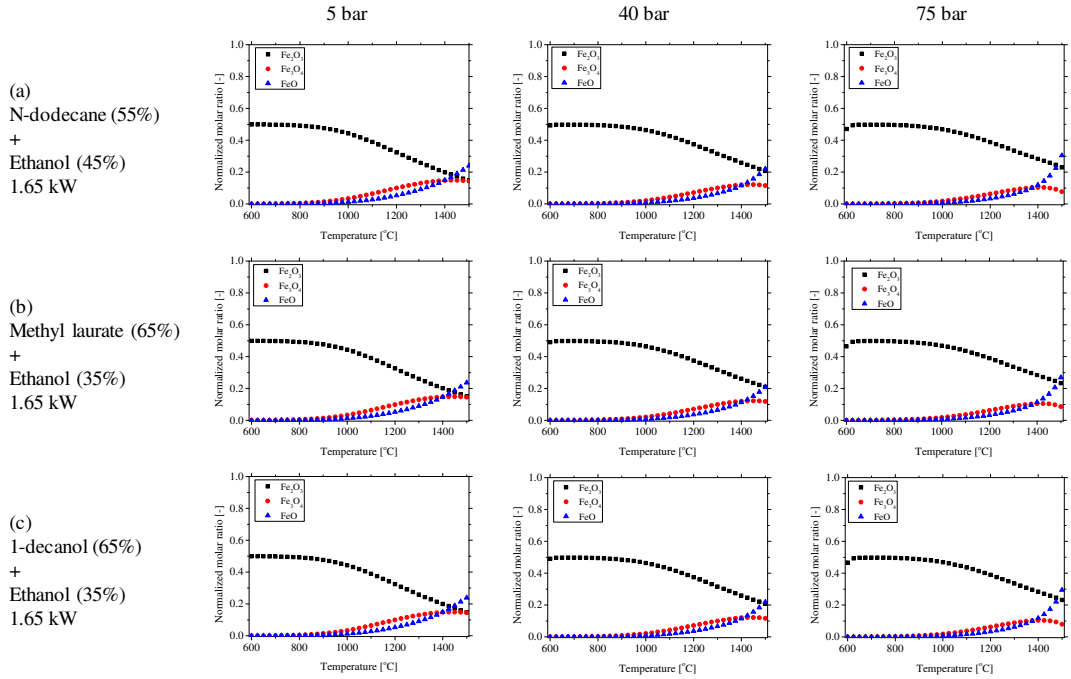

Figure S4- 6 Equilibrium calculations of chemical state of iron under different stating fuel and different pressures by means of Outokumpu HSC Chemistry for Windows (ver. 2.0). Dominant state of Fe in our experimental circumstances is oxidized one, being independent on pressure and fuel condition. Mean adiabatic combustion temperatures in our system are below 1,500 °C, and thus both Fe_2O_3 and FeO are mainly formed from the equilibrium point of view, being consistent with XPS analysis.

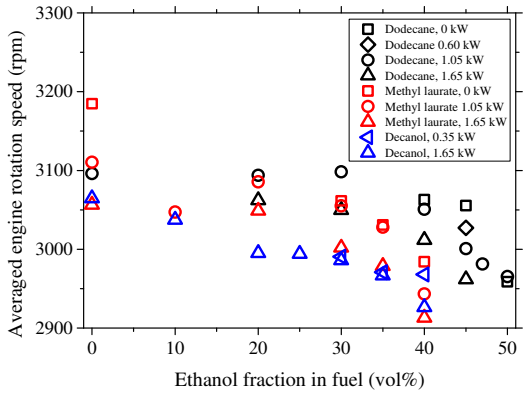

Figure S4- 7 Variations of averaged engine rotation speed as a function of fuel type, an ethanol fraction in fuel and an engine load. As a tendency, the fluctuation of an engine speed (The difference of maximum and minimum engine rotation speed) becomes large with an increase of an ethanol fraction in fuel (not shown here). Also, an engine speed declines gradually along with an ethanol fraction.

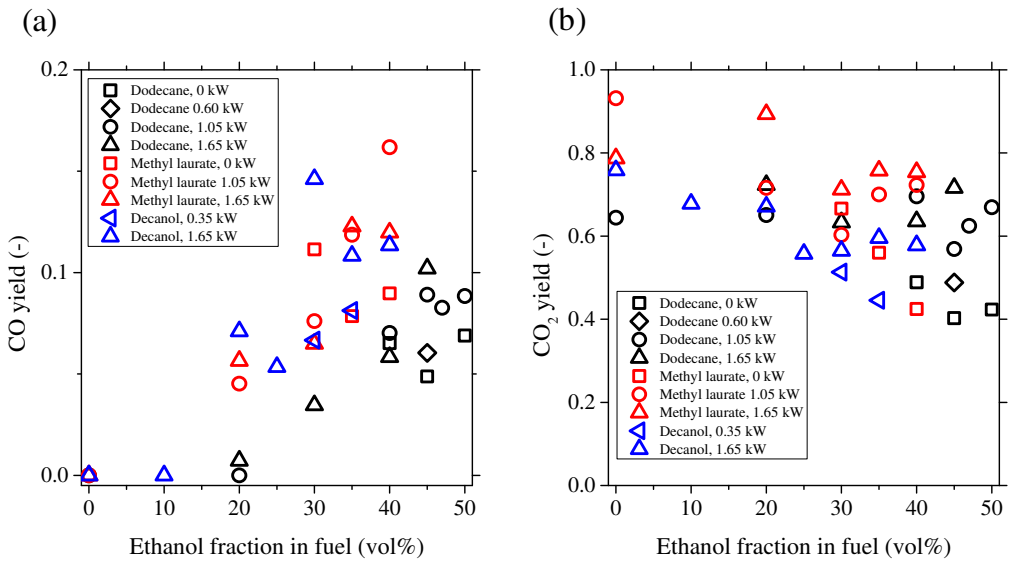

Figure S4- 8 Variations of (a) CO yield and (b) CO_2 yield in an exhaust as a function of fuel type, an ethanol fraction in fuel and an engine load. The calculation way of both yields is given in a similar manner expressed in the previous chapter. Larger CO yield is obtained using methyl laurate and 1-decanol than n-dodecane when compared at the equal ethanol fraction/engine load. The behavior of CO_2 yield resembles that of fuel conversion in Figure 4-4.

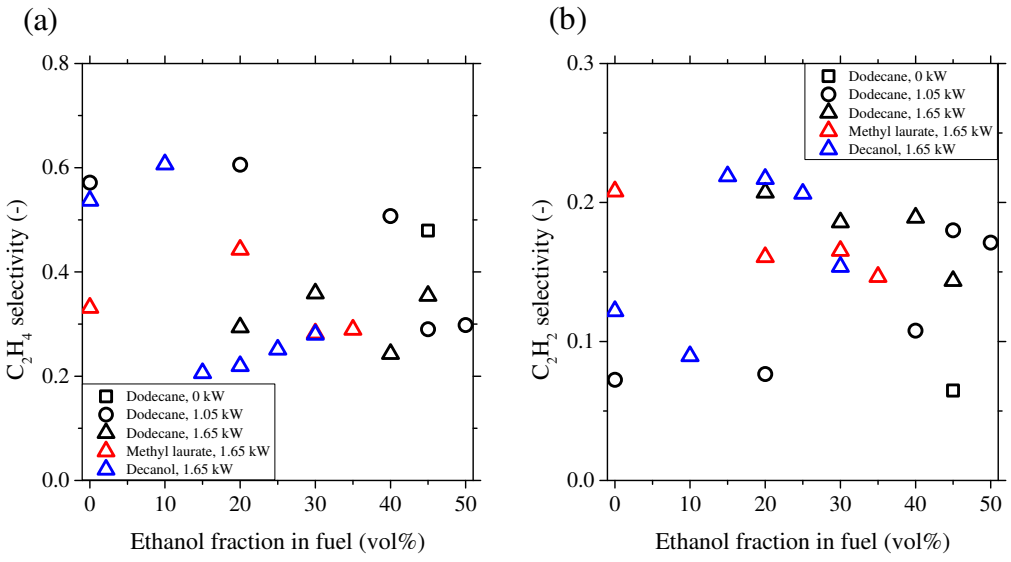

Figure S4- 9 Variations of (a) C_2H_4 selectivity and (b) C_2H_2 selectivity in an exhaust when fuel type is changed. The definition of selectivity is the ratio of ethylene or acetylene molar quantity in an exhaust to total molar quantity in an exhaust ranging from C1 to C3 hydrocarbons measured by means of gas chromatograph. No clear tendency is found.

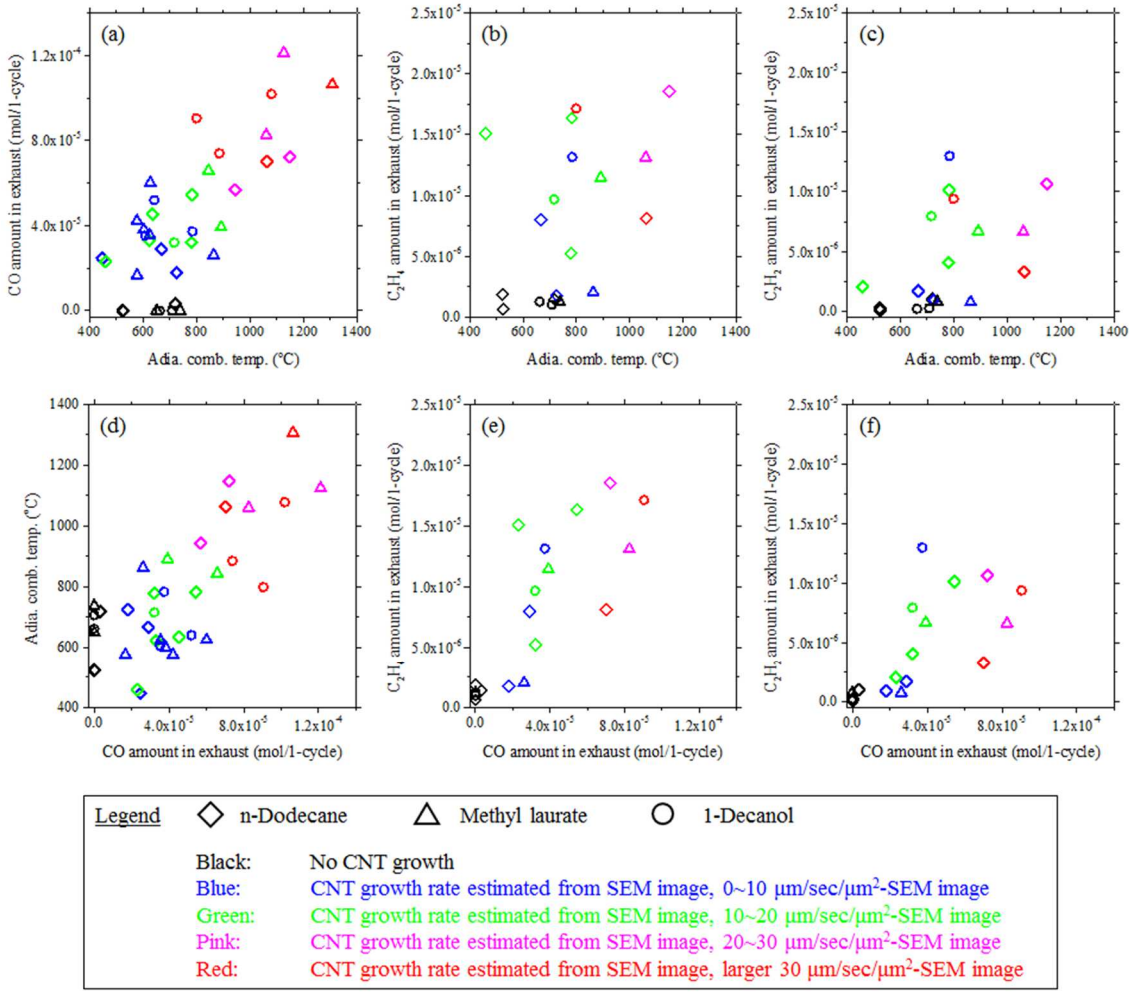

Figure S5- 1 Contour plots of CNT growth rates estimated from SEM micrographs using n-dodecane, methyl laurate and 1-decanol as main fuel. The correlation of (a) adiabatic combustion temperature vs. CO amounts in an exhaust, (b) adiabatic combustion temperature vs. C_2H_4 amounts in an exhaust, (c) adiabatic combustion temperature vs. C_2H_2 amount in an exhaust, (d) CO amounts in an exhaust vs. adiabatic combustion temperature, (e) CO amounts in an exhaust vs. C_2H_4 amounts in an exhaust and (f) CO amounts in an exhaust vs. C_2H_2 amounts in an exhaust. It should be noted that the same data with those in main manuscript are employed for the preparation of these contour plots. As a rough tendency, CNT growth rate is enhanced high combustion temperature and large amounts of hydrocarbons, which is especially noticeable in (a) and (d).

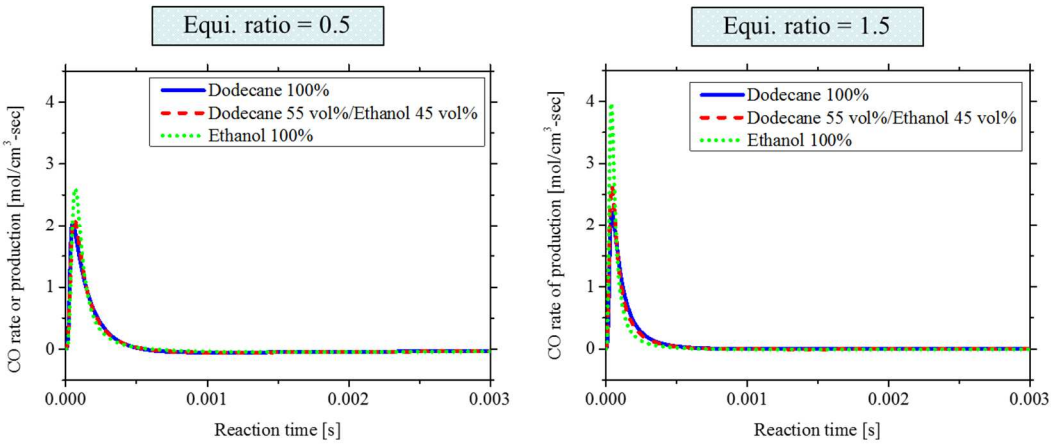

Figure S5- 2 CO rate of production simulated by CHEMKIN-PRO using a closed homogeneous reactor at 1250 K and 50 atm with different starting fuel. Irrespective of fuel rich/lean condition, CO production is increased with increasing an ethanol fraction in fuel.

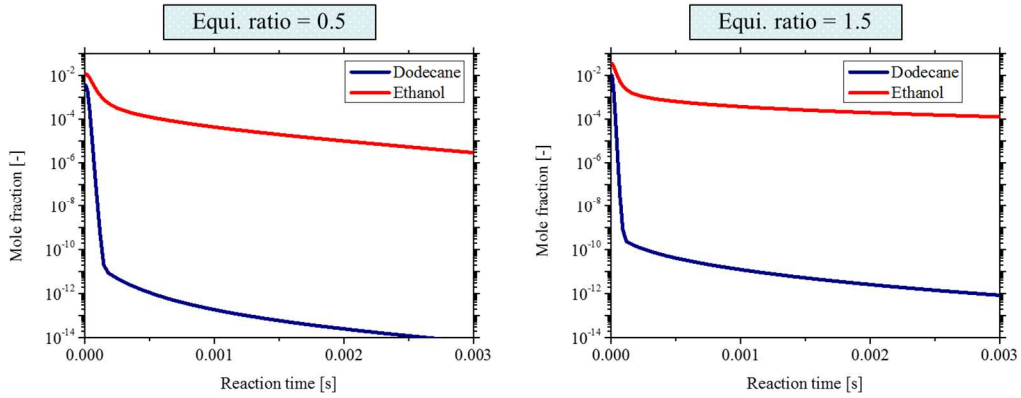

Figure S5- 3 The profile of normalized mole fraction of feedstock (n-dodecane/ethanol) simulated by CHEMKIN-PRO using a closed homogeneous reactor at 1250 K and 50 amt. Fuel condition was the mixture of n-dodecane (55 vol%) and ethanol (45 vol%). In both fuel rich/lean condition, consumption rate of n-dodecane is faster than that of ethanol, meaning that n-dodecane is easier to be oxidized.

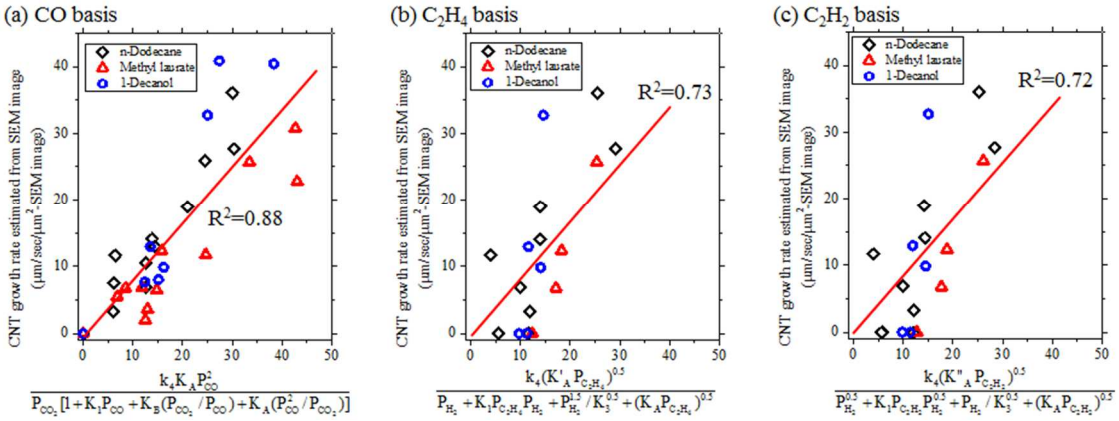

Figure S5- 4 Comparison of modeling performance using different hydrocarbons. This figure is extended to not only n-dodecane but also methyl laurate and 1-decanol as starting main fuel. (a) carbon monoxide basis, (b) ethylene basis and (c) acetylene basis. All modeling were carried out on the basis of the amounts in an exhaust gas in a similar manner stated in main manuscript. For modeling, the assumption that the rate-limiting step was carbon diffusion and other steps satisfied quasi-equilibrium was provided. Considering R^2, carbon monoxide is no less compelling CNT precursor even when modeling was extended to all main fuel used in this study. Fitting parameters same with those described in main manuscript were applied for preparing this figure.

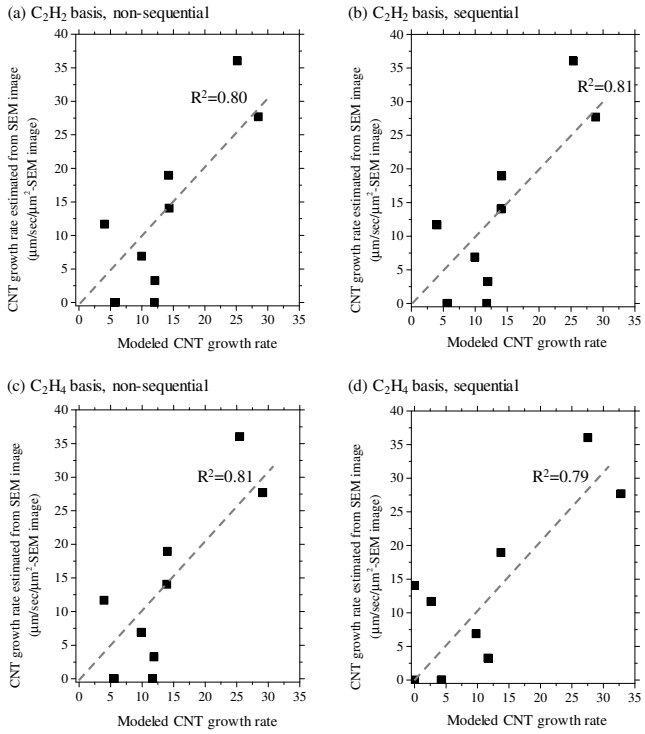

Figure S5- 5 Comparison of modeling performance in sequential surface reactions mode or non-sequential surface reactions mode in the use of acetylene or ethylene as a carbon source. (a) non-sequential manner using acetylene, (b) sequential manner using acetylene, (c) non-sequential manner using ethylene, and (d) sequential manner using ethylene. Only data related to n-dodecane are picked up. Non-sequential reaction manner coincides with the one described in the main manuscript (Chapter 5). This non-sequential manner is simplified reaction model. However, from the realistic point of view in surface reactions on catalytic surface, it is impractical that adsorbed molecules react with 4~6 reaction sites simultaneously, particularly in acetylene and ethylene. The cracking reaction of acetylene and ethylene should proceed in a sequential mode, where surface reaction sites take part in one by one. Here, we compared the fitting performance in non-sequential mode and sequential mode as shown above, and we confirmed that there is very less difference even when reaction sequence is simplified. The detailed procedure to give CNT growth rate in the sequential manner is expressed below.

- Acetylene (C_2H_2)

  We assumed that the cracking reaction using acetylene proceeds as follows in a sequential manner.

  $C_2H_2 + * \Leftrightarrow C_2H_2*$ (a)

  $C_2H_2* + * \Leftrightarrow C_2H* + H*$ (b)

  $C_2H* + * \Leftrightarrow C* + CH*$ (c)

  $CH* + * \Leftrightarrow C* + H*$ (d)

  $2H* \Leftrightarrow H_2 + 2*$ (e)

$C^* \Rightarrow C_{CNT} + *$ (f)

When carbon diffusion stage (step (f)) is assumed to be rate-determining and quasi-equilibrium is satisfied in other steps, modeled CNT growth rate can be estimated as below.

$$R'_{CNT} = \frac{k_f (K_a K_b K_c K_d K_e P_{C2H2})^{0.5}}{P_{H2}^{0.5} + K_a P_{C2H2} P_{H2}^{0.5} + P_{H2} / K_e^{0.5} + (K_a K_b K_c K_d K_e P_{C2H2})^{0.5} + K_a K_b K_e^{0.5} P_{C2H2} + (K_a K_b K_c P_{C2H2} P_{H2} / K_d)^{0.5}}$$

The meaning and definition of each symbol (e.g. k_i and K_i) is the same with that in the manuscript, e.g. k_i and K_i represent the rate constant and equilibrium constant in reaction step (i), respectively. By tuning fitting parameters, modeled CNT growth rate was calculated as shown in Figure S5-5 (b). Fitting parameters are summarized in Table S5-1, where the value in non-sequential and sequential manner is compared in the same column, e.g. k_{150} and k_{f0}.

- Ethylene (C_2H_4)

Sequential reactions of ethylene cracking become slightly complicated than the ones in acetylene. They proceed as follows.

$C_2H_4 + * \Leftrightarrow C_2H_4*$ (a)

$C_2H_4* + * \Leftrightarrow C_2H_3* + H*$ (b)

$C_2H_3* + * \Leftrightarrow C_2H_2* + H*$ (c)

$C_2H_2* + * \Leftrightarrow C_2H* + H*$ (d)

$C_2H* + * \Leftrightarrow C* + CH*$ (e)

$CH* + * \Leftrightarrow C* + H*$ (f)

$2H* \Leftrightarrow H_2 + 2*$ (g)

$C^* \Rightarrow C_{CNT} + *$ (h)

When carbon diffusion stage (step (h)) is assumed to be rate-determining and quasi-equilibrium is satisfied in other steps, modeled CNT growth rate can be estimated as below.

$$R''_{CNT} = \frac{k_h K_g (K_a K_b K_c K_d K_e K_f P_{C2H4} P_{H2})^{0.5}}{K_a P_{C2H4} P_{H2}^{1.5} + K_a K_b K_g^{0.5} P_{C2H4} P_{H2} + K_a K_b K_c K_g P_{C2H4} P_{H2}^{0.5} + K_a K_b K_c K_d K_g^{1.5} P_{C2H4} + (K_a K_b K_c K_d K_e K_g P_{C2H4} / K_f)^{0.5} P_{H2}}$$

$$\overline{+ K_g (K_a K_b K_c K_d K_e K_f P_{C2H4} P_{H2})^{0.5} + P_{H2}^2 / K_g^{0.5} + P_{H2}^{1.5}}$$

As well as in acetylene, fitting parameters were adjusted so that fitting performance became better as much as possible, Figure S5-5 (d). Fitting parameters determined here are summarized in Table S5-2.

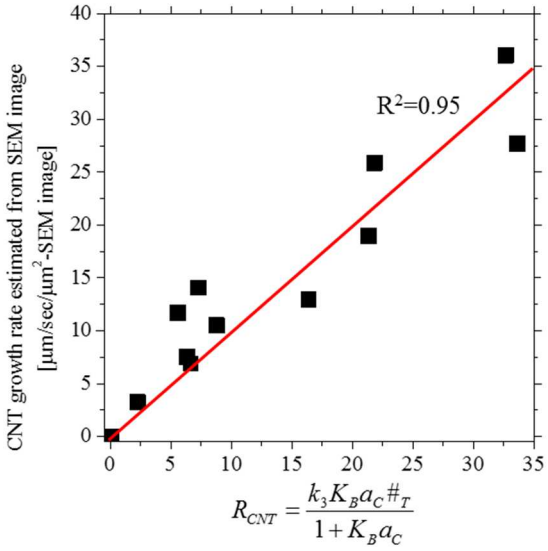

Figure S5- 6 Comparison of measured CNT growth rate and modeled one based on Eley-Rideal mechanism in CO disproportionation instead of Langmuir-Hinshelwood mechanism. Modeling using Eley-Rideal mechanism worked equally well with that using Langmuir-Hinshelwood mechanism.

We assumed that CO disproportionation reactions in Eley-Rideal mechanism proceed in the following three elemental reactions.

CO dissociative adsorption: $CO + * + \# \Leftrightarrow C\# + O*$ (1)

CO_2 desorption: $CO + O* \Leftrightarrow CO_2 + *$ (2)

Carbon diffusion: $C\# \Rightarrow C_{CNT} + \#$ (3)

where # and * signify adsorption site for carbon and oxygen on catalyst surface, respectively. If step (3), carbon diffusion, is assumed to be a rate-limiting step, CNT growth rate can be described as follows.

$$R_{CNT} = k_3 K_B a_c \#_T / (1 + K_B a_c)$$

where k_3 is a reaction rate constant in step (3), $K_B = K_1 K_2 / K_{eq}$ is an integrated equilibrium constant, K_1 is an equilibrium constant in step (1), K_2 is an equilibrium constant in step (2), K_{eq} is an equilibrium constant of overall CO disproportionation reaction ($2CO \Leftrightarrow C + CO_2$), a_c is defined as $K_{eq} P_{CO}^2 / P_{CO_2}$, $\#_T$ is total adsorption site number on catalyst surface. For fitting, we supposed that k_3 obeys Arrhenius equation and K_B is constant (independent on temperature). Then, each fitting parameter is indicated below.

$k_3 = 1.0 \times 10^8 \exp(-170\ [kJ/mol]/RT)$

$K_B = 1.0 \times 10^{-4}$

$\#_T = 4.0 \times 10^7$

Here, a_c, P_{CO} and P_{CO_2} are estimated according to measured data during experiments.

Table S5- 1 Comparison table showing fitting parameters in non-sequential manner and sequential manner for estimating modeled CNT growth rate when acetylene is used as a carbon source.

Non-sequential manner	Sequential manner
$k_{150} = 2.5 \times 10^2$ s^{-1}	$k_{f0} = 2.4 \times 10^2$ s^{-1}
$\Delta E_{15} = 25$ kJmol^{-1}	$\Delta E_f = 25$ kJmol^{-1}
$K_{120} = 1.0 \times 10^{-27}$ atm^{-1} at 873 K	$K_{a0} = 1.0 \times 10^{-27}$ atm^{-1} at 873 K
$\Delta H_{12} = -250$ kJmol^{-1}	$\Delta H_a = -250$ kJmol^{-1}
$K_{140} = 1.0 \times 10^{10}$ atm at 873 K	$K_{e0} = 1.0 \times 10^{10}$ atm at 873 K
$\Delta H_{14} = 60$ kJmol^{-1}	$\Delta H_e = 60$ kJmol^{-1}
$K_{D0} = 1.0 \times 10^4$ at 873 K	-
$\Delta H_D = -80$ kJmol^{-1}	-
-	$K_{b0} = 1.0 \times 10^5$ at 873 K
-	$\Delta H_b = 50$ kJmol^{-1} [(a)]
-	$K_{c0} = 1.0 \times 10^9$ at 873 K
-	$\Delta H_c = -40$ kJmol^{-1} [(a)]
-	$K_{d0} = 1.0 \times 10^9$ at 873 K
-	$\Delta H_d = 50$ kJmol^{-1} [(a)]

(a) Some newly added fitting parameters, ΔH_i, were determined in reference to previous publications [332,333,334,335]. However, the other newly added parameters such as K_i were determined arbitrarily due to the shortage of past literature data.

Table S5- 2 Comparison table showing fitting parameters in non-sequential manner and sequential manner for estimating modeled CNT growth rate when ethylene is used as a carbon source.

Non-sequential manner	Sequential manner
$k_{110} = 2.4 \times 10^2$ s^{-1}	$k_{h0} = 3.1 \times 10^2$ s^{-1}
$\Delta E_{11} = 25$ kJmol^{-1}	$\Delta E_f = 25$ kJmol^{-1}
$K_{80} = 5.0 \times 10^{-12}$ atm^{-1} at 873 K	$K_{a0} = 5.0 \times 10^{-12}$ atm^{-1} at 873 K
$\Delta H_8 = -60$ kJmol^{-1}	$\Delta H_a = -60$ kJmol^{-1}
$K_{100} = 1.0 \times 10^{10}$ atm at 873 K	$K_{g0} = 1.0 \times 10^{10}$ atm at 873 K
$\Delta H_{10} = 60$ kJmol^{-1}	$\Delta H_g = 60$ kJmol^{-1}
$K_{C0} = 1.0 \times 10^4$ at 873 K	-
$\Delta H_C = 100$ kJmol^{-1}	-
-	$K_{b0} = 1.0 \times 10^3$ at 873 K
-	$\Delta H_b = -40$ kJmol^{-1}
-	$K_{c0} = 1.0 \times 10^{10}$ at 873 K

-	ΔH_c = -50 kJmol^{-1}
-	K_{d0} = 1.0 × 10^5 at 873 K [(a)]
-	ΔH_d = 50 kJmol^{-1} [(a)]
-	K_{e0} = 1.0 × 10^9 at 873 K [(a)]
-	ΔH_e = -40 kJmol^{-1} [(a)]
-	K_{f0} = 1.0 × 10^9 at 873 K [(a)]
-	ΔH_f = 50 kJmol^{-1} [(a)]

(a) It should be noted that reaction step (b), (c) and (d) in acetylene cracking are corresponding to that (d), (e) and (f) in ethylene cracking, respectively. Thus, the similar values with each other were employed.

Kinetic/thermodynamic data for CHEMKIN simulation

(n-dodecane/ethanol/sulfur oxidation)


Reaction kinetics.txt


Thermodynamic properties.txt

(iron particle growth reaction)


Kinetic reactions.txt


Thermodynamics.txt

(methyl laurate/ethanol/sulfur oxidation)


Reaction kinetics.txt


Thermodynamic properties.txt

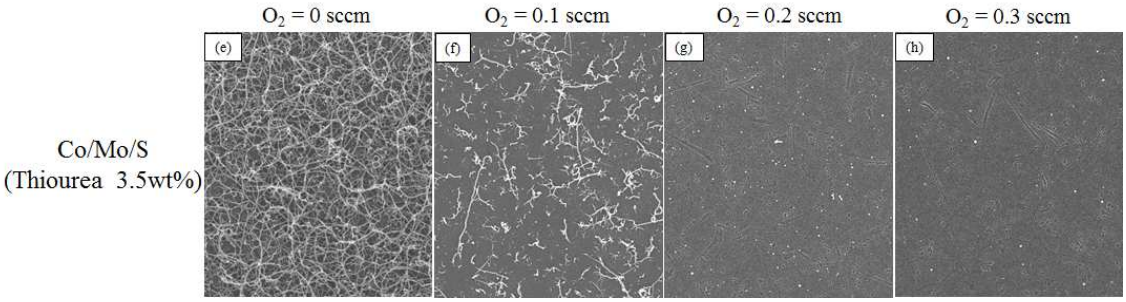

Figure S7- 1 SEM images showing the effects of O_2 in feed gas on CNT synthesis when thiourea was used as a sulfur source.

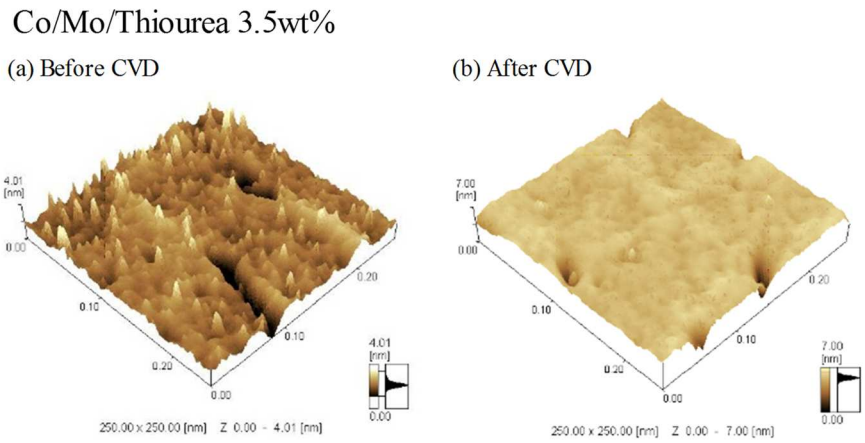

Figure S7- 2 AFM images of the substrate using thiourea. The images (a) before CVD and (b) after CVD (10 minutes at 800 ^oC).

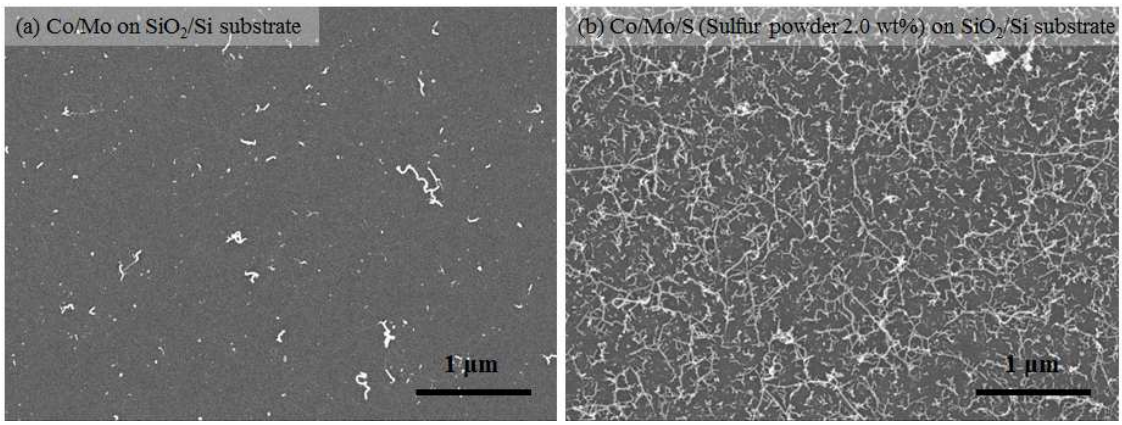

Figure S7- 3 SEM micrograph in the employment of SiO_2/Si substrate instead of quartz. (a) Co/Mo free from sulfur and (b) Co/Mo/S (Sulfur powder 2.0 wt%). CVD was performed at 800 ^oC for 30 minutes. It is obvious that the addition of sulfur is effective as well when SiO_2/Si substrate is used.

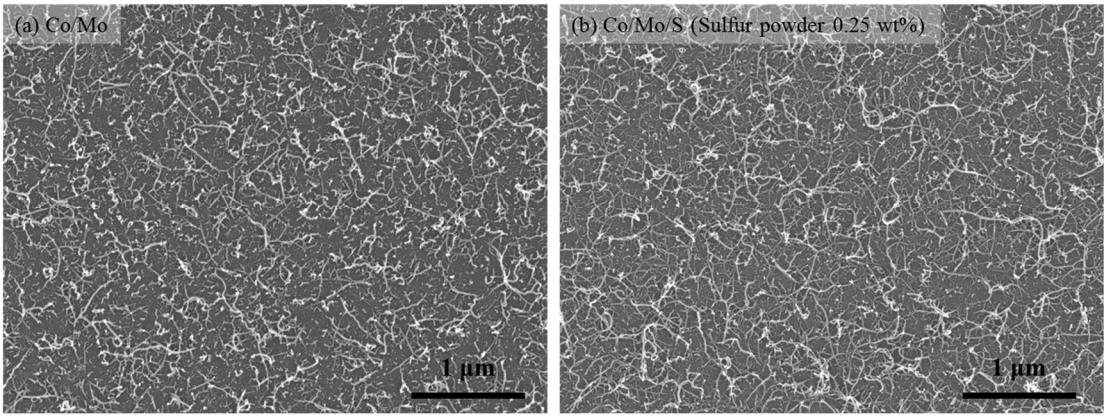

Figure S7- 4 SEM photographs when reduction procedure is changed from ordinary operation in (a) Co/Mo alone and (b) Co/Mo/S (Sulfur powder 0.25 wt%). CVD was performed at 800 ^{o}C for 30 minutes. Reduction operation using H_2 was initiated at the same time as heating from room temperature was started. Furnace temperature was kept at 400 ^{o}C for 30 minutes, and then heating was restarted up to 800 ^{o}C. Soon after temperature becomes 800 ^{o}C, CVD was carried out. When reduction procedure is varied, difference in CNT production between catalyst conditions becomes very small. It should be note that benzene was utilized as a solvent during dip-coating of sulfur powder.

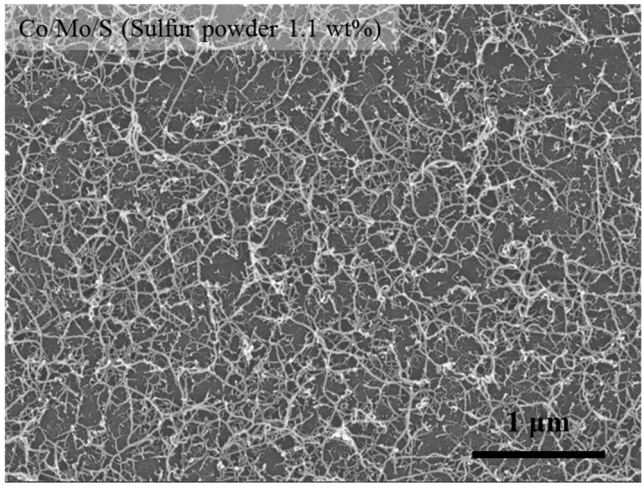

Figure S7- 5 SEM image in the use of mixed solution (ethanol + toluene) including Co precursor, Mo precursor and sulfur powder although ordinary procedure requires two separated step for dip-coating of Co/Mo and sulfur. Since CNT production is facilitated even in one step, there is chance that we are able to make preparation procedure simple.

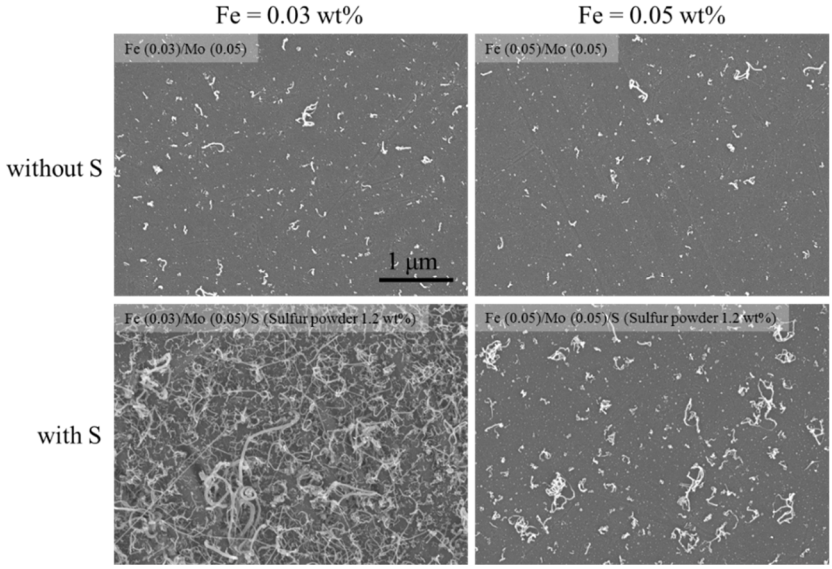

Figure S7- 6 SEM images when iron acetate is employed as a catalyst instead of cobalt acetate as a function of dissolved amounts of it in ethanol and with/without sulfur powder. It should be noted that reduction operation is different from Co/Mo case. Reduction was begun simultaneously with the temperature rising. Furthermore, reduction temperature was 750 ^{o}C and kept at this temperature for 15 minutes before CVD. CVD operation also differs from Co/Mo case, namely, CO of 45 sccm and H_2 of 4.5 sccm were fed in the absence of Ar for 60 minutes at 750 ^{o}C. Although the effect of sulfur addition is more evident in Fe = 0.03 wt%, it enhances CNT growth in Fe = 0.05 wt%.

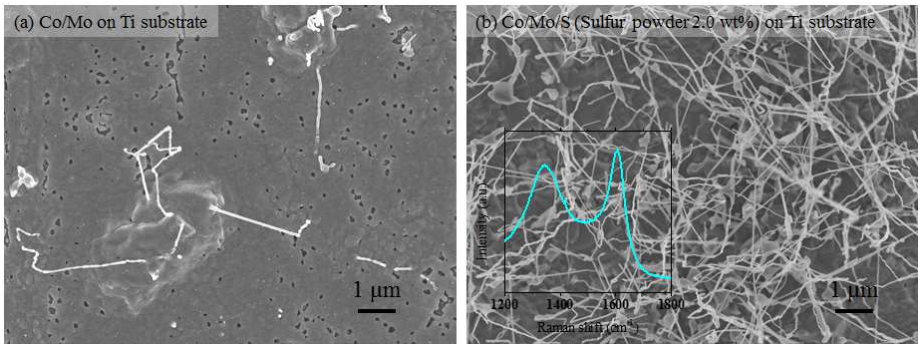

Figure S7- 7 SEM micrograph when Ti substrate was used in place of quartz. Ti substrate was calcined in air at 400 ^{o}C for 5 minutes before using in order to form TiO_2 layer. (a) catalyst condition was Co/Mo alone. (b) catalyst condition was Co/Mo/S (Sulfur powder 2.0 wt%). The reduction procedure was identical with that in quartz substrate, and CVD process where gas condition was consistent with that described in main manuscript was performed for 30 minutes at 800 ^{o}C. The effectiveness of sulfur for CNT growth can be recognized. Raman spectrum is inserted in (b), showing broad G and D peak, which is characteristic of MWNTs.

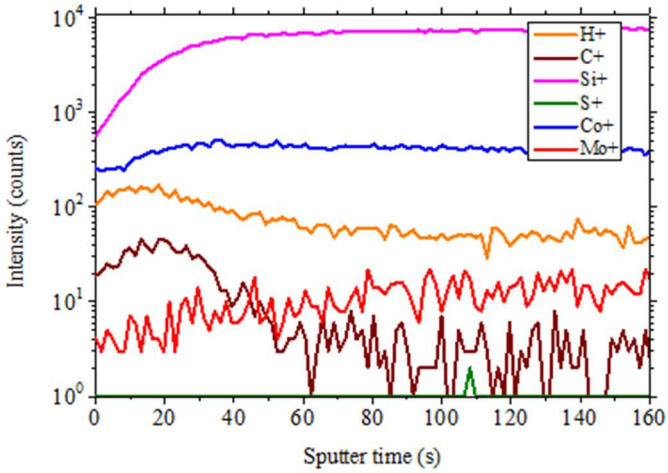

Figure S7- 8 Elemental depth profile of positive ions using TOF-SIMS. A sample is the one after a reduction (no CVD was performed) in the employment of Co/Mo/S (Sulfur powder 2.0 wt%). Due to low sputtering speed, elemental profile is less affected. The behavior in positive ions is less informative.

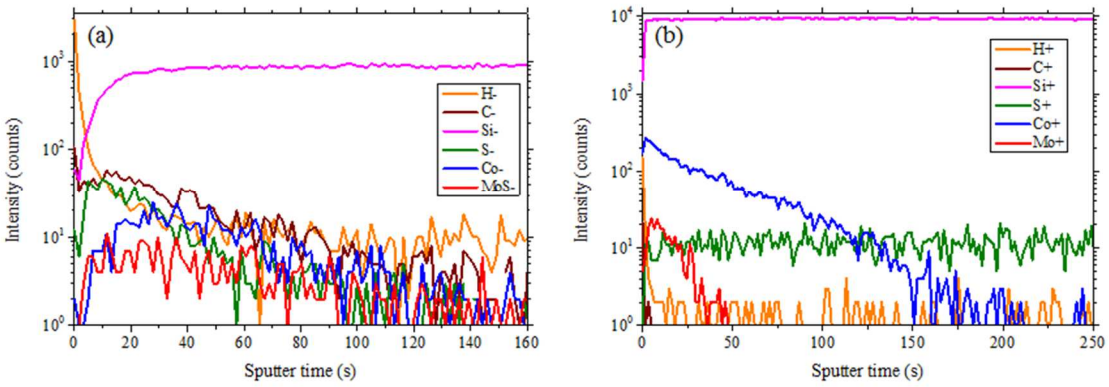

Figure S7- 9 Elemental depth profile using TOF-SIMS in a sample that Co/Mo/S (Sulfur powder 2.0 wt%) is used after CVD for 10 minutes at 800 ^{o}C. The profile of (a) negative ions and (b) positive ions. Both behaviors in negative/positive ions in these figure are well coincident with those in a sample performed up to reduction (no CVD).

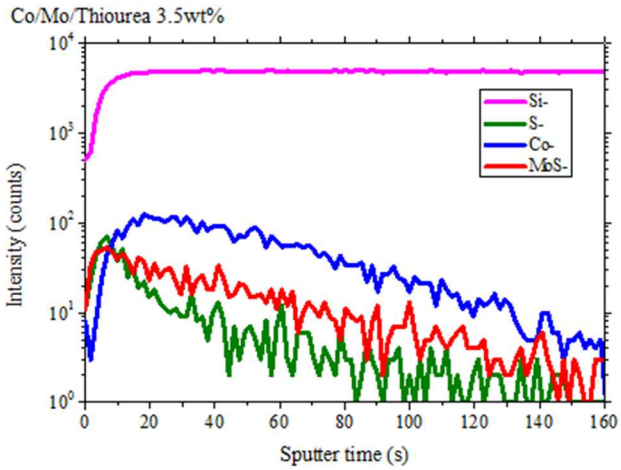

Figure S7- 10 Elemental depth profile of negative ions using TOF-SIMS. A sample is the one that thiourea was used as a sulfur source. Up to reduction operation was carried out (no CVD).

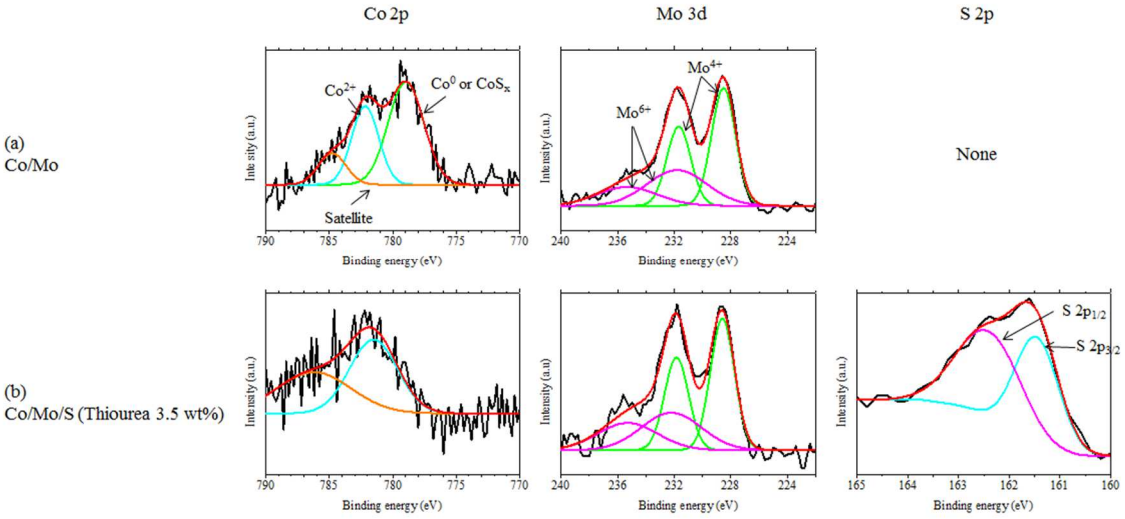

Figure S7- 11 XPS spectra of Co 2p, Mo 3d and S 2p in (a) Co/Mo alone and (b) Co/Mo/S (Thiourea 3.5 wt%). It should be noted that CVD at 800 ^{o}C for 10 minutes was carried out before analysis on Co and Mo. In case of S, multiple layers of Co/Mo/S were dip-coated and CVD was performed at 800 ^{o}C for 5 minutes before analysis. The chemical state of sulfur is identical with that in Co/Mo/S using sulfur powder describe in main manuscript.

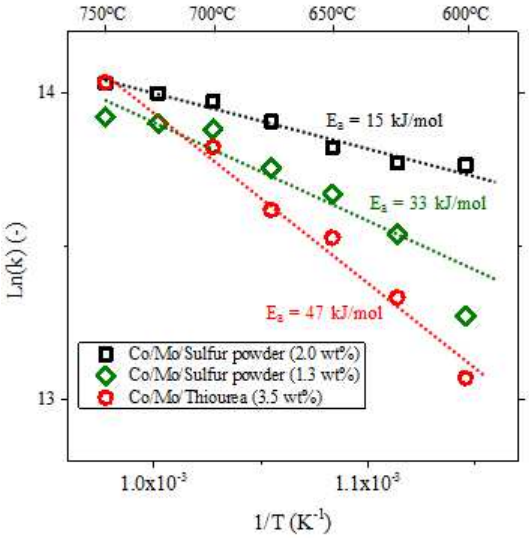

Figure S7- 12 The dependence of CNT growth rate on CVD temperature including Co/Mo/S (Sulfur powder 1.3 wt%) as new data. CNT growth rate is estimated through image treatment. Activation energy in Co/Mo/S (Sulfur powder 1.3 wt%) is almost an intermediate value between Co/Mo/S (Sulfur powder 2.0 wt%) and Co/Mo/S (Thiourea 3.5 wt%).

Research achievements

(1) Scientific journals (peer review)

1. S. Suzuki, S. Mori
   "Carbon nanotube-like materials in the exhaust from a diesel engine using gas oil/ethanol mixing fuel with catalysts and sulfur"
   Journal of the Air & Waste Management Association, **67**, pp.873–880, 2017 (本論文 第 2 章)
2. S. Suzuki, S. Mori
   "Flame synthesis of carbon nanotube through a diesel engine using normal dodecane/ethanol mixing fuel as a feedstock"
   Journal of Chemical Engineering of Japan, **50**, pp.178–185, 2017 (本論文 第 3 章)
3. S. Suzuki, S. Mori
   "Synthesis of carbon nanotubes from biofuel as a carbon source through a diesel engine"
   Diamond and Related Materials, **82**, pp.79–86, 2018 (本論文 第 4 章)
4. S. Suzuki, S. Mori
   "Considerations on the key precursor for the growth of carbon nanotubes using a diesel engine as a reactor"
   Chemical Engineering Science, **186**, pp.62–73, 2018 (本論文 第 5 章)
5. S. Suzuki, S. Mori
   "Promoted growth of carbon nanotubes by sulfur addition in chemical vapor deposition shown via Arrhenius law"
   Diamond and Related Materials, submitted (本論文 第 7 章)
6. S. Suzuki, S. Mori
   "Impacts of different sulfur sources as a promoter on the growth of carbon nanotubes in chemical vapor deposition"
   Chemical Physics Letters, submitted (本論文 第 7 章)
7. S. Suzuki, S. Mori
   "The role of sulfur in promoted growth of carbon nanotubes in chemical vapor deposition proposed through the characterizations on catalytic nanoparticles"
   Under preparation (本論文 第 7 章)

(2) Domestic conference (国内学会)

1. (査読なし、ポスター) ○鈴木俊介・森伸介
   "浮遊粒子触媒を用いたディーゼルエンジンにおけるカーボンナノチューブ(CNT)の火炎合成"
   化学工学会第 81 回年会、ZCA216、関西大学、2016 年 3 月

2. (査読なし、口頭) ○鈴木俊介・森伸介
   “反応器としてのディーゼルエンジンの利用-燃料への触媒源添加による燃焼過程中のカーボンナノチューブの合成-“
   日本機械学会 産業・化学機械と安全部門 研究発表講演 2016 夏、GS-2、関東学院大学、2016 年 6 月
3. (査読なし、口頭) ○鈴木俊介・森伸介
   “ドデカン/エタノール混合燃料を用いたディーゼルエンジンにおけるカーボンナノチューブの合成”
   化学工学会第 48 回秋季大会、M207、徳島大学、2016 年 9 月
4. (査読なし、口頭) ○鈴木俊介・森伸介
   “ディーゼルエンジンにおけるカーボンナノチューブの火炎合成に対する燃料の化学構造の影響”
   第 54 回燃焼シンポジウム、D224、仙台国際センター、2016 年 11 月
5. (査読なし、口頭) ○鈴木俊介・森伸介
   “ディーゼルエンジンにおけるカーボンナノチューブの合成に対する燃料種の影響と生成機構の考察”
   化学工学会第 82 回年会、G305、芝浦工業大学、2017 年 3 月
6. (査読なし、口頭) ○鈴木俊介・森伸介
   “バイオ燃料を使用したディーゼルエンジンにおけるカーボンナノチューブの合成”
   日本機械学会 産業・化学機械と安全部門 研究発表講演 2017 夏、GS-4、東京工業大学、2017 年 6 月
7. (査読なし、口頭) ○鈴木俊介・森伸介
   “CVD 法を用いたカーボンナノチューブ合成に対する硫黄の影響”
   化学工学会第 49 回秋季大会、BD118、名古屋大学、2017 年 9 月
8. (査読なし、口頭) ○鈴木俊介・森伸介
   “ディーゼルエンジンにおけるカーボンナノチューブの合成経路に関する考察”
   第 55 回燃焼シンポジウム、D342、富山国際会議場、2017 年 11 月
9. (査読なし、口頭) ○鈴木俊介・森伸介
   “ディーゼルエンジンを用いたカーボンナノチューブの合成機構および生成機構に関する研究”
   化学工学会第 83 回年会、K302、関西大学、2018 年 3 月

(3) International conference

1. (No peer review, poster) ○S. Suzuki, S. Mori
   “Effects of an ethanol addition on the growth of carbon nanotube during combustion in a

diesel engine”

28th International Conference on Diamond and Related Materials, P5.01, Gothenburg (Sweden), Sep.-2017

2. (No peer review, oral) ○S. Suzuki, S. Mori

“Flame synthesis of carbon nanotubes (CNTs) in a diesel engine using floating catalysts and n-dodecane/ethanol mixing fuel, and identification of CNT precursor”

10th World Congress of Chemical Engineering, OC-26146, Barcelona (Spain), Oct.-2017

3. (No peer review, oral) ○S. Suzuki, S. Mori

“Evaluation of sulfur role as a promoter for the growth of carbon nanotube in chemical vapor deposition”

2017 AIChE Annual Meeting, 287e, Minneapolis (U.S.A.), Oct.~Nov.-2017

Reference list

(Chapter 1)

[1] 鈴木孝幸、ディーゼルエンジンの徹底研究、東京、グランプリ出版、2012

[2] 畑村耕一、最新！自動車エンジン技術がわかる本、東京、ナツメ社、2009

[3] 水谷幸夫、燃焼工学第 3 版、東京、北森出版株式会社、2002

[4] 新岡嵩、河野通方、佐藤順一、燃焼現象の基礎第 1 版、東京、オーム社、2001

[5] http://www.densoautoparts.com.au/products/diesel-fuel-injectors/commonrail.aspx

[6] Y. Hiratsuka, Production of synthesis gas by an internal combustion engine, World Petroleum Congress, Frankfurt, 19-26 June 1963

[7] M. H. McMillian, S. A. Lawson, Experimental and modeling study of hydrogen/syngas production and particulate emissions from a natural gas-fueled partial oxidation engine, *Int. J. Hydrogen Energy* **31** (2006) 847–860

[8] G. A. Karim, N. P. W. Moore, Examination of rich mixture operation of a dual fuel engine, *SAE Tech. Paper* (1990) 901500

[9] G. A. Karim, N. P. W. Moore, The production of hydrogen by the partial oxidation of methane in a dual fuel engine, *SAE Tech. Paper* (1990) 901501

[10] G. A. Karim, I. Wierzba, The production of hydrogen through the uncatalyzed partial oxidation of methane in an internal combustion engine, *Int. J. Hydrogen Energy* **33** (2008) 2105–2110

[11] M. H. Morsy, Modeling study on the production of hydrogen/syngas via partial oxidation using a homogeneous charge compression ignition engine fueled with natural gas, *Int. J. Hydrogen Energy* **39** (2014) 1096–1104

[12] H. Gossler, O. Deutschmann, Numerical optimization and reaction flow analysis of syngas production via partial oxidation of natural gas in internal combustion engines, *Int. J. Hydrogen Energy* **40** (2015) 11046–11058

[13] L. Zhu, Z. He, Z Hu, X. Lu, J. Fang, W. Zhang, Z. Huang, In-cylinder thermochemical fuel reforming (TFR) in a spark-ignition natural gas engine, *Proc. Combust. Inst.* **36** (2017) 3487–3497

[14] Z. He, L. Zhu, Z. Xu, O. Kaario, A. Li, Z. Huang, Effects of ethanol enrichment on in-cylinder thermochemical fuel reforming (TFR) spark ignition natural gas engine, *Fuel* **197** (2017) 334–342

[15] E. G. Lim, E. E. Dames, K. D. Cedrone, A. J. Acocella, T. R. Needham, A. Arce, D. R. Cohn, L. Bromberg, W. K. Cheng, W. H. Green, The engine reformer: Syngas production in an engine for compact gas-to-liquid synthesis, *Can. J. Chem. Eng.* **94** (2016) 623–635

[16] D. M. Anderson, M. H. Nasr, T. M. Yun, P. A. Kottke, A. G. Fedorov, Sorption-enhanced variable-volume batch-membrane steam methane reforming at low temperature: Experimental demonstration and kinetic modeling, *Ind. Eng. Chem. Res.* **54** (2015) 8422–8436

[17] D. M. Anderson, T. M. Yun, P. A. Kottke, A. G. Fedorov, Comprehensive analysis of sorption enhanced steam methane reforming in a variable volume membrane reactor, *Ind. Eng. Chem. Res.* **56** (2017) 1758–1771

[18] C. D. Lagally, C. C. O. Reynolds, A. P. Grieshop, M. Kandlikar, Carbon nanotube and fullerene emissions from spark-ignited engines, *Aerosol Sci. Technol.* **46** (2012) 156–164

[19] H. S. Jung, A. Miller, K. Park, D. B. Kittelson, Carbon nanotubes among diesel exhaust particles: Real samples or contaminants?, *J. Air Waste Manage. Assoc.* **63** (2013) 1199–1204

[20] J. J. Swanson, R. Febo, A. M. Boies, D. B. Kittelson, Fuel sulfur and iron additives contribute to the formation of carbon nanotube-like structures in an internal combustion engine, *Environ. Sci. Technol. Lett.* **3** (2016) 364–368

[21] K. O. Lee, R. Cole, R. Sekar, M. Y. Choi, J. S. Kang, C. S. Bae, H. D. Shin, Morphological investigation of the microstructure, dimensions, and fractal geometry of diesel particulates, *Proc. Combust. Inst.* **29** (2002) 647–653

[22] J. Zhu, K. O. Lee, A. Yozgatligil, M. Y. Choi, Effects of engine operating conditions on morphology, microstructure, and fractal geometry of light-duty diesel engine particulates, *Proc. Combust. Inst.* **30** (2005) 2781–2789

[23] Y. Jung, C. Bae, Immaturity of soot particles in exhaust gas for low temperature diesel combustion in a direct injection compression ignition engine, *Fuel* **161** (2015) 312–322

[24] Z. Xu, X. Li, C. Guan, Z. Huang, Effects of injection pressure on diesel engine particle physico-chemical properties, *Aerosol Sci. Technol.* **48** (2014) 128–138
[25] Y. Jung, J. Hwang, C. Bae, Assessment of particulate matter in exhaust gas for biodiesel and diesel under conventional and low temperature combustion in a compression ignition engine, *Fuel* **165** (2016) 413–424
[26] M. J. Height, J. B. Howard, J. W. Tester, J. B. Vander Sande, Flame synthesis of single-walled carbon nanotubes, *Carbon* **42** (2004) 2295–2307
[27] R. L. Vander Wal, L. J. Hall, Flame synthesis of Fe catalyzed single-walled carbon nanotubes and Ni catalyzed nanofibers: Growth mechanisms and consequences, *Chem. Phys. Lett.* **349** (2001) 178–184
[28] C. J. Unrau, R. L. Axelbaum, P. Fraundoff, Single-walled carbon nanotube formation on iron oxide catalysts in diffusion flames, *J. Nanopart. Res.* **12** (2010) 2125–2133
[29] R. Barbella, A. Ciajolo, A. D'Anna, C. Bertoli, Pyrolysis and oxidation of n-tetradecane during combustion in a diesel engine, *Symp. Int. Combust.* **23** (1991) 1079–1085
[30] S. Tosaka, Y. Fujiwara, T. Murayama, Effect of fuel properties on particulate formation (thermal cracking and condensation polymerization process of fuels), *Trans. JSME B* **59** (1993) 2590–2595
[31] H. Noge, Y. Yoshihara, Y. Kidoguchi, K. Miwa, Soot precursor and PM formation in diffusion flame using thermally decomposed aliphatic fuel, *Trans. JSME B* **73** (2007) 328–334
[32] H. W. Kroto, J. R. Heath, S. C. O'Brien, R. F. Curl, R. E. Smalley, C60: Buckminsterfullerene, *Nature* **318** (1985) 162–163
[33] A. Oberlin, M. Endo, T. Koyama, Filamentous growth of carbon through benzene decomposition, *J. Cryst. Growth* **32** (1976) 335–349
[34] S. Iijima, Helical microtubules of graphitic carbon, *Nature* **354** (1991) 56–58
[35] フラーレン・ナノチューブ・グラフェン学会、カーボンナノチューブ・グラフェンハンドブック第１版、東京、コロナ社、2011
[36] C. Journet, W. K. Maser, P. Bernier, A. Loiseau, M. L. de la Chapelle, S. Lefrant, P. Deniard, R. Lee, J. E. Fisher, Large-scale production of single-walled carbon nanotubes by the electric-arc technique, *Nature* **388** (1997) 756–758
[37] H. Wang, K. Ghosh, Z. Li, T. Maruyama, S. Inoue, Y. Ando, Direct growth of single-walled carbon nanotube films and their optoelectric properties, *J. Phys. Chem. C* **113** (2009) 12079–12084
[38] H. Yoshida, T. Sugai, H. Shinohara, Fabrication, purification, and characterization of double-wall carbon nanotubes via pulsed arc discharge, *J. Phys. Chem. C* **112** (2008) 19908–19915
[39] A. Thess, R. Lee, P. Nikolaev, H. Dai, P. Petit, J. Robert, C. Xu, Y. H. Lee, S. G. Kim, A. G. Rinzler, D. T. Colbert, G. E. Scuseria, D. Tománek, J. E. Fischer, R. E. Smalley, Crystalline ropes of metallic carbon nanotubes, *Science* **273** (1996) 483–487
[40] S. Iijima, T. Wakabayashi, Y. Achiba, Structures of carbon soot prepared by laser ablation, *J. Phys. Chem.* **100** (1996) 5839–5843
[41] K. Kobayashi, B. Shukla, S. Ohmori, M. Kiyomiya, T. Hirai, Y. Kuwahara, T. Saito, Wall-number selectivity in single/double-wall carbon nanotube production by enhanced direct injection pyrolytic synthesis, *Jpn. J. Appl. Phys.* **52** (2013) 105102
[42] Y. Tian, M. Y. Timmermans, M. Partanen, A. G. Nasibulin, H. Jiang, Z. Zhu, E. I. Kauppinen, Growth of single-walled carbon nanotubes with controlled diameters and lengths by an aerosol method, *Carbon* **49** (2011) 4636–4643
[43] Z. Chen, D. Y. Kim, K. Hasegawa, T. Osawa, S. Noda, Over 99.6wt%-pure, sub-millimeter-long carbon nanotubes realized by fluidized-bed with careful control of the catalyst and carbon feeds, *Carbon* **80** (2014) 339–350
[44] C. Castro, M. Pinault, D. Porterat, C. Reynaud, M. Mayne-L'Hermite, The role of hydrogen in the aerosol-assisted chemical vapor deposition process in producing thin and densely packed vertically aligned carbon nanotubes, *Carbon* **61** (2013) 585–594
[45] B. T. Quinton, K. D. Leedy, J. W. Lawson, B. Tsao, J. D. Scofield, J. N. Merrett, Q. Zhang, K. Yost, S. M. Mukhopadhyay, Influence of oxide buffer layers on the growth of carbon nanotube arrays on carbon substrates, *Carbon* **87** (2015) 175–185
[46] B. Mas, B. Alemán, I. Dopico, I. Martin-Bragado, T. Naranjo, E. M. Pérez, J. J. Vilatela, Group 16 elements control the synthesis of continuous fibers of carbon nanotubes, *Carbon* **101** (2016) 458–

464
[47] Q. Zhang, J.-Q. Huang, M.-Q. Zhao, W.-Z. Qian, F. Wei, Carbon nanotube mass production: Principles and processes, *ChemSusChem* **4** (2011) 864–889
[48] P. Nikolaev, M. J. Bronikowski, R. K. Bradley, F. Rohmund, D. T. Colbert, K. A. Smith, R. E. Smalley, Gas-phase catalytic growth of single-walled carbon nanotubes from carbon monoxide, *Chem. Phys. Lett.* **313** (1999) 91–97
[49] B. Kitiyanan, W. E. Alvarez, J. H. Harwell, D. E. Resasco, Controlled production of single-wall carbon nanotubes by catalytic decomposition of CO on bimetallic Co–Mo catalysts, *Chem. Phys. Lett.* **317** (2000) 497–503
[50] M. Endo, Grow Carbon Fibers in the Vapour Phase, *CHEMTECH* **18** (1988) 568–576
[51] M. D. Diener, N. Nichelson, J. M. Alford, Synthesis of single-walled carbon nanotubes in flames, *J. Phys. Chem. B* **104** (2000) 9615–9620
[52] J. Z. Wen, H. Ritchter, W. H. Green, J. B. Howard, M. Treska, P. M. Jardim, J. B. Vander Sande, Experimental study of catalyst nanoparticle and single walled carbon nanotube formation in a controlled premixed combustion, *J. Mater. Chem.* **18** (2008) 1561–1569
[53] C. J. Unrau, V. R. Katta, R. L. Axelbaum, Characterization of diffusion flames for synthesis of single-walled carbon nanotubes, *Combust. Flame* **157** (2010) 1643–1648
[54] K. Masunaga, H. Ito, O. Fujita, Investigation of applying electric effect on carbon nanotube synthesis, *Asia-Pac. J. Chem. Eng.* **8** (2013) 246–253
[55] B. Hall, C. Zhuo, Y. A. Levendis, H. Richter, Influence of the fuel structure on the flame synthesis of carbon nanomaterials, *Carbon* **49** (2011) 3412–3423
[56] H. Oulanti, F. Laurent, T. Le-Huu, B. Durand, J. B. Donnet, Growth of carbon nanotubes on carbon fibers using the combustion flame oxy-acetylene method, *Carbon* **95** (2015) 261–267
[57] W. C. Hu, T. H. Lin, Ethanol flame synthesis of carbon nanotubes in deficient oxygen environments, *Nanotechnology* **27** (2016) 165602
[58] H. Richter, M. Treska, J. B. Howard, J. Z. Wen, S. B. Thomasson, A. A. Reading, P. M. Jardim, J. B. Vander Sande, Large scale combustion synthesis of single-walled carbon nanotubes and their characterization, *J. Nanosci. Nanotechnol.* **8** (2008) 6065–6074
[59] H. Takehara, M. Fujiwara, M. Arikawa, M. D. Diener, J. M. Alford, Experimental study of industrial scale fullerene production by combustion synthesis, *Carbon* **43** (2005) 311–319
[60] M. Arikawa, Fullerne – characteristics and synthesis/production methods, *TANSO* **224** (2006) 299–307

(Chapter 2)
[61] S. Yamamoto, D. Sakaguchi, H. Ueki, M. Ishida, Comparison of combustion characteristics of ethanol and butanol blended with gas oil in direct injection diesel engine, *Trans. JSME B* **79** (2013) 380–389
[62] H. An, W. M. Yang, J. Li, D. Z. Zhou, Modeling study of oxygenated fuels on diesel combustion: Effects of oxygen concentration, cetane number and C/H ratio, *Energy Convers. Manage.* **90** (2015) 261–271
[63] S. Maruyama, R. Kojima, Y. Miyauchi, S. Chiashi, M. Kohno, Low-temperature synthesis of high-purity single-walled carbon nanotubes from alcohol, *Chem. Phys. Lett.* **360** (2002) 229–234
[64] M. Hu, Y. Murakami, M. Ogura, S. Maruyama, T. Okubo, Morphology and chemical state of Co-Mo catalysts for growth of single-walled carbon nanotubes vertically aligned on quartz substrates, *J. Catal.* **225** (2004) 230–239
[65] D. Conroy, A. Moisala, S. Cardoso, A. Windle, J. Davidson, Carbon nanotube reactor: Ferrocene decomposition, iron particle growth, nanotube aggregation and scale-up, *Chem. Eng. Sci.* **65** (2010) 2965–2977
[66] B. Hou, R. Xiang, T. Inoue, E. Einarsson, S. Chiashi, J. Shiomi, A. Miyoshi, S. Maruyama, Decomposition of ethanol and dimethyl ether during chemical vapor deposition synthesis of single-walled carbon nanotubes, *Jpn. J. Appl. Phys.* **50** (2011) 065101
[67] B. Hall, C. Zhuo, Y. A. Levendis, H. Richter, Influence of the fuel structure on the flame synthesis of carbon nanomaterials, *Carbon* 49 (2011) 3412–3423
[68] H. S. Jung, A. Miller, K. Park, D. B. Kittelson, Carbon nanotubes among diesel exhaust particles:

Real samples or contaminants?, *J. Air Waste Manage. Assoc.* **63** (2013) 1199–1204
[69] J. J. Swanson, R. Febo, A. M. Boies, D. B. Kittelson, Fuel sulfur and iron additives contribute to the formation of carbon nanotube-like structures in an internal combustion engine, *Environ. Sci. Technol. Lett.* **3** (2016) 364–368
[70] M. S. Kim, N. M. Rodriguez, R. T. K. Baker, The interplay between sulfur adsorption and carbon deposition on cobalt catalysts, *J. Catal.* **143** (1993) 449–463
[71] G. G. Tibbetts, C. A. Bernardo, D. W. Gorkiewicz, R. L. Alig, Role of sulfur in the production of carbon fibers in the vapor phase, *Carbon* **32** (1994) 569–576
[72] W. C. Ren, F. Li, H. M. Cheng, Evidence for, and an understanding of, the initial nucleation of carbon nanotubes produced by a floating catalyst method, *J. Phys. Chem. B* **48** (2006) 16941–16946.
[73] L. Zhang, P. X. Hou, S. Li, C. Shi, H.-T. Cong, C. Liu, H.-M. Cheng, In situ TEM observations on the sulfur-assisted catalytic growth of single-wall carbon nanotubes, *J. Phys. Chem. Lett.* **5** (2014) 1427–1432
[74] T. Saito, W. C. Xu, S. Ohshima, H. Ago, M. Yumura, and S. Iijima, Supramolecular catalysts for the gas-phase synthesis of single-walled carbon nanotubes, *J. Phys. Chem. B* **110** (2006) 5849–5853

(Chapter 3)
[75] H. P. S. Shen, J. Steinberg, J. Vanderover, M. A. Oehlschlaeger, A shock tube study of the ignition of n-heptane, n-decane, n-dodecane, and n-tetradecane at elevated pressures, *Energy Fuels* **23** (2009) 2482–2489
[76] S. S. Vasu, D. F. Davidson, Z. Hong, V. Vasudevan, R. K. Hanson, n-Dodecane oxidation at high-pressures: Measurements of ignition delay times and OH concentration time-histories, *Proc. Combust. Inst.* **32** (2009) 173–180
[77] W. J. Pitz, Recent progress in the development of diesel surrogate fuels, CRC Report No. AVFL-18a (2009)
[78] K. Narayanaswamy, P. Pepiot, H. Pitsch, A chemical mechanism for low to high temperature oxidation of n-dodecane as a component of transportation fuel surrogates, *Combust. Flame* **161** (2014) 866–884
[79] T. Kamimoto, T. Minagawa, S. Kobori, A two-zzone model analysis of heat release rate in diesel engines, *SAE Tech. Paper* (1997) 972959
[80] A. Sadezky, H. Muckenhuber, H. Grothe, R. Niessner, U. Pöschl, Raman microspectroscopy of soot and related carbonaceous materials: Spectral analysis and structural information, *Carbon* **43** (2005) 1731–1742
[81] K. Hayashida, M. Uno, H. Ishitani, Effect of engine operating conditions on nanostructure and oxidation reactivity of soot particles from diesel engine, *Trans. JSME B* **79** (2013) 2228–2238
[82] H. J. Curran, E. M. Fisher, P.-A. Glaude, N. M. Marinov, W. J. Pitz, C. K. Westbrook, D. W. Layton, P. F. Flynn, R. P. Durrett, A. O. Zur Loye, O. C. Akinyemi, F. L. Dryer, Detailed chemical kinetic modeling of diesel combustion with oxygenated fuels, *SAE Tech. Paper* (2001) 010653
[83] G. Mittal, S. M. Burke, V. A. Davies, B. Parajuli, W. K. Metcalfe, H. J. Curran, Autoignition of ethanol in a rapid compression machine, *Combust. Flame* **161** (2014) 1164–1171
[84] M. J. Height, J. B. Howard, J. W. Tester, J. B. Vander Sande, Flame synthesis of single-walled carbon nanotubes, *Carbon* **42** (2004) 2295–2307
[85] C. J. Unrau, R. L. Axelbaum, Gas-phase synthesis of single-walled carbon nanotubes on catalysts producing high yield, *Carbon* **48** (2010) 1418–1424
[86] T. Saito, W. C. Xu, S. Ohshima, H. Ago, M. Yumura, S. Iijima, Supramolecular catalysts for the gas-phase synthesis of single-walled carbon nanotubes, *J. Phys. Chem. B* **110** (2006) 5849–5853
[87] K. Kobayashi, B. Shukla, S. Ohmori, M. Kiyomiya, T. Hirai, Y. Kuwahara, T. Saito, Wall-number selectivity in single/double-wall carbon nanotube production by enhanced direct injection pyrolytic synthesis, *Jpn. J. App. Phys.* **52** (2013) 105102
[88] P. Nikolaev, M. J. Bronikowski, R. K. Bradley, F. Rohmund, D. T. Colbert, K. A. Smith, R. E. Smalley, Gas-phase catalytic growth of single-walled carbon nanotubes from carbon monoxide, *Chem. Phys. Lett.* **313** (1999) 91–97
[89] R. L. Vander Wal, L. J. Hall, Flame synthesis of Fe catalyzed single-walled carbon nanotubes and Ni catalyzed nanofibers: Growth mechanisms and consequences, *Chem. Phys. Lett.* **349** (2001) 178–

184
[90] T. Tian, M. Y. Timmermans, M. Partanen, A. G. Nasibulin, H. Jiang, Z. Zhu, E. I. Kauppinen, Growth of single-walled carbon nanotubes with controlled diameters and lengths by an aerosol method, *Carbon* **49** (2011) 4636–4643
[91] T. X. Li, K. Kuwana, K. Saito, H. Zhang, Z. Chen, Temperature and carbon source effects on methane-air flame synthesis of CNTs, *Proc. Combust. Inst.* **32** (2009) 1855–1861
[92] H. Sato, Y. Hori, K. Hata, K. Seko, H. Nakahara, Y. Saito, Effect of catalyst oxidation on the growth of carbon nanotubes by thermal chemical vapor deposition, *J. App. Phys.* **100** (2006) 104321
[93] K. Liu, K. Jiang, C. Feng, Z. Chen, S. Fan, A growth mark method for studying growth mechanism of carbon nanotube arrays, *Carbon* **43** (2005) 2850–2856
[94] G. Zhong, S. Hofmann, F. Yan, H. Telg, J. H. Warner, D. Eder, C. Thomsen, W. I. Milne, J. Robertson, Acetylene: A key growth precursor for single-walled carbon nanotube forest, *J. Phys. Chem. C* **113** (2009) 17321–17325
[95] S. L. Pirard, S. Douven, C. Bossuot, G. Heyen, J.-P. Pirard, A kinetic study of multi-walled carbon nanotube synthesis by catalytic chemical vapor deposition using a Fe-Co/Al_2O_3 catalyst, *Carbon* **45** (2007) 1167–1175
[96] B. Shukla, T. Saito, M. Yumura, S. Iijima, An efficient carbon precursor for gas phase growth of SWCNTs, *Chem. Commun.* (2009) 3422–3424
[97] S. Inoue, D. Nakahara, Y. Matsumura, Precursor and formation mechanism in the synthesis of carbon nanotubes by chemical vapor deposition, *Chem. Phys. Lett.* **616–617** (2014) 217–221
[98] T. Ogura, Y. Sakai, A. Miyoshi, M. Koshi, P. Dagaut, Modeling of the oxidation of primary reference fuel in the presence of oxygenated octane improvers: Ethyl tert-butyl ether and ethanol, *Energy Fuels* **21** (2007) 3233–3239
[99] P. Saxena, F. A. Williams, Numerical and experimental studies of ethanol flames, *Proc. Combust. Inst.* 31 (2007) 1149–1156

(Chapter 4)
[100] S. Pinzi, P. Rounce, J. M. Herreros, A. Tsolakis, M. P. Dorado, The effect of biodiesel fatty acid composition on combustion and diesel engine exhaust emissions, *Fuel* **104** (2013) 170–182
[101] M. Chiba, K. Shimizu, H. Takahashi, Y. Sugiura, E. Seki, M. Harano, Diesel engine performance and emissions when using biodiesel fuel, *Jpn. Agric. Res. Q.* **48** (2014) 133–137
[102] H. K. Imdadul, N. W. M. Zulkifli, H. H. Masjuki, M. A. Kalam, M. Kamruzzaman, M. M. Rashed, H. K. Rashedul, A. Alwi, Experimental assessment of non-edible candlenut biodiesel and its blend characteristics as diesel engine fuel, *Environ. Sci. Pollut. Res.* **24** (2017) 2350–2363
[103] M. D. Cárdenasa, O. Armasa, C. Matab, F. Soto, Performance and pollutant emissions from transient operation of a common rail diesel engine fueled with different biodiesel fuels, *Fuel* **185** (2016) 743–762
[104] A. K. Agarwal, Biofuels (alcohols and biodiesel) applications as fuels for internal combustion engines, *Prog. Energy Combust. Sci.* **33** (2007) 233–271
[105] C. Saggese, A. Frassoldati, A. Cuoci, T. Faravalli, E. Ranzi, A lumped approach to the kinetic modeling of pyrolysis and combustion of biodiesel fuels, *Proc. Combust. Inst.* **34** (2013) 427–434
[106] W. Wang, S. Gowdagiri, M. A. Oehlschlaeger, The high-temperature autoignition of biodiesels and biodiesel components, *Combust. Flame* **161** (2014) 3014–3021
[107] O. Herbinet, W. J. Pitz, C. K. Westbrook, Detailed chemical kinetic oxidation mechanism for a biodiesel surrogate, *Combust. Flame* **154** (2008) 507–528
[108] Q. Feng, A. Jalali, A. M. Fincham, Y. L. Wang, T. T. Tsotsis, F. N. Egolfopoulos, Soot formation in flames of model biodiesel fuels, *Combust. Flame* **159** (2012) 1876–1893
[109] B. Kerschgens, L. Cai, H. Pitsch, B. Heuser, S. Pischiger, Di-n-buthylether, n-octanol, and n-octane as fuel candidates for diesel engine combustion, *Combust. Flame* **163** (2016) 66–78
[110] X. Liu, H. Wang, X. Wang, Z. Zheng, M. Yao, Experimental and modelling investigations of the diesel surrogate fuels in direct injection compression ignition combustion, *Appl. Energy* **189** (2017) 187–200
[111] H. P. S. Shen, J. Steinberg, J. Vanderover, M. A. Oehlschlaeger, A shock tube study of the ignition of n-heptane, n-decane, n-dodecane, and n-tetradecane at elevated pressures, *Energy Fuels* **23** (2009)

2482–2489
[112] D. Witkowski, K. Kondo, G. Vishwanathan, D. Rothamer, Evaluation of the sooting properties of real fuels and their commonly used surrogates in a laminar co-flow diffusion flame, *Combust. Flame* **160** (2013) 1129–1141
[113] J. Julis, W. Leiter, Synthesis of 1-octanol and 1,1-dioctyl ether from biomass-derived platform chemicals, *Angew. Chem. Int. Ed.* **51** (2012) 8615–8619
[114] M. Jakob, T. Hülser, A. Janssen, P. Adomeit, S. Pischinger, G. Grünefeld, Simultaneous high-speed visualization of soot luminosity and OH∗ chemiluminescence of alternative-fuel combustion in a HSDI diesel engine under realistic operating conditions, *Combust. Flame* **159** (2012) 2516–2529
[115] L. Cai, Y. Uygun, C. Togbé, H. Pitsch, H. Olivier, P. Dagaut, S. M. Sarathy, An experimental and modeling study of n-octanol combustion, *Proc. Combust. Inst.* **35** (2015) 419–427
[116] R. Kumar, R. K. Singh, D. P. Singh, Natural and waste hydrocarbon precursors for the synthesis of carbon based nanomaterials: Graphene and CNTs, *Renew. Sustain. Ener. Rev.* **58** (2016) 976–1006
[117] M. Kumar, Y. Ando, Single-wall and multi-wall carbon nanotubes from camphor – a botanical hydrocarbon, *Diam. Relat. Mater.* **12** (2003) 1845–1850
[118] E. F. Antunes, V. G. de Resende, U. A. Mengui, J. B. M. Cunha, E. J. Corat, M. Massi, Analyses of residual iron in carbon nanotubes produced by camphor/ferrocene pyrolysis and purified by high temperature annealing, *Appl. Surf. Sci.* **257** (2011) 8038–8043
[119] S. Musso, G. Fanchini, A. Tagliaferro, Growth of vertically aligned carbon nanotubes by CVD by evaporation of carbon precursors, *Diam. Relat. Mater.* **14** (2005) 784–789
[120] R. A. Afre, T. Soga, T. Jimbo, M. Kumar, Y. Ando, M. Sharon, Growth of vertically aligned carbon nanotubes on silicon and quartz substrate by spray pyrolysis of a natural precursor: Turpentine oil, *Chem. Phys. Lett.* **414** (2005) 6–10
[121] P. Ghosh, R. A. Afre, T. Soga, T. Jimbo, A simple method of producing single-walled carbon nanotubes from a natural precursor: Eucalyptus oil, *Mater. Lett.* **61** (2007) 3768–3770
[122] A. B. Suriani, A. A. Azira, S. F. Nik, R. Md Nor, M. Rusop, Synthesis of vertically aligned carbon nanotubes using natural palm oil as carbon precursor, *Mater. Lett.* **63** (2009) 2704–2706
[123] R. Kumar, R. M. Yadav, K. Awasthi, T. Shripathi, A. S. K. Sinha, R. S. Tiwari, O. N. Srivastava, Synthesis of carbon and carbon–nitrogen nanotubes using green precursor: Jatropha-derived biodiesel, *J. Exp. Nanosci.* **8** (2012) 606–620
[124] K. Awasthi, R. Kumar, H. Raghubanshi, S. Awasthi, R. Pandey, D. Singh, T.P. Yadav, O.N. Srivastava, Synthesis of nano-carbon (nanotubes, nanofibres, graphene) materials, *Bull. Mater. Sci.* **34** (2011) 607–614
[125] R. Kumar, R. K. Singh, P. Kumar, P. K. Dubey, R. S. Tiwari, O. N. Srivastava, Clean and efficient synthesis of graphene nanosheets and rectangular aligned-carbon nanotubes bundles using green botanical hydrocarbon precursor: Sesame oil, *Sci. Adv. Mater.* **6** (2014) 75–82
[126] H. J. Curran, E. M. Fisher, P. A. Glaude, N. M. Marinov, W. J. Pitz, C. K. Westbrook, D. W. Layton, P. F. Flynn, R. P. Durrett, A. O. Zur Loye, O. C. Akinyemi, F. L. Dryer, Detailed chemical kinetic modeling of diesel combustion with oxygenated fuels, *SAE Tech. Paper* (2001) 010653
[127] L. R. Cancino, M. Fikri, A. A. M. Oliveira, C. Schulz, Measurement and chemical kinetics modeling of shock-induced ignition of ethanol-air mixtures, *Energy Fuels* **24** (2010) 2830–2840
[128] S. M. Sarathy, P. Oßwald, N. Hansen, K. Kohse-Höinghaus, Alcohol combustion chemistry, *Prog. Energy Combust. Sci.* **44** (2014) 40–102
[129] A. G. Nasibulin, A. Moisala, D. P. Brown, H. Jiang, E. I. Kauppinen, A novel aerosol method for single walled carbon nanotube synthesis, *Chem. Phys. Lett.* **402** (2005) 227–232
[130] E. Teblum, Y. Gofer, C. L. Pint, G. D. Nessim, Role of catalyst oxidation state in the growth of vertically aligned carbon nanotubes, *J. Phys. Chem. C* **116** (2012) 24522–24528
[131] J. Z. Wen, M. Celnik, H. Richter, M. Treska, J. B. Vander Sande, M. Kraft, Modelling study of single walled carbon nanotube formation in a premixed flame, *J. Mater. Chem.* **18** (2008) 1582–1591
[132] H. Sato, Y. Hori, K. Hata, K. Seko, H. Nakahara, Y. Saito, Effect of catalyst oxidation on the growth of carbon nanotubes by thermal chemical vapor deposition, *J. Appl. Phys.* **100** (2006) 104321
[133] T. de los Arcos, P. Oelhafen, V. Thommen, D. Mathys, The influence of catalyst's oxidation degree on carbon nanotube growth as a substrate-independent parameter, *J. Phys. Chem. C* **111** (2007) 16392–16396

[134] C. J. Unrau, R. L. Axelbaum, P. Fraundoff, Single-walled carbon nanotube formation on iron oxide catalysts in diffusion flames, *J. Nanopart. Res.* **12** (2010) 2125–2133
[135] K. Nishimura, N. Okazaki, L. Pan, Y. Nakayama, In situ study of iron catalysts for carbon nanotube growth using X-ray diffraction analysis, *Jpn. J. Appl. Phys.* **43** (2004) L471–L474
[136] M. C. Altay, S. Eroglu, Thermodynamic analysis and chemical vapor deposition of multi-walled carbon nanotubes from pre-heated CH_4 using Fe_2O_3 particles as catalyst precursor, *J. Cryst. Growth* **364** (2013) 40–45
[137] R. T. K. Baker, J. R. Alonzo, J. A. Dumesic, D. J. C. Yates, Effect of the surface state of iron on filamentous carbon formation, *J. Catal.* **77** (1982) 74–84
[138] M. Kasper, K. Sattler, K. Siegmann, U. Matter, H. C. Siegmann, The influence of fuel additives on the formation of carbon during combustion, *J. Aerosol Sci.* **30** (1999) 217–225
[139] D. G. Nash, N. B. Swanson, W. T. Preston, T. L. B. Yelverton, W. L. Roberts, J. O. L. Wendt, W. P. Linak, Environmental implications of iron fuel borne catalysts and their effects on diesel particulate formation and composition, *J. Aerosol Sci.* **58** (2013) 50–61
[140] T. Hirasawa, C. J. Sung, Z. Yang, A. Joshi, H. Wang, Effect of ferrocene addition on sooting limits in laminar premixed ethylene-oxygen-argon flames, *Combust. Flame* **139** (2004) 288–299

(Chapter 5)
[141] Z. Luo, S. Som, S. M. Sarathy, M. Plomer, W. J. Pitz, D. E. Longman, T. F. Lu, Development and validation of an n-dodecane skeletal mechanism for spray combustion applications, *Combust. Theor. Model.* **18** (2014) 187–203
[142] L. R. Cancino, M. Fikri, A. A. M. Oliveira, C. Schulz, Measurement and chemical kinetics modeling of shock-induced ignition of ethanol-air mixtures, *Energy Fuels* **24** (2010) 2830–2840
[143] N. M. Marinov, A Detailed chemical kinetic model for high temperature ethanol oxidation, *Int. J. Chem. Kinet.* **31** (1999) 183–220
[144] H. Sugime, S. Noda, Cold-gas chemical vapor deposition to identify the key precursor for rapidly growing vertically-aligned single-wall and few-wall carbon nanotubes from pyrolyzed ethanol, *Carbon* **50** (2012) 2953–2960
[145] D. Bongartz, A. F. Ghoniem, Impact of sour gas composition on ignition delay and burning velocity in air and oxy-fuel combustion, *Combust. Flame* **162** (2015) 2749–2757
[146] T. Hirasawa, C. J. Sung, Z. Yang, A. Joshi, H. Wang, Effect of ferrocene addition on sooting limits in laminar premixed ethylene–oxygen–argon flames, *Combust. Flame* **139** (2004) 288–299
[147] K. Kuwana, K. Saito, Modeling ferrocene reactions and iron nanoparticle formation: Application to CVD synthesis of carbon nanotubes, *Proc. Combust. Inst.* **31** (2007) 1857–1864
[148] J. Z. Wen, C. F. Goldsmith, R. W. Ashcraft, W. H. Green, Detailed kinetic modeling of iron nanoparticle synthesis from the decomposition of $Fe(CO)_5$, *J. Phys. Chem. C* **111** (2007) 5677–5688
[149] M. D. Rumminger, D. Reinelt, V. Babushok, G. T. Linteris, Numerical study of the Inhibition of premixed and diffusion flames by iron pentacarbonyl, *Combust. Flame* **116** (1999) 207–219
[150] G. T. Linteris, M. D. Rumminger, V. I. Babushok, Premixed carbon monoxide-nitrous oxide-hydrogen flames: Measured and calculated burning velocities with and without $Fe(CO)_5$, *Combust. Flame* **122** (2000) 58–75
[151] P. E. Nolan, D. C. Lynch, A. H. Cutler, Carbon deposition and hydrocarbon formation on group VIII metal catalysts, *J. Phys. Chem. B* **102** (1998) 4165–4175
[152] M. Melander, K. Laasonen, Identifying the active sites for CO dissociation on Fe–BCC nanoclusters, *J. Mole. Catal. A* **406** (2015) 31–39
[153] O. Herbinet, J. Biet, M. H. Hakka, V. Warth, P. A. Glaude, A. Nicolle, F. Battin-Leclerc, Modeling study of the low-temperature oxidation of large methyl esters from C11 to C19, *Proc. Combust. Inst.* **33** (2011) 391–398
[154] P. B. Tøttrup, Kinetics of decomposition of carbon monoxide on a supported nickel catalyst, *J. Catal.* **42** (1976) 29–36
[155] J. Gałuszka, J. R. Chang, Y. Amenomiya, Disproportionation of carbon monoxide on supported nickel catalysts, *J. Catal.* **68** (1981) 172–181
[156] M. Audier, M. Coulon, Kinetic and microscopic aspects of catalytic carbon growth, *Carbon* **23** (1985) 317–323

[157] M. T. Tavares, I. Alstrup, C. A. Bernaldo, J. R. Rostrup-Nielsen, CO disproportionation on silica-supported nickel and nickel-copper catalysts, *J. Catal.* **147** (1994) 525–534
[158] C. T. Wirth, C. Zhang, G. Zhong, S. Hofmann, J. Robertson, Diffusion- and reaction-limited growth of carbon nanotube forests, *ACS Nano* **3** (2009) 3560–3566
[159] A. S. Anisimov, A. G. Nasibulin, H. Jiang, P. Launois, J. Cambedouzou, S. D. Shandakov, E. I. Kauppinen, Mechanistic investigations of single-walled carbon nanotube synthesis by ferrocene vapor decomposition in carbon monoxide, *Carbon* **48** (2010) 380–388
[160] M. V. Kharlamova, Investigation of growth dynamics of carbon nanotubes, *Beilstein J. Nanotechnol.* **8** (2017) 826–856
[161] L. J. Whitman, L. J. Richter, B. A. Gurney, J. S. Villarrubia, W. Ho, CO adsorption site occupations on Fe (111) vs coverage and temperature: The kinetics of adsorption and reaction, *J. Chem. Phys.* **90** (1989) 2050–2062
[162] T. C. Bromfield, D. C. Ferré, J. W. Niemantsverdriet, A DFT study of the adsorption and dissociation of CO on Fe (100): Influence of surface coverage on the nature of accessible adsorption states, *ChemPhysChem* **6** (2005) 254–260
[163] J. W. Snoeck, G. F. Froment, M. Fowles, Steam/CO_2 reforming of methane. Carbon filament formation by the boudouard reaction and gasification by CO_2, by H_2, and by steam: Kinetic study, *Ind. Eng. Chem. Res.* **41** (2002) 4252–4265
[164] D. C. Sorescu, D. L. Thompson, M. M. Hurley, C. F. Chabalowski, First-principles calculations of the adsorption, diffusion, and dissociation of a CO molecule on the Fe (100) surface, *Phys. Rev. B* **66** (2002) 035416
[165] D. P. Dobson, M. Wiedenbeck, Fe- and C-self-diffusion in liquid Fe_3C to 15 GPa, *Geophys. Res. Lett.* **29** (2002) 2006
[166] A. G. Nasibulin, P. Queipo, S. D. Shandakov, D. P. Brown, H. Jiang, P. V. Pikhitsa, O. V. Tolochko, E. I. Kauppinen, Studies on mechanism of single-walled carbon nanotube formation, *J. Nanosci. Nanotechnol.* **6** (2006) 1233–1246
[167] I. Astrup, On the kinetics of CO methanation on nickel surfaces, *J. Catal.* **151** (1995) 216–225
[168] Y. Benguerba, M. Virginie, C. Dumas, B. Ernst, Computational fluid dynamics study of the dry reforming of methane over Ni/Al_2O_3 catalyst in a membrane reactor. Coke deposition, *Kinet. Catal.* **58** (2017) 328–338
[169] C. C. Chang, C. H. Yeh, J. J. Ho, Theoretical study of selective hydrogenation in a mixture of acetylene and ethylene over Fe@W (111) bimetallic surfaces, *Appl. Catal. A* **462–463** (2013) 296–301
[170] A. Govender, D. Curulla-Ferré, M. Pérez-Jigato, H. Niemantsverdriet, First-principles elucidation of the surface chemistry of the C_2Hx (x = 0–6) adsorbate series on Fe (100), *Molecules* **18** (2013) 3806–3824
[171] H. Sellers, J. Gislason, Adsorption and desorption rate constants for small molecules on metal surfaces: An example of Trouton's rule, *Surf. Sci.* **426** (1999) 147–153
[172] J. W. Medlin, M. D. Allendorf, Theoretical study of the adsorption of acetylene on the (111) surfaces of Pd, Pt, Ni, and Rh, *J. Phys. Chem. B* **107** (2003) 217–223
[173] W. Huang, J. R. McCormick, R. F. Lobo, J. G. Chen, Selective hydrogenation of acetylene in the presence of ethylene on zeolite-supported bimetallic catalysts, *J. Catal.* **246** (2007) 40–51
[174] C. Zou, A. C. T. van Duin, D. C. Sorescu, Theoretical investigation of hydrogen adsorption and dissociation on iron and iron carbide surfaces using the ReaxFF reactive force field method, *Top. Catal.* **55** (2012) 391–401
[175] M. O. Ozbek, J. W. H. Niemantsverdriet, Elementary reactions of CO and H_2 on C-terminated χ-Fe_5C_2(001) surfaces, *J. Catal.* **317** (2014) 158–166
[176] J. E. Mueller, A. C. T. van Duin, W. A. Goddard III, Competing, coverage-dependent decomposition pathways for C_2Hy species on nickel (111), *J. Phys. Chem. C* **114** (2010) 20028–20041
[177] N. R. Franklin, H. Dai, An Enhanced CVD approach to extensive nanotube networks with directionality, *Adv. Mater.* **12** (2000) 890–894
[178] T. Y. Lee, J. H. Han, S. H. Choi, J. B. Yoo, C. Y. Park, T. Jung, S. Yu, W. K. Yi, I. T. Han, J. M. Kim, Effects of source gases on the growth of carbon nanotubes, *Diam. Relat. Mater.* **12** (2003) 851–855
[179] Y. Tian, Z. Hu, Y. Yang, X. Wang, X. Chen, H. Xu, Q. Wu, W. Ji, Y. Chen, In situ TA-MS study

of the six-membered-ring-based growth of carbon nanotubes with benzene precursor, *J. Am. Chem. Soc.* **126** (2004) 1180–1183
[180] G. Eres, A. A. Kinkhabwala, H. Cui, D. B. Geohegan, A. A. Puretzky, D. H. Lowndes, Molecular beam-controlled nucleation and growth of vertically aligned single-wall carbon nanotube arrays, *J. Phys. Chem. B* **109** (2005) 16684–16694
[181] S. M. Kim, Y. Zhang, K. B. K. Teo, M. S. Bell, L. Gangloff, X. Wang, W. I. Milne, J. Wu, J. Jiao, S.-B. Lee, SWCNT growth on Al/Fe/Mo investigated by in situ mass spectroscopy, *Nanotechnology* **18** (2007) 185709
[182] G. Zhong, S. Hofmann, F. Yan, H. Telg, J. H. Warner, D. Eder, C. Thomsen, W. I. Milne, J. Robertson, Acetylene: A key growth precursor for single-walled carbon nanotube forests, *J. Phys. Chem. C* **113** (2009) 17321–17325
[183] B. Shukla, T. Saito, S. Ohmori, M. Koshi, M. Yumura, S. Iijima, Interdependency of gas phase intermediates and chemical vapor deposition growth of single wall carbon nanotubes, *Chem. Mater.* **22** (2010) 6035–6043
[184] S. Inoue, D. Nakahara, Y. Matsumura, Precursor and formation mechanism in the synthesis of carbon nanotubes by chemical vapor deposition, *Chem. Phys. Lett.* **616-617** (2014) 217–221
[185] Y. Zhang, B. Wang, Q. Yu, Y. Tian, A new understanding of carbon nanotube growth: Different functions of carbon species, *Appl. Surf. Sci.* **332** (2015) 756–760
[186] E. Teblum, A. Itzhak, E. Shawat-Avraham, M. Muallem, R. Yemini, G. D. Nessim, Differential preheating of hydrocarbon decomposition and water vapor formation shows that single ring aromatic hydrocarbons enhance vertically aligned carbon nanotubes growth, *Carbon* **109** (2016) 727–736
[187] S. D. Shandakov, A. V. Kosobutsky, M. S. Rybakov, O. G. Sevostyanov, D. M. Russakov, M. V. Lomakin, A. I. Vershinina, I. M. Chirkova, Effect of gaseous and condensate products of ethanol decomposition on aerosol CVD synthesis of single-walled carbon nanotubes, *Carbon* **126** (2018) 522–532
[188] D. N. Futaba, J. Goto, S. Yasuda, T. Yamada, M. Yumura, K. Hata, General rules governing the highly efficient growth of carbon nanotubes, *Adv. Mater.* **21** (2009) 4811–4815
[189] I. V. Anoshkin, A. G. Nasibulin, Y. Tian, B. Liu, H. Jiang, E. I. Kauppinen, Hybrid carbon source for single-walled carbon nanotube synthesis by aerosol CVD method, *Carbon* **78** (2014) 130–136
[190] C. J. Unrau, V. R. Katta, R. L. Axelbaum, Characterization of diffusion flames for synthesis of single-walled carbon nanotubes, *Combust. Flame* **157** (2010) 1643–1648
[191] B. Hall, C. Zhuo, Y. A. Levendis, H. Richter, Influence of the fuel structure on the flame synthesis of carbon nanomaterials, *Carbon* **49** (2011) 3412–3423
[192] R. L. Vander Wal, L. J. Hall, G. M. Berger, Optimization of flame synthesis for carbon nanotubes using supported catalyst, *J. Phys. Chem. B* **106** (2002) 13122–13132
[193] S. Naha, S. Sen, A. K. De, I. K. Puri, A detailed model for the flame synthesis of carbon nanotubes and nanofibers, *Proc. Combust. Inst.* **31** (2007) 1821–1829
[194] J. Z. Wen, M. Celnik, H. Richter, M. Treska, J. B. Vander Sande, M. Kraft, Modelling study of single walled carbon nanotube formation in a premixed flame, *J. Mater. Chem.* **18** (2008) 1582–1591
[195] T. X. Li, K. Kuwana, K. Saito, H. Zhang, Z. Chen, Temperature and carbon source effects on methane-air flame synthesis of CNTs, *Proc. Combust. Inst.* **32** (2009) 1855–1861
[196] P. Nikolaev, Gas-phase production of single-walled carbon nanotubes from carbon monoxide: A review of the hipco process, *J. Nanosci. Nanotechnol.* **4** (2004) 307–316

(Chapter 6)
[197] H. An, W. M. Yang, A. Maghbouli, J. Li, S. K. Chou, K. J. Chua, A numerical study on a hydrogen assisted diesel engine, *Int. J. Hydrogen Energy* **38** (2013) 2919–2928
[198] Y. Karagöz, T. Sandalcı, L. Yüksek, A. S. Dalkılıç, Engine performance and emission effectcs of diesel burns by hydrogen on different engine loads, *Int. J. Hydrogen Energy* **40** (2015) 6702–6713
[199] J. H. Zhou, C. S. Cheung, W. Z. Zhao, Z. Ning, C. W. Leung, Impact of intake hydrogen enrichment on morphology, structure and oxidation reactivity of diesel particulate, *Appl. Energy* **160** (2015) 442–455
[200] J. J. Hernández, M. Lapuerta, J. Barba, Separate effect of H_2, CH_4 and CO on diesel engine performance and emissions under partial diesel fuel replacement, *Fuel* **165** (2016) 173–184

[201] P. Rosha, A. Dhir, S. K. Mohapatra, Influence of gaseous fuel induction on the various engine characteristics of a dual fuel compression ignition engine: A review, *Renew. Sustain. Ener. Rev.* **82** (2018) 3333–3349
[202] T. Lakshmanan, G. Nagarajan, Experimental investigation of timed manifold injection of acetylene in direct injection diesel engine in dual fuel mode, *Energy* **35** (2010) 3172–3178
[203] A. K. Srivastava, S. L. Soni, D. Sharma, D. Sonar, N. L. Jain, Effect of compression ratio on performance, emission and combustion characteristics of diesel–acetylene-fuelled single-cylinder stationary CI engine, *Clean Technol. Environ. Policy* **19** (2017) 1361–1372
[204] M. Jansons, R. Florea, K. Zha, E. Florea, The Combined effect of HCHO and C_2H_4 addition on combustion in an optically accessible diesel engine fueled with JP-8, *SAE Int. J. Engines* **4** (2011) 2048–2064
[205] M. R. Abu Mansor, M. M. Abbood, T. I. Mohamad, The influence of varying hydrogen-methane-diesel mixture ratio on the combustion characteristics and emissions of a direct injection diesel engine, *Fuel* **190** (2017) 281–291
[206] Y. Karagöz, İ. Güler, T. Sandalcı, L. Yüksek, A. S. Dalkılıç, S. Wongwises, Effects of hydrogen and methane addition on combustion characteristics, emissions, and performance of a CI engine, *Int. J. Hydrogen Energy* **41** (2016) 1313–1325
[207] N. N. Mustafi, R. R. Raine, Electron microscopy investigation of particulate matter from a dual fuel engine, *Aerosol Sci. Technol.* **43** (2009) 951–960
[208] N. N. Mustafi, R. R. Raine, B. James, Characterization of exhaust particulates from a dual fuel engine by TGA, XPS, and Raman techniques, *Aerosol Sci. Technol.* **44** (2010) 954–963

(Chapter 7)
[209] H. Qiu, Z. Shi, L. Guan, L. You, M. Gao, S. Zhang, J. Qiu, Z. Gu, High-efficient synthesis of double-walled carbon nanotubes by arc discharge method using chloride as a promoter, *Carbon* **44** (2006) 516–521
[210] C. Ghemes, A. Ghemes, M. Okada, H. Mimura, T. Nakano, Y. Inoue, Study of growth enhancement of multiwalled carbon nanotubes by chlorine-assisted chemical vapor deposition, *Jpn. J. Appl. Phys.* **52** (2013) 035202
[211] F. Benissad-Aissani, H. Aït-Amar, M. C. Schouler, P. Gadelle, The role of phosphorus in the growth of vapour-grown carbon fibres obtained by catalytic decomposition of hydrocarbons, *Carbon* **42** (2004) 2163–2168
[212] L. Ci, H. Zhu, B. Wei, J. Liang, C. Xu, D. Wu, Phosphorus – a new element for promoting growth of carbon filaments by the floating catalyst method, *Carbon* **37** (1999) 1652–1654
[213] L. Huang, B. Wu, J. Chen, Y. Xue, Y. Liu, H. Kajiura, Y. Li, Synthesis of single-walled carbon nanotubes by an arc-discharge method using selenium as a promoter, *Carbon* **49** (2011) 4792–4800
[214] B. Mas, B. Alemán, I. Dopico, I. Martin-Bragado, T. Naranjo, E. M. Pérez, J. J. Vilatela, Group 16 elements control the synthesis of continuous fibers of carbon nanotubes, *Carbon* **101** (2016) 458–464
[215] M. S. Kim, N. M. Rodriguez, R. T. K. Baker, The interplay between sulfur adsorption and carbon deposition on cobalt catalysts, *J. Catal.* **143** (1993) 449–463
[216] G. G. Tibbetts, C. A. Bernardo, D. W. Gorkiewicz, R. L. Alig, Role of sulfur in the production of carbon fibers in the vapor phase, *Carbon* **32** (1994) 569–576
[217] H. M. Cheng, F. Li, G. Su, H. Y. Pan, L. L. He, X. Sun, M. S. Dresselhaus, Large-scale and low-cost synthesis of single-walled carbon nanotubes by the catalytic pyrolysis of hydrocarbons, *Appl. Phys. Lett.* **72** (1998) 3282–3284
[218] H. Ago, S. Ohshima, K. Uchida, M. Yumura, Gas-Phase synthesis of single-wall carbon nanotubes from colloidal solution of metal nanoparticles, *J. Phys. Chem. B* **105** (2001) 10453–10456
[219] H. W. Zhu, C. L. Xu, D. H. Wu, B. Q. Wei, R. Vajtai, P. M. Ajayan, Direct synthesis of long single-walled carbon nanotube strands, *Science* **296** (2002) 884–886
[220] Y. L. Li, I. A. Kinloch, A. H. Windle, Direct spinning of carbon nanotube fibers from chemical vapor deposition synthesis, *Science* **304** (2004) 276–278
[221] W. Ren, F. Li, H. M. Cheng, Evidence for, and an understanding of, the initial nucleation of carbon nanotubes produced by a floating catalyst method, *J. Phys. Chem. B* **110** (2006) 16941–16946

[222] W. Ren, F. Li, S. Bai, H. M. Cheng, The effect of sulfur on the structure of carbon nanotubes produced by a floating catalyst method, *J. Nanosci. Nanotechnol.* **6** (2006) 1339–1345
[223] A. Barreiro, C. Kramberger, M. H. Rümmeli, A. Grüneis, D. Grimm, S. Hampel, T. Gemming, B. Büchner, A. Bachtold, T. Pichler, Control of the single-wall carbon nanotube mean diameter in sulphur promoted aerosol-assisted chemical vapour deposition, *Carbon* **45** (2007) 55–61
[224] M. S. Motta, A. Moisala, I. A. Kinloch, A. H. Windle, The role of sulphur in the synthesis of carbon nanotubes by chemical vapour deposition at high temperatures, *J. Nanosci. Nanotechnol.* **8** (2008) 2442–2449
[225] T. P. McNicholas, L. Ding, D. Yuan, J. Liu, Density enhancement of aligned single-walled carbon nanotube thin films on quartz substrates by sulfur-assisted synthesis, *Nano Lett.* **9** (2009) 3646–3650
[226] V. Reguero, B. Alemán, B. Mas, J. J. Vilatela, Controlling carbon nanotube type in macroscopic fibers synthesized by the direct spinning process, *Chem. Mater.* **26** (2014) 3550–3557
[227] C. H. Kiang, W. A. III Goddard, R. Beyers, J. R. Salem, D. S. Bethune, Catalytic synthesis of single-layer carbon nanotubes with a wide range of diameters, *J. Phys. Chem.* **98** (1994) 6612–6618
[228] J. J. Swanson, R. Febo, A. M. Boies, D. B. Kittelson, Fuel sulfur and iron additives contribute to the formation of carbon nanotube-like structures in an internal combustion engine, *Environ. Sci. Technol. Lett.* **3** (2016) 364–368
[229] J. Wei, H. Zhu, Y. Jia, Q. Shu, C. Li, K. Wang, B. Wei, Y. Zhu, Z. Wang, J. Luo, W. Liu, D. Wu, The effect of sulfur on the number of layers in a carbon nanotube, *Carbon* **45** (2007) 2152–2158
[230] L. Zhang, P. X. Hou, S. Li, C. Shi, H. T. Cong, C. Liu, H. M. Cheng, In situ TEM observations on the sulfur-assisted catalytic growth of single-wall carbon nanotubes, *J. Phys. Chem. Lett.* **5** (2014) 1427–1432
[231] A. J. McCue, J. A. Anderson, Sulfur as a catalyst promoter or selectivity modifier in heterogeneous catalysis, *Catal. Sci. Technol.* **4** (2014) 272–294
[232] C. N. R. Rao, A. Govindaraj, Carbon nanotubes from organometallic precursors, *Acc. Chem. Res.* **35** (2002) 998–1007
[233] C. Vallés, M. Pérez-Mendoza, P. Castell, M. T. Martínez, W. K. Maser, A. M. Benito, Towards helical and Y-shaped carbon nanotubes: The role of sulfur in CVD processes, *Nanotechnology* **17** (2006) 4292
[234] G. H. Du, W. Z. Li, Y. Q. Liu, Y. Ding, Z. L. Wang, Growth of carbon nanotubes by pyrolysis of thiophene, *J. Phys. Chem. C* **111** (2007) 14293–14298
[235] J. M. Romo-Herrera, B. G. Sumpter, D. A. Cullen, H. Terrones, E. Cruz-Silva, D. J. Smith, V. Meunier and M. Terrones, An atomistic branching mechanism for carbon nanotubes: Sulfur as the triggering agent, *Angew. Chem. Int. Ed.* **47** (2008) 2948–2953
[236] H. L. Ma, Y. Y. Wang, G. Q. Jin, X. Y. Guo, Structural changes in carbon produced by a sulfur-aided catalytic chemical vapor deposition, *New Carbon Mater.* **24** (2009) 13–17
[237] Q. Su, G. Zhong, J. Li, G. Du, B. Xu, Branched carbon nanotubes synthesized by pyrolysis of dimethyl sulfide over Fe/MgO catalyst and their luminescent property, *Physica E* **43** (2011) 1224–1228
[238] C. Wang, L. Zhan, Y. L. Wang, W. M. Qiao, X. Liang, L. C. Ling, Effect of sulfur on the growth of carbon nanotubes by detonation-assisted chemical vapor deposition, *Appl. Surf. Sci.* **257** (2010) 932–936
[239] L. Ci, Z. Rao, Z. Zhou, D. Tang, X. Yan, Y. Liang, D. Liu, H. Yuan, W. Zhou, G. Wang, W. Liu and S. Xie, Double wall carbon nanotubes promoted by sulfur in a floating iron catalyst CVD system, *Chem. Phys. Lett.* **359** (2002) 63–67
[240] B. Yu, C. Liu, P. X. Hou, Y. Tian, S. Li, B. Liu, F. Li, E. I. Kauppinen, H. M. Cheng, Bulk synthesis of large diameter semiconducting single-walled carbon nanotubes by oxygen-assisted floating catalyst chemical vapor deposition, *J. Am. Chem. Soc.* **133** (2011) 5232–5235
[241] K. S. Kim, C. T. Kingston, D. Ruth, M. Barnes, B. Simard, Synthesis of high quality single-walled carbon nanotubes with purity enhancement and diameter control by liquid precursor Ar–H_2 plasma spraying, *Chem. Eng. J.* **250** (2014) 331–341
[242] L. Ci, J. Wei, B. Wei, J. Liang, C. Xu, D. Wu, Carbon nanofibers and single-walled carbon nanotubes prepared by the floating catalyst method, *Carbon* **39** (2001) 329–335
[243] R. M. Sundaram, K. K. K. Koziol and A. H. Windle, Continuous direct spinning of fibers of

single-walled carbon nanotubes with metallic chirality, *Adv. Mater.* **23** (2011) 5064–5068
[244] H. Wang, K. Goh, R. Xue, D. Yu, W. Jiang, R. Lau and Y. Chen, Sulfur doped Co/SiO_2 catalysts for chirally selective synthesis of single walled carbon nanotubes, *Chem. Commun.* **49** (2013) 2031–2033
[245] Y. Yuan, L. Wei, W. Jiang, K. Goh, R. Jiang, R. Lau, Y. Chen, Sulfur-induced chirality changes in single-walled carbon nanotube synthesis by ethanol chemical vapor deposition on a Co/SiO_2 catalyst, *J. Mater. Chem. A* **3** (2015) 3310–3319
[246] Y. Yuan, H. E. Karahan, C. Yildirim, L. Wei, Ö. Birer, S. Zhai, R. Lau, Y. Chen, "Smart poisoning" of Co/SiO_2 catalysts by sulfidation for chirality-selective synthesis of (9,8) single-walled carbon nanotubes, *Nanoscale* **8** (2016) 17705–17713
[247] H. Wang, F. Ren, C. Liu, R. Si, D. Yu, L. D. Pfefferle, G. L. Haller, Y. Chen, $CoSO_4/SiO_2$ catalyst for selective synthesis of (9,8) single-walled carbon nanotubes: Effect of catalyst calcination, *J. Catal.* **300** (2013) 91–101
[248] H. Wang, L. Wei, F. Ren, Q. Wang, L. D. Pfefferle, G. L. Haller, Y. Chen, Chiral-selective $CoSO_4/SiO_2$ catalyst for (9,8) single-walled carbon nanotube growth, *ACS Nano* **7** (2013) 614–626
[249] S. H. Lee, J. Park, H. R. Kim, J. Lee, K. H. Lee, Synthesis of high-quality carbon nanotube fibers by controlling the effects of sulfur on the catalyst agglomeration during the direct spinning process, *RSC Adv.* **5** (2016) 41894–41900
[250] W. E. Alvarez, B. Kitiyanan, A. Borgna, D. E. Resasco, Synergism of Co and Mo in the catalytic production of single-wall carbon nanotubes by decomposition of CO, *Carbon* **39** (2001) 547–558
[251] A. Monzon, G. Lolli, S. Cosma, S. B. Mohamed, D. E. Resasco, Kinetic modeling of the SWNT growth by CO disproportionation on CoMo catalysts, *J. Nanosci. Nanotechnol.* **8** (2008) 6141–6152
[252] H. Sugime, S. Noda, S. Maruyama, Y. Yamaguchi, Multiple "optimum" conditions for Co–Mo catalyzed growth of vertically aligned single-walled carbon nanotube forests, *Carbon* **47** (2009) 234–241
[253] N. Fukaya, D. Y. Kim, S. Kishimoto, S. Noda, Y. Ohno, One-step sub-10 μm patterning of carbon-nanotube thin films for transparent conductor applications, *ACS Nano* **8** (2014) 3285–3293
[254] V. Jourdain, C. Bichara, Current understanding of the carbon nanotubes in catalytic chemical vapor deposition. *Carbon* **58** (2013) 2–39
[255] D. Potoczna-Petru, L. Kępiński, Reduction study of Co_3O_4 model catalyst by electron microscopy, *Catal. Lett.* **73** (2001) 41–46
[256] X. Ma, Y. Cai, X. Li, S. Wen, Growth and microstructure of Co-filled carbon nanotubes, *Mater. Sci. Eng. A* **357** (2003) 308–313
[257] L. Guo, F. Liang, X. Wen, S. Yang, L. He, W. Zheng, C. Chen, Q. Zhong, Uniform magnetic chains of hollow cobalt mesospheres from one-pot synthesis and their assembly in solution, *Adv. Func. Mater.* **17** (2007) 425–430
[258] G. Du, Y. Zhou, B. Xu, Preparation of carbon nanotubes by pyrolysis of dimethyl sulfide, *Mater. Charact.* **61** (2010) 427–432
[259] H. Rau, Range of homogeneity and defect energetics in $Co_{1-x}S$, *J. Phys. Chem. Solids* **37** (1976) 931–934
[260] Y. O. Chen, Y. A. Chang, Thermodynamics and phase relationships of transition metal-sulfur systems: I. the cobalt-sulfur system, *Metall. Trans. B* **9B** (1978) 61–67
[261] B. Alemán, M. M. Bernal, B. Mas, E. M. Pérez, V. Reguero, G. Xu, Y. Cuia, J. J. Vilatela, Inherent predominance of high chiral angle metallic carbon nanotubes in continuous fibers grown from a molten catalyst, *Nanoscale* **8** (2016) 4236–4244
[262] C. Wu, V. Sahajwalla, Influence of melt carbon and sulfur on the wetting of solid graphite by Fe-C-S melts, *Metall. Mater. Trans. B* **29B** (1998) 471–477
[263] M. Hu, Y. Murakami, M. Ogura, S. Maruyama, T. Okubo, Morphology and chemical state of Co-Mo catalysts for growth of single-walled carbon nanotubes vertically aligned on quartz substrates, *J. Catal.* **225** (2004) 230–239
[264] H. Sugime, S. Esconjauregui, L. D'Arsié, J. Yang, A. W. Robertson, R. A. Oliver, S. Bhardwaj, C. Cepek, J. Robertson, Low-temperature growth of carbon nanotube forests consisting of tubes with narrow inner spacing using Co/Al/Mo catalyst on conductive supports, *ACS Appl. Mater. Interfaces* **7** (2015) 16819–16827

[265] E. Heydari-Bafrooei, N. S. Shamszadeh, Synergetic effect of CoNPs and graphene as cocatalysts for enhanced electrocatalytic hydrogen evolution activity of MoS_2, *RSC Adv.* **6** (2016) 95979–95986
[266] A. Galtayries, J. Grimblot, Formation and electronic properties of oxide and sulphide films of Co, Ni and Mo studied by XPS, *J. Electron Spectrosc. Relat. Phenom.* **98-99** (1999) 267–275
[267] Y. Okamoto, K. Ochiai, M. Kawano, K. Kobayashi, T. Kubota, Effects of support on the activity of Co–Mo sulfide model catalysts, *Appl. Catal. A* **226** (2002) 115–127
[268] A. D. Gandubert, E. Krebs, C. Legens, D. Costa, D. Guillaume, P. Raybaud, Optimal promoter edge decoration of CoMoS catalysts: A combined theoretical and experimental study, *Catal. Today* **130** (2008) 149–159
[269] Y. Pan, Y. Liu, C. Liu, Phase- and morphology-controlled synthesis of cobalt sulfide nanocrystals and comparison of their catalytic activities for hydrogen evolution, *Appl. Surf. Sci.* **357** (2015) 1133–1140
[270] Z. Wu, X. Yuan, H. Wang, Z. Wu, L. Jiang, H. Wang, L. Zhang, Z. Xiao, X. Chen, G. Zeng, Facile synthesis of a novel full-spectrum-responsive $Co_{2.67}S_4$ nanoparticles for UV-, vis- and NIR-driven photocatalysis, *Appl. Catal. B* **202** (2017) 104–111
[271] A. Jorio, R. Saito, J. H. Hafner, C. M. Lieber, M. Hunter, T. McClure, G. Dresselhaus, M. S. Dresselhaus, Structural (n, m) determination of isolated single-wall carbon nanotubes by resonant Raman scattering, *Phys. Rev. Lett.* **86** (2001) 1118–1121
[272] P. T. Araujo, S. K. Doorn, S. Kilina, S. Tretiak, E. Einarsson, S. Maruyama, H. Chacham, M. A. Pimenta, A. Jorio, Third and fourth optical transitions in semiconducting carbon nanotubes, *Phys. Rev. Lett.* **98** (2007) 067401
[273] A. Ansaldo, V. Skakalova, E. Di Zitti, D. Ricci, S. Roth, Catalytic chemical vapour deposition growth of single wall carbon nanotube films on different substrates for transparent electronic devices, *Phys. Status Solidi B* **244** (2007) 3935–3938
[274] J. Li, K. Otsuka, X. Zhang, S. Maruyama, J. Liu, Selective synthesis of large diameter, highly conductive and high density single-walled carbon nanotubes by a thiophene-assisted chemical vapor deposition method on transparent substrates, *Nanoscale* **8** (2016) 14156–14162
[275] Z. Chen, X.D. Chen, H. Wang, X. Li, L. Lin, K. Chen, H. Ci, X. Wu, Y. Zhang, Y. Zhang, Z. Liu, One-step growth of graphene/carbon nanotube hybrid films on soda-lime glass for transparent conducting applications, *Adv. Electron. Mater.* **3** (2017) 1700212
[276] M. V. Kharlamova, Investigation of growth dynamics of carbon nanotubes, *Beilstein J. Nanotechnol.* **8** (2017) 826–856
[277] G. D. Lee, S. Han, J. Yu, J. Ihm, Catalytic decomposition of acetylene on Fe(001): A first-principles study, *Phys. Rev. B* **66** (2002) 081403(R)
[278] S. Hofmann, G. Csányi, A. C. Ferrari, M. C. Payne, J. Robertson, Surface diffusion: The low activation energy path for nanotube growth, *Phys. Rev. Lett.* **95** (2005) 036101
[279] Y. Wang, X. Gao, H. J. Qian, Y. Ohta, X. Wu, G. Eres, K. Morokuma, S. Irle, Quantum chemical simulations reveal acetylene-based growth mechanisms in the chemical vapor deposition synthesis of carbo in nanotubes, *Carbon* **72** (2014) 22–37
[280] J. W. Snoeck, G. F. Froment, M. Fowles, Steam/CO_2 reforming of methane. Carbon filament formation by the Boudouard reaction and gasification by CO_2, by H_2, and by steam: Kinetic study, *Ind. Eng. Chem. Res.* **41** (2002) 4252–4265
[281] T. C. Bromfield, D. C. Ferré, J. W. Niemantsverdriet, A DFT study of the adsorption and dissociation of CO on Fe (100): Influence of surface coverage on the nature of accessible adsorption states, *ChemPhysChem* **6** (2005) 254–260
[282] D. Borthwick, V. Fiorin, S. J. Jenkins, D. A. King, Facile dissociation of CO on Fe {2 1 1}: Evidence from microcalorimetry and first-principles theory, *Surf. Sci.* **602** (2008) 2325–2332
[283] M. Melander, L. Laasonen, Identifying the active sites for CO dissociation on Fe–BCC nanoclusters, *J. Mol. Catal. A: Chem.* **406** (2015) 31–39
[284] D. Curulla-Ferré, A. Govender, T. C. Bromfield, J. W. Niemantsverdriet, A DFT study of the adsorption and dissociation of CO on sulfur-precovered Fe(100), *J. Phys. Chem. B* **110** (2006) 13897–13904
[285] K. Habermehl-Ćwirzeń, J. Lahtinen, Sulfur poisoning of the CO adsorption on Co (0 0 0 1), *Surf. Sci.* **573** (2004) 183–190

[286] Y. T. Lee, J. Park, Y. S. Choi, H. Ryu, H. J. Lee, Temperature-dependent growth of vertically aligned carbon nanotubes in the range 800–1100 °C, *J. Phys. Chem. B* **106** (2002) 7614–7618
[287] K. Liu, K. Jiang, C. Feng, Z. Chen, S. Fan, A growth mark method for studying growth mechanism of carbon nanotube arrays, *Carbon* **43** (2005) 2850–2856
[288] C. T. Wirth, C. Zhang, G. Zhong, S. Hofmann, J. Robertson, Diffusion- and reaction-limited growth of carbon nanotube forests, *ACS Nano* **3** (2009) 3560–3566
[289] A. S. Anisimov, A. G. Nasibulin, H. Jiang, P. Launois, J. Cambedouzou, S. D. Shandakov, E. I. Kauppinen, Mechanistic investigations of single-walled carbon nanotube synthesis by ferrocene vapor decomposition in carbon monoxide, *Carbon* **48** (2010) 380–388
[290] C. Ducati, I. Alexandrou, M. Chhowalla, G. A. J. Amaratunga, J. Robertson, Temperature selective growth of carbon nanotubes by chemical vapor deposition, *J. Appl. Phys.* **92** (2002) 3299
[291] N. S. Kim, Y. T. Lee, J. Park, J. B. Han, Y. S. Choi, S. Y. Choi, J. Choo, G. H. Lee, Vertically aligned carbon nanotubes grown by pyrolysis of iron, cobalt, and nickel phthalocyanines, *J. Phys. Chem. B* **107** (2003) 9249–9255
[292] K. Bartsch, K. Biedermann, T. Gemming, A. Leonhardt, On the diffusion-controlled growth of multiwalled carbon nanotubes, *J. Appl. Phys.* **97** (2005) 114301
[293] E. Einarsson, Y. Murakami, M. Kadowaki, S. Maruyama, Growth dynamics of vertically aligned single-walled carbon nanotubes from in situ measurements, *Carbon* **46** (2008) 923–930
[294] P. Vinten, J. Lefebvre, P. Finnie, Kinetic critical temperature and optimized chemical vapor deposition growth of carbon nanotubes, *Chem. Phys. Lett.* **469** (2009) 293–297
[295] R. Smoluchowski, Diffusion rate of carbon in iron-cobalt alloys, *Phys. Rev.* **62** (1942) 539–544
[296] A. E. Lord, D. N. Beshers, The mechanical damping of iron from room temperature to 400°c at 7 megacycles/sec, *Acta Metall.* **14** (1966) 1659–1672
[297] Y. Iijima, F. Makuta, R. P. Agarwala, K. Hirano, Diffusion of carbon in cobalt, *Mater. Trans., JIM* **30** (1989) 984–990
[298] R. B. McLellan, C. Ko, M. L. Wasz, The diffusion of carbon in solid cobalt, *J. Phys. Chem. Solids* **53** (1992) 1269–1273
[299] A. Gorbunov, O. Jost, W. Pompe, A. Graff, Solid–liquid–solid growth mechanism of single-wall carbon nanotubes, *Carbon* **40** (2002) 113–118
[300] Y. Kawai, Diffusion of sulfur in liquid iron. I: Diffusion in pure iron, *Sci. Rep. Res. Inst. Tohoku Univ. Ser. A Phys. Chem. Metall.* **9** (1957) 78–83
[301] W. Jost, *Diffusion in solids, liquids, gases*, Academic Press Inc., New York, 1960
[302] J. F. Mojica, L. L. Levenson, Bulk-to-surface precipitation and surface diffusion of carbon on polycrystalline nickel, *Surf. Sci.* **59** (1976) 447–460
[303] B. Li, Q. Zhang, L. Chen, P. Cui, X. Pan, Vacancy-mediated diffusion of carbon in cobalt and its influence on CO activation, *Phys. Chem. Chem. Phys.* **12** (2010) 7848–7855
[304] M. Lin, J. P. Y. Tan, C. Boothroyd, K. P. Loh, E. S. Tok, Y. L. Foo, Direct observation of single-walled carbon nanotube growth at the atomistic scale, *Nano Lett.* **6** (2006) 449–452
[305] Q. Yuan, H. Hu, F. Ding, Threshold barrier of carbon nanotube growth, *Phys. Rev. Lett.* **107** (2011) 156101
[306] A. G. Nasibulin, P. Queipo, S. D. Shandakov, D. P. Brown, H. Jiang, P. V. Pikhitsa, O. V. Tolochko, E. I. Kauppinen, Studies on mechanism of single-walled carbon nanotube formation, *J. Nanosci. Nanotechnol.* **6** (2006) 1233–1246
[307] E. Fitzer, S. Weisenburger, Evidence of catalytic effect of sulphur on graphitization between 1400 and 2000°C, *Carbon* **14** (1976) 195–198
[308] S. R. Brandtzæg, H. A. Øye, A possible mechanism of sulphur-induced graphitization, *Carbon* **26** (1988) 163–168
[309] J. M. Jiménez Mateos, E. Romero, C. Gómez De Salazar, XRD study of petroleum cokes by line profile analysis: Relations among heat treatment, structure, and sulphur content, *Carbon* **31** (1993) 1159–1178
[310] Y. Xie, S. D. McAllister, S. A. Hyde, J. P. Sundararajan, B. A. FouetioKengne, D. N. McIlroy, I. F. Cheng, Sulfur as an important co-factor in the formation of multilayer graphene in the thermolyzed asphalt reaction, *J. Mater. Chem.* **22** (2012) 5723–5729
[311] G. Carotenuto, V. Romeo, S. De Nicola, L. Nicolais, Graphite nanoplatelet chemical cross-

linking by elemental sulfur, *Nanoscale Res. Lett.* **8** (2013) 94
[312] J. C. Burgos, E. Jones, P. B. Balbuena, Effect of the metal-substrate interaction strength on the growth of single-walled carbon nanotubes, *J. Phys. Chem. C* **115** (2011) 7668–7675
[313] A. J. Page, F. Ding, S. Irle, K. Morokuma, Insights into carbon nanotube and graphene formation mechanisms from molecular simulations: A review, *Rep. Prog. Phys.* **78** (2015) 036501
[314] P. Sahoo, T. Debroy, M. J. Mcnallan, Surface tension of binary metal – surface active solute systems under conditions relevant to welding metallurgy, *Metall. Mater. Trans. B* **19B** (1988) 483–491
[315] C. Wu, V. Sahajwalla, Influence of melt carbon and sulfur on the wetting of solid graphite by Fe-C-S melts, *Metall. Mater. Trans. B* **29B** (1998) 471–477
[316] S. Wang, Q. Gao, J. Wang, Thermodynamic analysis of decomposition of thiourea and thiourea oxides, *J. Phys. Chem. B* **109** (2005) 17281–17289
[317] Z. D. Wang, M. Yoshida, B. George, Theoretical study on the thermal decomposition of thiourea, *Comput. Theor. Chem.* **1017** (2013) 91–98
[318] S. W. Pattinson, R. E. Diaz, N. A. Stelmashenko, A. H. Windle, C. Ducati, E. A. Stach, K. K. K. Koziol, In situ observation of the effect of nitrogen on carbon nanotube synthesis, *Chem. Mater.* **25** (2013) 2921–2923
[319] B. G. Sumpter, V. Meunier, J. M. Romo-Herrera, E. Cruz-Silva, D. A. Cullen, H. Terrones, D. J. Smith, M. Terrones, Nitrogen-mediated carbon nanotube growth: diameter reduction, metallicity, bundle dispersability, and bamboo-like structure formation, *ACS Nano* **1** (2007) 369–375
[320] S. Taubert, K. Laasonen, Initial stages of growth of nitrogen-doped single-walled carbon nanotubes, *J. Phys. Chem. C* **116** (2012) 18538–18549
[321] X. Gu, G. M. Michal, F. Ernst, H. Kahn, A. H. Heuer, Numerical simulations of carbon and nitrogen composition-depth profiles in nitrocarburized austenitic stainless steels, *Metall. Mater. Trans. A* **45A** (2014) 4268–4279
[322] H. Göhring, A. Leineweber, E. J. Mittemeijer, N and C interstitial diffusion and thermodynamic interactions in ε-iron carbonitride, *Metall. Mater. Trans. A* **46A** (2015) 3612–3626
[323] D. Wu, Y. Ge, H. Kahn, F. Ernst, A. H. Heuer, Diffusion profiles after nitrocarburizing austenitic stainless steel, *Surf. Coat. Technol.* **279** (2015) 180–185
[324] D. W. Morgan, J. A. Kitchener, Solutions in liquid iron. Part 3: – Diffusion of cobalt and carbon, *Trans. Faraday Soc.* **50** (1954) 51–60
[325] J. R. G. da Silva, R. B. McLellan, Diffusion of carbon and nitrogen in B.C.C. iron, *Mater. Sci. Eng.* **26** (1976) 83–87
[326] M. Inoue, Y. Kojima, T. Choh, S. Uekawa, Y. Yamada, On the mechanism of diffusion coefficients of nitrogen in the liquid iron, *Tetsu-to-Hagane* **59** (1973) 205–213
[327] T. Belmonte, M. Gouné, H. Michel, Numerical modeling of interstitial diffusion in binary systems. Application to iron nitriding, *Mater. Sci. Eng. A* **302** (2001) 246–257
[328] T. Saito, Y. Kawai, K. Maruya, M. Maki, Diffusion of some alloying elements in liquid iron, *Sci. Rep. Res. Inst. Tohoku Univ. A Phys. Chem. Metall.* **11** (1959) 401–410
[329] A. Hoshino, T. Araki, Diffusion of sulfur in gamma iron, *Tetsu-to-Hagane* **56** (1970) 252–257
[330] H. Oikawa, Lattice diffusion in iron – A review, *Tetsu-to-Hagane* **68** (1982) 1489–1497

(Appendix)

[331] Y. Yanowitz, M. A. Rarcliff, R. L. McCormick, J. D. Taylor, M. J. Murphy, Compendium of experimental cetane numbers, *NREL Technical Report* (2014) TP-5400-61693
[332] G.-D. Lee, S. Han, J. Yu, J. Ihm, Catalytic decomposition of acetylene on Fe(001): A first-principles study, *Phys. Rev. B* **66** (2002) 081403
[333] Z.-X Chen, H. A. Aleksandrov, D. Basaran, N. Rösch, Transformations of ethylene on the Pd(111) surface: A density functional study, *J. Phys. Chem. C* **114** (2010) 17683–17692
[334] D. Basaran, H. A. Aleksandrov, Z.-X. Chen, Z.-J. Zhao, N. Rösch, Decomposition of ethylene on transition metal surfaces M(111). A comparative DFT study of model reactions for M=Pd, Pt, Rh, Ni, *J. Mole. Catal. A* **344** (2011) 37–46
[335] Y. Wang, X. Gao, H.-J. Qian, Y. Ohta, X. Wu, G. Eres, K. Morokuma, S. Irle, Quantum chemical simulations reveal acetylene-based growth mechanisms in the chemical vapor deposition synthesis of carbon nanotubes, *Carbon* **72** (2014) 22–37